

**Developing Real Driving CO₂ Emission Factors for Hybrid Cars
Through on Road Testing and Microscale Modelling**

Richard James Acklom Riley

Submitted in accordance with the requirements for the degree of
Doctor of Philosophy

The University of Leeds
School of Chemical and Process Engineering
Doctoral Training Centre in Low Carbon Technologies

July, 2016

The candidate confirms that the work submitted is his own and that appropriate credit has been given where reference has been made to the work of others.

This copy has been supplied on the understanding that it is copyright material and that no quotation from the thesis may be published without proper acknowledgement.

The right of Richard James Acklom Riley to be identified as Author of this work has been asserted by him in accordance with the Copyright, Designs and Patents Act 1988.

© 2016 The University of Leeds and Richard James Acklom Riley

Acknowledgements

I would like to express my heartfelt thanks to all those who have aided me throughout the completion of this thesis. To my supervisors Dr. James Tate, Dr. Hu Li and Dr. Zia Wadud who have guided me through the winding path that is a PhD. For their ideas and direction getting the project started and their support throughout to get the project finished.

To John Tubby, from Leeds City Council, who set up and organised our work with the Leeds taxi fleet. For his tireless efforts to engage with the taxi community and organise interviews. To Mike Utting from the Leeds Joint Taxi Council and head of Streamline Cabs for his great insight into how the Leeds taxi community operates.

To the Engineering and Physical Science Research Council (EPSRC) for funding my work and giving me the freedom to choose my area of study.

Special thanks to all my friends in Leeds, both those from my undergrad and those I have met on the Low Carbon DTC. You have made the last four and a half years' great fun and a thesis bearable. Particular thanks to Steve and Laura for being great housemates and giving me somewhere to stay when I had no home. To Josh for being a great friend from the first days, I arrived in Leeds. To Clare for making it all more fun and teaching me that transport studies are really geography and no less because of it. To Jannik, my ever-present drinking companion, for teaching me much about a little bit of everything.

The biggest thank you of all to my family, my parents, sister and my girlfriend Hattie who have all been incredibly supportive throughout my seclusion while writing this thesis. Without them, I would never have got this far.

Abstract

Vehicle type approval CO₂ emission figures form the basis for many countries' national policy to reduce transport's contribution to anthropogenic climate change. However, it has become increasingly apparent that the vehicle type approval testing procedure used in Europe is not fit for purpose. There is, therefore, a need for representative real world emission factors that can be used to inform consumers, aid policy makers and provide an accurate benchmark from which type approval figures can be compared.

In this work, two methods are explored to assess their feasibility to provide robust CO₂ emission figures. The first is on-road vehicle activity tracking, using data collected from the vehicle controller area network. This method was chosen as it has the potential to provide large quantities of cheap, reliable data and has been demonstrated by recording over 40 parameters during testing of a third-generation Toyota Prius. This data has been used to analyse the vehicle powertrain control and provide a clear understanding of the control mechanisms that balance the engine and electrical power systems, present a comparison of the emissions of conventional and hybrid taxis giving local policy makers the underlying evidence required to introduce strong policies to reduce urban emissions from taxis and build a microscale emission model for accurate and detailed emission forecasts.

The second method is microscale vehicle modelling, defined as very short time step models (1 second or less) that capture vehicle and location specific details within the model. The model requires vehicle speed and road gradient data as input and outputs second-by-second cumulative and total fuel consumed and CO₂ emissions. The model has been validated against independent data (chassis dynamometer data collected by Argonne National Laboratory) and is now a powerful tool to help assess the effects of local policies (geofences, changes in the speed limit, incentives for hybrid vehicle uptake) or schemes (eco-driving) on the CO₂ emissions from hybrid vehicles.

This work has further developed these two methods in two ways. Firstly, by demonstrating the accuracy of controller area network data collected in vehicle activity tracking. Secondly, by demonstrating the precision of emission models built using real-world data, despite the data noise caused by real world conditions. In conclusion, these methods are well suited to providing representative real world CO₂ emission factors, especially if the methods are combined. This is because vehicle activity tracking can provide the large amount of data needed for vehicle modelling and a vehicle model can provide situation specific emission factors, which, in contrary to many current emissions factors, are not only dependent on vehicle average speeds.

Table of Contents

Acknowledgements	iii
Abstract	iv
Table of Contents	vi
List of Tables	xii
List of Figures	xiv
List of Abbreviations	xx
Nomenclature	xxiii
Chapter 1 Introduction	1
1.1 Motivation.....	1
1.2 Aims and Objectives.....	5
1.3 Thesis Outline	7
1.4 Thesis Contributions.....	10
Chapter 2 Background Literature	13
2.1 Introduction	13
2.2 Vehicle Emission Policy.....	13
2.2.1 Problems with Regulation 443/2009.....	16
2.2.1.1 Test Cycle	18
2.2.1.2 Test Procedure.....	20
2.2.1.3 Conformity Testing	23
2.2.1.4 Real World Testing.....	24
2.3 Vehicle Testing Methods	25
2.3.1 Chassis Dynamometer.....	25
2.3.2 Portable Emissions Measurement Systems (PEMS).....	28
2.3.3 Emissions Delay	29
2.3.4 Portable Activity Measurement Systems (PAMS).....	31
2.3.4.1 Vehicle Controller Area Network (CAN).....	31
2.3.4.2 On-Board Diagnostics (OBD) Link.....	31
2.3.4.3 Use of Vehicle CAN Data Collected from the OBD Port ..	33
2.4 Fuel Consumption and Emissions Modelling	37
2.4.1 Models Based on External Variables	40
2.4.1.1 VT-Micro	40
2.4.1.2 VERSIT+ LD	41
2.4.1.3 MOVES (Motor Vehicle Emission Simulator)	45

2.4.2 Models Based on Internal Variables	48
2.4.2.1 PHEM (Passenger car and Heavy duty vehicle Emission Model).....	48
2.4.2.2 CMEM (Comprehensive Modal Emission Model)	51
2.4.2.3 VeTESS (Vehicle Transient Emissions Simulation Software)	55
2.4.2.4 EMIT (Emissions from Traffic).....	58
2.4.2.5 PERE (Physical Emissions Rate Estimator)	60
2.4.2.6 Kaishan Zhang Microscale Model	62
2.4.2.7 Delia Ajtay Modal Model	64
2.4.3 Vehicle Component Models	65
2.4.3.1 ADVISOR (Advanced Vehicle Simulator)	66
2.4.3.2 PSAT (Powertrain Systems Analysis Toolkit) / Autonomie	67
2.4.3.3 Ricardo in-House Model.....	69
2.4.3.4 AVL CRUISE	71
2.5 Conclusions	72
Chapter 3 Portable Activity Measurement System (PAMS) Testing Methodology.....	74
3.1 Introduction	74
3.2 Testing Equipment	75
3.2.1 Test Vehicle.....	75
3.2.1.1 Development of Toyota Prius	75
3.2.1.2 Vehicle Specification.....	75
3.2.2 Data Loggers.....	77
3.2.2.1 Racelogic Data Logger.....	77
3.2.2.2 HEM Data Logger	78
3.3 Testing Methodology	81
3.3.1 On-Road Data Collection.....	81
3.3.1.1 Taxi Data Collection Campaign.....	82
3.3.1.1.1 Interviews with Taxi Drivers	82
3.3.1.1.2 Test Routes	83
3.3.1.1.3 Test Procedure	85
3.3.1.2 Commuter Data Collection Campaign	87
3.3.1.2.1 City Test Route	88

3.3.1.2.2 Motorway Test Route	89
3.3.2 Data Post Processing	90
3.4 Test Data Distribution	91
3.5 Fuel Consumption Determination	94
3.5.1 Injection Rate.....	94
3.5.2 Mass Air Flow	94
3.5.3 Fuel Consumption Method Comparison.....	95
3.6 Conclusions.....	96
Chapter 4 Analysis of a Hybrid Vehicle.....	98
4.1 Introduction	98
4.2 Literature Review	99
4.2.1 Vehicle Physical Specification.....	99
4.2.1.1 Powertrain.....	99
4.2.1.2 Engine.....	101
4.2.1.3 Aftertreatment System.....	103
4.2.2 Vehicle Control	104
4.2.2.1 Main Operating Modes	104
4.2.2.2 Overarching Control	105
4.2.2.3 Component Control	106
4.2.2.3.1 Engine.....	106
4.2.2.3.2 Generator.....	106
4.2.2.3.3 Motor.....	106
4.2.2.3.4 Battery	107
4.2.2.4 Additional Operating Modes	107
4.2.2.4.1 Cold Starts	107
4.2.2.4.2 Low Battery SOC	108
4.3 Analysis of the PAMS Test Data.....	109
4.3.1 Overview of Vehicle Design	109
4.3.2 Vehicle Control	114
4.3.2.1 Overview of Power Flow Paths.....	114
4.3.2.2 Overarching Control	117
4.3.2.3 Component Control	122

4.3.2.3.1 Engine	122
4.3.2.3.1.1 Engine Speed and Torque Operation	122
4.3.2.3.1.2 Engine Fuel Consumption	126
4.3.2.3.2 Generator	127
4.3.2.4 Additional Operating Modes	128
4.3.2.4.1 Cold Start.....	129
4.3.2.4.1.1 Cabin Heating Off.....	131
4.3.2.4.1.2 Cabin Heating On.....	135
4.3.2.4.1.3 Effect of Battery SOC on Cold Engine Operation.....	138
4.3.2.4.2 Low Battery SOC	139
4.3.2.4.3 Fuel Cut	140
4.3.3 Effect of SOC and coolant temperature on fuel consumption.....	142
4.3.3.1 Battery SOC Effect on Fuel Consumption	144
4.3.3.2 Engine Coolant Temperature Effect on Fuel Consumption	146
4.4 Conclusions	147
Chapter 5 Potential of Hybrid Vehicles to Reduce Emissions from Taxi Fleets	150
5.1 Introduction	150
5.2 Literature Review	154
5.3 Leeds Taxi Fleet Overview	155
5.4 Results and Discussion	161
5.4.1 Taxi Driving Pattern	161
5.4.2 Driving Styles	164
5.4.3 Fuel Consumption and CO ₂ Emissions	165
5.4.3.1 Mode 1, Vehicle Stationary Mode	170
5.4.3.2 Mode 2, Pure Electric Mode	170
5.4.3.3 Mode 3, Hybrid Electric Mode	173
5.4.4 NO _x Emissions	179
5.4.5 Business Case.....	185
5.4.5.1 New Vehicle Business Case	186

5.4.5.2 Second Hand Vehicles Business Case	186
5.4.5.3 Sensitivity of Payback Time to Vehicle Mileage.....	187
5.4.5.4 Sensitivity of Payback Time to Fuel Price.....	188
5.4.5.5 Anecdotal Evidence from Taxi Driver Interview	190
5.5 Policy Options to Encourage the Uptake of Hybrid Taxis.....	191
5.5.1 Vehicle Licencing, Emission Limits, or Technology Requirements	191
5.5.2 Financial Incentives	193
5.5.3 Vehicle Licencing.....	193
5.5.4 Taxi Rank	194
5.5.5 Restricted Zone or Lane Access	195
5.5.6 Green Taxi Image	195
5.5.7 Taxi Community Engagement.....	196
5.5.8 Consumer Engagement.....	197
5.5.9 Reducing the Price of Second Hand Hybrid Vehicles.....	197
5.6 Conclusions.....	199
Chapter 6 Hybrid Vehicle Model Creation and Validation	201
6.1 Introduction	201
6.2 Model Creation.....	202
6.2.1 Model Input.....	204
6.2.2 Model Components.....	204
6.2.2.1 Tractive Power	207
6.2.2.2 Engine.....	208
6.2.2.2.1 Engine Cooling Sub-Model.....	209
6.2.2.2.2 Engine On Sub-Model.....	212
6.2.2.2.3 Engine Off Sub-Model.....	214
6.2.2.2.4 Engine Power Sub-Model.....	217
6.2.2.2.5 Engine Speed and Torque Sub-Model	221
6.2.2.2.6 Engine Fuel Consumption Sub-Model	224
6.2.2.3 Motor and Inverter.....	228
6.2.2.4 Generator and Inverter	237
6.2.2.5 Battery	243
6.2.2.5.1 Predicted Battery Power Demand	244

6.2.2.5.2 Actual Battery Power Demand	245
6.2.2.5.3 Battery SOC.....	249
6.2.3 Additional Model Control Modes	252
6.2.3.1 Cold Start.....	252
6.2.3.2 Low Battery SOC	255
6.3 Model Validation.....	256
6.3.1 Validation Database	256
6.4 Model Applications	272
6.4.1 Introduction.....	272
6.4.2 Geofence Model Application	274
6.4.3 Geofence Model Results	278
6.5 Conclusions	282
Chapter 7 Conclusions.....	285
7.1 Further Work	289
Glossary	291
List of References.....	292

List of Tables

Table 2.1: Penalty per car in manufacturers fleet if the average fleet CO ₂ emissions exceed limit (European Commission, 2016).....	14
Table 2.2: Super credits multiplication factor (European Commission, 2016)	16
Table 2.3: Benefits and drawbacks of chassis dynamometer testing (Franco et al., 2013; Kadijk & Ligterink, 2012; Transport & Environment, 2015a; Weilenmann, Soltic, & Ajtay, 2003)	27
Table 2.4: Benefits and drawbacks of PEMS testing (Franco et al., 2013; Ortenzi & Costagliola, 2010; Sandhu & Frey, 2013; Weilenmann et al., 2003).....	29
Table 2.5: Classification of model parameters used in the development of VERSIT+ LD (Smit et al., 2007).	44
Table 2.6: MOVES, VSP and speed bins (Coordinating Research Council, 2010).....	47
Table 2.7: Model input parameters (Scora & Barth, 2006).....	53
Table 2.8: CMEM CO ₂ emissions validation (Scora & Barth, 2006).....	55
Table 3.1: Third generation Toyota Prius specification (Rask et al., 2010).....	76
Table 3.2: Racelogic parameters collected by Racelogic unit	78
Table 3.3: HEM Mini Logger parameters collected	80
Table 3.4: Summary of data collection and applications	82
Table 3.5: Taxi testing overview	87
Table 4.1: EPA vehicle specific power modes (US Environmental Protection Agency, 2002)	144
Table 5.1: Fuel economy, fuel consumption and CO ₂ emissions for the three vehicle technologies and three driving styles	167
Table 5.2: Toyota Prius operating modes	168
Table 5.3: Fuel saving achieved by Prius in each operating mode	169
Table 5.4: Comparison between PAMS taxi data and the London Urban, Suburban and motorway drive cycles	181
Table 5.5: NO _x saving achieved, by road type, through switching from diesel to petrol, or conventional vehicles to petrol hybrid.....	182
Table 5.6: Percentage time and percentage NO _x saving, by switching from conventional to hybrid vehicles, split by Prius stationary, Prius pure electric mode and Prius hybrid electric mode	183
Table 5.7: Fuel saving and payback times for purchasing a new hybrid taxi	186
Table 5.8: Fuel saving and payback times for purchasing a second-hand hybrid taxi.....	187
Table 6.1: Tractive power model: inputs and outputs	207

Table 6.2: Engine coolant sub-model: inputs and outputs	209
Table 6.3: Engine power sub-model: inputs and outputs	217
Table 6.4: Engine speed and torque sub-model: inputs and outputs	221
Table 6.5: Engine fuel consumption sub-model: inputs and outputs	224
Table 6.6: Motor model: inputs and outputs	228
Table 6.7: Generator model: inputs and outputs	237
Table 6.8: Predicted battery power sub-model: inputs and outputs	244
Table 6.9: Battery power sub-model: inputs and outputs.....	245
Table 6.10: Battery SOC sub-model: inputs and outputs	249
Table 6.11: Validation database, parameters collected.....	258
Table 6.12: Error in modelled fuel consumption over five validation cycles.	261

List of Figures

Figure 1.1: Thesis chapter overview and interconnection	7
Figure 2.1: CO ₂ limit value curve 2015 and 2021 with manufacturer's progress 2013. Adapted from (The International Council on Clean Transportation, 2014).....	15
Figure 2.2: Gap between type-approval and real-world CO ₂ emissions figures. Adapted from (Mock, Tietge, et al., 2014).....	17
Figure 2.3: Chassis dynamometer test cycles (A) NEDC, (B) WLTC	20
Figure 2.4: Type approval testing flexibilities leading to divergence between test and real world CO ₂ emission figures in 2002, 2010, 2014, 2020 and 2025 (Element Energy & The International Council on Clean Transportation, 2015).....	22
Figure 2.5: Schematic representation of a chassis dynamometer emission testing facility (Franco et al., 2013)	26
Figure 2.6: Methodology to calculate emission parameters (Pelkmans et al., 2004).....	57
Figure 3.1: Racelogic module setup	77
Figure 3.2: Leeds four taxi test routes with route height profile	84
Figure 3.3: Route one, city test route	89
Figure 3.4: Route two, motorway test route	90
Figure 3.5: PAMS database distribution across vehicle speed and acceleration	92
Figure 3.6: PAMS database distribution across road gradient.....	92
Figure 3.7: PAMS database distribution across ambient temperature.....	93
Figure 3.8: Comparison of PAMS injection and MAF fuel consumption methods.....	96
Figure 4.1: Schematic of the Toyota Prius drivetrain	100
Figure 4.2: Schematic of the Toyota Prius transmission	100
Figure 4.3: Percentage of engine power passing through the mechanical path, over vehicle speed and tractive torque, when the Prius is operating in hybrid electric mode	111
Figure 4.4: Density plot over vehicle speed and tractive torque, when the Prius is operating in hybrid electric mode	112
Figure 4.5: Vehicle speed against tractive torque when the Prius is operating in pure electric mode	114
Figure 4.6: Power flow diagram for the Toyota Prius powertrain. Red lines, electrical path. Blue lines, mechanical path.....	115
Figure 4.7: Prius tractive power, engine power, battery power, predicted engine power and predicted battery power during transient driving ...	118

Figure 4.8: Battery power as a function of battery SOC and rate of change of tractive power.....	119
Figure 4.9: Prius powertrain response to three separate harsh acceleration events	121
Figure 4.10: Prius engine speed and torque operating points with engine target operating line in red.....	123
Figure 4.11: Prius engine operation during transient driving. A, tractive power and change in tractive power colour coded by run time. B, engine speed against engine torque colour coded by run time. Red line, engine optimum path	124
Figure 4.12: Prius engine operation at 40 km/h. A, engine speed against engine torque, colour coded by vehicle traction torque. B, engine speed against engine torque, colour coded by battery power.....	126
Figure 4.13: Prius engine fuel consumption map.....	127
Figure 4.14: Engine power delivered to the sun gear against generator power, colour coded by change in engine speed	128
Figure 4.15: Prius engine speed and torque under different engine coolant temperatures	130
Figure 4.16: Prius engine coolant temperature against engine efficiency. Blue, all data. Red, cold start engine idling data	131
Figure 4.17: Prius cold powertrain operation at the start of a run with cabin heating off.....	132
Figure 4.18: Prius cold powertrain operation in the middle of a run with cabin heating off.....	134
Figure 4.19: Prius powertrain response to vehicle driving demand during cold start at the beginning of a run with cabin heating off	135
Figure 4.20: Prius cold powertrain operation at the start of a run with cabin heating on.....	136
Figure 4.21: Prius warm powertrain operation at the start of a run with cabin heating on.....	137
Figure 4.22: Effect of battery SOC on cold powertrain operation at the start of a run with cabin heating on.....	139
Figure 4.23: Prius powertrain operation during a low battery SOC event	140
Figure 4.24: Prius vehicle speed, tractive power, engine power, engine speed, engine torque and fuel consumption during fuel cut.....	141
Figure 4.25: Prius engine power, generator power, motor power and battery power during fuel cut.....	142
Figure 4.26: Prius percentage time, percentage time with the engine off and fuel consumption by tractive power mode.....	143
Figure 4.27: Prius percentage time, percentage time with the engine off and fuel consumption by tractive power mode, split by batter SOC	145

Figure 4.28: Prius percentage time, percentage time with the engine off and fuel consumption by tractive power mode, split by engine coolant temperature	147
Figure 5.1: Leeds hackney carriage fleet makeup, broken down by powertrain, body type and engine size.....	156
Figure 5.2: Leeds private hire fleet makeup, broken down by powertrain, body type and engine size.....	157
Figure 5.3: Number and proportion of taxi vehicles on the A660 in a 24 hour period. Bar chart, percentage of vehicle fleet. Line chart, number of taxi vehicles.....	159
Figure 5.4: Leeds hackney carriage and PHV fleet, year of vehicle first registration	160
Figure 5.5: Leeds hackney carriage and PHV fleet makeup, by vehicle make and model	161
Figure 5.6: Vehicle Speed against VSP for six data sets. Top-panel (a) Toyota Prius test data, (b) Toyota Prius test data with taxi rank data removed, (c) PCO Cenex London taxi driving cycle. Bottom-panel (d) Urban Dynamometer Driving Schedule (UDDS), (e) New European Drive Cycle (NEDC), (f) Worldwide harmonized Light-duty Test Cycle (WLTC).....	163
Figure 5.7: Vehicle speed against vehicle acceleration, for the three taxi driving styles	165
Figure 5.8: Engine power and fuel consumption for the hybrid, petrol and diesel vehicles, colour coded by Prius operating mode	170
Figure 5.9: Petrol engine speed versus torque, at each gear ratio, when the Prius is in pure electric mode.....	171
Figure 5.10: Diesel engine speed versus torque, at each gear ratio, when the Prius is in pure electric mode.....	172
Figure 5.11: Petrol engine speed versus torque, at each gear ratio, when the Prius is in hybrid electric mode	175
Figure 5.12: Diesel engine speed versus torque, at each gear ratio, when the Prius is in hybrid electric mode	175
Figure 5.13: Prius engine speed versus torque, at each gear ratio, when the Prius is in hybrid electric mode	176
Figure 5.14: Comparing petrol and hybrid engine speed versus torque, by segment, over the engine map.....	177
Figure 5.15: Comparing diesel and hybrid engine speed versus torque, by segment, over the engine map.....	178
Figure 5.16: Petrol and petrol hybrid NOx emissions, colour coded by Prius mode. Clear, vehicle stationary. Blue, pure electric mode. Red, hybrid electric mode	185
Figure 5.17: Change in payback time with changing mileage for switching from a petrol or diesel taxi to a hybrid taxi.....	188

Figure 5.18: Change in payback time with change in petrol fuel price for switching from a petrol taxi to a petrol hybrid taxi.....	189
Figure 5.19: Change in payback time with changing petrol and diesel prices for switching from a diesel taxi to a petrol hybrid taxi	190
Figure 6.1: Toyota Prius powertrain overview. Sub-models underlined. Parameters calculated within each model in Red.....	205
Figure 6.2: Sub-model inputs and outputs	207
Figure 6.3: Prius engine coolant temperature, cooling over time	210
Figure 6.4: Prius engine coolant temperature, heating over time	211
Figure 6.5: Test data and modelled engine coolant temperature	212
Figure 6.6: Prius engine, battery, motor and tractive power at engine on.....	213
Figure 6.7: Prius battery SOC against motor power, at engine on. Blue dots represent raw data. Red line is a corrected linear best fit.....	214
Figure 6.8: Prius battery SOC against tractive power, at engine off. Blue dots represent raw data. Red line is a corrected linear best fit.....	216
Figure 6.9: Calculating engine power from tractive and battery power. Blue dots represent raw data. Red line is a linear best fit fitted over two power ranges (-20-0kW, 0-80kW)	218
Figure 6.10: Prius engine operational area and power limit	220
Figure 6.11: Engine power error against sub-model inputs, tractive power and battery power	221
Figure 6.12: Calculating engine speed from engine power. Blue dots represent raw data. Red line is a quartic best fit curve	222
Figure 6.13: Prius engine idle speed as a function of engine coolant temperature	223
Figure 6.14: Engine fuel consumption, test data against model data. Blue dots represent raw data. Red line is a linear best fit	226
Figure 6.15: Fuel consumption error against model inputs, engine speed, torque and temperature	227
Figure 6.16: Tractive power against motor power at the start of microtrips. Blue dots represent raw data. Red line is a linear best fit.....	230
Figure 6.17: Tractive power against motor power in Prius pure electric mode. Blue dots represent raw data. Red line is a linear best fit.....	231
Figure 6.18: Prius motor operational area and power limit.....	233
Figure 6.19: Prius Motor and inverter efficiency map. Adapted from (Burress et al., 2011).....	234
Figure 6.20: Motor power error against model input, tractive power, when the Prius is operating in pure electric mode	235
Figure 6.21: Motor power error against model inputs, generator, battery and tractive power, when the Prius is operating in hybrid electric mode	236

Figure 6.22: Sun gear power versus generator power with lines fitted at nine bands of rate of change of engine speed. Blue dots represent raw data. Red lines are linear best fit.....	239
Figure 6.23: Gradient of lines fitted to generator power as a function of rate of change of engine speed. Blue dots represent raw data. Red line is a cubic curve best fit.....	240
Figure 6.24: Prius generator operational area and power limit	241
Figure 6.25: Prius generator and inverter efficiency map. Adapted from (Burress et al., 2011)	242
Figure 6.26: Generator model error, against model inputs, motor speed, engine speed and engine torque.....	243
Figure 6.27: Battery SOC against battery power, under normal engine on conditions. Blue dots represent raw data. Red line is a linear best fit.	245
Figure 6.28: Prius battery operational area and power limit	247
Figure 6.29: Vehicle speed against battery regeneration power	248
Figure 6.30: Battery power error against model inputs, motor and engine power	249
Figure 6.31: Battery SOC error, test versus modelled data	251
Figure 6.32: Battery power demand as a function of battery SOC at low catalyst temperatures. Blue dots represent raw data. Red line is a linear best fit over the battery SOC range from 30-65%. The range from 65-80% is assumed based on the finding in Figure 6.33	254
Figure 6.33: Battery power demand as a function of battery SOC at low coolant temperatures. Blue dots represent raw data. Red line is a linear best fit fitted over three battery SOC ranges (30-65%, 65-68%, 68-80%).....	255
Figure 6.34: Battery power demand as a function of battery SOC during a low battery SOC event. Blue dots represent raw data. Red line is a linear best fit	256
Figure 6.35: Validation drive cycles. A, HWFET. B, UDDS. C, US06. D, Steady State	257
Figure 6.36: Vehicle speed and acceleration distribution for the validation database	259
Figure 6.37: Model validated against HWFET cycle.....	265
Figure 6.38: Model validated against UDDS cycle with hot start	266
Figure 6.39: Model validated against UDDS cycle with cold start	267
Figure 6.40: Model validated against US06 cycle	268
Figure 6.41: Model validated against steady state speed cycle	269
Figure 6.42: Validation fuel consumption against model fuel consumption	270
Figure 6.43: Fuel consumption error against tractive power for five validation cycles.....	271

Figure 6.44: Roadmap of Leeds marked with geofence zones	275
Figure 6.45: Predicted battery power as a function of battery SOC for the original and geofence model.....	276
Figure 6.46: Original and geofence model battery SOC over the four taxi driving cycles. Colour coded by geofence zone. Green, outer zone. Blue, inner zone	280
Figure 6.47: Boxplot of fuel consumption, left to right. Original model all data. Original model excluding vehicle stationary data. Geofence model all data. Geofence model excluding vehicle stationary data.	281
Figure 6.48: Cumulative fuel consumption, original versus geofence model, over the four taxi driving cycles. Colour coded by geofence zone. Green, outer zone. Blue, inner zone	282

List of Abbreviations

ADVISOR	Advanced Vehicle Simulator
AFV	Alternative Fuelled Vehicles
BEV	Battery Electric Vehicle
CAN	Controller Area Network
CAPS	Controller, Actuator, Plant, Sensor
CMEM	Comprehensive Modal Emission Model
COP	Conference of Parties
DfT	Department for Transport
DOHC	Double Over Head Cam
DSM	Digital Surface Model
ECU	Electronic Control Unit
EHRS	Exhaust Heat Recirculation System
EI	Emission Index
EMIT	Emissions from Traffic
EOBD	European On-Board Diagnostics
EPA	Environmental Protection Agency
ETCS-I	Electronic Throttle Control System with intelligence
EU	European Union
EUDC	Extra Urban Drive Cycle
FR	Fuel Rate
FTP-75	Federal Test Procedure 75
GUI	Graphical User Interface
HE	Hybrid Electric
HTBR	Hierarchical Tree Based Regression
HWFET	Highway Fuel Economy Test
ICCT	International Council on Clean Transportation

ICE	Internal Combustion Engine
IPCC	Intergovernmental Panel on Climate Change
ITS	Intelligent Transport Systems
LDC	London Drive Cycles
LDT	Light Duty Truck
LDV	Light Duty Vehicle
LEV	Low Emission Vehicle
LEZ	Low Emission Zone
LiDAR	Light Detection and Ranging
MAF	Mass Air Flow
MAP	Manifold Absolut Pressure
MOVES	Motor Vehicle Emission Simulator
MPG	Miles Per Gallon
MPV	Multi-Purpose Vehicle
MSRG	Motor Speed Reduction Gear
NEDC	New European Drive Cycle
Ni-MH	Nickle Metal Hydride
OBD	On-Board Diagnostics
PAMS	Portable Activity Measurement Systems
PE	Pure Electric
PEMS	Portable Emission Measurement Systems
PERE	Physical Emissions Rate Estimator
PG	Planetary Gear
PHEM	Passenger car and Heavy duty vehicle Emission Model
PHEV	Plug-in Hybrid Electric Vehicle
PHV	Private Hire Vehicle
PID	Parameter ID's
PSAT	Powertrain Systems Analysis Toolkit

PZEV	Partial Zero Emission Vehicles
RDE	Real Driving Emission
SCR	Selective Catalytic Reduction
SOC	State of Charge
SULEV	Super Ultra Low Emission Vehicles
TfL	Transport for London
THS	Toyota Hybrid System
TWC	Three Way Catalyst
UDC	Urban Drive Cycle
UDDS	Urban Dynamometer Driving Schedule
ULEV	Ultra-Low Emission Vehicles
ULEZ	Ultra-Low Emission Zone
UNFCCC	United Nations Framework Convention on Climate Change
VeTESS	Vehicle Transient Emissions Simulation Software
VIN	Vehicle Identification Number
VSP	Vehicle Specific Power
VVT-I	Variable Valve Timing with intelligence
WAV	Wheel Chair Accessible Vehicle
WLTC	Worldwide harmonised Light-duty vehicles Test Cycle
WLTP	Worldwide harmonised Light-duty vehicles Testing Procedure
ZEC	Zero Emission Capable

Nomenclature

A, B, C = Vehicle Coast Down Rolling, Rotating and Aerodynamic Resistance Coefficients

A_r = Vehicle Frontal Area (m^2)

a = Vehicle Acceleration (m/s^2)

B = Speed Correction to Rolling Resistance Coefficient ($kW/(m/s)^2$)

b_{mep} = Brake Mean Effective Pressure

C_D = Aerodynamic Drag Coefficient ($kW/(m/s)^3$)

C_R = Rolling Resistance ($kW/m/s$)

D_{Wheel} = Dynamic Wheel Diameter (m)

dF/dt = Fuel Use Rate (kW)

E_{b^+AUX} = Total Auxiliary Brake Energy During Powered Driving (kJ)

E_{BR} = Total Braking Energy Required at the Road-Tyre Interface (kJ)

E_{Final} = Final Steady State Emissions

E_{New} = New Steady State Emissions

E_{Prev} = Previous Emissions Rate

E_{TR} = Total Tractive Energy Required at the Road-Tyre Interface During Powered Driving (kJ)

f_{mep} = Friction Mean Effective Pressure

$fr_{0,1,2,3,4}$ = Rolling Resistance Coefficients

F_{TR} = Tractive Force (N)

g = Gravitational Constant ($9.81 m/s^2$)

GC = Ground Clearance (m)

(g/g_{top}) = Gear Ratio in Selected Gear

H = Vehicle Height (m)

H_f = Fuel Heating Value (MJ/kg)

I = Moment of Inertia (kg/m^2)

i = Species (fuel consumption, CO, HC)

i_{axle} = Transmission Ratio of Axle

i_{Gear} = Transmission Ratio of the Gear in use

I_w = Polar Moment of Inertia of the Wheel (kg/m^2)

j = Species (NO, HC, CO, CO₂, fuel consumption)

K = Engine Friction Factor (kJ/rev/litre)

LHV = Lower Heating Value of Fuel

m = Vehicle Mass (kg)

m_f^+ = Mass of Fuel Consumed in a Drive Cycle During Powered Driving (kg)

m_f^- = Mass of Fuel Consumed in a Drive Cycle During Braking (kg)

m_f^0 = Mass of Fuel Consumed in a Drive Cycle During Idling (kg)

\bar{m}_f^- = Time Averaged Fuel Mass Flow Rate During Braking (kg/s)

\dot{m}_f^0 = Fuel Mass Flow Rate During Idle (s)

\bar{m}_i = Average Mass Emission Rate for Species i (g/s)

N = Engine Speed (rps)

$(N/v)_{\text{top}}$ = rpm to Speed Ratio in Top Gear

$N_{r,s}$ = No. of Gear Teeth on the Ring or Sun Gear

P = Engine Power Output (kW)

P_0 = Fraction of Power Demand of Auxiliaries to Auxiliaries Rated Power

P_{Aux} = Power Demand of Auxiliary Systems (W)

P_b = Brake Output Power of the Engine (kW)

$P_{b,\text{AUX}}$ = Brake Power Required by Vehicle Auxiliaries (kW)

P_{dr} = Power to overcome driving resistances (kW)

P_{Engine} = Power Demand on Engine (W)

P_{map} = Manifold Absolute Pressure (kPa)

P_{Rated} = Rated Power of all Auxiliaries (W)

P_{Tract} = Power Required at the Wheel (kW)

r_0 = Tyre Rolling Resistance Coefficient

r_w = Effective Rolling Radius of the Wheel (m)

S = Total Distance Driven over a Drive Cycle (km)

T = Torque (Nm)

T_x = Time Increment (s)

t = Time (s)

Δt = Index for Averaging Period

v = Vehicle Velocity (m/s)

V = Engine Displacement (litres)

W = Vehicle Width (m)

x = Average Emissions Over Previous 15s

y = Difference Between the Two Steady State Emissions Values

α = Coefficient (m/s²)

β = Coefficient (kg/m.s²)

γ = Coefficient (m/s²)

ε = Rotational Mass Factor

ε_j = Model Residual for species j

η = Engine Indicated Efficiency

$\eta_{b,MAX}$ = Maximum Brake Thermal Efficiency

$\tilde{\eta}_b$ = Fuel-Consumption-Weighted Average Brake Thermal Efficiency over the powered segment of a driving schedule

η_{dr} = Instantaneous Drivetrain Efficiency

$\tilde{\eta}_{dr}$ = Energy-Transfer-Weighted Average Drivetrain Efficiency over the Powered Driving Segment of a Drive Cycle

η_m = Mechanical Efficiency

η_t = Transmission and Drivetrain Efficiency

η_{Trans} = Transmission Efficiency

η_V = Volumetric Efficiency

θ = Road Gradient Angle (degree)

λ = Equivalence Ratio (stoichiometric air fuel ratio over actual air fuel ratio)

ρ = Air Mass Density (1.225 kg/m³)

ρ_f = Density of Fuel (kg/litre)

τ_c = Time Constant

ϕ = Equivalence Ratio

ω = Rotational Speed

Superscript

- = Decelerating

+ = Powered Driving

0 = Idling

Subscript

c = Pinion Gear Carrier

e = Engine

m = Motor

r = Ring Gear

s = Sun Gear

w = Wheel

Chapter 1

Introduction

1.1 Motivation

Although evidence of anthropogenic climate change mounted throughout the twentieth century, it was not until the creation of the Intergovernmental Panel on Climate Change (IPCC) and the United Nations Framework Convention on Climate Change (UNFCCC) in 1988 and 1992 respectively, that there has been a concerted endeavour by the global scientific and political communities to define, understand and tackle the problem of our changing climate (Intergovernmental Panel on Climate Change, 2014b; United Nations Framework Convention on Climate Change, 2016).

The IPCC was set up to collate all scientific knowledge on climate change and its impacts. Now having completed their fifth assessment report the IPCC has the extensive evidence required to clearly present the human causes and consequences of climate change. The IPCC has found that climate change will affect the world's weather resulting in an increased probability of heat waves, drought, floods, cyclones and wildfires, these, in turn, affect the quality and quantity of fresh water, crop yields and many natural ecosystems. This will effect humanities ability to access food, water, settlement and infrastructure, all of these are necessary for maintaining stable human civilisations, it is therefore of the utmost importance that new technological, political and social solutions are found to limit the worst effects of climate change (Intergovernmental Panel on Climate Change, 2014a).

Based on the findings of the IPCC, the UNFCCC has worked to create a political framework for tackling climate change. The latest meeting of the Conference of Parties (COP) occurred in Paris in December 2015. The conference ended with a legally binding

agreement by all 196 countries involved to limit global warming to 2°C, above preindustrial levels, and to aim for 1.5°C. To achieve the overall target each nation has put forward its own emission reduction target. At the moment, these targets are not legally binding and fall a long way short of meeting the global target. Five-year reviews have been added to the agreement in the hope that the ambition of the national targets will be increased and will in time match the reductions needed to meet the global target (Pointel, 2015). Whether the Paris agreement achieved enough to start us on the path to meeting the 2°C target is not yet clear, but what is clear is that the intentions displayed in Paris will significantly increase the risk of investing in fossil fuels and our current heavy dependence on fossil fuel cannot outlast this century.

When tackling anthropogenic climate change, reducing emissions from the transport sector is important for two reasons. Firstly, the transport sector is now the largest consumer of energy in developed countries (Transport & Environment, 2015c), resulting in a high proportion of emissions, both globally, 14% (United States Environmental Protection Agency, 2014), and in the European Union (EU), 24% (European Commission, 2012). Secondly, transport emissions are growing rapidly across the board, despite policies and technologies designed to reverse the trend. Globally, transport energy use is expected to double by 2050 due to the much higher use of private vehicles and road freight, especially in economically developing countries like China and India. With the uptake of large numbers of vehicles in developing regions, the number of light-duty vehicles is expected to rise from 700 million in 2005 to between 2 and 3 billion in 2015. The policies and technologies currently in place will struggle to meet this increase in demand and emission look set to continue to grow (International Energy Agency, 2009). In the EU the transport sector is the only sector that has not achieved an emission reduction since 1990 (European Commission, 2012), this has resulted in the share of emissions originating from transport rising from 15% in 1990 to 22% in 2013 (eurostat, 2015). As transport emissions globally are dominated, 75% (International Energy Agency, 2009), by road transport emissions from cars and trucks, with a similar situation,

72% (European Commission, 2012), in the EU, it is clear that tackling car emissions is an essential part of any strategy to combat climate change.

This work will focus on CO₂ emissions from cars rather than looking at any of the four pollutants covered by the Euro standards. CO₂ emissions have been chosen for this research for two reasons. Firstly, while the other pollutants are important for air quality, health and in some cases climate change, CO₂ is the main greenhouse gas pollutant emitted by light-duty vehicles. In the UK 116.6 MtCO₂e of the 117.9 MtCO₂e produced from transport is CO₂ with the rest made up by methane and nitrous oxide (UK Department of Energy & Climate Change, 2016). Secondly, CO₂ is directly correlated with fuel consumption, by producing both figures the results can be used to inform top-down policies aimed at manufacturers, while also driving bottom-up change by influencing consumer choice.

To combat the rising CO₂ emissions from cars, many regions like America, China and the EU have brought in vehicle CO₂ emission standards. This standard was first introduced in the EU in 2009, and the regulation requires that the average CO₂ emissions of all new cars sold in the EU must be below 130 g/km in 2015 and below 95 g/km in 2021 (European Commission, 2016). By continually bringing down the standards every five years it is hoped that the fleet efficiency will rapidly decrease and this, predominantly by itself, will meet the EU strategy laid out in the 2011 transport white paper 'Roadmap to a Single European Transport Area – Towards a competitive and resource efficient transport system' which sets out a target of reducing transport emissions by 60% between 1990 and 2050 (European Commission, 2011).

The effectiveness of the EU emission standards has been severely hampered by problems with the vehicle testing method. An unrepresentative testing cycle and lax testing procedures have meant that the emission reductions achieved on paper have not resulted in the same emission reduction on the road. To combat this, a new test cycle and procedure is to be introduced in 2017, but this is not expected to halt the growing

gap between type-approval and real-world emissions (Element Energy & The International Council on Clean Transportation, 2015).

This problem is still worse for advanced powertrains like hybrid vehicles where the gap can be 5 to 10% higher than for conventional vehicles (Mock, Tietge, et al., 2014). Due to the lack of representative real world CO₂ emission data for hybrid vehicles and because they are the bestselling advanced powertrain on the road today in Europe (European Automobile Manufacturers Association, 2016), this work will focus on hybrid vehicles as an area with high potential impact.

The data created during vehicle type approval not only forms the basis for EU emission standards but is also used by national and regional governments to set taxes, incentives and other policies, aimed at reducing road transport emissions. This means that without accurate type-approval numbers no large shift in vehicle emissions will be achieved and the EU will fail to meet its climate change goals (Mock, Tietge, et al., 2014).

In the effort to overcome the problems with EU vehicle emission policy, new independent emission data is vitally important. Vehicle data collected on chassis dynamometers or on the road, with Portable Emission Measurement Systems (PEMS) and Portable Activity Measurement Systems (PAMS), has proved to be invaluable in three main ways. Firstly, independent on road tests can be used alongside not to exceed limits as part of vehicle testing to ensure vehicle emission reduction technology performs on the road. Secondly, the data highlights flexibilities in the test procedure that manufacturers are using to artificially lower emission figures. This encourages and informs the development of more robust policies, as has been the case throughout the development of the Worldwide harmonised Light-duty vehicles Testing Procedure (WLTP). Thirdly, the data can show when manufacturers have been cheating the vehicle emission tests, as was the case with VW in the dieselgate scandal. Independent testing by the International Council on Clean Transportation (ICCT) started an Environmental Protection Agency (EPA)

investigation that revealed a global use of illegal defeat devices that had not been picked up by type approval testing (The International Council on Clean Transportation, 2015a).

This thesis will look at PAMS vehicle testing and vehicle modelling as methods for analysing vehicles and collecting CO₂ emission data. Unlike the more commonly used methods of chassis dynamometer and PEMS testing, these methods are not well suited to type approval testing because, in the case of PAMS testing, CO₂ is the only pollutant that can be measured, and in the case of modelling, it is very time consuming and has accuracy and independence concerns. However, these methods can be used to collect large amounts of representative real world data at very low costs. This makes them very useful for providing consumer information, informing policymakers about local policy decisions and for contributing to the global pool of independent real world data that acts as a check on the quality of type approval testing.

1.2 Aims and Objectives

This project aims to provide real-world fuel consumption and CO₂ emission data for hybrid vehicles through data collection on the road and microscale modelling. The project will demonstrate the potential uses of on-road data for analysing new vehicle technologies, informing local policy makers, providing consumer information and model development. It is intended that this data, by providing evidence to local policy makers and consumers, will accelerate the uptake of hybrid vehicles in urban areas, especially within the taxi driving community. The project aims to build the simplest, most computationally efficient model that is capable of predicting fuel consumption to within 5%. To achieve this the model must make a number of assumption these include vehicle mass is constant and is not affected by the weight of the testing equipment or passengers, auxiliary power demand is zero and the vehicle rolling and aerodynamic resistance coefficients are constant and are not affected by the road condition or wind

speed. The adaptability of the model will be demonstrated by analysing a future policy that could not be tested on the road or in a laboratory.

The objectives of this project are to:

1. Develop a vehicle activity data collection method that records a wide range of internal and external vehicle parameters, including fuel consumption. This will be the focus of Chapter 3.
2. Conduct a detailed analysis of the Toyota Prius powertrain controls using the vehicle activity data collected. This will be the focus of Chapter 4.
3. Use vehicle activity tracking and vehicle modelling, in the commercial modelling environment PHEM, to analyse the potential fuel and emission saving of hybrid taxis in the Leeds taxi fleet. This will be the focus of Chapter 5.
4. Build, validate and demonstrate a microscale CO₂ emission model, of a hybrid vehicle, based on real world data. This will be the focus of Chapter 6.

1.3 Thesis Outline



Figure 1.1: Thesis chapter overview and interconnection

Chapter one presented here lays out the reasoning for further developing vehicle data collection methods and collecting new on-road vehicle activity and emission data.

Chapter two reviews the current literature in a number of areas to provide context for the work laid out later in the thesis. This includes a more detailed appraisal of the EU CO₂

emission standards. An assessment of the advantages and disadvantages of chassis dynamometer and PEMS testing, alongside a more detailed discussion of PAMS testing. This includes an assessment of the advantages and disadvantages of PAMS, as well as methods and uses. The chapter finishes with a review of the most commonly used academic and industrial microscale emission models.

Chapter three details the vehicle testing method used in this research. The chapter starts with a detailed description and specification of the test vehicle and data loggers. This is followed by an explanation of the data collection method, which is split into two parts, data collection on the road and data post processing, to correct for GPS error and to add road gradient to the data files. A brief description of the data is then given to provide an overview of the data size and distribution. Finally, the chapter looks at the different methods of calculating fuel consumption based on the data collected and provides an argument as to why one method is used over the other.

Chapter four is a detailed analysis of the third generation Toyota Prius powertrain technology and control. The chapter is split into two main sections. The first reviews the literature and presents details on the Prius technology, including the powertrain design, engine and after treatment systems, as well as looking at the vehicle overall control and component control. The second section uses data collected during this project to conduct a more in-depth analysis, this covers the same areas covered during the literature review but adds more details about the vehicle control. This section touches on the general powertrain control, but this is brief as it has been fairly well covered in the literature, greater detail, however, is given on powertrain control under cold starts and during low battery State of Charge (SOC), as this is an area other researchers, who do most of their testing on a chassis dynamometer, struggle to collect large amount of data on. Combined the two sections of this chapter give the reader a detailed understanding of the Toyota Prius.

Chapter five presents an emission and economic evaluation of Leeds City Councils proposed plans to encourage the uptake of petrol hybrid vehicles in the Leeds taxi fleet. The chapter starts by reviewing the literature on the emission benefits of hybrid vehicles as taxis. This is followed by an overview of the Leeds taxi fleet, to set the context of the work. The next section gives a description of the data collection campaign used to collect data about the Prius and the Passenger car and Heavy duty vehicle Emission Model (PHEM) modelling used to create comparative data for a petrol and diesel vehicle. The data collected is analysed to answer five questions. These are; is taxi driving significantly different from type approval drive cycles, do the three driving styles used during testing represent the full range of city driving and are the three styles significantly different from each other, does the petrol hybrid significantly outperform the conventional vehicles in terms of CO₂ emissions and fuel consumption, does the petrol hybrid significantly outperform the conventional vehicles in terms of NO_x emissions and is there a business case for using petrol hybrid vehicles as taxis in Leeds. The chapter finishes by reviewing the literature of policies used to date to encourage the uptake of hybrid vehicles in taxi fleets and makes some suggestions for policies that could be used in Leeds.

Chapter six covers the building, validation and application of a microscale emission model of the Toyota Prius. This chapter goes through each sub-model explaining how the components fit into the overall model, the data used and how the model was fitted. The error between the sub-model and the source data is also given wherever it makes sense to do so. The overall model is then validated against five drive cycles recorded on a chassis dynamometer by Argonne National Laboratory. The two data sets are compared over the four parameters they have in common, fuel consumption, engine speed, battery SOC and coolant temperature. The chapter finishes with an example application of the model. Transport for London (TfL) put forward the idea of geofenced zones, inside which hybrid taxis and buses will only be allowed to drive in Pure Electric (PE) mode (Transport for London, 2014). To assess the feasibility of a similar scheme in

Leeds, the model is used to drive the taxi drive cycles developed in chapter five, but with the restrictions of geofenced zones in the city centre.

Chapter seven concludes the thesis, summarising the findings of all previous chapters. This chapter also outlines areas of further work that could be conducted in the future to build upon the ideas and methods presented in this thesis.

1.4 Thesis Contributions

Collecting data from the vehicle Controller Area Network (CAN) has been a central part of PEMS data collection since the On-Board Diagnostics (OBD II) and European On-Board Diagnostics (EOBD) standards became widespread in the fleet (Y. Gao & Checkel, 2007; Krimmer & Venigalla, 2006; Rubino, Bonnel, Hummel, & Krasenbrink, 2007). Researchers can now collect enough parameters from the vehicle CAN that the method can be combined with GPS tracking to form a useful standalone vehicle data collection method called PAMS. Researchers have been able to collect a wide range of parameters using PAMS, especially for hybrid vehicles. However, the full potential of PAMS as a method has yet to be explored.

In this thesis, an expanded range of parameters has been collected that covers the operating states of the engine, motor and battery, the three main components of a hybrid drivetrain. The data has been used in two novel ways that highlight the potential of this data collection method for future research. Firstly, the data has been used to interpret the control systems of the Toyota Prius. Due to the complexity of the Prius control, this has only previously been achieved by combining component and whole vehicle chassis dynamometer testing with additional sensors added to the vehicle (Burress et al., 2011; Rask, Duoba, Lohse-Busch, & Bocci, 2010). The same control patterns have been found using both methods, proving the validity of PAMS testing for this purpose. The Toyota Prius is one of the most studied vehicles and so most of the controls have been demonstrated. Despite this, in areas of cold start and low battery SOC, which are difficult

to measure repeatedly during chassis dynamometer testing, PAMS data has added new knowledge about the Prius control. This project has proved the potential of PAMS data for analysing the control mechanisms of advanced vehicle technologies. As this method is applied to new vehicles, as they enter the market, it could provide an invaluable research tool for explaining their performance on the road (Riley & Tate, 2016).

Secondly, the data has been used to build a microscale CO₂ emissions and fuel consumption model. Vehicle CAN data has been used occasionally in the literature to build simple correlations, for conventional vehicle, between vehicle activity and fuel consumption (Hu, Frey, & Washburn, 2016; Xu, Yu, & Song, 2011), but this work presents the first use of this data to build a complex model of a hybrid vehicle. Few accurate hybrid vehicle models have been built because of the large amounts of internal vehicle data required. This project has demonstrated that PAMS is an effective method for collecting much of the internal and external data needed for model building. The model fuel consumption has been validated against independent chassis dynamometer data collect by Argonne National Laboratory. By building the model from PAMS data and validating it, to within 5%, against chassis dynamometer data, the accuracy of a wide range of parameters collected from the vehicle CAN has been verified for the first time.

PAMS data also has great potential for supporting local policy makers and providing consumer information. The cost effectiveness of PAMS allows local data to be collected to inform a specific policy or local group. To demonstrate this PAMS data collection from the Prius was used to inform local policy makers and taxi drivers about the potential fuel and emissions saving of using hybrid vehicles as taxis. While some papers estimate the benefits of hybrid vehicles, by comparing conventional vehicles and hybrid vehicles in city driving. This work is the first to compare a petrol and diesel vehicle to a hybrid vehicle over commonly used taxi routes including the taxi rank. It is important to include the taxi rank as it is one of the key difference between an ordinary driver on the road and a taxi.

It also adds a significant additional amount of idling time in which the difference in fuel consumption between the conventional and hybrid vehicle is always growing.

Chapter 2

Background Literature

2.1 Introduction

This chapter reviews the current literature related to vehicle emission policy, testing and modelling. This includes:

1. A review of the EU regulation 443/2009 that sets vehicle CO₂ emission standards for manufacturers and a discussion of why this policy has failed to deliver the expected real world vehicle CO₂ emission savings.
2. An analysis of the advantages and disadvantages of different vehicle testing methods including chassis dynamometer, PEMS and PAMS testing, with an evaluation of the potential for each of these methods to contribute towards accurate vehicle testing for legislation, local policy, consumer information and model building.
3. A comparative review of the microscale emission models available in the academic literature and the leading commercial models including the model inputs, outputs, method and any validation published to date.

2.2 Vehicle Emission Policy

At an EU level, there is only one overarching policy, aimed at vehicle manufacturers, that is designed to reduce CO₂ emissions from passenger cars, Regulation 443/2009. This policy was introduced in 2009 and it set a fleet-wide average CO₂ target of 130 gCO₂/km for new cars sold in the EU by 2015. This policy was updated in 2014 with Regulation 333/2014, which set a new target of 95 gCO₂/km to be achieved by 95% of manufacturer's fleets by 2020 and 100% of the fleet by 2021 (European Commission, 2016).

On paper, this policy has been incredibly successful. Very strong financial penalties for not meeting the targets, outlined in Table 2.1, have forced manufacturers to make CO₂ reduction a key part of their company focus. This has resulted in an 18% reduction in new car CO₂ emissions since 2007 and is expected to produce a 40% reduction between 2007 and 2021 (European Commission, 2016).

Table 2.1: Penalty per car in manufacturers fleet if the average fleet CO₂ emissions exceed limit (European Commission, 2016)

Cost	Rule
€ 5	For 1 st g/km over limit
€ 15	For 2 nd g/km over limit
€ 25	For 3 rd g/km over limit
€ 95	For each subsequent g/km over limit
€ 95	For all exceedances from 2019

The average fleet target is not the same for every manufacturer. Instead, a limit value curve has been created that converts manufacturers average fleet mass into their CO₂ target. This allows manufacturers of large sports utility vehicles and multi-purpose vehicles to emit more than manufacturers of small city cars while ensuring the industry as a whole meets the target (European Commission, 2016). Figure 2.1 shows the limit value curve for the 2015 and 2021 targets along with some manufacturers fleet CO₂ figures from 2013 (The International Council on Clean Transportation, 2014).

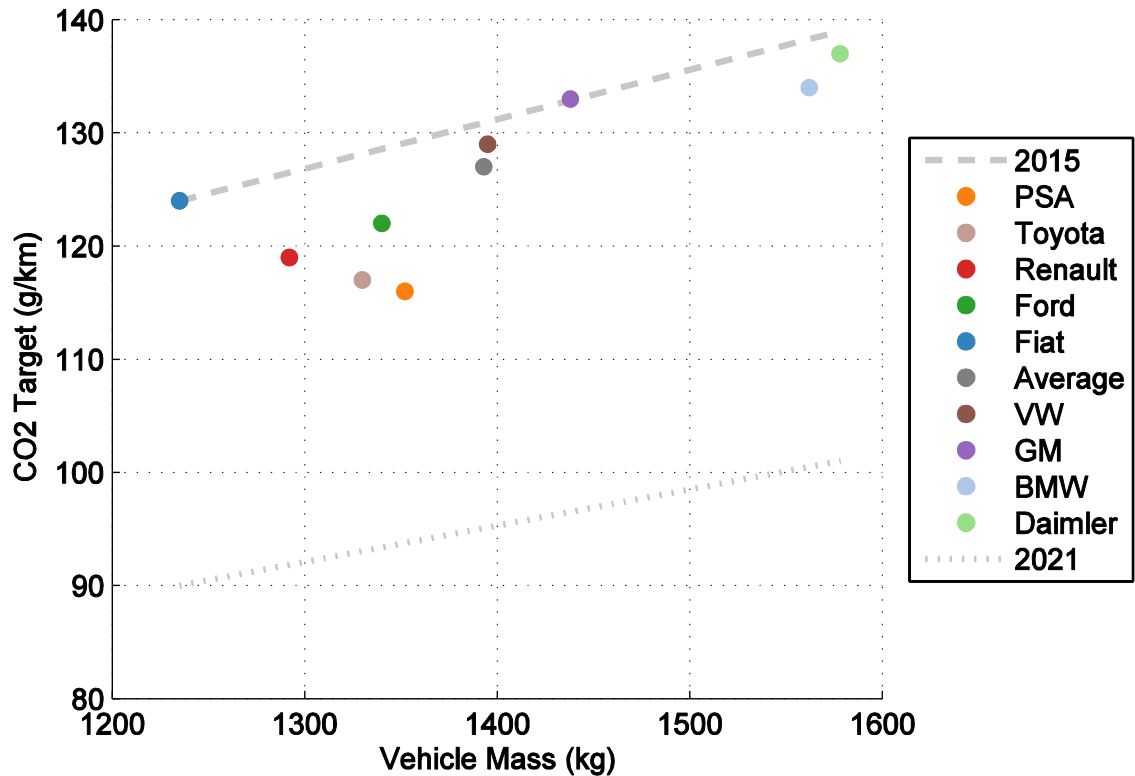


Figure 2.1: CO₂ limit value curve 2015 and 2021 with manufacturer's progress 2013. Adapted from (The International Council on Clean Transportation, 2014)

The policy also includes other incentives to encourage the development of future emission reduction technologies. Eco-innovations allow manufacturers to claim up to 7 g/km per year off their fleet average emissions. This can be claimed for introducing technologies to the fleet that do not result in major benefits in the type approval procedure but can be independently shown to improve emissions in the real world. Super credits incentivise very low emission cars by allowing manufacturers to count vehicles with CO₂ emissions less than 50g/km multiple times in their fleet average. This scheme has been implemented for both targets with slightly different limits. For the 2015 target, there was no limit on how much of a fleet reduction could be achieved with the scheme. For the 2021 target, the scheme can only contribute 7.5g/km worth of fleet reductions over three years. Table 2.2 shows how super credits have been implemented in the 2015 and 2021 targets (European Commission, 2016).

Table 2.2: Super credits multiplication factor (European Commission, 2016)

Multiplication Factor	Date of use
3.5	2012 – 2013
2.5	2014
1.5	2015
1	2016 - 2019
2	2020
1.67	2021
1.33	2022
1	2023

Super credits have also appeared to be a success. The number of plug-in hybrid and pure electric models on the market in the EU has increased from just three models made by three manufacturers in 2010 to 27 models made by 17 manufacturers in 2014. Over the same time period, Plug-in Hybrid Electric Vehicle (PHEV) and Battery Electric Vehicle (BEV) sales in the EU have grown from a few hundred to over 70,000. Although there are several other policies encouraging the uptake of PHEV and BEV, it seems clear that for manufacturers at least, sales of these vehicles and super credits has become an important part of their strategy to meet the EU CO₂ regulations (Thiel, Krause, & Dilara, 2015).

2.2.1 Problems with Regulation 443/2009

The effectiveness of Regulation 443/2009 and 333/2014 to bring about a reduction in the CO₂ emissions from cars in the real world, rather than just in type approval testing, has increasingly come under question. There has always been a difference between the emissions of a car tested in a laboratory and those tested on the road. However, since the introduction of mandatory CO₂ targets, the difference has increased sharply from just 8% in 2001 to 40% in 2014 (Transport & Environment, 2015b).

Figure 2.2 shows the percentage difference between the EU type approval figures and real world CO₂ data collected by several organisations across Europe. There is a worrying trend, of not just an increasing difference, but an almost exponential growth in the difference between type-approval and real-world emissions (Mock, Tietge, et al., 2014). Since 2012 the growth in the difference between the two figures has outstripped the reduction in type approval CO₂ figures. This means that for three years when the industry has reported its greatest reduction in fleet emissions ever, it has actually achieved no reduction in real world CO₂ emissions (Transport & Environment, 2015b).

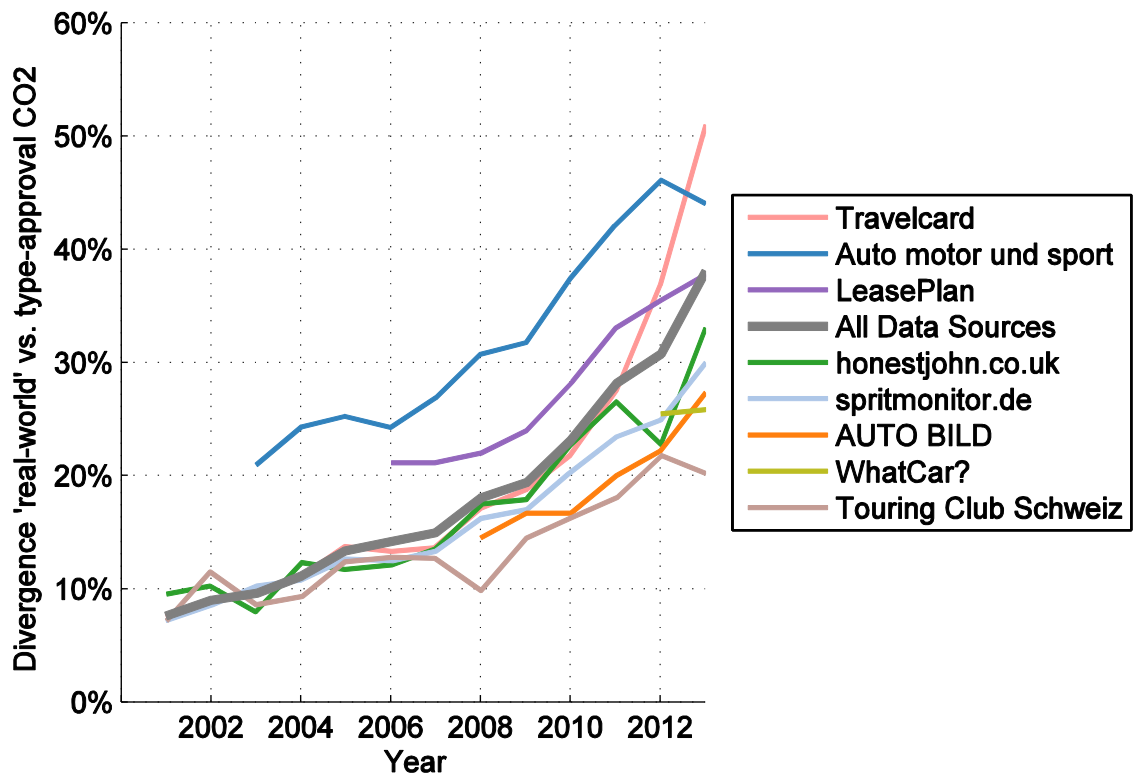


Figure 2.2: Gap between type-approval and real-world CO₂ emissions figures. Adapted from (Mock, Tietge, et al., 2014)

The reasons manufacturers are allowed to manipulate the type approval figures is because of a wide range of faults and flexibilities in the design and wording of the test cycle and the test procedure, known as the New European Drive Cycle (NEDC). This was known about when Regulation 443/2009 was first suggested and so in 2009, at the

same time as mandatory CO₂ targets were introduced, a project was launched to create a new test cycle and test procedure called the Worldwide harmonised Light-duty Test Procedure/Cycle (WLTP/C). The WLTP was finished in 2014, but further work was required if the WLTP was going to be introduced before 2021, as the 2021 target was agreed over the NEDC (Ciuffo et al., 2015). A correlation tool has recently been finished and agreed that will convert test results over the WLTC back to NEDC figures allowing the WLTP to be introduced in 2018 (Transport & Environment, 2016).

2.2.1.1 Test Cycle

Part of the problem with type approval testing is that the NEDC is very unrepresentative of real world driving in Europe today. This is clear when comparing the NEDC to the new WLTC cycle in Figure 2.3. The NEDC is what is called a steady state cycle which means it is made up of constant speed and acceleration phases. The original version of the NEDC was designed for testing air quality pollutants in very busy European cities in the 1960's - 1970's. This has resulted in a cycle with low average speeds and high percentage idle, reflecting city driving, along with low acceleration levels that reflect the lower powered vehicles on the road in the 1970's. The cycle was designed for repeatability and ease of scientific testing, the designers had no idea it would be used for type approval testing, where large sum of money rested on the outcome of the test, so it is unsurprising that the cycle is very simplistic and easy for manufacturers to optimise (DieselNet, 2013; Mock, Kuhlwein, et al., 2014).

By comparison, the WLTC was created using a large database of real world driving. In both cases complex statistical methods were used to cluster section of driving data by driving type/speed, then one or several representative sections were chosen from each cluster and combined to create a cycle. This method means that the speed trace in the cycles was actually driven under real world conditions, and so apart from some smoothing required to make the cycle drivable on the chassis dynamometer, they do represent the short term speed fluctuation seen in real world driving. Whether the whole

cycle represents real world driving depends on the proportion of the different cluster types included in the cycle. As all drivers spend different amounts of time driving on different road types and in different traffic conditions, it is impossible to create a cycle that represents any individual, but on the whole the WLTC is generally accepted as being reasonably representative of the average driving conditions found in Europe (Ciuffo et al., 2015).

The CO₂ emissions from a test cycle are predominantly dependent on four key factors, the percentage idling, the dynamicity, the average speed and the cycle length. Increased idling time increases the emissions because they are measured in g/km and idling results in emissions with no km covered. More dynamic cycles have higher accelerations which require more engine power and therefore fuel, very fast speed changes also result in un-optimised air fuel ratios, especially in turbocharged engines, resulting in higher fuel use. Most cars have an optimal efficiency at speeds between 60-100km/h, the more time the cycle spends in this speed band the lower the emissions will be. Engines produce much higher CO₂ emissions under cold conditions, the longer the cycle the less cold start emissions affect the overall results (Marotta & Tutuianu, 2012).

Surprisingly the CO₂ emissions over the NEDC and WLTC are very similar (Marotta, Pavlovic, Ciuffo, Serra, & Fontaras, 2015; Marotta & Tutuianu, 2012; Mock, Kuhlwein, et al., 2014). The WLTC emissions are increased compared to the NEDC due to the higher dynamicity of the cycle but are decreased because of the much lower percentage idling time, more optimum speed range and lower effect of a cold start due to the longer cycle. It is clear that a new cycle alone will not close the gap between test and real world emission figures, but the new cycle does have some benefits. By reducing the idle time and increasing the power demand of the cycle, vehicle technologies such as stop-start, downsizing and hybridisation, which are particularly effective under NEDC conditions, but which often don't give the same benefits in the real world, are not overly encouraged (Element Energy & The International Council on Clean Transportation, 2015).

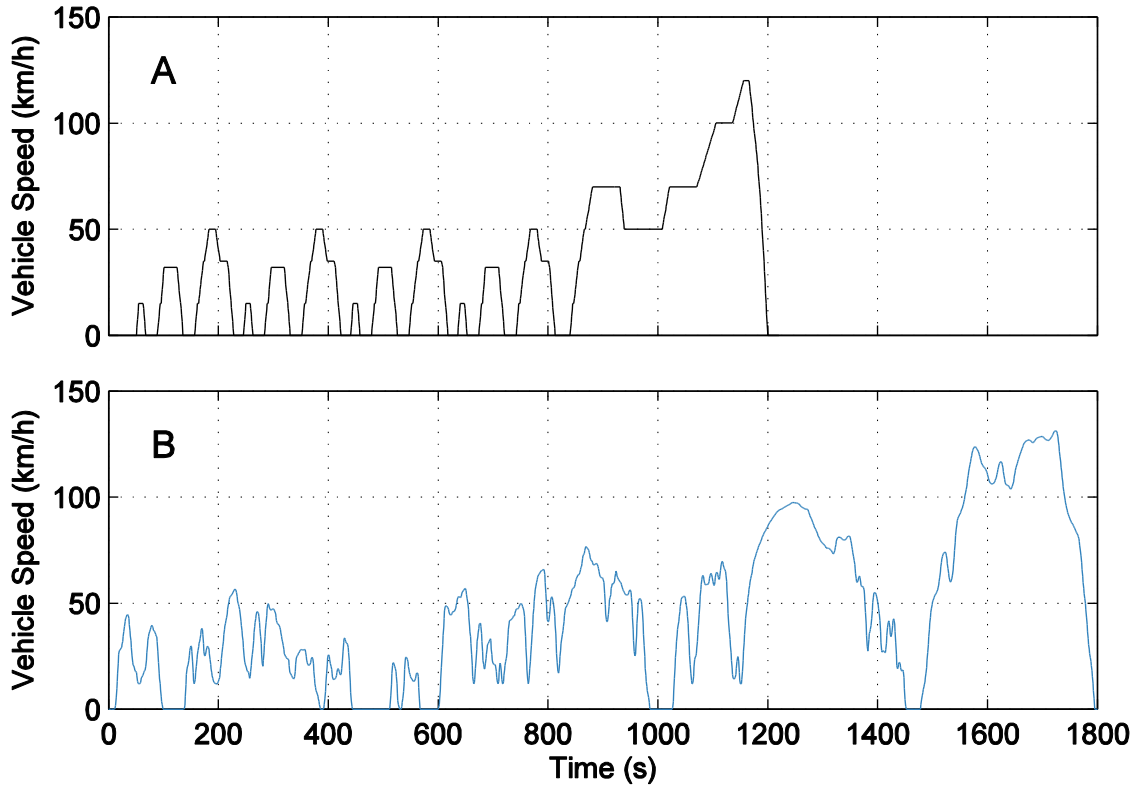


Figure 2.3: Chassis dynamometer test cycles (A) NEDC, (B) WLTC

2.2.1.2 Test Procedure

In the past, the dominant factor affecting the gap between type-approval and real-world CO₂ emissions figures has been ambiguity in the NEDC testing procedure. As type approval CO₂ and fuel consumption figures have become more important to consumers and legislation has enforced emission limits, manufacturers have increasingly used allowed flexibilities in the vehicle testing method to reduce type approval figures (Transport & Environment, 2015a).

Figure 2.4 shows how the gap has grown over time due to increased use of these flexibilities. In Figure 2.4 the brown region represents road load determination, blue, chassis dynamometer testing method, green, vehicle technology and orange, other. The greatest growth up until now has been in the brown and blue regions, which reflect the areas that manufacturers can currently influence directly. The green region depends on

the technology that manufacturers bring out in the future, it takes time for technology development to respond to the 2009 regulation, but by 2020 it plays a significant role in the growing gap. By changing test procedures in 2017/2018 the gap for new cars sold in 2020 will be reduced from 49% to 23%, this will reduce fleet emissions by 3MtCO₂ per year. Most of this change results from stricter and more realistic definitions of the vehicle condition during road load and chassis dynamometer testing in the new test procedure. In this respect, the WLTP will be successful because it will close many loopholes that are currently causing the issue. However, once WLTP has been used by manufacturers for some time the gap is expected to grow again. This growth is expected to arise from increasing PHEV fleet penetration, self-learning vehicle modes, gear change optimisation, driving trace optimisation, new road load determination methods and tyre selection and preparation (Element Energy & The International Council on Clean Transportation, 2015).

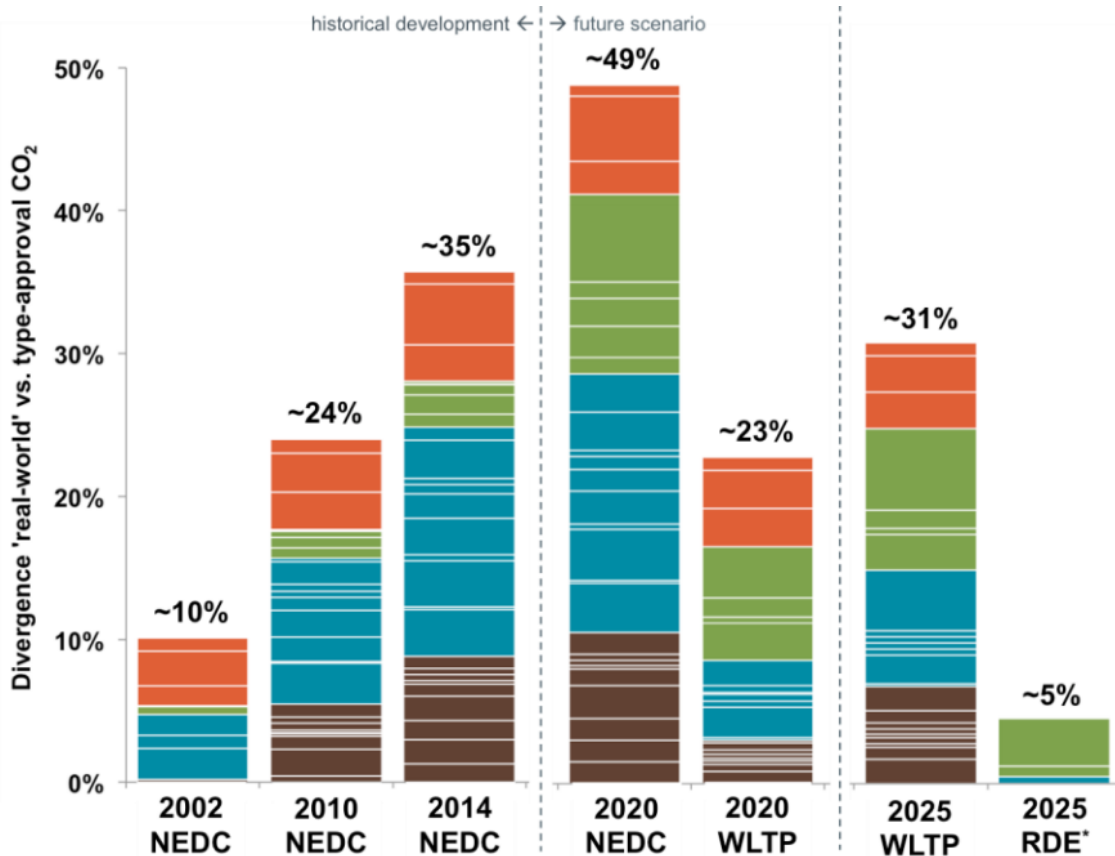


Figure 2.4: Type approval testing flexibilities leading to divergence between test and real world CO₂ emission figures in 2002, 2010, 2014, 2020 and 2025 (Element Energy & The International Council on Clean Transportation, 2015)

The WLTP has been well designed to meet current emission testing problems. The new more representative drive cycle reduces the gap due to current technologies like stop-start, engine downsizing and turbocharging. The better test procedure overcomes many of the current ambiguity and representativeness issues. However, it is unable to cover the effects of upcoming and near future technologies such as plug-in hybrids and intelligent vehicle mode selection or adaptive vehicle mode selection (Element Energy & The International Council on Clean Transportation, 2015). It is, therefore, clear that the extensive research capabilities of the vehicle manufacturers and the speed at which technology is changing will result in new testing flexibilities being found and exploited, leaving the WLTP/C with many of the same problems as its predecessor the NEDC.

2.2.1.3 Conformity Testing

A key difference between EU and USA type approval testing is the level of independent conformity testing carried out in the USA, which helps to ensure the quality of vehicle testing. In the EU the manufacturer, with some checks from licencing agency, performs the coast down test, laboratory testing, conformity of production and in use surveillance tests. The results of the coast down test are considered private data of the manufacturer and are not made public. The laboratory testing only has to be of a representative vehicle of the vehicle family tested. The conformity of production is conducted by the manufacturer and only has to be within 8% of the original test figure, while the regulator only checks that the manufacturer has quality management systems in place. In-use conformity is only conducted on exhaust emission not CO₂ and there is no sign that this will be introduced (Mock & German, 2015).

By comparison, in the USA the EPA has the legal authority and testing capacity to perform independent checks of the manufacturers testing at every stage of the process. In the USA road-load coefficients measured by the manufacture are made public and the EPA periodically carries out its own testing to check that the coefficient measured by manufacturers are reasonable. If a discrepancy is found the manufacturer is fined and all laboratory tests based on the coast down figures have to be redone. The laboratory testing is conducted on the highest selling vehicle type from each family and testing must include enough vehicle configurations as to cover 90% of all cars sold each year. The EPA also conducts its own laboratory tests on 15% of all vehicle types to ensure the quality of testing. The EPA has the power to pull vehicles straight from the assembly line to check the conformity of production, but the area was so strongly enforced in the early years of the law that it is no longer considered a problem area and few vehicles are independently tested. In-use conformity is mostly conducted by manufacturers who have to test one to five vehicles per family at low and high mileages, with all the result supplied to the regulator. However, the EPA still conducts its own in use conformity testing on a

small number of randomly selected in-use vehicles as a secondary check (Mock & German, 2015).

Conformity checking in the USA has resulted in a number of manufacturers getting fined and emission figures being corrected (Mock & German, 2015). However, conformity checks by regulators did not pick up the use of defeat devices by VW, the testing was instead carried out by a third party (The International Council on Clean Transportation, 2015a), but the EPA experience of checking and prosecuting manufacturers for other illegal behaviour in the past is likely to have played an important role in ensuring that evidence of illegal behaviour does not go uninvestigated. It is clear that data is required to check manufacturers at every stage of the type approval process. This ideally should be carried out by a regulatory body with powers to fine manufacturers for non-compliance, but data from third party testing also has an important part to play in checking that manufactures follow both the letter and the intent of the law.

2.2.1.4 Real World Testing

In the wake of growing evidence that diesel vehicles were emitting very high levels of NO_x, which culminated in 'dieseldate', the EU is now looking into Real Driving Emission (RDE) testing of air quality pollutants. RDE involves testing vehicles outside of the laboratory using PEMS. This is an important step forward, but the current legislation has several key flaws. Firstly, testing is only planned for the pre-production vehicles, termed 'Golden Vehicle', used for type approval and not on full production vehicles on the road. Secondly, conformity factors have been added that increase the Euro standard limits that manufacturers have to meet. The conformity factor has been set at 2.1 at the introduction of RDE in 2017, dropping to 1.5 in 2020. Thirdly, the RDE test does not include many real world conditions such as cold starts. Fourthly, the RDE test will only allow a narrow range of driving conditions rather than the broad range of driving styles seen in the real world (The International Council on Clean Transportation, 2015b).

Even with its current flaws, RDE testing is likely to become an important part of more accurate and representative vehicle type approval. It is, therefore, short sighted that CO₂ emissions will not be included in RDE testing even though the PEMS equipment used to do the testing can measure CO₂. Figure 2.4 shows that RDE testing could have a much larger impact on reducing the gap between CO₂ type approval and real world emissions than a new laboratory drive cycle or test procedure, in fact, it is the only policy currently on the table that can achieve this goal. However, while RDE for CO₂ is not currently being considered by the EU it will take some time before it could be brought into effect. This leaves real world CO₂ data collected by independent organisations as the only check against manufacturer cheating, legal or illegal, of the type approval process.

2.3 Vehicle Testing Methods

Chassis dynamometer testing in a laboratory is used for type approval testing because it has good repeatability which makes it a fair comparison between different manufacturers. However, it also has some clear limitations that have partly led to the problems with Regulation 443/2009. The next section looks in more detail at the different methods for collected vehicle emission data and how their different benefits and drawbacks can be combined to create more robust vehicle testing.

2.3.1 Chassis Dynamometer

Figure 2.5 displays a chassis dynamometer set up. The vehicles driven wheels are placed on a large roller which is connected through a gear box to a dynamometer which measures the power and torque from the car. An electronic brake is used to simulate a road load force which accounts for the driving resistances like aerodynamic drag and rolling resistance, that are experienced when the car is driven on a real road (Franco et al., 2013).

The car is driven by a trained test driver or robot who operates the vehicle according to a set speed, time trace and gear shift schedule displayed on the driver's aid. The exhaust gases collected at the exhaust pipe are diluted with ambient air then pass through a series of gas analysers to give instantaneous emission rates. After the gases have passed through the analysers they are collected in sampling bags, the total emissions collected in the sampling bags are analysed to give total emissions over the cycle, usually expressed as emissions per km (Franco et al., 2013).

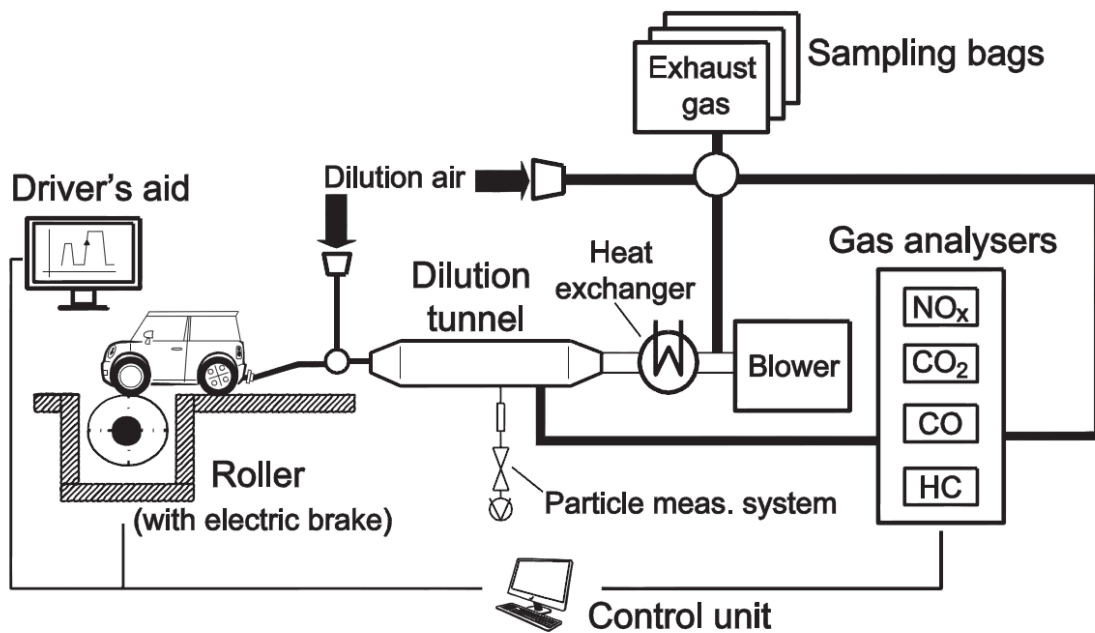


Figure 2.5: Schematic representation of a chassis dynamometer emission testing facility (Franco et al., 2013)

Table 2.3: Benefits and drawbacks of chassis dynamometer testing (Franco et al., 2013; Kadijk & Ligterink, 2012; Transport & Environment, 2015a; Weilenmann, Soltic, & Ajtay, 2003)

Benefits	Drawbacks
<p>Many testing facilities in the EU are built to the same standards and many testing variables can be measured or controlled. This provides results that can be fairly compared between test runs, facilities and vehicle manufacturers.</p>	<p>Very high-speed transients that often occur in real-world driving are difficult to replicate in a laboratory, either because the dynamometer can't handle the acceleration or because it makes the drive cycle impossible to repeat accurately.</p>
<p>Testing facility standards required for type approval testing and space for large complex gas analysers results in high accuracy of results.</p>	<p>Real world conditions such as changes in temperature, humidity, gradient, cornering and wind are difficult to include in testing and are therefore rarely considered.</p>
<p>Newer testing facilities can simulate a wide range of outdoor conditions using climate control.</p>	<p>Testing often uses road load factors measured by manufacturers which can be unrepresentative of the real road loads.</p>
<p>Greater control of testing conditions allows researchers to study the effect of changing a single variable on emissions.</p>	<p>Quality of results dependent on good drive cycle creation, which requires lots of real-world data collection.</p>
<p>A wide range of emission species can be recorded, depending on the laboratory. Studies have recorded CO₂, CO, NO_x, THC, PM, PN, Ammonia, Methane, Benzene and Toluene.</p>	<p>Due to the high cost of equipment and technicians needed to run testing, testing is expensive and therefore quite short. This makes it difficult to create representative drive cycles.</p>
	<p>Factors such as tire pressure have to be set at unrealistic values for safe testing.</p>
	<p>Parameters such as road load and inertia setting have a very large effect on the final result and can easily be manipulated. Whereas these parameters are largely pre-set during on-road testing.</p>
	<p>Emission delay and spreading must be corrected for if emissions are to be linked to engine parameters.</p>

2.3.2 Portable Emissions Measurement Systems (PEMS)

PEMS is an on-board analysis system that allows for the testing of a wide range of exhaust emissions (CO, CO₂, HC, NO_x) under real world operating condition. The system consists of an exhaust pipe attachment that directs a fraction of the exhaust gases through heated exhaust lines to the gas analysers, the attachment also has a pitot tube for measuring exhaust gas flow rate and thermocouples for measuring exhaust gas temperature.

Ambient air is collected at the front of the car to establish the ambient temperature, humidity and pollutant concentrations. A GPS system is used to track the location of the car from which the cars speed and acceleration can be calculated and an engine scanner can be connected to the OBD link in the car to collect data (manifold pressure, vehicle speed, engine speed, air intake temperature, coolant temperature, air intake mass flow rate, percentage wide open throttle, open/closed loop flag etc.), the whole system can be run off the car's battery through the cigarette lighter socket or a battery pack can be used if more accurate results are required. All the data is logged on a laptop during the study. Altogether the PEMS weights around 80kg which equates to carrying one extra passenger (M. Weiss et al., 2011).

Table 2.4: Benefits and drawbacks of PEMS testing (Franco et al., 2013; Ortenzi & Costagliola, 2010; Sandhu & Frey, 2013; Weilenmann et al., 2003)

Benefits	Drawbacks
By testing on the road real world conditions that affect emissions are taken into account in testing.	Uncontrollable ambient and traffic conditions result in poor repeatability and makes vehicle to vehicle comparisons difficult.
Any driving style or conditions that can be experienced on the road could be tested.	Variability between runs means more data needs to be collected for each project.
Regulated emission species can be recorded, including CO ₂ , CO, NO _x , THC, PM and PN.	Due to the high cost of equipment and technicians needed to run testing, testing is expensive and therefore quite short.
Development in transportable gas analysers means PEMS analysers can now match stationary analysers for accuracy and response time.	Not all parameters can be controlled or measured, this makes studying the effect of a single variable on emissions more difficult.
The method can be combined with a not to exceed limit to act as a check on chassis dynamometer type approval figures.	Emission delay and spreading must be corrected for if emissions are to be linked to engine parameters.
PEMS testing is cheaper than chassis dynamometer testing allowing longer tests of more vehicles.	No consistent method for testing is used making the results less comparable.

2.3.3 Emissions Delay

Emission signal delay and spreading is a major drawback to chassis dynamometer and PEMS testing. These effects combined make it very difficult to accurately align the emission data to vehicle and engine conditions. This makes the data difficult to use for microscopic emission model building or validation and analysing vehicle performance under different conditions.

The exhaust gases are transported from the cylinder exhaust valve through the vehicle exhaust system (including the turbocharger, exhaust after-treatment systems and exhaust silencer), up the sampling line and through the analyser. There is, therefore, a delay in time between when the pollutant is created in the engine cylinder and when it is recorded by the analyser, for correct emission assignment this delay must be corrected for (Weilenmann et al., 2003).

Two phenomena are related to the delay, first travel time down the pipes. This depends on the size of the exhaust system, the displacement of the engine and the engine speed. Low load, low speed operation results in a long delay and high load, high speed operation results in a short delay. The transport time is much longer in petrol vehicle because of the use of a throttle plate for power control, this causes very low exhaust flow volumes at low speeds. For a typical 1.6L engine the delay between the engine and tailpipe can be up to 1.5s for a diesel and 6.5s for a petrol (Weilenmann et al., 2003).

The second part of the delay is caused by the mixing of the exhaust gases, especially in catalysts and silencers etc. this causes the emission peaks to spread resulting in a smoothing of the emission plot. This both reduces the emissions that should have been assigned to a particular operating point and wrongly assigns emissions to other operating points. The combined effects of delays in the exhaust pipes, sample lines and the analyser delay can result in a travel time delay of up to 15s and a smoothing effect of up to 10s. These delays can be significantly worse for chassis dynamometer testing facilities with constant volume sampling where the delay can be up to 25s and the smoothing effect up to 20s. With engine conditions and emissions changing at a frequency of 3-5Hz it is clear that these two time delay effects, if not corrected for, will undermine the usefulness of the data (Weilenmann et al., 2003).

2.3.4 Portable Activity Measurement Systems (PAMS)

2.3.4.1 Vehicle Controller Area Network (CAN)

Modern vehicles rely on a large number of inbuilt sensors to provide data on the cars current state, an Electronic Control Unit (ECU) to create control signals based on the sensors inputs and actuators to change vehicle operation based on ECU commands. The data created by each sensor and controller is passed to every sensor, controller and actuator in the system using the CAN communications protocol (Johansson, Törngren, & Nielsen, 2005). The CAN consists of two wires, a high voltage CAN wire and a low voltage CAN wire, all devices attach to the two wires and the binary information is sent as a voltage difference between the two wires (Fairhurst, 2016).

CAN transmissions are called frames, a frame consists of up to 8 bytes of data surrounded by a number of identifiers; these set the signal priority, identify the data and can be used to request data from another device. Each of the 8 bytes of data in a frame can be made up of 8 bits so a single transmission can contain between 0 and 64 binary signals. In the network all devices receive all data transmitted, the CAN controller chip on each device then filters the signal so that it only received data related to its own operation. At the beginning of each transmission the device transmits a piece of code stating the transmissions level of importance, if two devices try to transmit data at the same time the more import data continues to send and the less important data stops sending and waits until it is the highest priority signal trying to transmit on the network (National Instruments, 2014).

2.3.4.2 On-Board Diagnostics (OBD) Link

After the Clean Air Act was passed in the USA in 1970 manufacturers had to develop more complex engine control and after treatment systems. These devices had to be checked throughout the vehicle life to make sure the vehicle stayed emissions compliant. If the emission control technology sensed a problem it activated a warning light on the

dashboard to tell the driver to take the car to a garage, it also activates an error code which the mechanic can pick up to identify the fault. To make it easier for mechanics to check faults, the plug and diagnostic test signals have been standardised. The current USA standard is OBD-II which has been mandatory on vehicles since 1996 (Martin, 2015). The same standard called European OBD (EOBD) were phased-in in the EU between 2000 and 2005 (Ferris, 2009).

The EOBD has a 16 pin plug; two pins are connected to the two CAN wires. To access data transmitted on the CAN a database of Parameter ID's (PID) is required, where each PID relates to a particular sensor or ECU signal. The EOBD standard defines a range of PID that are useful to mechanics when diagnosing vehicles. Each manufacturer also has a large number of company specific PID which are either not disclosed or are very expensive to obtain. The PID contains information about the channel name, data location (start bit, number of bits), scaling factor, offset, units and min, max range. This allows the CAN message to be converted into data in scientific units (National Instruments, 2014).

The SAE standard for OBD-II defines ten operating modes, although not all vehicles have all modes. Mode 1 gives some basic diagnostic figures such as engine speed, temperature and oxygen sensor readings, each one with its unique PID. This does not mean that manufacturers have to use these PID, only that they can't use them for anything else. Mode 2 is a freeze frame of CAN data when a fault occurred. Mode 3 displays fault codes. Mode 4 clears fault codes. Mode 5 is only used on older vehicles and is not relevant here. Mode 6 gives information about channels that are not constantly monitored. Mode 7 shows unconfirmed fault codes. Mode 8 is not used in Europe. Mode 9 gives vehicle specification like the Vehicle Identification Number (VIN). Mode 10 gives fault codes. These cannot be cleared by a mechanic they are only cleared when the car drives a certain distance without the fault reoccurring (Outils OBD Facile, 2016).

2.3.4.3 Use of Vehicle CAN Data Collected from the OBD Port

Since the introduction of OBD-II and EOBD researchers have used vehicle activity data collected from the vehicle CAN as part of larger data collection campaigns. CAN data collection has been most widely used as part of PEMS measurements and is now considered a fairly standard part, alongside GPS tracking and the PEMS gas analysers, of a PEMS setup (Franco, Posada Sánchez, German, & Mock, 2014). The vehicle CAN data provides two functions in PEMS testing. Firstly, some studies use standard PID such as engine speed and Mass Air Flow (MAF) to estimate exhaust mass flow rate, which is required to convert the gas analyser readings from gas concentration to pollutant mass/volume (Kousoulidou et al., 2010; Rakha, Ahn, El-Shawarby, & Jang, 2004). Secondly, many studies now analyse emissions by splitting the emissions into segments based on vehicle speed, vehicle acceleration or Vehicle Specific Power (VSP). By splitting the data by vehicle activity, overall trends can be observed in large quantities of data and the results are more applicable to real world situations (Hu et al., 2016; Xu et al., 2011). Vehicle CAN data can be relied on for these two functions even though the PID available change from car to car because vehicle speed is always available, engine speed is mostly included and mass fuel flow, MAF, Manifold Absolute Pressure (MAP), intake air temperature, and coolant temperature is sometimes included (H C Frey et al., 2011). This data has expanded the potential of PEMS results, allowing researchers to study the effects of a wide range of vehicle activity parameters on emissions, including, ambient temperature, cold starts, driving style and road gradient (Della Ragione, Meccariello, Prati, Costagliola, & Ragione, 2014; H Christopher Frey, Boroujeni, Hu, & Liu, 2013; Prati, Meccariello, Della Ragione, & Costagliola, 2015; Varella, Gonçalves, Duarte, & Farias, 2016)

Vehicle activity data from the vehicle CAN has also allowed PEMS data to be used to build simple emission models. These often bin emissions by VSP and vehicle speed and then predict emissions for a given VSP trace (Henry Christopher Frey & Sun, 2011; Xu

et al., 2011). The most widely used model of this type, that uses PEMS data in model creation, is the Motor Vehicle Emission Simulator (MOVES) (Koupal, Cumberworth, Michaels, Beardsley, & Brzezinski, 2003). The prediction ability of these models can be improved by fitting the emissions data to internal vehicle parameters, such as MAP, engine speed and engine torque, rather than external vehicle parameters, such as vehicle speed (H. Christopher Frey, Zhang, & Roupail, 2010; Hu et al., 2016). This method has the drawback that emission values can't be estimated directly from vehicle speed traces, but these engine maps can be connected to models such as ADVISOR (Advanced Vehicle Simulator) to overcome this problem (Kousoulidou et al., 2010).

Vehicle CAN data also has great potential beyond supporting PEMS data collection. These uses include building drive cycles, understanding driving behaviour, providing consumer information and feedback, analysing local policy decisions, checking vehicles for defeat devices and very high emissions exceedances, analysing advanced vehicle technologies and building models to predict CO₂ emissions, either simple average speed emission curves, VSP bin models, or complete vehicle models.

Vehicle CAN data has three main benefits that make it very useful for building drive cycles and correcting type approval fuel consumption figures for consumer use. These are, testing is much cheaper than chassis dynamometer or PEMS testing, this means lots of data, from many vehicles, over a long period of time can be collected. Also, because no technician is needed to run the equipment the vehicles can be driven by their owners over their normal day to day driving patterns (Nam, 2009).

Vehicle CAN data can be used to provide instantaneous feedback to the driver about their driving style and suggest changes that will improve the vehicle fuel consumption. Eco-driving tries to avoid harsh accelerations and braking as well as late gear shifting. By collecting vehicle speed, vehicle acceleration, throttle position, engine speed and fuel consumption data eco-driving devices can provide the driver with audio and visual feedback that has been shown to be effective in improving people driving style and

reducing fuel consumption (Hari, Brace, Vagg, Poxon, & Ash, 2012; Magana & Munoz-Organero, 2015; Munoz-Organero & Magana, 2013).

As the OBD main function is checking that the exhaust after-treatment systems are functioning correctly, several parameters that can indicate very high exhaust emissions are sent over the vehicle CAN. These parameters could be used on a large scale to check for very high emission exceedances. With the introduction of Selective Catalytic Reduction (SCR) for reduction of NO_x emissions in diesel exhausts, vehicles must be fitted with NO_x sensors to check that the SCR is functioning correctly. The NO_x signal from this sensor can be collected with an OBD scanner without the use of PEMS equipment. This signal, while not as accurate as data collected from PEMS, can be used to study the trends in NO_x emissions, find large NO_x exceedances and to check for the use of defeat devices (Price, Wang, & Pauly, 2015).

Both standard and non-standard PID have been successfully collected from hybrid vehicles to analyse the technologies performance on the road. Collecting these parameters is particularly important for studies focusing on the hybrid vehicle as the emissions and fuel consumption of hybrid vehicles are not only dependent on the current driving demand but also on a range of internal variables such as engine temperature, battery temperature and battery SOC. Several studies by a research group in Rome has collected vehicle speed, engine speed, MAF, MAP, throttle position, air-fuel ratio, engine load, oxygen sensor voltage, fuel tank level, coolant temperature, catalyst temperature, ambient temperature, ambient pressure, lambda sensor voltage, absolute load, EGR, ignition advance and battery voltage, for the Honda Civic hybrid (A Alessandrini, Filippi, Orecchini, & Ortenzi, 2006; Adriano Alessandrini, Orecchini, Ortenzi, & Villatico Campbell, 2009; Ortenzi & Costagliola, 2010). Another research group from Lisbon has collected a similar range of parameters along with battery SOC from the Prius, Plug-in Prius and Ampera (G. Duarte, Lopes, Goncalves, & Farias, 2013; G. O. Duarte, Varella, Gonçaves, & Farias, 2014). Only one study by Coelho & Luzia (2010) collected detailed

information about the hybrid battery and electrical motors, these are important parameters for analysing the power flow through the powertrain. They collected fuel consumption, engine speed, vehicle speed, throttle position, motor speed, motor torque, battery voltage and current, battery SOC and ambient temperature for the Lexus RX 400h (Coelho & Luzia, 2010). These studies show that this method has potential and that these variables can be collected on a range of hybrid and plug-in hybrid vehicles. However, none of these studies collects all the fundamental parameters needed to analyse the drivetrain, these are engine speed, torque, temperature and fuel input, motor speed and torque, and battery current, voltage and SOC. Also, none of these studies use the data collected to analyse vehicle control at the drivetrain level, which would have provided a more detailed explanation of the observed emission trends.

Several studies have built emission models, based on real world data, using vehicle CAN activity data and PEMS emission data (H. Christopher Frey et al., 2010; Hu et al., 2016). However, few studies have used vehicle CAN data alone to build CO₂ emission and fuel consumption models. This is despite vehicle CAN data having four key benefits that make it suitable for building microscale models. Firstly, large amounts of data, needed to fit the different parameters of the model together, can be collected in a short period of time, at low costs. Secondly, the vehicle activity and fuel consumption data are time aligned, meaning there is no need for complex exhaust delay correction, as needed for models built from PEMS data. Thirdly, data can be collected at up to 10 Hz, which makes it suitable for building microscale models that run at 1 Hz or more. Lastly, the data includes real world effects on fuel consumption that are trying to be captured in the model (Den Braven, Abdel-Rahim, Henrickson, & Battles, 2012; Weilenmann et al., 2003). This method has potential for conventional vehicles, which can be modelled using several standard PID, vehicle speed, road gradient, engine coolant temperature, engine speed and fuel consumption. The method has greater potential for hybrid vehicles, which can't be modelled using the basic parameters collected during PEMS or chassis dynamometer

testing, but can be modelled in great detail if the full range of vehicle CAN parameters are available.

The vehicle CAN data collected in this project, and described in Chapter 3, goes beyond the five to fifteen parameters collected in most studies. Instead, testing has access to over 500 parameters, of which twenty-seven have been selected. It is only by collecting activity and condition data for the engine, motors and battery that the whole powertrain can be analysed and modelled. Throughout the rest of this thesis, PAMS will be used to describe a data collection method that combines, the collection of a wide range of vehicle CAN parameters that details the operation of the vehicle and all its major powertrain components, with vehicle GPS tracking.

2.4 Fuel Consumption and Emissions Modelling

There is a wide range of scales that could be used to classify vehicle models. Faris et al. 2011 classified the models in the academic literature by five fundamental parameters. These are the scale of the input variables, the formulation approach, the main input variable, the state variable and the number of dimensions. For each of these classification approaches the models can be grouped by the modelling method (Faris, Rakha, Kafafy, Idres, & Elmoselhy, 2011).

If the models are grouped by the scale of the input then they can be split into microscopic, mesoscopic and macroscopic models. Microscopic models require second by second input information about the vehicle and road, to produce instantaneous emission figures as an output. The advantage of this type of modelling is that it can represent transient conditions allowing it to produce results that accurately predict real world figures. This comes with the drawback that they are very time consuming to create, validate and run. Mesoscopic models use aggregated input information, this allows for decreased computing time, but as the frequency of data input decreases the ability to track short time scale transients is lost, and the accuracy declines. Macroscopic models use even

more aggregated data, this reduces the computation time, thus allowing these models to predict the emissions of large transport systems, although important parameters like driving style and individual car technologies are disregarded (Faris et al., 2011).

The different formulation approaches to modelling are analytical, empirical, statistical and graphical. The analytical approach has the advantage of being based on physical principles, and therefore allows the results to be interpreted to give insight into the cause of emissions. These models can be very complex and often require very long development and running times. Empirical models are used to fit curves to measured results, or bin data, in an emission matrix; this can either be done on a vehicle or component basis. The more components that are modelled the longer the development time, but the greater the explanatory power of the model. Empirical models can be fast running with minimal model development time, but the models require a large source database and the expertise to collect the data, this can be very time consuming and expensive. Due to the complexity of modern vehicle systems, empirical data is used in all the models considered here, either as the main modelling method or as correction factors to analytical models (Faris et al., 2011).

The main input variable can either be average speed, instantaneous speed, or vehicle specific power. Guensler et al. 1993 showed that average speed is inadequate to model emissions which can fluctuate over very short time periods (Guensler, Washington, & Sperling, 1993). Instantaneous speed is included in most of the models discussed here as it is a good explanatory variable of emissions. VSP is increasingly being used in models (alongside instantaneous speed) because additional engine loads such as auxiliary use, and road gradient can be included in the VSP calculation (Faris et al., 2011).

Depending on the required accuracy of the model the engine state can either be modelled at crank angle resolution which models the effects of all four of the engine strokes, or by a mean value model using average figures for the engine over a whole

cycle. Crank angle models will not be considered here as they are unnecessarily complex to model emissions to the accuracy required (Faris et al., 2011).

Hybrid vehicle are particularly difficult to model because unlike conventional vehicles which operate the same way and produce the same emissions when subjected to a particular vehicle load, hybrid vehicles have a hysteresis effect caused by the changing battery SOC. This means that to predict the current vehicle emissions, either the current vehicle states must be known, or the whole vehicle must have been modelled accurately from a point where the vehicle state was known. This requirement for accurate modelling of the vehicle internal components over short time periods makes mesoscale and macroscale models unsuitable for studying the potential of hybrid vehicles.

Microscopic scale models are given many names in the literature, instantaneous, modal, continuous, and online but they all pertain to models based on 1Hz, or higher, emission measurement data, with the capacity to predict emissions on a second by second basis (Ajtay, 2005). There are three predominant modelling methods that are used in all the major microscopic models, emissions maps, regression analysis, and load models. Emission mapping is a method that consists of a 2D, or occasionally 3D matrix, where each individual cell contains an average emission rate. Each cell represents a combination of factors that are linked to the emissions in that cell. Common parameters used for emission matrices are speed and acceleration, although other models have used speed and speed multiplied by acceleration and speed and VSP. Regression modelling is a statistical method where equations or parameters are fitted to empirical data. Some models use regression analysis for the whole model with speed and acceleration as the explanatory variables, other models use the techniques to create correction factors for cold start and transients etc. Load based modelling is an analytical method based on physical principals, it is the preferred method as it can encompass all engine loads resulting in a high accuracy. The models are based on engine power, engine out torque, or VSP (Cappiello, Chabini, Nam, Lue, & Abou Zeid, 2002).

2.4.1 Models Based on External Variables

Emission models based on external variables are often used at the meso end of the micro scale. These models can predict emissions at 1Hz but are really designed to model short sections of road over a several second period. These models are mostly used to analyse emissions on a road network where only vehicle speed through the network is known (Koupal, Beardsley, Brzezinski, Warila, & Faler, 2010; Smit, Smokers, & Rabe, 2007).

2.4.1.1 VT-Micro

VT-Micro is a statistical model based on a combination of emission matrices and regression analysis, it was developed by researchers at the Virginia Tech Transportation Institute and was first published in 1999. The model aims to estimate non steady state emissions. The source data consists of chassis dynamometer testing of 60 randomly selected vehicles, made between 1986 and 1996, and tested over 12 EPA real world cycles LA04, LA92, ST01, CARB and the New York drive cycles (Rakha, Ahn, & Trani, 2004).

The input to the model is the basic vehicle specification that the model uses to select the vehicle categories, the speed trace and road grade. The output is emission rates per second, and over the whole cycle, for HC, CO, NO_x, CO₂ and fuel consumption (Rakha, Ahn, & Trani, 2004).

The modelling method starts by binning all the emissions data. A single speed acceleration matrix is created for each vehicle category and pollutant; there are 5 Light Duty Vehicle (LDV) and 2 Light-Duty Truck (LDT) categories and four pollutants. All the data collected over the different drive cycles, and for all the vehicles in a category, are entered into the same matrix. The values in each cell of the matrix are averaged to give a single value per cell. The speed bins ranged from 0-120km/h at 1km/h intervals and

the acceleration bins ranged from -6 to 10km/h/s at increments of 1km/h/s (Rakha, Ahn, & Trani, 2004).

Once the input data has thus been simplified the model employs regression analysis to fit linear, quadratic, cubic and quartic terms of the input (speed and acceleration) to the output (emissions). The work resulted in Equation 2.1 and 2.2 to predict emissions. Different coefficients K and I are used for accelerating, idling, cruising and deceleration. The natural logarithm term is used to ensure that no negative values of emissions are produced (Rakha, Ahn, & Trani, 2004).

$$\text{Instantaneous Emission} = \sum_{I=1}^3 \sum_{J=1}^3 \exp(k_{I,J} \cdot v_I \cdot a_J) \text{ for } a \geq 0 \quad \text{Eq. 2.1}$$

$$\text{Instantaneous Emission} = \sum_{I=1}^3 \sum_{J=1}^3 \exp(I_{I,J} \cdot v_I \cdot a_J) \text{ for } a < 0 \quad \text{Eq. 2.2}$$

The model was validated against the EPA database from which the model was created. Over the ARTA drive cycle, the modelled CO₂ values are 2% high for one of the LDT models and 7% high for one of the LDV models when compared to laboratory testing over the entire drive cycle. Validation has shown that this model cannot be used outside of the speed, acceleration range of the input data, as emissions at higher speed, acceleration do not follow the same trends (Rakha, Ahn, & Trani, 2004).

2.4.1.2 VERSIT+ LD

VERSIT+LD is a fully empirical, statistical model developed by TNO. The aim of the model is to use mean emission factors to predict emissions caused by traffic streams for all vehicle categories and traffic situations (Smit et al., 2007).

The source data was collected on a chassis dynamometer over cycles designed to represent real world operation in the Netherlands. The model is based on a database of 12,000 tests over 153 speed traces. This large sample was thought necessary because an accurate statistical model requires a large representative database. The database is

continually growing, as on-going testing done at TNO are added, this ensures that the model is based on the current driving conditions and vehicle technologies (Smit et al., 2007).

The inputs to the model are a driving pattern (recorded directly on the road) or a driving cycle (created to represent certain traffic situations) and vehicle parameters. The model output is emission factors for CO, HC, NO_x, PM₁₀, fuel consumption and CO₂ for each vehicle category and traffic situation or road network (Smit et al., 2007).

The model works by calculating a range of variables for each vehicle class and pollutant. The model then uses a selection of these variables in a multiple linear regression analysis to predict emissions (g/km), variables are given in Table 2.5. The emissions are then corrected for the effects of cold start, vehicle ageing and AC use.

The methodology follows several steps. Step one, regression analysis assumes that the variance (difference in emissions between vehicles within a category) is not related to the mean emissions over a set cycle. This is not true for the data set used, the variance increases with the mean. To overcome this a log transformation of both the individual vehicle emissions and the mean emissions over the cycle is performed to produce a variance that is not directly related to the mean emissions. The emission figures within each vehicle category are then averaged to produce a single representative vehicle per category (Smit, Smokers, Schoen, & Hensema, 2006).

Step two, create a list of variables to be used in the model. For each vehicle category and pollutant, a subset of the 34 variables is chosen based on, best prediction, low bias and a minimum number of variable to decrease computation requirements. To find “the best fit an automatic variable selection procedure has been employed using Mallows’ C_p criterion” (Smit et al., 2006). This method creates a linear regression model using all possible combinations of the defined variables.

Step three involves estimation of the model constants. This was done using a weighted generalised regression model employing the maximum likelihood method. Step four, the

model is verified to ensure that it gives a good fit to the dataset on which the model is based (Smit et al., 2006).

Table 2.5: Classification of model parameters used in the development of VERSIT+ LD (Smit et al., 2007).

Variable	Location Statistic	Dispersion Statistic
Stop	Number of stops per km, mean stop time	-
Driving mode proportion	Percentage idle time, acceleration time, deceleration time	-
1 st derivative "speed"	Mean speed, max speed, running speed, log mean speed, unit travel time	Standard deviation (SD) of speed and running speed, coefficient of variation of speed and running speed, total absolute difference in instantaneous speed per km
2 nd derivative "acceleration"	Mean acceleration and deceleration, max acceleration and deceleration	SD of acceleration and deceleration, coefficient of variation of acceleration and deceleration, root mean square acceleration
3 rd derivative "Δ acceleration"	Mean change in acceleration and deceleration over one and two seconds, summed change of acceleration and deceleration per unit distance	-
Power demand "inertia resistance"	Mean power, mean acceleration and deceleration power, relative positive acceleration	SD of power, acceleration power and deceleration power
Power demand "rolling and drivetrain resistance"	Relative positive speed, relative squared speed, relative positive squared speed, positive kinetic energy	-
Power demand "Aerodynamic drag"	Relative cubic speed, relative positive cubic speed	-
Impulse variables	Positive and negative speed impulse, positive and negative acceleration impulse, positive and negative speed acceleration impulse	-

The model was validated against a small subsets of the original database from which the model was created. For fuel consumption, the model is within 5% of the measured figures for nearly all drive cycles. The agreement was good but this is to be expected as the data is included in the model creation (Smit et al., 2006).

2.4.1.3 MOVES (Motor Vehicle Emission Simulator)

MOVES is a statistical, empirical model based on vehicle load. The model has been created by the EPA to replace MOBILE. Work on MOVES started in 2001 and an initial simplified example version of MOVES was released in 2005. This has been built upon and a complete version of MOVES was released in 2012, with an update in 2014 (US Environmental Protection Agency, 2013, 2014). The model aims to predict emissions of air pollutants and air toxics at multiple scales, from individual vehicles up to regional and national scale, from all sources (tailpipe, evaporation, brake wear, tyre wear), to provide state and local governments with the tools to meet air quality and transport planning (Koupal et al., 2010).

The source data for the model comes from many databases and projects that the EPA is connected to, including work by most of the US national laboratories and universities. This includes data from multiple sources, chassis dynamometer, inspection/maintenance, PEMS and remote sensing. The inputs to the model are vehicle type (13 categories covering motorcycles, cars, trucks and buses), vehicle specification, fuel specification, location (road type), scale, ambient conditions, traffic situation (drive cycle), road gradient, time span (days, months, years) and emission sources of interest. These inputs are for a project scale model; modelling at county or national level requires different information (US Environmental Protection Agency, 2012). Within each vehicle category for cars, there is a growing proportion of Alternative Fuelled Vehicles (AFV) that are included in the average emissions for that category, but AFV are not independently modelled in MOVES (US Environmental Protection Agency, 2010). The outputs of the model are emissions either as a total figure or emission rates (g/mile). The model covers

a wide range of pollutants HC, CO, NO_x (NO, NO₂), NH₃, SO₂, PM_{10,2.5}, CO₂, CH₄, N₂O and toxics (Benzene etc.). The user can specify how the output should be broken down, vehicle class, road type, emission process, fuel type or model year. The output can also be specified by scale, national, county or project level (Koupal et al., 2010).

The methodology started by trying to find a vehicle variable that best correlated to emissions. Early on in the project Hierarchical Tree Based Regression (HTBR) statistical analysis was used to find the best explanatory variable. The analysis showed that VSP is the best choice when compared to, speed, acceleration, temperature, engine displacement, number of cylinders, AC usage, odometer reading, model year and net weight. The model works by creating VSP, speed matrices for each vehicle category and pollutant (Koupal, Hart, Brzezinski, Giannelli, & Bailey, 2002), VSP is calculated using Equation 2.3. When looking at aggregated vehicles, assumptions can be made for rolling resistance and drag, allowing Equation 2.3 to be simplified to Equation 2.4 (Xu et al., 2011). Second by second (1Hz) emission data is input into the matrices for all vehicles within a category, over every drive cycle, and from all the different emission collection methods. The data within each cell of the matrices is averaged to give a single value. The size of the VSP bins, Table 8.3.1.7.1, was chosen so that the emissions in every bin are significantly different from those in neighbouring bins and no bin should represent more than 10% of the total emissions. The driving location and road grade are used to calculate VSP and vehicle speed, which is used to lookup emission values from the matrices. Other information input into the model regarding fuel type, ambient conditions, mileage, technology, standard and emitter category is used to apply correction factors to the emissions (Koupal et al., 2002).

$$VSP = v \cdot (a \cdot (1 + \varepsilon) + g \cdot \text{grade} + g \cdot C_r) + \frac{\rho \cdot C_D \cdot A_r \cdot v^3}{2 \cdot m} \quad \text{Eq. 2.3}$$

$$VSP = v \cdot (1.1 \cdot a + 9.81 \cdot \sin(\text{atan}(\text{grade})) + 0.132 + 0.000302 \cdot v^3) \quad \text{Eq. 2.4}$$

Table 2.6: MOVES, VSP and speed bins (Coordinating Research Council, 2010).

Condition	VSP (kW/tonne)	Speed (mph)
Braking	-	-
Idling	-	-
Low Speed Coasting	<0	1≤Speed<25
Cruise/Acceleration	0≤VSP<3	1≤Speed<25
Cruise/Acceleration	3≤VSP<6	1≤Speed<25
Cruise/Acceleration	6≤VSP<9	1≤Speed<25
Cruise/Acceleration	9≤VSP<12	1≤Speed<25
Cruise/Acceleration	>12	1≤Speed<25
Moderate Speed Coasting	<0	25≤Speed<50
Cruise/Acceleration	0≤VSP<3	25≤Speed<50
Cruise/Acceleration	3≤VSP<6	25≤Speed<50
Cruise/Acceleration	6≤VSP<9	25≤Speed<50
Cruise/Acceleration	9≤VSP<12	25≤Speed<50
Cruise/Acceleration	12≤VSP<18	25≤Speed<50
Cruise/Acceleration	18≤VSP<24	25≤Speed<50
Cruise/Acceleration	24≤VSP<30	25≤Speed<50
Cruise/Acceleration	>30	25≤Speed<50
Cruise/Acceleration	<6	>50
Cruise/Acceleration	6≤VSP<12	>50
Cruise/Acceleration	12≤VSP<18	>50
Cruise/Acceleration	18≤VSP<24	>50
Cruise/Acceleration	24≤VSP<30	>50
Cruise/Acceleration	>30	>50

The original model MOVES GHG had 14 VSP bins and was validated against an independent data source for CO₂. The model results were within 14 to -8% of the real test data. To improve the accuracy the current model has 23 bins based on vehicle speed and VSP (Koupal et al., 2002). As the model is not designed to look at emissions from individual vehicles detailed validation at the microscale has not been conducted. The model has been validated against highway statistics for total national fuel use and the model agrees with statistics to within 3% for petrol and diesel (Choi & Koupal, 2011).

2.4.2 Models Based on Internal Variables

Emission models based on engine variables give a better prediction of emissions than those based on vehicle variables. However, the model requires more information about the drivetrain and assumptions need to be made about the driver's gear selection pattern (Hu et al., 2016). While a reasonable approximation of a conventional vehicle's emissions, at a given second, can be made based on external parameters alone, this is not the case for hybrid vehicles where the engine power is strongly affected by the battery SOC. This effect is most strongly pronounced during city driving where the engine could be on or off during the same driving demand based on the battery SOC. This excludes the use of models based on external vehicle parameters from use later on in this study.

2.4.2.1 PHEM (Passenger car and Heavy duty vehicle Emission Model)

PHEM was first developed in 2000 by the Institute for internal combustion engines and thermodynamics at Graz University of Technology, as part of the ARTEMIS project. The model has been continually updated and now covers Euro 0 to Euro 6 petrol and diesel vehicles, as well as hybrid and electric vehicles (Kuhlwein et al., 2013). The aim of the project is "to predict fuel consumption and emissions for any single type of car, as well as for average car fleets for a given speed profile, for various loading, slopes and gear shift strategies" (Zallinger, Anh, & Hausberger, 2005).

The source data for the model comes from the ARTEMIS database. This consists of data collected by the 300 ARTEMIS partners and includes hundreds of tested vehicles. No set testing criteria were set out before testing so the database includes testing of over 874 sub-cycles and comprises a total of 31,479 individual tests. The database includes emission factors for the regulated pollutants, CO, CO₂, fuel consumption, THC, NO_x, PM, as well as 398 non-regulated pollutants (Andre, 2005). Additional testing has been conducted to update the model, with 80 Euro 5 and 20 Euro 6 vehicles tested on a chassis dynamometer (Kuhlwein et al., 2013). All the data used for the PHEM model is corrected for the emission time delay caused by the gas transport through the exhaust system.

The model requires specific input data about each car modelled, some of this data can be found in the literature (vehicle mass, aerodynamic drag coefficients, frontal area, auxiliaries rated power, and transmission ratios) and some has to be calculated using coast down tests or measured on the vehicle in the laboratory (rolling resistance coefficients, inertia of rotating parts, mass of individual parts). The model also requires detailed input data about the vehicle driving demand, including 1Hz vehicle speed and road gradient. The model outputs engine power, engine speed, fuel consumption, CO₂, CO, HC, NO_x, and PM emissions per second and per drive cycle (Luz & Hausberger, 2010).

The modelling methodology starts by using the input of a driving cycle and road gradient, to calculate the required engine power based on the driving resistances and losses shown in Equation 2.5 – 2.12. The engine speed is calculated based on vehicle speed, wheel size, differential ratio, transmission ratios and a gear shift model, shown in Equation 2.13. The gear shift model is based on the engine speed, when the engine speed moves above or below a fixed threshold the gear is changed up or down accordingly (several laws are in place to govern when a gear change can occur). Once engine power and speed has been calculated for an instantaneous vehicle speed and

gradient, the model looks up the emissions from the engine map, which was created using the modified Shepard interpolation method and the test data. This is done for every second of the drive cycle and the results are integrated to give a cycle total emissions value. Empirically based correction factors are used to increase engine map emissions during engine transients (Luz & Hausberger, 2010).

$$P_{Engine} = P_{Rolling} + P_{Aero} + P_{Acceleration} + P_{Gradient} + P_{Trans} + P_{Aux} \quad Eq. 2.5$$

$$P_{Rolling} = m \cdot g \cdot (fr_0 + fr_1 \cdot v + fr_2 \cdot v^2 + fr_3 \cdot v^3 + fr_4 \cdot v^4) \cdot v \quad Eq. 2.6$$

$$P_{Aero} = C_D \cdot A \cdot \frac{\rho}{2} \cdot v^3 \quad Eq. 2.7$$

$$P_{Acceleration} = (m_{Vehicle} + m_{Rot} + m_{Loading}) \cdot a \cdot v \quad Eq. 2.8$$

$$m_{Rot} = \left(\frac{1}{2} \cdot m_{Wheels} \right) + I_{Mot} \cdot \left(\frac{i_{Axle} \cdot i_{Gear}}{r_{Wheel}} \right)^2 + I_{Trans} \cdot \left(\frac{i_{Axle}}{r_{Wheel}} \right)^2 \quad Eq. 2.9$$

$$P_{Gradient} = m \cdot g \cdot Grad \cdot \frac{1}{100} \cdot v \quad Eq. 2.10$$

$$P_{Trans} = \frac{P_{dr}}{\eta_{Trans}} - P_{dr} \quad Eq. 2.11$$

$$P_{Aux} = P_0 \cdot P_{Rated} \quad Eq. 2.12$$

$$n = v \cdot 60 \cdot i_{Axle} \cdot i_{Gear} \cdot \frac{1}{D_{Wheel} \cdot \pi} \quad Eq. 2.13$$

The model has been validated for an average car, created by averaging the engine maps of multiple cars, against chassis dynamometer tests, over 12 real world cycles. The validation is based on different drive cycles to those used in the model creation and the fuel consumption results match those of the model very well. This shows that the model is robust over a wide range conditions, but as only overall emissions were presented it is impossible to study which vehicle operating conditions result in the model error (Zallinger et al., 2005). PHEM is considered one of the most advanced and robust

models in Europe (CH2M Hill, 2013), because of this PHEM will be used for modelling petrol and diesel vehicles in Chapter 5 of this thesis.

2.4.2.2 CMEM (Comprehensive Modal Emission Model)

CMEM was initially developed in 1995 by the CE-CERT at the University of California-Riverside, University of Michigan and Lawrence Berkeley National Laboratory, as part of a five-year project. The model has subsequently been updated to reflect the changing vehicle fleet and now includes Ultra Low Emission Vehicles (ULEV), Super Ultra Low Emission Vehicles (SULEV) and Partial Zero Emission Vehicles (PZEV). The model aims to predict vehicle emissions over transport corridors, by predicting the emissions of individual, average composite vehicles, which have been designed to represent each vehicle category (Barth, An, Norbeck, & Ross, 1996; Scora & Barth, 2006; University of California, 2016).

The source data for the model was second by second emissions collected for hundreds of vehicles specifically chosen to represent all the vehicle categories in the USA fleet. All vehicles were tested on a chassis dynamometer over the Federal Test Procedure 75 (FTP-75), US06 and MEC01 cycles. As FTP-75 and US06 are not modal cycles they lack prolonged operation at idle, cruise, acceleration and deceleration, therefore, as part of the CMEM project the MEC01 modal cycle was developed. This cycle was designed to cover the full range of accelerations and decelerations that most cars were capable of, as well as cruising at different speeds, speed fluctuations and constant power driving (Barth et al., 1996; Scora & Barth, 2006).

The input parameters to the model have been categorised into three groups. The readily available parameters are variables that can be collected from the literature. The calibrated parameters are variables that have to be measured or approximated using chassis dynamometer testing and a process of regression analysis or optimisation. The calibrated parameters are broken into two groups, insensitive parameters (roughly calculated, with only a minor effect on results) and sensitive parameters (calculated in

detail, with a large effect on results). All the required inputs are presented in Table 2.7. The model outputs instantaneous emissions of CO, HC, NO_x and CO₂, as well as fuel consumption per second and total fuel consumption (Barth et al., 1996; Scora & Barth, 2006).

Table 2.7: Model input parameters (Scora & Barth, 2006)

Readily Available Parameters	Calibrated Parameters	
	Insensitive Parameters	Sensitive Parameters
Specific Vehicle	Emission Parameters	Cold Start Parameters
Vehicle Mass Engine Displacement Engine Idle Speed Coast down Power Engine Speed/Vehicle Speed Max Torque Engine Speed at Max Torque Max Power Engine Speed at Max Power Number of Gears	CO Enrichment Coefficient CO Index Coefficient HC Index Coefficient HC Residual Value NOx stoichiometric Index NOx Enrichment Index NOx FR Threshold	Cold Start Catalyst Coefficients for CO, HC and NOx Cold Fuel/Air Equivalence Ratio Surrogate Temperature Reach Stoichiometric Cold HC Multiplier Cold NO Multiplier
Generic Vehicle	Fuel	Hot Catalyst
Indicated Efficiency Max Drivetrain Efficiency Gear Ratios	Engine Friction Factor Drivetrain Efficiency Coefficients	Hot Max Catalyst Efficiencies for CO, HC, NOx Hot Catalyst Coefficients for CO, HC, NOx NOx Catalyst Tip-in Coefficient
Operating Variables	Enleanment	Enrichment
Road Grade Accessory Power Speed Trace Soak Time Specific Humidity	Max HC Lean Rate Transition HC Lean Rate HC Lean Threshold Value HC Lean Release Rate Ratio of O ₂ and EHC Lean Fuel/Air Equivalence Ratio	Max Fuel/Air Equivalence Ratio SP Threshold Factor
	Soak-time	
	Soak Time Engine Coefficient for CO, HC, NOx Soak-time Catalyst Coefficient for CO, HC, NOx	

The model has 26 vehicle categories, each one modelled using the basic procedure described here. The model uses Equation 2.14 to calculate the vehicle tractive power demand and Equation 2.15 to convert this to engine power demand. The engine speed is calculated from vehicle speed and the gear shift schedule. The model has four operating modes, cold start, stoichiometric, enrichment and enleanment, these are calculated based on how long the model has been running for and engine power. Engine power and model operating mode are used to calculate air/fuel equivalence ratio, which alongside engine speed and engine power is used to calculate fuel rate. The final output emissions are calculated from the fuel rate, the engine emissions per unit fuel and the catalyst pass fraction (Barth et al., 1996; Scora & Barth, 2006).

$$P_{Tract} = \frac{m}{1000} \cdot v \cdot (a + g \cdot \sin\theta) + \left(m \cdot g \cdot C_R \cdot \frac{\rho}{2} \cdot v^2 \cdot A_r \cdot C_D \right) \cdot \frac{v}{1000} \quad Eq. 2.14$$

$$P_{Engine} = \frac{P_{Tract}}{\eta_{tf}} + P_{Aux} \quad Eq. 2.15$$

The model has been validated against independent data over the FTP and US06 cycles. The validation compares actual vehicles tested to average composite vehicles within each model category. The validation results are presented in Table 2.8. While the results are not a great match, a reasonable proportion of the difference could be down to the difference in the tested vehicle and the category average vehicle. While CMEM is capable of predicting emissions from an individual vehicle over a micro-scale time frame it is clear that the accuracy of the model limits its use to modelling whole road sections (Scora & Barth, 2006).

Table 2.8: CMEM CO₂ emissions validation (Scora & Barth, 2006)

Statistic	FTP Bag 3 Cycle	US06 Cycle
Average Emissions g/s	3.5	5.1
Average Bias	0.53	0.22
Maximum Bias	2.9	4.3
Minimum Bias	-1.7	-3.2
Slope	0.94	0.86
Y-Intercept	10	46
R-Squared	0.99	0.87

2.4.2.3 VeTESS (Vehicle Transient Emissions Simulation Software)

VeTess was developed under the EC 5th Framework DECADE project by MIRA, IDIADA Automotive Technology, the Centre of Logistics and Expert Systems GmbH and Vlaamse Instelling voor Technologisch Onderzoek NV. VeTESS is an advanced quasi steady state model that aims to accurately predict emissions by including dynamic engine behaviour (Pelkmans, Debal, Hood, Hauser, & Delgado, 2004).

The source data consists of various tests for three vehicles, a Euro IV petrol car (VW Polo 1.4L 16V), a Euro III diesel car (Skoda Octavia 1.9L TDi 90) and a Euro II diesel light commercial vehicle (Citroen Jumper 2.5D). These vehicles were tested in the real world in Mol and Barcelona over urban, rural and motorway conditions, on a proving ground at IDIADA and on a chassis dynamometer at CLE, IDIADA and MIRA. The chassis dynamometer tests were carried out over the NEDC and Mol cycle. The engines were removed from all the vehicles and steady state engine maps were created on engine dynamometers. The cars were then tested on a chassis dynamometer looking at the effects of the drive cycle, tire pressure, vehicle mass, gear shifting, intake air flow, fuel quality, ambient temperature, ambient humidity and ac use on emissions, to find the parameters that had the greatest effect on each pollutant. The drive cycle, vehicle mass,

gear shift strategy and AC use were found to be the most important parameters followed by the ambient conditions (Pelkmans et al., 2004).

The exact calculation of engine speed and torque for this model is not discussed in the literature, although they appear to follow much the same method as PHEM, and therefore will require the same input parameters. The model output is instantaneous and whole cycle emission factors for CO, HC, NO_x, CO₂, PM and fuel consumption (Pelkmans et al., 2004).

The method for this model differs from others as instead of having a normal engine map based on emissions at set engine speeds and engine torques, this model has 3D maps based on engine speed, engine torque and change in engine torque. The change in engine torque is modelled as a step change in torque that occurs at constant engine speed when the accelerator pedal is pressed. This third parameter allows the model to relate emissions to the rate of change of engine torque, and therefore more accurately model transients. The engine speed is calculated based on the vehicle speed and transmission ratios. The engine torque is calculated using Equation 2.16 and power losses through the powertrain. Once the engine speed, torque and change in torque have been calculated they are the input variable to the four engine maps (Pelkmans et al., 2004).

Total Force = Acceleration Resistance + Climbing Resistance

+Rolling Resistance + Aerodynamic Resistance *Eq. 2.16*

During a change in speed the emissions are modelled based on four main variables, steady state emission rate (emission rate under steady state conditions), jump fraction (following a change in torque, the ratio of immediate emission rate to final emission rate), time constant (a measure of how the emission rate returns to steady state conditions after the torque change) and transient emissions (the amount of additional emissions caused by the torque change) (Pelkmans et al., 2004).

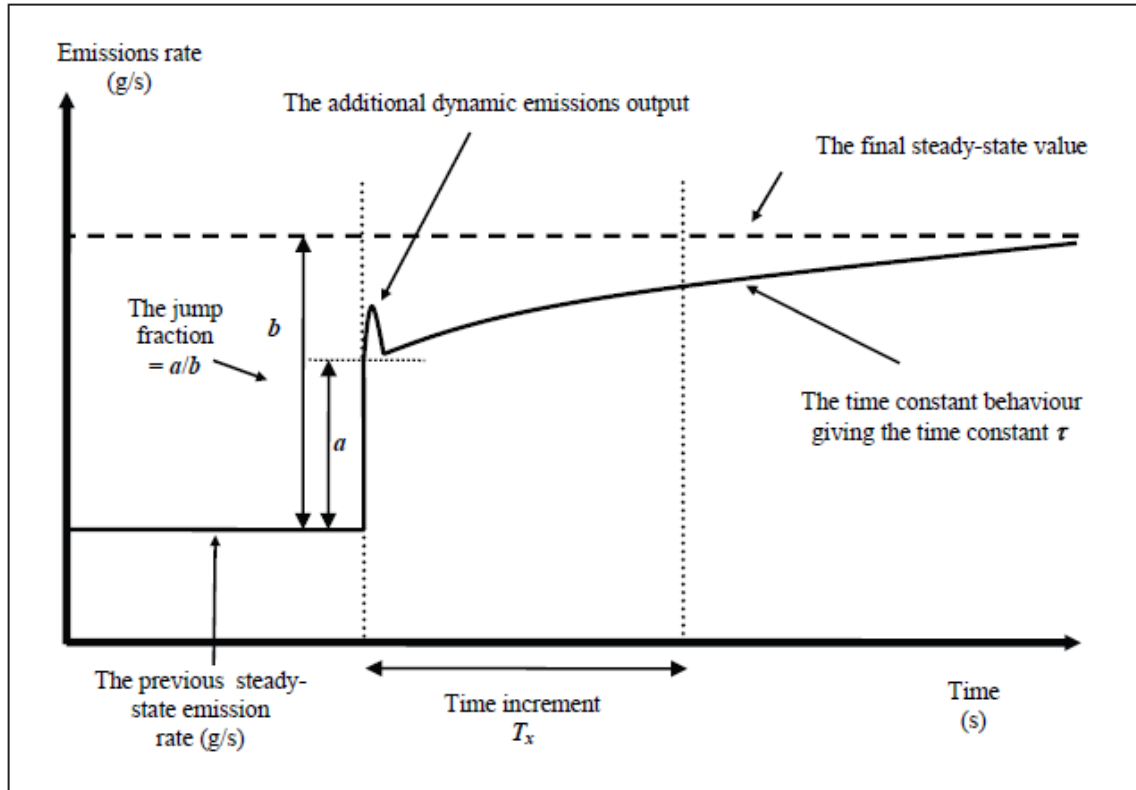


Figure 2.6: Methodology to calculate emission parameters (Pelkmans et al., 2004).

When a change in speed occurs the model works through three steps shown in Figure 2.6.

Step 1. Multiply previous steady state emission rate by a time increment.

$$Area = E_{prev} \times T_x \quad Eq. 2.17$$

Step 2. Look up constants x and y from the jump fraction map.

$$Area = \left(E_{prev} + \left(\frac{x}{y} \times (E_{final} - E_{prev}) \right) \right) \times T_x \quad Eq. 2.18$$

Step 3. An exponential function is used to better estimate the new steady state emissions.

$$1 - e^{-\frac{t(s) - 15(s)}{\tau ct(s)}} \quad Eq. 2.19$$

The exponential equation considers values between the jump fraction mean and the upper steady state value to find a time constant value at which the exponential function best fits the measured data. The final area under the curve shown in Figure 2.6 is the emissions over that time step and is calculated using Equation 2.20.

$$Area = \left(\left(E_{Prev} + \left(\left(\frac{x}{y} \right) \times (E_{Final} - E_{Prev}) \right) \right) \times T_x \right) + \left(\left(\left(1 - e^{-\frac{t}{\tau c}} \right) \times \left(E_{New} - \left(\frac{x}{y} \right) \times (E_{New} - E_{Prev}) \right) - E_{Prev} \right) \times 0.5 \right) \times T_x \quad Eq. 2.20$$

The model has been validated for the three subject vehicles to an accuracy of 5% for CO₂. However, fuel consumption figures can have an error as large as 20% when the gear shifting strategy used in the model does not reflect those used in practice. The model's transient correction increased the fuel consumption by 6% for diesel and 10% for petrol vehicles (Pelkmans et al., 2004).

2.4.2.4 EMIT (Emissions from Traffic)

EMIT is a statistical model based on vehicle load and was created by the Massachusetts Institute of Technology and Ford Motor Company. The model aims to estimate emissions for average vehicles that represent the many vehicle categories. The source data for the model is the NCHRP database which consists of emissions data collected on chassis dynamometer between 1996 and 1999, by the University of California Riverside, and was also used for the CMEM model. The database has hundreds of vehicles split into 26 categories by technology, mileage, power to weight ratio and emissions (Cappiello et al., 2002).

For input, the model requires the speed trace, instantaneous acceleration, road grade and auxiliary power requirements, as well as some basic vehicle specification available from manufacturers. All other parameters are calculated from this basic set of inputs.

The model output is engine out and tailpipe emissions of CO₂, CO, HC and NO_x as well as fuel consumption on a second by second basis (Cappiello et al., 2002).

At each instant during vehicle testing the vehicle speed, acceleration and fuelling rate (FR) is recorded. The FR is calculated using Equation 2.21 as a carbon balance and acceleration is calculated from vehicle speed. The method directly relates fuelling rate to engine power requirements by statistically calibrating the coefficients in Equation 2.22 and 2.23 to test data. Every parameter in Equation 2.22 and 2.23 is known from vehicle testing or can be calculated from known values, engine speed from vehicle speed, gear ratio and engine peak torque, friction factor is a function of engine speed, and drivetrain efficiency is a function of vehicle speed and specific power. The data for all the vehicles within a category over every drive cycle is input into the equations and a statistical approach is used to determine the A, B and C values that best match the vehicle's speed and acceleration to the measured FR. A vehicle category, a speed trace and the A, B and C coefficients can then be used to predict FR. The engines out emissions are modelled as the product of FR and an Emission Index (EI) which is mass of emission per unit mass of fuel, and tailpipe emissions are engine out emissions multiplied by the catalyst pass fraction (Cappiello et al., 2002).

$$FR = \left(\frac{CO_2}{44} + \frac{CO}{28} \right) \times (12 + 1 \times 1.85) + HC \quad Eq. 2.21$$

$$FR = \phi \cdot \left(K \cdot N \cdot V + \frac{P}{\eta} \right) \text{ for } P > 0 \quad Eq. 2.22$$

$$FR = K_{Idle} \cdot N_{Idle} \cdot V \text{ for } P = 0 \quad Eq. 2.23$$

$$P = \frac{P_{Tract}}{\eta_{dr}} + P_{Aux} \quad Eq. 2.24$$

$$P_{Tract} = A \cdot v + B \cdot v^2 + C \cdot v^3 + m \cdot a \cdot v + m \cdot g \cdot \sin\theta \cdot v \quad Eq. 2.25$$

The model is validated with the data from the US06 cycle that was not used in model calibration. The fuel consumption and CO₂ overall emissions were within 5.3% and -2.6%

of the measured results respectively. This gives a high R^2 value of roughly 0.95 in most cases (Cappiello et al., 2002).

2.4.2.5 PERE (Physical Emissions Rate Estimator)

PERE is an empirical model based on vehicle load. The model has been developed to support MOVES by modelling advanced technology vehicles, advanced petrol and diesel engines, hybrid electric vehicles and hydrogen fuel cell hybrids. The model aims to predict fuel consumption for average vehicles that represent likely future market segments (Nam, 2004).

The source data for the model comes from the EPA certification database. In the USA manufacturers are forced to publish coast down test data used to calculate road load. This information can then be used to calculate power from rolling, rotating and aerodynamic resistances. The required model inputs are model year, vehicle weight, body type, engine displacement, motor power and fuel type. The output is second by second and whole cycle fuel consumption (Nam, 2004).

The method used for conventional vehicles is a backwards facing model that uses the vehicle speed profile and vehicle characteristics as inputs for Equation 2.26 to calculate the engine power demand; if coast down test data is available then Equation 2.28 can be used instead. ϵ is assumed to be 0.1, C_R ranges between 0.008 – 0.013, C_D and A_r are supplied by manufacturers and A, B and C are calculated from the coast down tests. It has been found that Equation 2.26 underestimates fuel consumption and that Equation 2.28 is more accurate, but it supplies no explanation for the results (Nam, 2004).

$$P_b = VSP \cdot m = m \cdot v(a \cdot (1 + \epsilon) + g \cdot \text{grade} + g \cdot C_R) + \frac{1}{2} \cdot \rho \cdot C_D \cdot A_r \cdot v^3 \quad \text{Eq. 2.26}$$

$$A_r = (H - GC) \cdot W \cdot 0.93 \quad \text{Eq. 2.27}$$

$$P_b = A \cdot v + B \cdot v^2 + C \cdot v^3 + m \cdot v(a + g \cdot \text{grade}) \quad \text{Eq. 2.28}$$

The petrol engine is modelled using the method described in (Ross, 1997). In Equation 2.29, η is the indicated or thermal efficiency (fraction of fuel energy converted to useful

work), f_{mep} represents the mechanical losses due to friction, pumping and auxiliary load, and b_{mep} represents brake power and can be obtained from Equation 2.26 or Equation 2.28. Plotting fuel mep against b_{mep} gives a straight line for a large range of engines over different operating conditions. From this straight line relationship η , f_{mep} and k can be calculated. This straight line relationship does not hold true close to WOT operation and so the model is only accurate at lower engine loads. The model uses generic peak torque and power curves taken from (M. A. Weiss, Heywood, Drake, Schafer, & AuYeung, 2000) and corrected to the engine size using relationships developed in (Sandoval & Heywood, 2003). These curves are used to determine the gear shift strategy and cut point for hybrid systems (Nam, 2004).

$$Fuel\ mep = \frac{k+b_{mep}}{\eta} = \frac{f_{mep}+b_{mep}}{\eta} \quad Eq. 2.29$$

For the transmission model the engine speed is calculated using Equation 2.30; under the current model $(N/v)_{top}$ is assumed constant and the transmission is downshifted at high speeds or loads when the torque demand is higher than the max torque curve. The model assumes all transmissions are 5 speed manuals with a transmission plus drive train efficiency of 0.88. When engine and drivetrain efficiencies are included the fuelling rate is calculated using Equation 2.31 (Nam, 2004).

$$N = \left(\frac{N}{v}\right)_{top} \cdot \left(\frac{60\ rps}{1\ rpm}\right) \cdot \left(\frac{g}{g_{top}}\right) \cdot v \quad Eq. 2.30$$

$$FR = \varphi \frac{\left(k \cdot N \cdot V + \frac{\left(\frac{P_b}{\eta_t} + P_{Aux}\right)}{\eta}\right)}{LHV} \quad Eq. 2.31$$

For diesel engine vehicles the same method is used, but the factors are changed, indicated efficiency is set to 0.45, the friction values are changed, the max engine speed is decreased by 25% and the weight of the vehicle is increased by 4%, relative to a similar size petrol vehicle. Advanced ICE vehicles are modelled with different efficiency and friction coefficients based on figures from the academic literature (Nam, 2004).

Hybrid vehicles are modelled based on the control logic described by (M. A. Weiss et al., 2000). The system is controlled so that at low power the car is run off the motor alone, at medium power the car is run off the engine alone and at high power the car is driven by both the motor and the engine. The system has regenerative braking to recharge the batteries. The motor drive is limited by the model so that the battery SOC is sustained over the FTP-75 and Highway Fuel Economy Test (HWFET) cycles. The motor has a set efficiency of 76% when motoring and 61% during regenerative braking, this covers the efficiency of the motor and inverter etc. The battery is assumed to be 95% efficient in discharge and 85% efficient while charging. The mild hybrid model is given a 0.936kWhr battery pack and the full hybrid is assumed to have a 1.31kWhr battery pack. The weight of hybrids vehicle has been calculated based on a direct comparison between hybrid and non-hybrid models with the same vehicle body. A petrol hybrid is assumed to be 7% heavier than an ICE petrol and a diesel hybrid is assumed to be 4% heavier than a petrol hybrid of a similar size (Nam, 2004).

The model is validated against FTP-75 and HWFET figures measured during the EPA certification process. Most conventional vehicles are accurate over the two cycles to within 5%. The model always underestimates fuel consumption at the beginning of the cycle because it does not model cold start effects. The model has good accuracy for the advanced ICE vehicles, within 5%, but over estimates fuel consumption for the Prius by 12-18%, over the FTP-75. This is due to the simple control system used and inaccurate modelling of the Prius advanced regenerative braking system (Nam, 2004).

2.4.2.6 Kaishan Zhang Microscale Model

The model is presented in Kaishan Zhang PhD thesis, completed in 2006. The PhD was completed at North Carolina State University under the direction of Dr. H. Christopher Frey. The project “aims to develop vehicle specific energy use and emission models to capture episodic events during real world driving” and to use this to compare intra and inter vehicle variability (Zhang, 2006).

The source data consisted of 10 vehicles tested using PEMS equipment on the road. The vehicles had engine displacement ranging from 2.2-5.3L and model years 1997-2005. Testing was conducted over multiple routes between fixed start and end points, chosen to represent busy residential and business areas. Six routes were chosen to cover a wide range of driving conditions, road types and gradients, and the tests were conducted at different times of day to cover a range of ambient conditions and peak, non-peak traffic conditions. A total of 230hr of data was collected covering 9322 miles across the 10 vehicles and three drivers. Emissions were collected using a Montana PEMS system, road grade was calculated using Light Detection and Ranging (LiDAR), GPS was used to set the routes, the on-board diagnostic link was used to collect data on vehicle speed, acceleration, engine speed, manifold absolute pressure, intake air temperature, throttle position percentage and coolant temperature. A quality assurance code was used on all PEMS data to detect and correct the errors in the data. At the beginning of the data collection runs the accelerator pedal is depressed rapidly to produce a CO spike. This event is used to align the engine scanner data with the gas analyser (Zhang, 2006).

The input data for the model is the speed trace and road grade. Two modelling methods were used; one based on internal vehicle data and one on external vehicle data. The internal model requires additional information, manifold absolute pressure and engine speed, whereas the external model can be run on a drive cycle alone. The model output is average emission values over 3-12 second periods for NO, HC, CO, CO₂ and fuel rate (Zhang, 2006).

The internal model uses Equation 2.32, where coefficient a is used to fit the model to the measured results using regression fitting. The external model uses Equation 2.33 where the coefficients A, B, C and D were used to fit the model to the measured data using regression fitting. Due to the slow response time of the analysers, 3 second to reach

63% of real emission input value, it was decided to use consecutive averaging of the emissions and vehicle activity data in the model (Zhang, 2006).

$$\bar{m}_i^{\Delta t} = a_i \cdot \overline{P_{map}} \cdot \bar{N}^{\Delta t} \quad Eq. 2.32$$

$$\bar{m}_j^{\Delta t} = A_j \cdot \bar{a}v^{\Delta t} + B_j \cdot \bar{v}^{\Delta t} + C_j \cdot \bar{v}r^{\Delta t} + D_j \cdot \bar{v}^3{}^{\Delta t} + \varepsilon_j \quad Eq. 2.33$$

The model was validated against a subset of the original database that was split off for validation purposes. The internal model had an R^2 ranging from 0.88 to 0.99 for fuel rate across the 10 vehicle models. The external model had an R^2 ranging from 0.77 to 0.94 for fuel rate across the 10 vehicle models (Zhang, 2006).

2.4.2.7 Delia Ajtay Modal Model

The model is presented in Delia Ajtay PhD thesis, completed in 2005. The PhD was completed at the Swiss Federal Institute of Technology Zurich under the direction of Dr. Martin Weilenmann, during this PhD work the group developed the emission delay correction method now used by PHEM and other major models. The aim of the project was to model the exhaust gas transport system to reconstruct engine out emissions as well as developing a simple transient emission model (Ajtay, 2005).

The source data for the model is 20 vehicles tested on a chassis dynamometer over the R1-R4 and CADC real world cycles. The cars consisted of 3 pre-Euro 1, 10 gasoline Euro 3 and 7 diesel Euro 2, chosen to represent the Swiss vehicle fleet. Vehicle emissions, vehicle speed, manifold pressure, engine speed, temperature and humidity were all measured on a 10Hz basis (Ajtay, 2005).

The inputs to the model are speed trace, road grade, gear shift schedule, auxiliary use and vehicle specifications. The model also requires engine power demand to calculate torque unless torque is measured on the chassis dynamometer. The power demand can be calculated using the methods used in PHEM and this would require the same inputs as PHEM. The model outputs are emissions of NO_x, CO, HC, CO₂ and fuel consumption

factors in g for the whole cycle and as emission rates in g/km, at a frequency of 10Hz (Ajtay, 2005).

The method is based on a series of emission matrices used as emission lookup tables. The matrices use bmep calculated using Equation 2.34 and engine speed as the inputs. Each car and pollutant combination have a matrix, all data is entered into the cells of the matrix and then values within each cell are averaged. The matrices are all 16 by 16 with a coarse outer grid and a fine inner grid to reduce interpolation. At 10Hz frequency the model calculates the bmep and engine speed from speed trace and vehicle specification and then looks up an interpolated emission value from the matrices using bilinear interpolation (Ajtay, 2005).

$$bmep = \frac{T_e \cdot 4 \cdot \pi}{V_d} \quad Eq. 2.34$$

For NO_x, CO and HC a transient model was created using 3D matrices based on bmep, engine speed and the derivative of manifold pressure, but the results for CO₂ were accurate enough using the simpler model that it was not included in the transient model (Ajtay, 2005).

The model was validated using a fraction of the source data. The source data includes 16 drive cycles, 15 were used for model creation the 16th for validation. The measured and modelled emission factors were compared at a vehicle category level. The relative error for CO₂ for the Euro 1 category was 1.5%, for Euro 2 it was 2% and Euro 3 it was 1.5% (Ajtay, 2005).

2.4.3 Vehicle Component Models

Vehicle component models have a library of drivetrain components that can be slotted together in many different combinations, to replicate existing vehicles or trail new vehicle designs (AVL, 2009). These are the most powerful models from the point of view of the user, especially for building hybrid vehicle powertrains where many different combinations of components and component sizing are possible, but building the

component library involves large amounts of testing which is usually beyond the abilities of most academic institutions. Therefore, these models are usually government funded projects or commercial enterprises, and in both cases, OEM support is usually required (AVL, 2009; Markel et al., 2002; Ricardo Inc., 2008; Rousseau & Halbach, 2010).

2.4.3.1 ADVISOR (Advanced Vehicle Simulator)

Advisor is an empirical model that was created by the National Renewable Energy Laboratory in 1994, on behalf of the US Department of Energy, and runs in the MATLAB/Simulink environment. The aim of the model is to provide the engineering community with a package capable of modelling fuel consumption, performance and emissions for advanced alternative technologies (Markel et al., 2002).

The source data for the model is individual component testing by one of the national laboratories, to provide steady state efficiency maps. On the user interface, the user has to input the vehicle components, their configuration and sizing. The user also chooses from over 40 drive cycles which include the full range of driving operating (driving styles, road grade). The model outputs the performance of each component in the vehicle (engine speed, engine torque, battery voltage etc.) and the performance of the vehicle, as well as fuel consumption and emissions on a second by second basis and integrated over the entire cycle (Markel et al., 2002).

The model structure composes a database of text files to populate a Matlab code for each component. The components are connected through a Simulink vehicle model, which comprises the user interface. Each component has been tested to provide an efficiency, fuel consumption or emission map or index. The required power at the wheels is transferred through the model to each component where it is corrected for the losses in that component. Until a speed and torque requirement can be fed to the engine map which uses the points to interpolate fuel consumption and emission figures (Markel et al., 2002).

The model was validated by Virginia Tech against a series hybrid vehicle in 1997. The model fuel consumption was compared to chassis dynamometer results over the FTP-75 and HWFET cycles. The modelled fuel economy is within 12-19% of the tested figures (Senger, Merkle, & Nelson, 1998).

2.4.3.2 PSAT (Powertrain Systems Analysis Toolkit) / Autonomie

PSAT is an empirical forward facing model developed by Argonne National Laboratory, with contributions from Ford, General Motors and Daimler-Chrysler, on behalf of the US Department for Energy (Rousseau et al., 2001). Autonomie has been created by Argonne National Laboratory to replace PSAT, the project started in 2007 and ended in 2010 and has been funded by the Department for Energy and General Motors. The project aims to “accelerate the development and introduction of advanced technologies” this will be done by reducing the time and cost of new vehicle development (Rousseau & Halbach, 2010).

The source data for this model is very varied with multiple models present in the model library. The current library is based predominantly on models created from laboratory testing at Argonne, combined with several industry models (GT-Power, AMESim, SimScape and CarSim) and in-house data from General Motors. The model library can be added to by users so the source data is updated over time to reflect the latest technology (Halbach, Sharer, Pagerit, Rousseau, & Folkerts, 2010).

The inputs to the model are specified by the user on the Graphical User Interface (GUI). Here the user has to set the vehicle configuration, vehicle component parameters, model fidelity, drive cycle and environmental conditions. The model inputs can be limited to configuring the vehicle structure or can be used to redefine models or add in new models from outside Autonomie. The user can access the data flow at any point in the model, allowing the model output to include the input and output values for any component or subcomponent. The model also outputs fuel consumption over the drive cycle (Halbach et al., 2010).

The model works by having an overall structure in Simulink which is capable of interacting with many other vehicle simulation packages allowing advanced industry models like GT-Power, AMESim and CarSim to be integrated into a single modelling environment (V.Gopal & Rousseau, 2011). The model is based on the concept of 'plug and play' this means that multiple models exist for the different components and for the same component but at varying degrees of complexity. All of these models can be connected together interchangeably allowing quick creation of a model that fits the accuracy requirements of the specific project. The basic engine model used in most cases is a fuel consumption map based on chassis dynamometer testing that correlates engine speed and torque to fuel consumption for every instant of the drive cycle. The model works by automating the connection of models chosen from the model library by the user in the GUI, this saves the user the time of connecting all the models together and avoids the many user errors likely to be inherent to that process. As the overall model automatically connects component models it also adds blocks before and after models that are needed to convert code types or correct units, thus allowing for rapid model integration (Halbach et al., 2010).

The model is capable of any arrangement of components, but for ease of use the model is organised in a hierarchy. The top level contains the environment, driver, vehicle propulsion controller, for HEV, and the vehicle propulsion architecture (engine, battery etc.). Each component is structured using a controller, actuator, plant, sensor (CAPS) configuration. Depending on the component it may not have all the systems, for example, the driver component only needs a controller. Many components can have subcomponents depending on the required accuracy of the model and these subcomponents are again organised under the CAPS system. The whole system is set up to mimic the physical layout of the actual vehicle to make model construction and use as intuitive as possible (Halbach et al., 2010).

The model has been validated for the Toyota Prius 2010. The model fuel consumption, over the FTP-75 and HWFET drive cycles, was compared with data collected at Argonne on the chassis dynamometer. The difference in fuel consumption between the test and model results was -3.36, -1.42, 4.13 and -1.69%, the difference in battery SOC was -3.36, 2.66, 0.51 and 1.92 over the Urban Dynamometer Driving Schedule (UDDS), LA92, HWFET and US06 cycles respectively (N. Kim, Rousseau, & Rask, 2012).

2.4.3.3 Ricardo in-House Model

The Ricardo model is an analytical physics-based model. This detailed model is forward facing using a 'driver' model to control the accelerator and brakes in an attempt to follow the speed trace. The model's initial aim was to predict the CO₂ emission reduction potential of future engine, drivetrain and vehicle technologies (Ricardo Inc., 2008). The model has been further developed and can now be used to study vehicle performance, fuel consumption, emissions and energy flows throughout the powertrain (Ricardo Inc., 2016).

The source data for the model is Ricardo's large in-house database. This information has been collected by sections of the company working on vehicle technology research and development, as well as from the many OEM that Ricardo works alongside (Ricardo Inc., 2008).

There are many model inputs the basic ones are presented here by source.

Published data (Source).

- Equivalent test weight (EPA vehicle certification database)
- Gross vehicle weight (manufacturers website)
- Gross combined weight (manufacturers website)
- Road load coefficients (EPA vehicle certification database)
- Vehicle dimensions (manufacturers website)
- Tyre size (manufacturers website)

- Engine displacement, rated horse power, rated torque and technology used (manufacturers website)
- Transmission gear ratio (various websites)
- Final drive ratio (manufacturers website, EPA certification database)

Ricardo propriety data.

- Transmission hydraulic losses and gear efficiency
- Engine, transmission and driveline rotational inertia
- Driveline spin losses
- Transmission shift and torque converter lockup strategy
- Vehicle frontal area, coefficient of drag
- Tyre rolling resistance
- Vehicle weight distribution and centre of gravity

The model outputs fuel consumption and emissions, as well as energy flow and losses for each powertrain component, on a time interval and whole cycle basis (Ricardo Inc., 2008, 2016).

The Ricardo modelling method starts from the EPA coast down coefficients A, B and C to calculate the vehicle load while driving. The model consists of a sub-model for most components, each sub-model is designed to input and output parameters like speed, torque, heat etc.. From the output values of the sub-models efficiency factors are calculated and imposed on the outgoing values. The efficiency and engine fuelling maps are all created from in-house testing by Ricardo (Kasab, Shepard, Casadei, Huang, & Brandao, 2012).

The main sub-models include fuel consumption engine maps based on in-house testing data across the full range of engine speeds and loads. A turbo lag model. A warm up model that uses a cooling circuit to calculate engine warm up times. An accessories model that assumes most auxiliary can be set as a constant additional engine load, apart from power steering which is modelled as an engine speed dependent load. The auxiliary

loads that use power from the battery rather than directly off the engine, this also includes the alternator inefficiency. A transmission efficiency model based on empirical formulas from in-house testing that sets an individual inefficiency for every gear and includes hydraulic pumping losses. A differential model. A tyre model that calculates the rolling resistance and vehicle speed, based on tyre rolling radius, rotational inertia, slip at peak tyre force, maximum friction coefficient and tyre rolling resistance coefficients. A driver model that controls the vehicle speed and braking and allows for accurate modelling of vehicle performance (Ricardo Inc., 2008).

The model has been validated against in-house test data and EPA certification data. The model predicts fuel consumption with a 1-3% error for 5 vehicles covering a diverse range of cars and light duty trucks (National Academy of Engineering, 2011).

2.4.3.4 AVL CRUISE

AVL Cruise is an analytical model built by AVL over the last twenty years. The model is designed as a tool for vehicle component, powertrain, control systems and whole vehicle development, from concept through to vehicle launch. The model allows for the optimisation of fuel consumption, emissions, driving performance and drivability. The model architecture is modular allowing the modeller to build conventional, hybrid and electric vehicles from pre-tested components, based on performance maps, in the vehicle model library. Models can be built using AVL model components or using imported data from other vehicle or component testing. Models can include sub-models for combustion engines, exhaust after-treatment systems, clutches, transmissions, vehicle and component control, wheels, motors, batteries, electronics, capacitors, converters and inverters, brakes, auxiliary systems, driver and environmental conditions. Models can be built at many different levels of complexity depending on the required output and the model can output data on any component or for the whole vehicle (AVL, 2009, 2016). A model of the Toyota Prius built in AVL Cruise was validated over three cycles, with the error ranging from 1 to 3 % for CO₂ emissions (Jones, 2011).

2.5 Conclusions

To overcome the current shortcomings of Regulation 443/2009 will require not just a new test cycle and testing procedure, but conformity testing, similar to that currently carried out in the USA, and real world PEMS testing of production vehicles. The dieselgate scandal has shown that type approval testing will always need to be supported by extensive real world testing, if regulations are to be successfully enforced and updated to match the latest vehicle technology. It is, therefore, important that new real world vehicle testing procedures are developed and verified, giving regulators the tools they need to legislate the car market.

To overcome the current problem of test data not representing real world emissions, PEMS data is the best solution, as it can be collected under any real world condition and a wide range of pollutants can be measured accurately. However, the PEMS method is expensive and this can make it unsuitable for delivering person specific information or for analysing a local policy. PEMS data also has an emission delay which makes it very difficult to align the emissions with the vehicle or engine operation, making it challenging to use PEMS data to analyse a specific technology or for emission model building. If the focus of the study is real world CO₂ emissions, rather than air quality emissions then PAMS testing could offer a good alternative to PEMS testing as it is cheaper and does not have an emission delay.

Real-world vehicle testing is not always an option, either due to the cost or because the work is a feasibility study and the testing conditions do not yet exist. In this case, modelling can be a powerful tool to study the situation and provide situation-specific results. Development and application of models is currently hampered by access to vehicle data to build and validate the models and so further development of PAMS data collection methods could also improve the range and accuracy of models available.

The review of the current models available has fed into the design of the model presented in chapter 6. From this review, a number of model design decisions have been made.

These include:

1. The model must be based on internal variables (engine speed and torque) if it is to meet the accuracy requirements of this project.
2. The model should add something new to the collection of models available in the literature. This will be achieved by building a model based on real world vehicle activity data.
3. Detailed, independent model validation is lacking from many models and this makes them less powerful tools as the outputs can't be used to inform important decision making. It is, therefore, very important that the model is rigorously validated.
4. There are many equations for calculating vehicle power. This study will use the one used in the Physical Emissions Rate Estimator as this is based on three resistance coefficients A, B and C which are freely published for all vehicles sold in the USA by the EPA.
5. The model should be backward facing (the engine matches the vehicle demand exactly) rather than forward facing (a driver sub model controls the throttle to try and match the desired vehicle speed). This has been chosen because the model will be run over real world vehicle speed time traces and the model should match these exactly, rather than running the model over drive cycles where the model should predict a human driver's speed profile over the drive cycle.

Chapter 3

Portable Activity Measurement System (PAMS) Testing

Methodology

3.1 Introduction

This chapter presents the PAMS data collection method that is used to build two databases of real world data. One to study the potential of hybrid vehicles as taxis in Leeds and one to analyse the Toyota Prius powertrain controls and build a microscale model. This chapter includes:

1. A detailed description of the vehicle tested, the two sets of data logging equipment used and the parameters recorded.
2. A testing methodology including when the data was collected, who drove the vehicle and the amount of data recorded.
3. An explanation of the two databases created and the test routes driven.
4. The data post processing methodology which includes adding road gradient data to the PAMS data, based on vehicle location and a digital surface model.
5. An analysis of the distribution of the data collected to ensure a wide range of testing conditions have been incorporated into the database.
6. An examination of the different methods for calculating fuel consumption from the parameters collected and a reasoned argument to explain why one method has been chosen for this work.

3.2 Testing Equipment

3.2.1 Test Vehicle

3.2.1.1 Development of Toyota Prius

This work focuses on the Toyota Prius because it is the bestselling hybrid vehicle on the market today (Toyota, 2012). There have been four generations of the Toyota Prius released so far. The first generation was launched in 1997 and came to the UK in 2000. The second generation was launched in the UK in 2004, the third generation in August 2009 and fourth generation has just been released, after its introduction at the Frankfurt motor show in September 2015 (Toyota, 2015b).

3.2.1.2 Vehicle Specification

The vehicle tested in this project was a 2009 third generation Toyota Prius. The vehicle was purchased second hand from a registered Toyota dealer in 2014 with 26,000 miles on the odometer. A detailed vehicle specification is presented in Table 3.1.

The Prius has two motors as part of its powertrain. The larger motor which provides traction power during all-electric mode driving will be referred to as the motor and the smaller motor which normally transfers power from the engine to the battery will be called the generator. For both motors, motoring will be denoted by positive power and generating by negative power. In line with this, negative battery power signifies battery charging and positive power battery discharging.

Table 3.1: Third generation Toyota Prius specification (Rask et al., 2010)

Parameter	Value
Year of Registration	2009
Vehicle Weight	1370 kg
Vehicle Mileage	42,000 km (26,000 miles)
Engine Type	Aluminium double overhead cam (DOHC) 16-valve VVT-i 4-cylinder
Engine Displacement	1.8 litres (1798 cc)
Engine Bore x Stroke	80.5 mm x 88.4 mm (3.17 in x 3.48 in)
Engine Compression Ratio	13.0:1
Engine Valvetrain	Variable Valve Timing with intelligence (VVT-i)
Engine Induction System	Sequential multi-point EFI with Electronic Throttle Control System with intelligence (ETCS-i)
Engine Power Output	73 kW @ 5200 rpm
Engine Torque	142 Nm @ 4000 rpm
Motor Type	Permanent magnet AC synchronous motor
Motor Power Output	60 kW
Motor Torque	207 Nm
Motor Voltage	650 V
Generator Type	Permanent magnet AC synchronous motor
Generator Power Output	42 kW
Generator Voltage	650 V
Traction Battery Type	Sealed Nickel-Metal Hydride (Ni-MH)
Traction Battery Power Output	27 kW
Traction Battery Cell Number	168
Traction Battery Cell Voltage	1.2 V
Traction Battery Voltage	201.6 V
Traction Battery Capacity	6.5 Ah

3.2.2 Data Loggers

The vehicle was fitted with two vehicle activity measurement devices, one from Racelogic and a second from HEM Data Corporation.

3.2.2.1 Racelogic Data Logger

The Racelogic setup comprised a VBOX Lite II, connected to a CAN02 module and an IMU03 module. All the modules are powered through the VBOX Lite II which is connected to a 12V cigarette lighter power socket in the car. Data collected by all the modules is logged by the VBOX Lite II onto a 2GB compact flash memory card at 2Hz. The CAN02 module is connected to the car CAN via a CAN GO Click connector that clips over the two CAN wires behind the dashboard. The VBOX Lite II and CAN02 modules are stored in the central compartment between the front two seats as this compartment has a 12V power source. The IMU03 is bolted to a custom built frame that that is connected to the passenger seat running rails, this provides a firm connection between the module and the chassis. Figure 3.1 shows how the Racelogic setup is connected and Table 3.2 presents the parameters collected by each module (Racelogic, 2014).

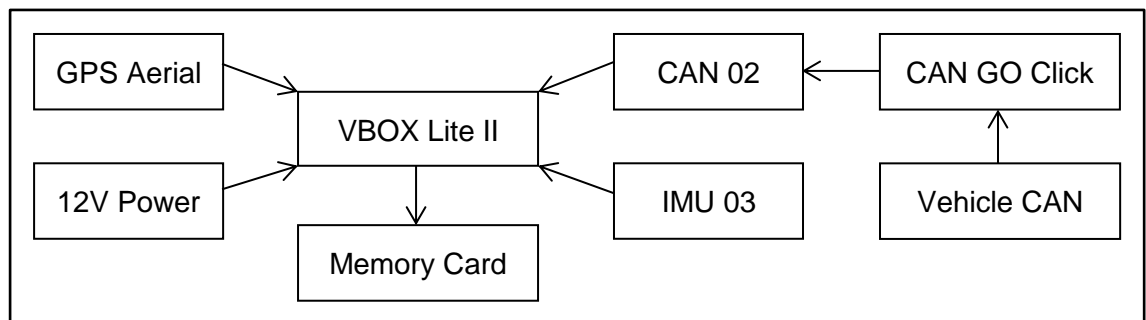


Figure 3.1: Racelogic module setup

Table 3.2: Racelogic parameters collected by Racelogic unit

Module	Parameters Collected	Units
VBOX Lite II	Number of Satellites	-
	Time Elapsed	Seconds
	Latitude	Minutes
	Longitude	Minutes
	Vehicle Velocity (based on satellite position data)	km/h
	Heading	Degrees
	Height	Meters
	Vertical Velocity	m/s
CAN02	Brake Pedal	-
	Wheel Speed	km/h
	Odometer Reading	Miles
	Vehicle Velocity (based on CAN data)	km/h
	Engine Speed	RPM
IMU 03	Yaw Rate	°/s
	Pitch Rate	°/s
	Roll Rate	°/s
	X Acceleration	g
	Y Acceleration	g
	Z Acceleration	g

3.2.2.2 HEM Data Logger

The HEM Data Corporation data logger used was the HEM Data DAWN OBD Mini Logger. This module plugs directly into the vehicle OBDII port, found under the steering wheel. It does not require a separate power source and it logs data directly onto a 32GB

microSD memory card at 2Hz. Along with the data logger, a database of Toyota Prius specific enhanced OBD parameter ID's were purchased from HEM Data Corporation. The database contains over 500 parameter ID's, the data logger was programmed with twenty-seven parameters from the database. The specific parameters collected in this study are presented in Table 3.3 (HEM Data, 2016).

Table 3.3: HEM Mini Logger parameters collected

Parameters Collected	Units
Time Elapsed	Seconds
Throttle Position	%
Vehicle Velocity	km/h
Calculated Load	%
Vehicle Load	%
Road Surface Gradient	m/s ²
Ambient Temperature	°C
Coolant Temperature	°C
Engine Warm Up Request	-
Catalyst Temperature	°C
Mass Air Flow (MAF)	g/s
Air Fuel Ratio	-
Fuel Injection Volume	ml
Fuel Cut Condition	-
Engine Speed	RPM
Engine Torque	Nm
Engine Power	kW
Generator Speed	RPM
Generator Torque	Nm
Motor Speed	RPM
Motor Torque	Nm
SOC	%
Traction Battery Current	Amps
Traction Battery Voltage	Volts
Air conditioning Request	-
Air conditioning Consumption Power	Watts

3.3 Testing Methodology

3.3.1 On-Road Data Collection

All the data for this project was collected between January and July 2015 in order to include the full range of ambient temperature and weather conditions common in the UK. The test driver for all the data was a 24 year old male, multiple test drivers would have been preferable to give a range of driving styles; however, due to time constraints, this was not possible. Instead, the driver was given three driving styles, described in Section 3.3.1.1.3, to follow on different test runs. Throughout the testing period the driver completed regular test runs under urban/congested, urban/uncongested, and motorway conditions. In total over 700,000 recording were taken, this equates to around 100 hours or 4 days of driving data covering 2,500 km (1550 miles).

The time and routes driven needed to be carefully selected to provide the best data for the given application. For this work there are three different applications for the data: 1) analysis of the Prius drivetrain and controls, 2) modelling the vehicle and 3) studying taxi use. Two databases were created, database A for studying the drivetrain controls and modelling the vehicle and B for studying taxi use, summarised in Table 3.4.

Table 3.4: Summary of data collection and applications

Data Application	Database	Test Routes in Database
Studying drivetrain controls	A	City route, motorway route, taxi route 1, taxi route 2, taxi route 3, taxi route 4
Vehicle modelling	A	City route, motorway route, taxi route 1, taxi route 2, taxi route 3, taxi route 4
Studying taxis	B	Taxi route 1, taxi route 2, taxi route 3, taxi route 4

3.3.1.1 Taxi Data Collection Campaign

3.3.1.1.1 Interviews with Taxi Drivers

Leeds City Council conducted two interviews in order to better understand the Leeds taxi driving community. The first interview was with the Head of Streamline Cabs, one of a small number of companies that represents the taxi drivers of Leeds. As a previous taxi driver and one of the leading representatives of the Leeds taxi driving community, he was able to provide a lot of background information about taxi driving in Leeds. The results of this interview informed the taxi test routes chosen in this project, presented in the next section.

The second interview was with one of the three drivers currently driving a hybrid taxi in Leeds. All three drivers were invited to come in and discuss their experiences of using a hybrid vehicle as a taxi in Leeds, but only one person contacted responded. The results of this interview are compared against this studies fuel consumption findings in Section 5.4.5.5.

3.3.1.1.2 Test Routes

The routes driven for the taxi study were chosen after discussion with taxi drivers. From these discussions, we learned that a usual taxi drivers shift is 12 hours, consists of 10-15 jobs, 8-9 hours of driving, 3-4 hours of queuing, 50% of jobs travel to around band A, 25% of jobs travel to around band B and the final 25% could be anywhere beyond band B, probably around band C, see Figure 3.2. Each route starts at a taxi drop-off location, heads into the city centre to the train station, queues through the station taxi rank and then heads out of the city centre to a different drop-off point. Figure 3.2 shows the routes used, with annotations showing the route start point (S), finish point (F), the location of the train station and the distances for bands A, B and C (*Interview Head of Streamline Cabs, 2015, Unpublished Data*).

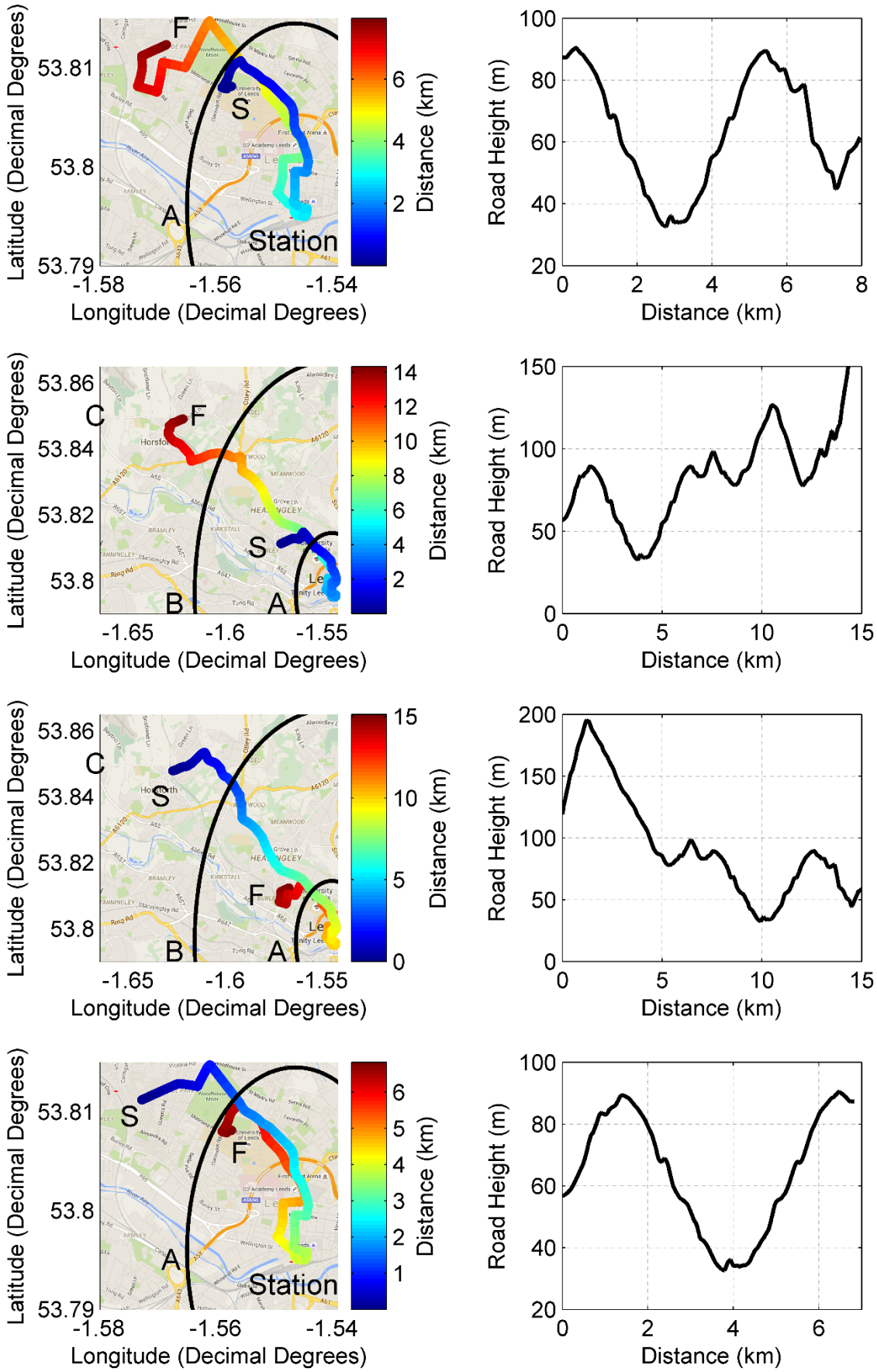


Figure 3.2: Leeds four taxi test routes with route height profile

3.3.1.1.3 Test Procedure

In this study driving tests were conducted between 28th April 2015 and 21st May 2015, this period was chosen as it does not include any school or university holidays that may affect the traffic. Driving was conducted on Tuesdays, Wednesdays and Thursdays, as Mondays and Fridays were expected to be irregular. Each day 8 trips were driven, 4 in the morning, starting at 7.15am and ending between 10.00 - 10.30am, and the same 4 trips in the afternoon, starting at 2 pm and ending between 5.15 – 6.00 pm. The vehicle test routes were chosen to include similar levels of urban and suburban driving to real taxis. The test timings were chosen to include roughly equal amounts of peak and off-peak traffic conditions, where peak times are estimated to be between 7.30am, and 9.30am in the morning and 4.00pm, and 6.00pm in the evening. Each day of testing is roughly half the number of hours and trips of a real taxi shift.

As we could not ensure that the test drivers driving style was similar to real taxi drivers, three driving styles were used to cover the full range of driving styles possible. Each day the driver tried to drive in a particular driving style; calm, normal, or aggressive. Each week contained three days of testing and each day the driver followed one of the three different driving styles. Testing was conducted over three consecutive weeks so each driving style was repeated three times. In total 9 days of driving were conducted, this corresponds to 72 trips, 24 driving calmly, 24 driving normally and 24 driving aggressively. In total over 50 hours corresponding to 780km (484 miles) were driven during testing.

During calm driving, the cars eco mode was selected, which provides the driver with feedback showing the power demanded and suggests an optimum target level, to minimise the use of the ICE. The driver aims to keep the power demand close to this optimum level while accelerating up to the speed limit. The driver also aims to decelerate slowly so that the power from regeneration does not exceed the battery maximum charge rate.

During normal driving, the car is left in its default mode, which is the mode the car is in when turned on. In this mode, the driver is given no feedback from the car about their driving style. The driver aims to follow the traffic, matching their driving with the acceleration, speed and deceleration of the neighbouring cars.

During aggressive driving, the cars power mode is selected. In this mode, the driver is given no feedback from the car about their driving style. In these tests, the driver aims to pull away from stops quickly and break later coming up to stops. The driver also changes lane more regularly to be in the fastest lane or to move further up the queue at traffic lights, while always obeying road speed limits.

Table 3.5: Taxi testing overview

Parameter	Calm	Normal	Aggressive
Number of Runs	24	24	24
Total Time (hours)	17.3	16.3	15.9
Total Distance (km)	260	260	260
Route 1 Time (min)	38.5	37.4	38.4
Route 1 Distance (km)	7.68	7.69	7.69
Route 2 Time (min)	51.8	48.6	50.0
Route 2 Distance (km)	14.2	14.2	14.2
Route 3 Time (min)	48.4	46.8	42.6
Route 3 Distance (km)	14.8	14.8	14.8
Route 4 Time (min)	34.8	29.7	28.6
Route 4 Distance (km)	6.68	6.70	6.70
Peak Time (hours)	9.36	9.12	8.30
Peak Distance (km)	139	142	136
Off Peak Time (hours)	7.98	7.13	7.65
Off Peak Distance (km)	121	119	124
Idle Time (hours)	6.72	6.63	6.76
Average Speed (km/h)	15.0	16.0	16.3
Average Positive Acceleration (m/s/s)	0.188	0.237	0.274
Average Negative Acceleration (m/s/s)	-0.221	-0.255	-0.268

3.3.1.2 Commuter Data Collection Campaign

To ensure this work captures the full range of Prius drivetrain operating modes and controls and to build a model capable of representing all Prius operation it is important

that the testing procedure cover the widest range of driving situations possible. This includes different ambient temperatures and weather, driving styles, road types and traffic conditions. As the taxi database B did not achieve this it was supplemented with data over two routes, City and Motorway route, which were regularly driven at rush hour and non-rush hour, throughout the testing period (January to July), on top of runs completed for business travel, to create database A which is more representative of driving in the UK.

3.3.1.2.1 City Test Route

City route, presented in Figure 3.3 is designed to follow a common commuting route from the north of Leeds into the city centre. The route starts on the outer ring road with a speed limit of 97 km/h (60 mph), this is followed by the A660 which connects the outer ring road to the centre of town, the speed limit of this road is 48 km/h (30 mph). The A660 passes through Headingley on the way into town, this area is built up with housing and shops, becoming congested at rush hour due to three pedestrian traffic light crossing. The route goes through the centre of town and round the inner ring road, with a speed limit of 48 km/h (30 mph), before heading back to the starting point along the same route. The complete loop covers around 21 km (13 miles) and takes between 40 minutes and 2 hours to complete.

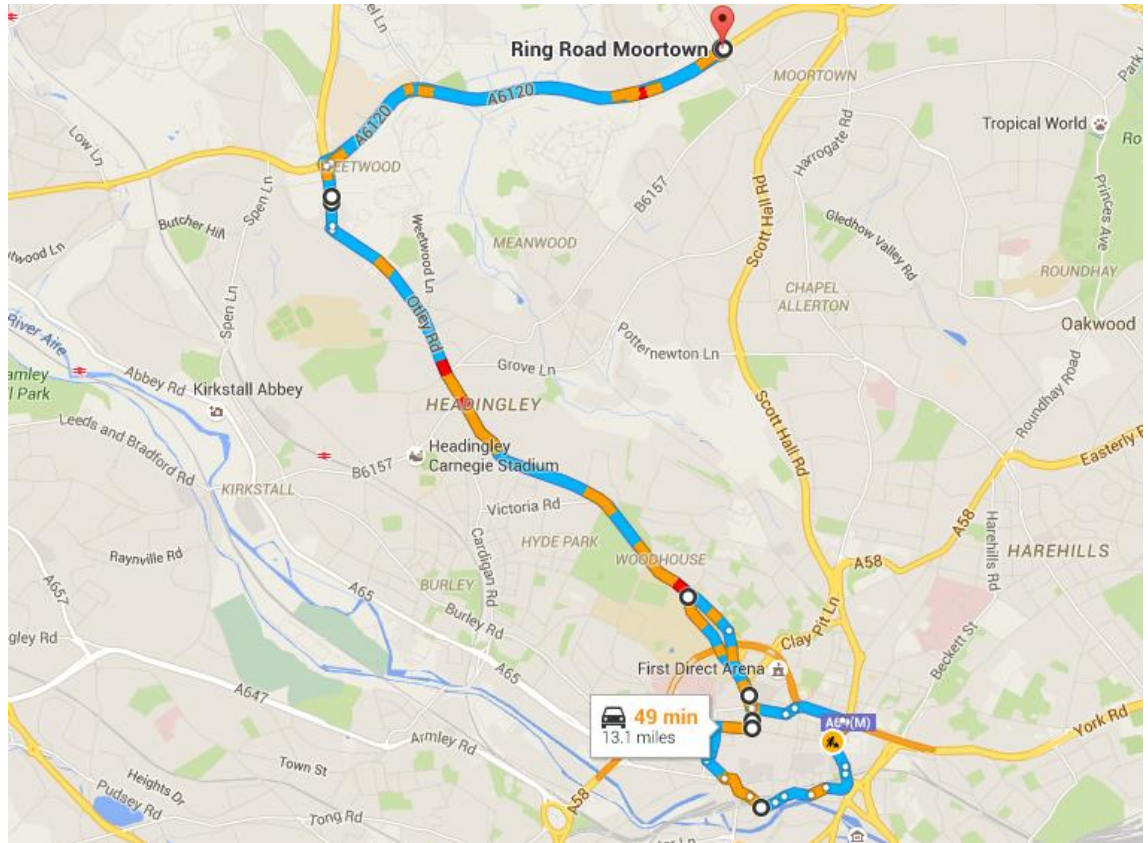


Figure 3.3: Route one, city test route

3.3.1.2.2 Motorway Test Route

Motorway route, presented in Figure 3.4 was designed to include motorway driving and follows a regular commuting route from the south side of Leeds. The route starts at junction 26 on the M62, passing along the M1 and M621 heading into the centre of Leeds. This slightly less direct route was chosen because it increases the amount of motorway driving in the route. All of these roads have a speed limit of 113 km/h (70 mph). The route then heads into the city centre, to the University, starting on a dual carriage way with a speed limit of 64 km/h (40 mph) and finishing by cutting through residential roads with a speed limit of 48 km/h (30 mph). The loop covers around 58 km (36 miles) and takes between 50 minutes and 2 hours to complete.

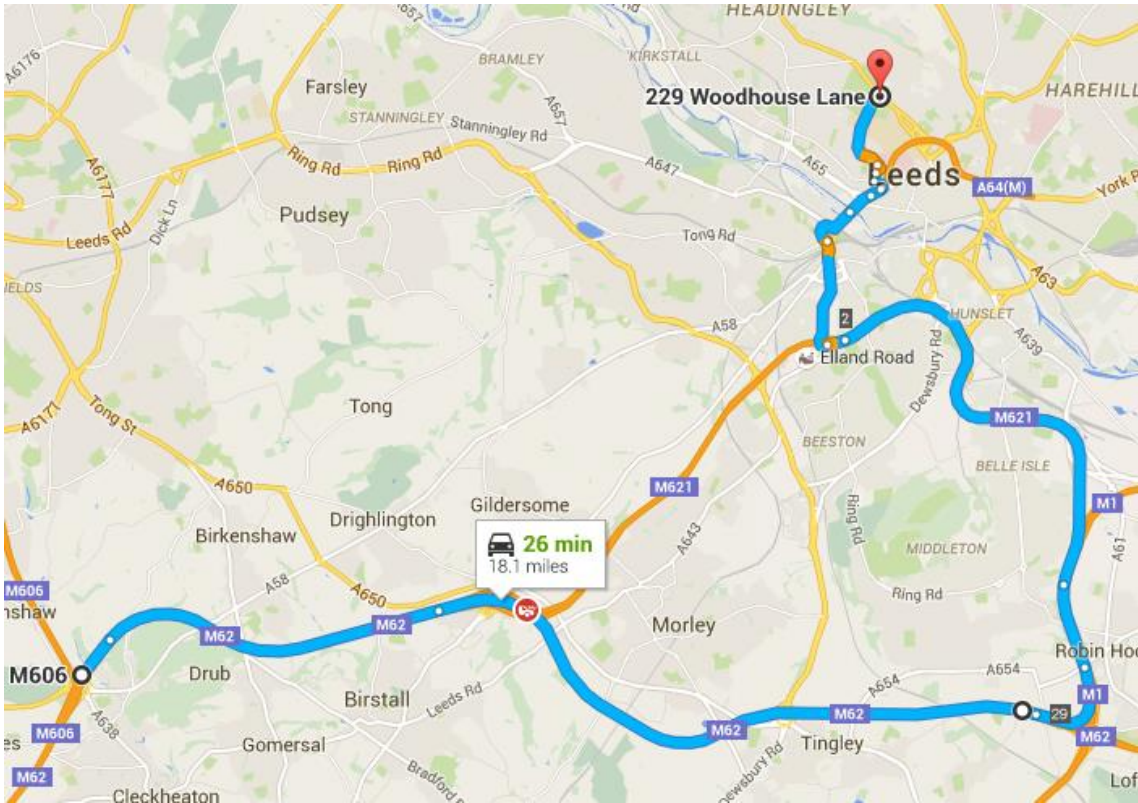


Figure 3.4: Route two, motorway test route

3.3.2 Data Post Processing

Accurately recording vehicle location and road gradient is very important for calculating instantaneous vehicle power demand. Road gradient was recorded as an acceleration by the IMU 03 and is also available as a CAN channel through the HEM mini logger. In both cases, it was found that the data required complex filtering to remove the effects of the uneven road surface and the vehicle suspension, especially when the vehicle accelerated away from, or came to, a stop.

Instead, a road gradient method based on Wyatt et al. 2013 has been developed. This method uses a Digital Surface Model (DSM) created from 2m LiDAR data. In this method, a map of Leeds road network is overlaid onto the DSM in ArcGIS, a mapping software, and the height above sea level is extracted from the DSM at regular points along the road network. This data is then filtered to remove positive spikes from the data, caused

by overhanging trees or buildings and then smoothed, using a moving average, to give a gradient profile free from unrealistic gradient changes (Wyatt, Li, & Tate, 2013).

The Racelogic GPS is accurate to within 1.5 m, 95% of the time (Racelogic, 2008). This means the GPS reading never falls on the road network used to extract the height data from the DSM. To overcome this problem the routes driven are extracted from the road network data and all the GPS data is corrected to the nearest point on the road network routes. In some cases where the vehicle drives under a bridge or the GPS inaccuracy, at low speeds, results in the points jumping backwards, this first correction is not enough. A second correction based on vehicle speed, predicts the vehicle position based on the previous point and the vehicle speed. This correction is used to prevent the points from moving backwards along the route, stops the points from moving when the vehicle is stationary and inserts new points when overhanging structures or tall buildings cause major errors in the GPS position.

3.4 Test Data Distribution

To be confident in the analysis of the vehicle and the model's predictive abilities, it is important that the database collected incorporates the full range of vehicle operating conditions regularly experienced in the real world. Figure 3.5, 3.6 and 3.7 show the range of vehicle speed, road gradient and ambient temperature data covered by all the data collected (database A). The database gives good coverage of the different travel regimes from urban congested to free flow high-speed motorway driving and should provide a robust basis for vehicle analysis and modelling. The distribution of vehicle speeds and accelerations collected in this project is a good match with the distribution of the EU data used to build the WLTC. Indicating that the data collected is reasonably representative of EU driving (Tutuianu et al., 2015).

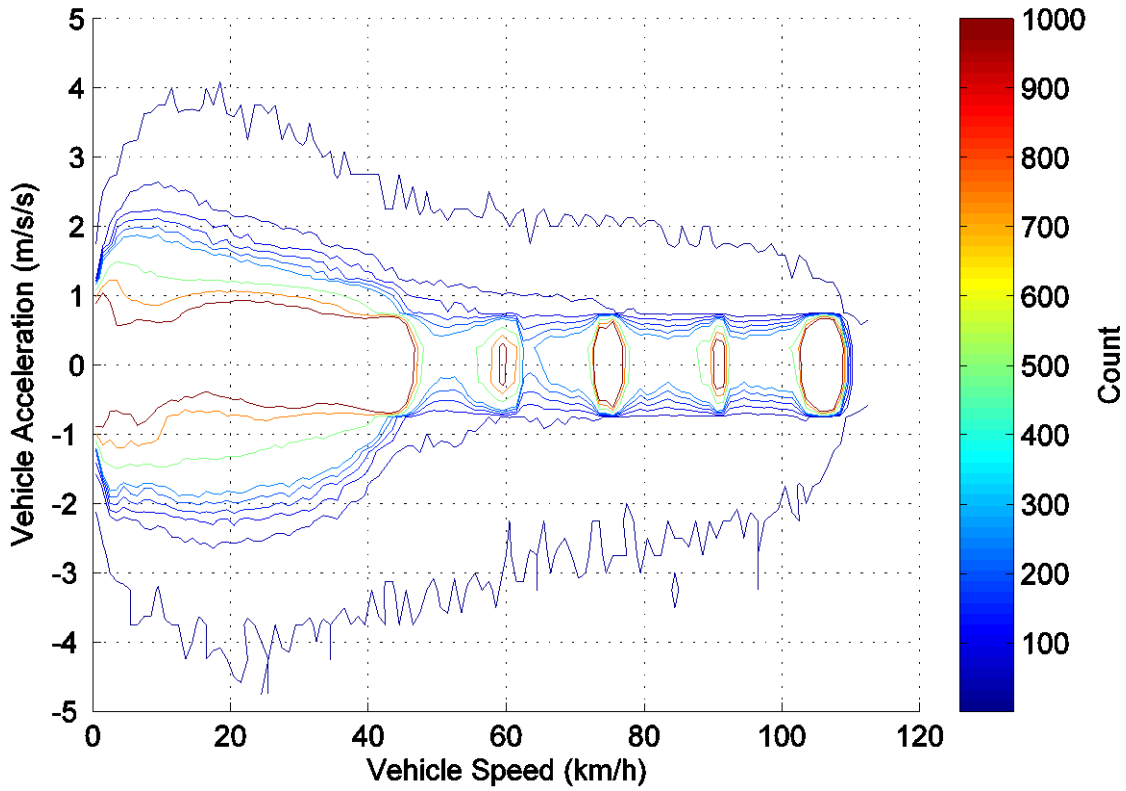


Figure 3.5: PAMS database distribution across vehicle speed and acceleration

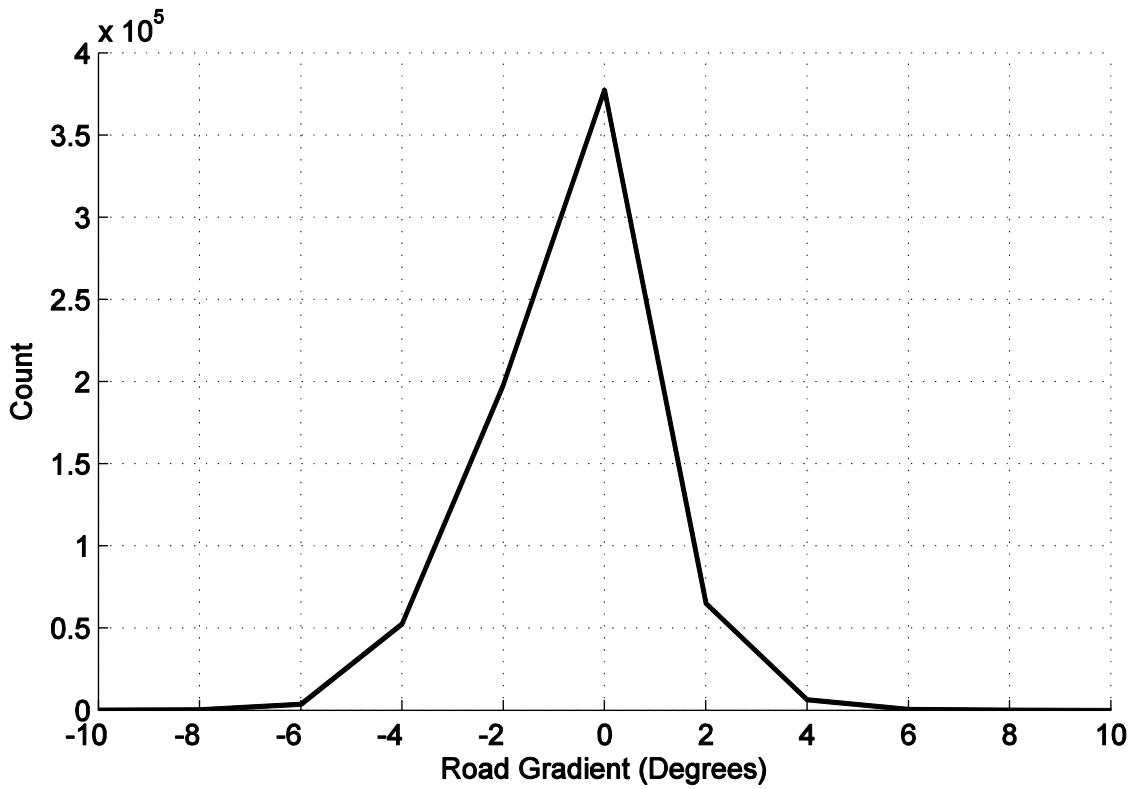


Figure 3.6: PAMS database distribution across road gradient

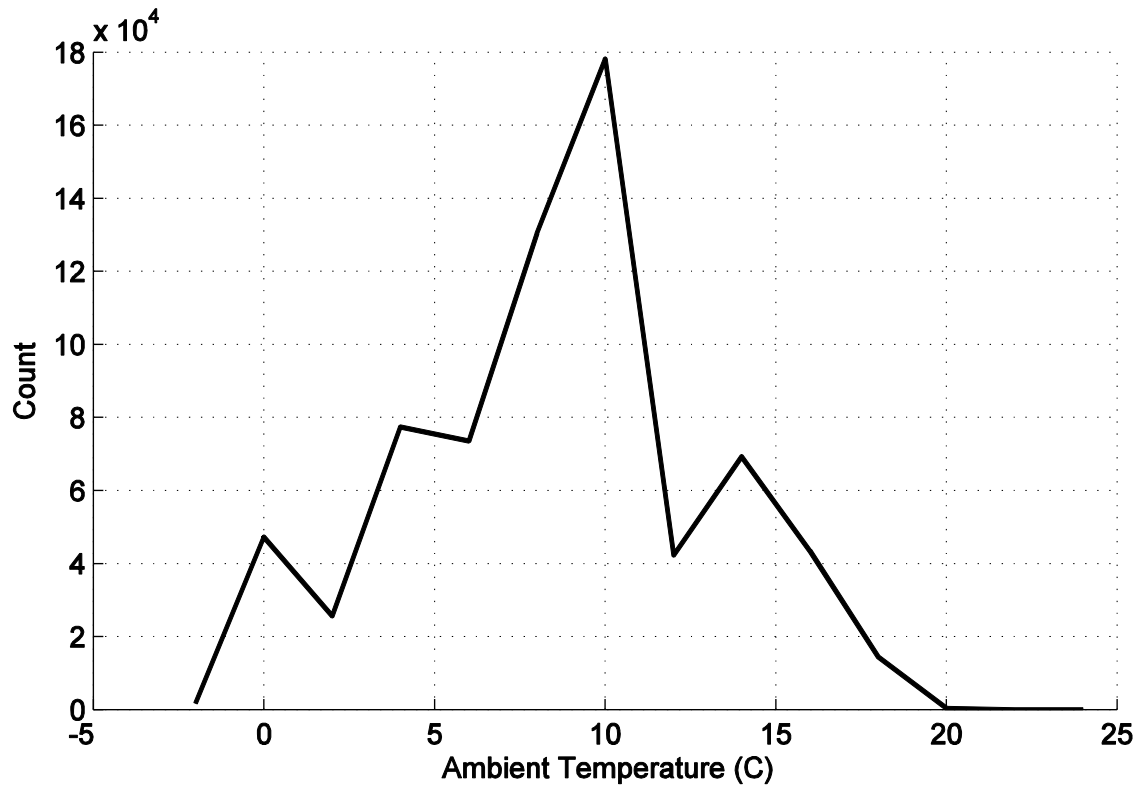


Figure 3.7: PAMS database distribution across ambient temperature

The database can also be separated by cabin heating on or off. The cabin heating off database includes over 550,000 readings and the cabin heating on database around 150,000 readings. The cabin heating off database was collected over the whole testing period and includes the full range of ambient temperatures. The cabin heating on database was only collected early on in the year and only includes colder ambient temperatures.

Unfortunately, due to the complexity of collected road gradient data, tractive power is only available for a subset of the full database (database A). This was carefully collected so as to include both urban and motorway driving, and to include a good spread of data across all vehicle speeds. This section of the database has 380,000 readings and forms the core data that is used for all vehicle analysis and modelling.

3.5 Fuel Consumption Determination

The HEM data logger collects two groups of parameters that can be used to calculate fuel consumption. The first method is based on the rate of fuel delivered at the fuel injector and the second on the MAF into the engine. The next two sections outline the two calculation methods and then a comparison is made in the third section to rationalise why one method is taken forward for use in this work.

3.5.1 Injection Rate

The fuel injection volume obtained from the HEM system is a measure of the last 10 injections in cylinder one. This is converted into fuel rate using Equation 3.1. The drawback of this method is that it assumes that the current fuel injection rate is one tenth of the last ten fuel injections (Timothy H. DeFries et al., 2014).

$$Fr = \frac{F_{Inj} \times N_C \times RPS \times Inj_{Rate}}{N_I} \quad Eq. 3.1$$

Fr = Fuel Rate (ml/s)

F_{Inj} = Fuel Injection Volume (ml)

N_C = Number of Engine Cylinders

RPS = Engine Speed (RPS)

Inj_{Rate} = Number of Injections per Engine Revolution

N_I = Number of Fuel Injections Measured by Fuel Injection Volume

3.5.2 Mass Air Flow

This method calculates the fuel consumption rate in ml/s using Equation 3.2. The equation calculates the amount of fuel required for stoichiometric combustion based on the MAF and then corrects this figure for non-stoichiometric combustion based on lambda. Lambda is the ratio of the actual air-fuel ratio to the stoichiometric air-fuel ratio

and is calculated using the O₂ level in the exhaust stream, measured by the wide band oxygen sensor (Timothy H. DeFries et al., 2014).

$$Fr = \frac{MAF}{\rho_F \times \lambda \times AF_{St}} \quad Eq. 3.2$$

MAF = Mass Air Flow (g/s)

P_F = Fuel Density (g/ml)

λ = Lambda, Fuel Equivalence Ratio

AF_{st} = Stoichiometric Air Fuel Ratio

3.5.3 Fuel Consumption Method Comparison

These two methods were compared by DeFries et al. 2013. They found the injection method total fuel consumption to be 3.3% higher than the MAF method and the average instantaneous percentage difference to be 22% higher. This agrees well with the data collected in this project, which found a total difference of 4.77% and an average instantaneous difference of 18.6%.

The two fuel consumption methods have not been compared against chassis dynamometer data, so there is no definitive answer to say which method is more accurate. However, when comparing the two methods on a Prius DeFries et al. 2013 found that most of the difference occurred during engine transients, especially *engine on* and *off*. The MAF method has a faster response to changes in engine load, while the injection method data often lags behind the MAF data by 1 second. When the two methods were compared on a Toyota Camry it was found that the majority of the error occurred when the throttle input was very low, the MAF signalled dropped down and the injection signalled response was slow and took time to follow. In this situation, it is expected that the MAF signal is correct (T.H. DeFries, Sabisch, & Kishan, 2013).

Figure 3.8 shows an *engine on* event from the test data, it is clear that the situation where the throttle drops to zero and the injection fuel consumption overshoots found by DeFries

et al. 2013 on the Toyota Camry is also occurring in the Toyota Prius test data. To try and quantify the effect of this overshoot the difference between the two methods was compared for the last three seconds of each *engine on* event. It was found that 40% of the difference between the two signals where the injection value was higher than the MAF value occurred during this engine off phase.

Based on the findings of DeFries et al. 2013 and analysis of the test data, it has been found that the MAF based method, of computing fuel consumption, reacts better to the transient changes of the engine, resulting in a better correlation with engine load. Good time alignment with the other test parameters is an important characteristic of good empirical modelling data, it has therefore been decided to use the MAF based approach in this study.

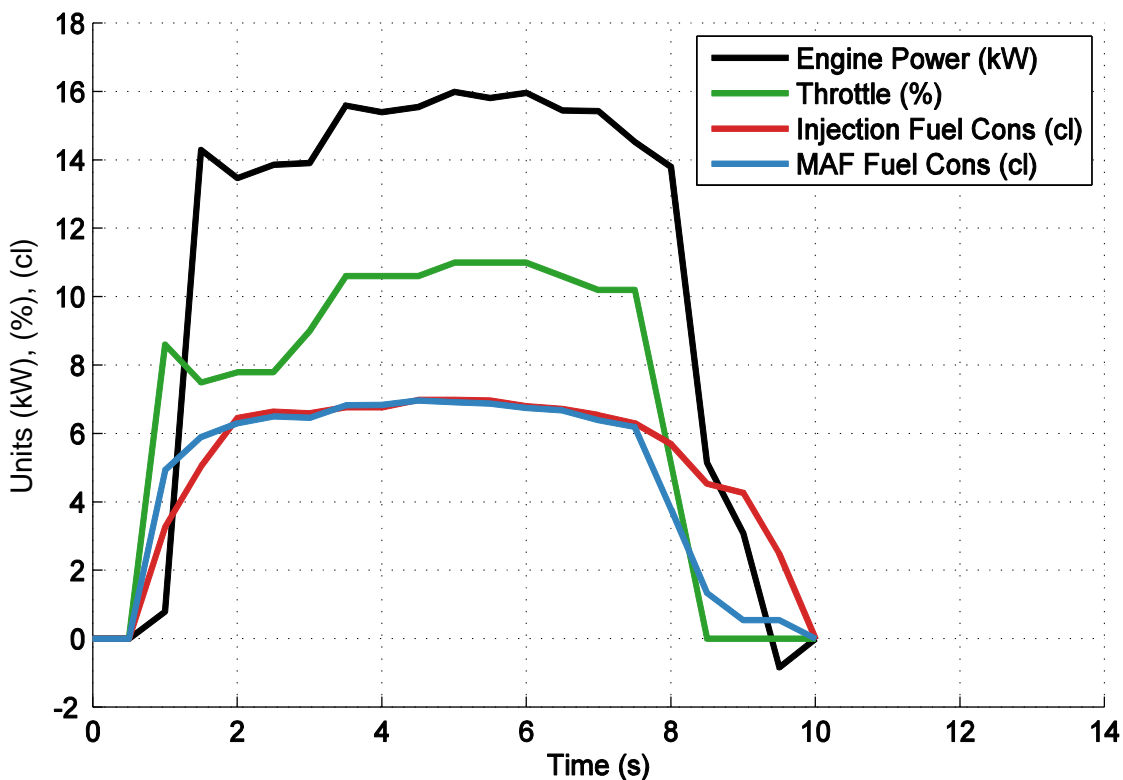


Figure 3.8: Comparison of PAMS injection and MAF fuel consumption methods

3.6 Conclusions

A successful method has been developed that can collect both external and internal vehicle activity data. The data is well distributed across vehicle speed, acceleration, road

gradient and ambient temperature. By covering the full range of driving conditions the data will form a strong basis for vehicle analysis in Chapter 4 and vehicle modelling in Chapter 6. An accurate fuel consumption method has been presented that provides high-frequency data that is well time aligned to engine operation. The success of this method is demonstrated in Chapter 6 by building a model from the data and validating the model against independent data from a chassis dynamometer.

Chapter 4

Analysis of a Hybrid Vehicle

4.1 Introduction

This chapter presents an in-depth analysis of the powertrain controls of a third generation Toyota Prius based on the real-world activity data in database A and discussed in Chapter 3. This includes:

1. A systematic review of the academic literature to present a complete picture of the current understanding of the Toyota Prius powertrain design and controls.
2. An assessment of all the known Prius powertrain controls using the PAMS data from chapter 3 to demonstrating that the PAMS data can accurately display all the Prius powertrain control patterns that have been found using other data collection methods.
3. A further analysis of the PAMS data to discover new aspects of the Prius powertrain control that have not been previously published in the public domain.

In the past, an in-depth understanding of the complexities of vehicle powertrains has been left up to engineers working for vehicle manufacturers. However, as academics, consultants and policymakers, spend more time working with, and on, vehicle emission models, local vehicle emission policies and national vehicle emission standards. It is increasingly important that vehicles are understood to avoid, the inappropriate use of models, misdirected local policy and weak nation vehicle standards that allow emission breaches like the VW emission scandal last year.

Most of our understanding of how the Toyota Prius operates comes from vehicle testing conducted by several National Laboratories in the USA. This testing included taking the vehicle to pieces and testing individual components, as well as whole vehicle chassis dynamometer testing with sensors located between components to measure the

operation of each component (Burress et al., 2011; Rask et al., 2010). This level of detailed testing is necessary to understand how the vehicle works, but it is an impractical method when so many different vehicle makes and models need to be examined.

4.2 Literature Review

4.2.1 Vehicle Physical Specification

The basic vehicle specification and component sizing are given in Section 3.2.1. This subsection provides a more detailed explanation of the vehicle powertrain, engine and after-treatment systems, as the design of these systems strongly influences the emission results presented in Chapter five and Chapter six.

4.2.1.1 Powertrain

The Toyota Prius drivetrain is a series-parallel, or power split design. The schematic shown in Figure 4.1 below shows the drivetrain configuration with a motor, generator and engine connected together via two planetary gear sets. The Motor Speed Reduction Gear (MSRG) has a fixed carrier gear, this means the gear set acts as a normal gear with a fixed gear ratio (Lee, Lee, McDonald, Sanchez, & Nam, 2014).

In the main Planetary Gear (PG) set both the sun gear and the carrier gears can move independently of the ring gear but not independently of each other. This means that for every vehicle speed there is a generator speed that allows the engine to operate at the desired optimum engine speed. This is obviously limited by the minimum and maximum speeds of the generator, but under normal driving conditions, it allows the engine speed

to be set independently of the vehicle speed (Arata, Leamy, Meisel, Cunefare, & Taylor, 2011).

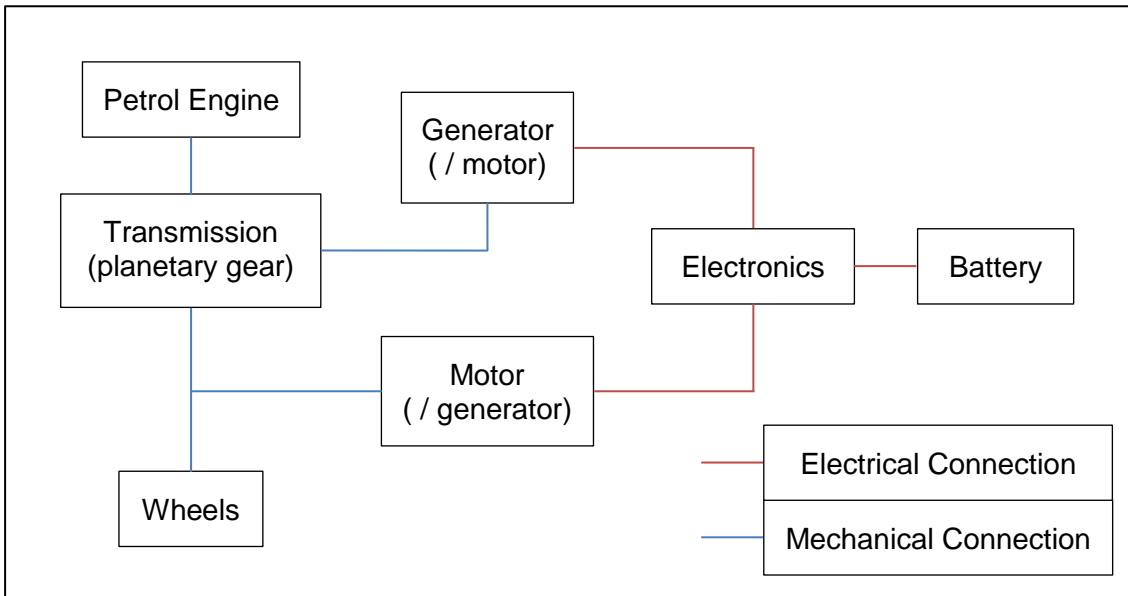


Figure 4.1: Schematic of the Toyota Prius drivetrain

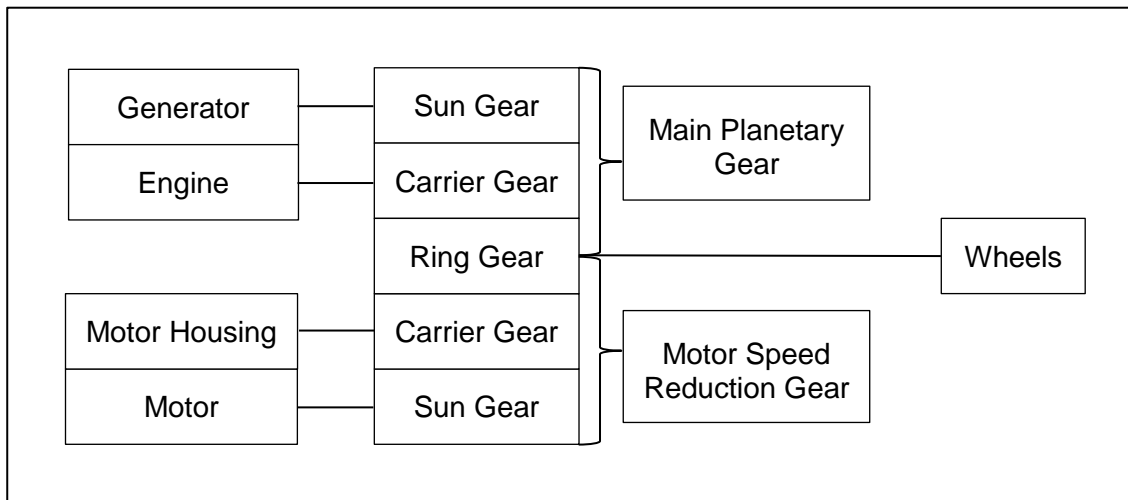


Figure 4.2: Schematic of the Toyota Prius transmission

The literature often defines the power flow through the power split powertrain as either power directed through the mechanical or electric paths. The mechanical path takes power directly from the engine through the main planetary gear to the wheels. The electrical path covers a wide range of other options, but predominantly it refers to power from the engine that passes to the main planetary gear, to the generator, to the motor, to the motor speed reduction gear, to wheels. However, due to the gear ratios used in the Prius powertrain under certain motor speed, engine speed conditions the generator

will slow to a stop and start rotating backwards. When the generator speed drops to zero, this is known as the mechanical point and it is the most efficient operating condition for the powertrain. When the generator spins in reverse it acts as a motor and the normal electric path changes so that the generator acts as a motor and the motor acts as a generator (Arata et al., 2011).

The mechanical path has similar features to a parallel hybrid vehicle, with an efficient drivetrain, but very limited opportunity to improve engine efficiency through better control. The parallel architecture is most efficient during motorway driving when the engine is already in an efficient operating range and the drivetrain transmits the power with minimum losses (Liu, 2013).

The electrical path is similar to a series hybrid vehicle, it has the benefit that it partially decouples the engine operation from the vehicle demand, this helps to optimise the engine efficiency at all times. The drawback of the electrical path is the added inefficiencies of converting the power from mechanical power to electrical power and back again. The series configuration is most effective in city driving when shifting the engine to a more efficient operating point outweighs drivetrain losses. The power split architecture tries to outperform series and parallel hybrids by exploiting the benefits of each drivetrain. The drawback of this design is the very complex control required for it to operate effectively in all the varied conditions experienced in the real world (Liu, 2013).

4.2.1.2 Engine

The third generation Toyota Prius engine employs several technologies that have helped to improve the engine efficiency above other vehicle models and previous Prius generations. The key trio of technologies used in the Prius to reduce fuel consumption are, large engine displacement, Atkinson cycle with late inlet valve closing and cooled EGR at all engine loads. These technologies are, in some cases only beneficial, and in other cases only possible, in a hybrid powertrain (Kawamoto, Naiki, Kawai, Shikida, & Tomatsuri, 2009).

The larger engine displacement reduces heat loss and allows the engine to meet higher power demands at lower engine speeds which reduces frictional losses. This is true for all engines, but in conventional vehicles, these gains at higher powers are offset by increased pumping losses at low engine powers. Whereas, in the hybrid powertrain low powers are met by the motor and thus low engine power operation is mostly avoided (Kawamoto et al., 2009).

The Atkinson cycle uses late inlet valve closing to decouple the engine compression ratio from the expansion ratio. In most petrol engines the compression and therefore the expansion ratio is limited by engine knock, but in the Atkinson cycle, the compression ratio can be reduced to avoid this problem. This allows a 13:1 expansion ratio in the Prius engine which is much higher than the normal 10:1 found in most petrol engines. The higher expansion ratio means the expanding combustion gases do more work on the piston and therefore the engine is more efficient (Kawamoto et al., 2009). The Atkinson cycle is not used in conventional vehicles because it produces low engine output torque, especially at low engine speeds. In a conventional vehicle, this would result in unacceptable vehicle performance, but the Prius powertrain has the support of the motor which can deliver maximum torque at zero revolutions, thus overcoming the shortfalls of the Atkinson cycle engine (Committee on the Assessment of Technologies for Improving Fuel Economy of Light-Duty Vehicles, 2015).

Late inlet valve closing combined with cooled EGR has other benefits. During low load conditions, the Prius engine uses late inlet valve closing and EGR to reduce the air-fuel mixture coming into the cylinder. These two technologies combined allow less use of the engine throttle which reduces low load pumping losses (Kawamoto et al., 2009).

Under high load conditions, the inlet valve is closed earlier to get more air and fuel into the cylinder. This leads to higher compression ratios and engine knock problems. To avoid engine knock many engines delay spark timing, this results in combustion later on in the cylinder expansion which reduces maximum combustion temperatures and engine

efficiency. To reduce spark timing delay the Prius engine uses EGR under high load conditions to cool the combustion. This is not possible in a conventional engine because the whole cylinder volume is needed for air and fuel at high power. The Prius engine, by comparison, is oversized allowing space in the cylinder for EGR even with the maximum power requirements for stoichiometric air and fuel. Using EGR at maximum power allows for higher compression ratios and earlier spark timing without engine knock. In a conventional vehicle high exhaust gas temperatures at high engine load can lead to catalyst damage, this is overcome by injecting fuel into the cylinder late in the combustion cycle. The Prius overcomes this fuel penalty by using cooled EGR at maximum engine load (Kawamoto et al., 2009).

The engine also benefits from being in a hybrid powertrain in ways beyond the engine technology that can be used. The Prius planetary gear decouples the engine speed from the vehicle speed. This allows the Prius engine to operate along an optimised engine speed, torque path, which avoids operating the engine in the most inefficient regions of the engine map (Kawamoto et al., 2009).

The third generation Prius now also uses an electric, rather than a belt driven water pump. This means engine cooling water flow is independent of engine speed. This provides additional cooling at high loads to reduce knock and less cooling during cold starts to speed up engine warm up. This has a strong positive effect on fuel consumption because the engine will not turn off until it has been warmed up (Kawamoto et al., 2009).

4.2.1.3 Aftertreatment System

The Toyota Prius after-treatment system consists of two Three Way Catalysts (TWC) followed by the Exhaust Heat Recirculation System (EHRS). The EHRS is a heat exchanger that uses exhaust gases to heat the engine coolant water during engine cold starts when the cabin heating is on. The key benefit of a hybrid vehicle is that it can turn its engine off for large sections of urban cycles. However, during a cold start, the engine has to stay on to heat up the engine and catalysts, so fuel savings from switching off the

engine are not achieved. When cabin heating is used the heat comes from the engine coolant water, this increases the amount of time it takes for the engine to warm up, forcing the engine to stay on longer. The EHRS tries to overcome this problem with hybrid vehicles by adding as much extra heat to the coolant water every time the engine is on. The EHRS is used throughout engine warm up until a bypass valve opens when the engine coolant temperatures reaches 90°C (Mike Duoba, 2011).

4.2.2 Vehicle Control

4.2.2.1 Main Operating Modes

These are the five basic operating modes of the Toyota Prius presented in the literature.

- Operating mode one, Pure Electric (PE) mode. The vehicle is accelerating at low speeds, the engine is off and the battery supplies power to the motor which drives the vehicle (Toyota, 2015c). The battery in the Prius is quite small and so PE mode is very limited. The car is capable of driving at speeds up to 50 km/h, for a distance up to 1.2 miles, before the engine needs to start to charge the battery (Toyota, 2015b).
- Operating mode two, Hybrid Electric (HE) mode. The vehicle is accelerating or cruising at higher speeds and the engine is on. The engine power is being delivered to the wheels along the two powertrain pathways and some of the power passing through the electrical path is recharging the battery (Toyota, 2015a).
- Operating mode three, full acceleration mode. The vehicle is accelerating very quickly, the engine is on and the battery is supporting the engine during the high power demand (Toyota, 2015a).
- Operating mode four, regeneration mode. The vehicle is slowing down, the tractive power demand is negative and the motor is regenerating power from the momentum of the vehicle to recharge the battery (Toyota, 2015a).

- Operating mode five, the vehicle is stationary and the engine is off (Toyota, 2015a).

4.2.2.2 Overarching Control

The most important parameter in the control of the Prius is the tractive power demand, which is the power at the wheels required to drive the vehicle. Tractive power is calculated from vehicle speed and tractive torque demand, which is calculated by the vehicle, as a function of vehicle speed and accelerator pedal input. The overarching control strategy uses tractive power demand and battery SOC to switch the vehicle between PE and HE mode, to minimise fuel consumption and maintain battery SOC (N. Kim et al., 2012).

The engine turns on when the tractive power goes above a set threshold. The power threshold is a linear function of battery SOC, so that at low battery SOC the engine turns on at lower powers to protect the battery. Once the engine has turned on the battery power is a linear function of battery SOC, at low SOC the battery demands power from the engine and at high SOC the battery assists the engine in driving the vehicle. The flip point from battery charging, to discharging, is 60% SOC, so the control strategy naturally maintains the battery SOC close to this target. To meet the demands of the vehicle and battery the engine target power is a function of the vehicle tractive power, battery demand power and efficiency losses through the powertrain (N. Kim et al., 2012; Namwook. Kim & Rousseau, 2015; Namwook Kim, Rousseau, & Rask, 2012).

The engine turns off either directly or through the fuel cut path. During direct *engine off* the power threshold is a function of tractive power and battery SOC similar to *engine on*, but set at a tractive power threshold. When the driver takes their foot off the accelerator pedal the tractive power demand drops very quickly, and so it is very difficult to pin point the location of the *engine off* threshold. Instead Kim et al. 2012 uses the driver releasing the accelerator pedal as the control signal for *engine off*. The control parameter for switching between direct *engine off* and fuel cut is vehicle speed. At vehicle speeds less

than 20 m/s (72 km/h, 45 mph) the engine turns off directly. At vehicle speeds greater than 20 m/s (72 km/h, 45 mph) the engine switches to fuel cut mode where the engine speed is maintained at idle speed and the fuel to the engine is cut. This control method is used to help turn the *engine on* smoothly, if suddenly required, at high vehicle speeds. Once in fuel cut mode the engine will either switch on again due to driving demand or switch off when the vehicle speed drops below 20 m/s (72 km/h, 45 mph) (N. Kim et al., 2012).

4.2.2.3 Component Control

4.2.2.3.1 Engine

The engine follows an optimised path across the engine speed, torque map. This means that in theory there is only one engine speed, torque value pair for each engine power (Namwook Kim et al., 2012).

4.2.2.3.2 Generator

The generator speed is a function of engine speed and motor speed, defined by the gear ratios of the planetary gear set. When the engine is on, the generator torque is controlled to maintain the engine along its optimised engine path (Namwook. Kim & Rousseau, 2015).

4.2.2.3.3 Motor

The motor is directly connected to the wheels so the motor speed is a function of vehicle speed. When the engine is on the motor torque is controlled to provide the battery with its demanded power (Namwook. Kim & Rousseau, 2015). When no pedal inputs are provided by the driver the motor provides negative torque at vehicle speeds greater than 16 km/h and positive torque at vehicle speeds below 16 km/h. This control is enacted to provide a driving experience similar to an automatic vehicle, for driver comfort. During regeneration mode, the motor power is limited to 27 kW, as this is the battery charging power limit. At very low vehicle speeds the motor stops regenerating and the mechanical

brake acts alone to bring the vehicle to a stop. This is done to provide a smooth vehicle stop for drivers comfort (N. Kim et al., 2012).

4.2.2.3.4 Battery

Battery efficiency is expected to be a function of battery SOC, battery charge and discharge rates and battery temperature (Dhameja, 2002). Kim et al. 2014 found no correlation between battery SOC and battery efficiency, possibly because the battery only operates over a narrow SOC range. If this is the case there should be a linear relationship between battery SOC and battery power and this is what Kim et al. 2014 found in their test data (Namwook Kim, Rousseau, Lee, & Lohse-Busch, 2014).

Battery internal resistance is a cubic function of battery temperature, with the highest resistances occurring at low temperatures and the lowest resistances seen under hot battery operation. Battery temperature has a strong effect on battery efficiency, it might, therefore, be expected that the battery power demand would be adjusted to compensate for this effect. However, Kim et al. 2015 found that while maximum battery charge and discharge rates are limited at high battery temperatures, there was no correlation between battery temperature and battery power demand (Namwook. Kim & Rousseau, 2015).

4.2.2.4 Additional Operating Modes

4.2.2.4.1 Cold Starts

The engine also turns on, independent of tractive power demand, during an engine cold start. An engine cold start occurs when the engine coolant temperature drops below the low-temperature limit. Kim et al. 2015 found this limit to be 53°C, while Kim et al. 2014 found a limit of 52°C and Barrieu et al. 2011 found that when the cabin heating is on the temperature limit is between 55 - 65°C depending on the cabin heating demand, and when the cabin heating is off the limit is 40°C (Barrieu, 2011; Namwook. Kim & Rousseau, 2015; Namwook Kim et al., 2014).

Kim et al. 2015 found three control options based on engine coolant temperature. In the hot situation, greater than 90°C, the vehicle follows the *engine on, off* controls specified in Section 4.2.2.2. In the middle-temperature range, 50 - 90°C, the engine turns on due to the standard controls given in Section 4.2.2.2, but does not turn off until the engine is hot. During a cold start, less than 50°C, the engine turns on straight away and idles. For the first minute, the engine provides no propulsion torque to the vehicle, after this the engine drives the vehicle but runs at idle speed, not at normal running speed. The engine stays on until the vehicle speed drops to zero or the coolant temperature is hot (Namwook. Kim & Rousseau, 2015).

Kim et al. 2012 suggest the first minute of the cold start when the engine does not drive the vehicle is not set by time but runs until the coolant temperature reaches 35°C (N. Kim et al., 2012), while Duoba et al. 2011 proposes that this first section of the engine warm up is not designed to heat up the engine but aims to warm up the TWC, while causes minimum emissions of air quality pollutants (Michael Duoba, Lohse-Busch, Rask, & Carlson, 2011; Mike Duoba, 2011).

The cold start exhibits lower engine efficiencies especially when the engine is idling and no power demand is required. The engine path across the engine speed, torque map is also slightly different during cold start, displaying slightly higher torque values at every engine speed. The engine idle speed is also a function of engine coolant temperature, starting high at very cold temperatures and dropping to hot engine idle speed when the coolant temperature reaches 80°C (Namwook. Kim & Rousseau, 2015).

4.2.2.4.2 Low Battery SOC

The engine can also turn on, independent of tractive power demand, if the battery SOC is too low (Namwook Kim et al., 2014).

4.3 Analysis of the PAMS Test Data

As the dominant hybrid powertrain on the market, it is not surprising that the Toyota Hybrid System (THS) has been so well documented in the academic literature. However, the methods of vehicle testing used in the literature are impractical for testing large numbers of vehicles and the details given are insufficient to build the complete picture of the powertrain operation needed to develop an accurate model of the vehicle architecture.

The PAMS methodology presented in Chapter 3 is particularly well suited to overcoming this information gap, for two reasons. Firstly, the literature is limited to a small number of test runs, over a limited number of drive cycles. Whereas real world PAMS testing covers on-road driving conditions not experienced in the laboratory and is cheap enough that a wide range of vehicle conditions can be tested multiple times. This helps to examine control thresholds, especially during cold vehicle operation which requires many runs to observe. Secondly, this method is recording the same vehicle CAN parameters that the car is using to control the vehicle. This means that, unlike an instrumented car, the signal accuracy and timing is less important because the vehicle control thresholds are based on the data that is being recorded.

The data used in this analysis is the full database collected. This includes the data collected for the taxi study and the additional data collected to broaden the testing conditions covered.

4.3.1 Overview of Vehicle Design

Very little is written in the literature about the structural design of the Prius powertrain beyond stating its physical characteristics (Burress et al., 2011). The large difference in efficiency between the two powertrain power paths makes it vital to understand the physical design of the powertrain, as it will have a strong impact on the overall system controls.

As the literature indicates, the mechanical point where the generator is stationary is the most efficient operating condition for the Prius powertrain (Arata et al., 2011). The generator speed is a function of vehicle speed and engine speed. This means there is an engine speed for every vehicle speed that will give the best powertrain efficiency.

Figure 4.2 shows the percentage of engine power flowing through the mechanical path, and therefore the percentage of engine power flowing through the electrical path, at every vehicle speed and tractive torque. At vehicle speeds less than 40 km/h (25 mph) the engine speed that results in the mechanical point is less than 900 RPM which is the engine's lowest idle speed. This means that if the engine does turn on at these low vehicle speeds, at least 50% of the engine power will pass through the electrical path, resulting in high drivetrain losses. At vehicle speeds greater than 40 km/h (25 mph) the Prius gearing has been designed so that at each vehicle speed, a slight vehicle acceleration results in a tractive power demand, and therefore engine power demand, that according to the engine optimised path gives the engine speed needed for the mechanical point. Higher or lower accelerations, road gradient and battery power demand all alter the engine power demand, and therefore shift the engine speed away from the desired engine speed for the mechanical point. However, as Figure 4.3 and 4.4 show, by designing the gearing so that the mechanical point occurs under the commonest driving conditions most of the data points at speeds greater than 50 km/h (31 mph) have a mechanical path usage greater than 60%. The exception to this is high speed, low torque driving, where the generator spins backwards and operates as a motor. Under these conditions electrical path usage increases resulting in higher powertrain losses, these conditions are avoided, as much as possible, by switching the vehicle to fuel cut mode.

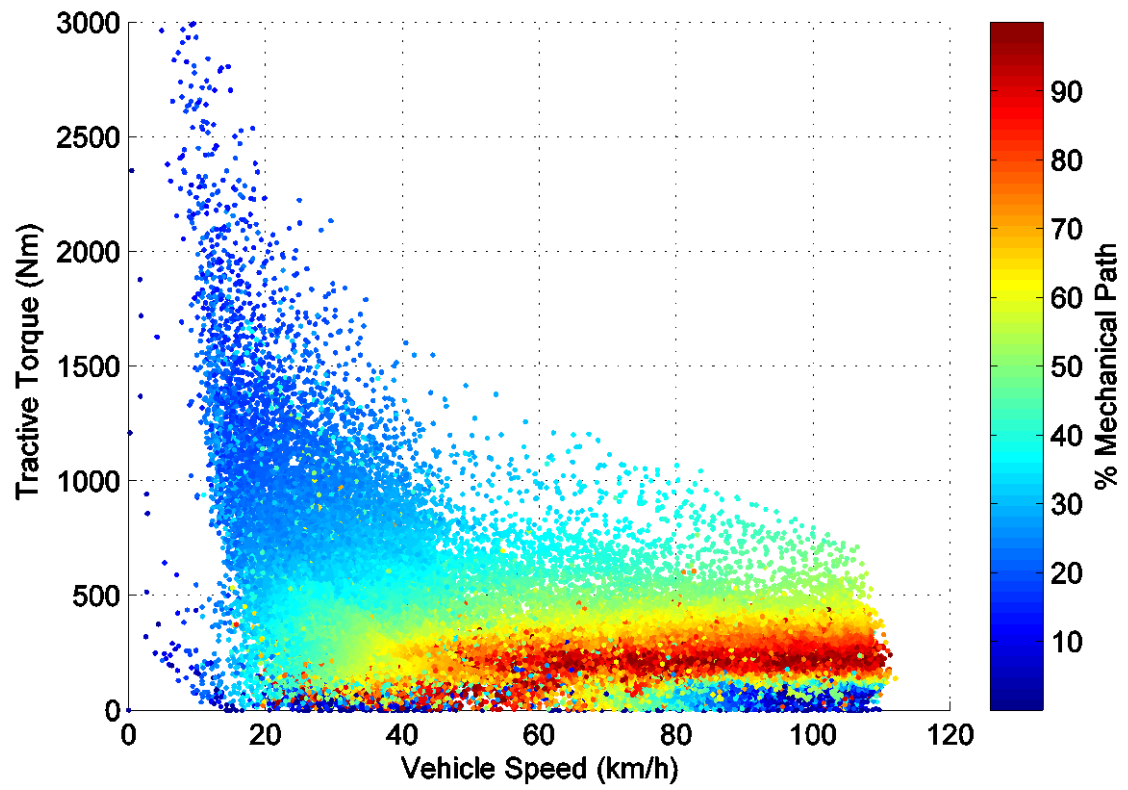


Figure 4.3: Percentage of engine power passing through the mechanical path, over vehicle speed and tractive torque, when the Prius is operating in hybrid electric mode

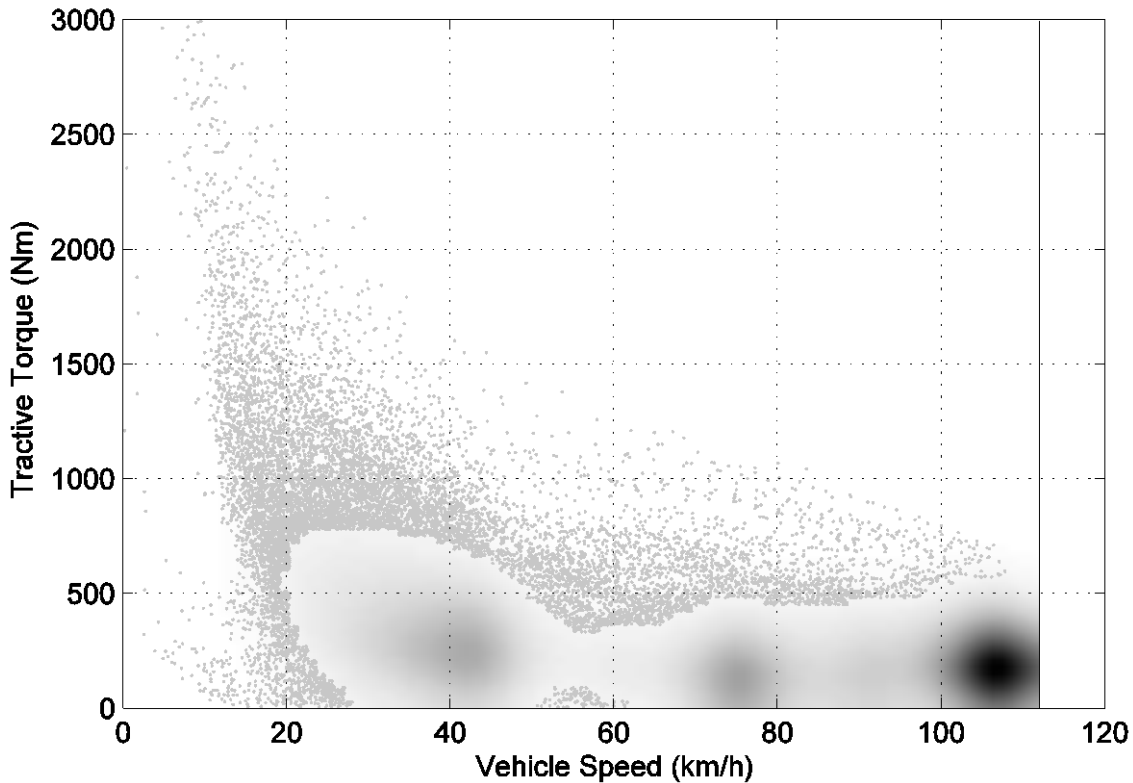


Figure 4.4: Density plot over vehicle speed and tractive torque, when the Prius is operating in hybrid electric mode

Figure 4.5 displays the observed vehicle speed and tractive torque when the vehicle is operating in PE mode. By comparing Figure 4.3 with 4.5 it is evident that PE mode can match much of the vehicle demand in the areas where, if the engine is on, electrical path usage is highest. There is an area between 10 and 50 km/h (6 and 31 mph) where if the tractive torque is very high the battery can't meet the power demand and the engine has to turn on. However, as Figure 4.4 shows this only accounts for a relatively small number of the vehicle operating points in real world driving. Far more important, because of the regularity with which it occurs, is PE modes ability to meet driving demand below 500 Nm of tractive torque and below 40 km/h (25 mph). The highest power points in PE mode track the bottom of the orange/red zone that starts at 40 km/h (25 mph) in Figure 4.3. This means that the electric capabilities of the vehicle have been designed so that in many cases, as the vehicle accelerates it operates in PE mode throughout the low vehicle speed zone where the engine and drivetrain operate at lower efficiencies and

then once the vehicle speed has reached the point where the drivetrain can operate more like a parallel hybrid the engine turns on. By designing the vehicle in this way the motor and Internal Combustion Engine (ICE) complement each other, both allowing the other to be designed and operated for maximum efficiency within their niche.

As Figure 4.3 and 4.5 show, *engine on* points do exist below the capabilities of the electric drive system. This could be because of low engine coolant temperatures, low battery SOC or aggressive driving. As the literature highlighted the *engine off* power threshold is below the *engine on* power threshold (N. Kim et al., 2012). This means aggressive acceleration can result in an *engine on* at low vehicle speeds, then when the driver is constrained by the speed limit, or the traffic, and the vehicle power demand drops back into a power region where PE mode could meet the driving demand the engine is still on. Aggressive driving can, therefore, have a double negative effect on the Prius fuel consumption, demanding more power to drive the same distance and forcing the *engine on*, to operate at low engine and drivetrain efficiencies.

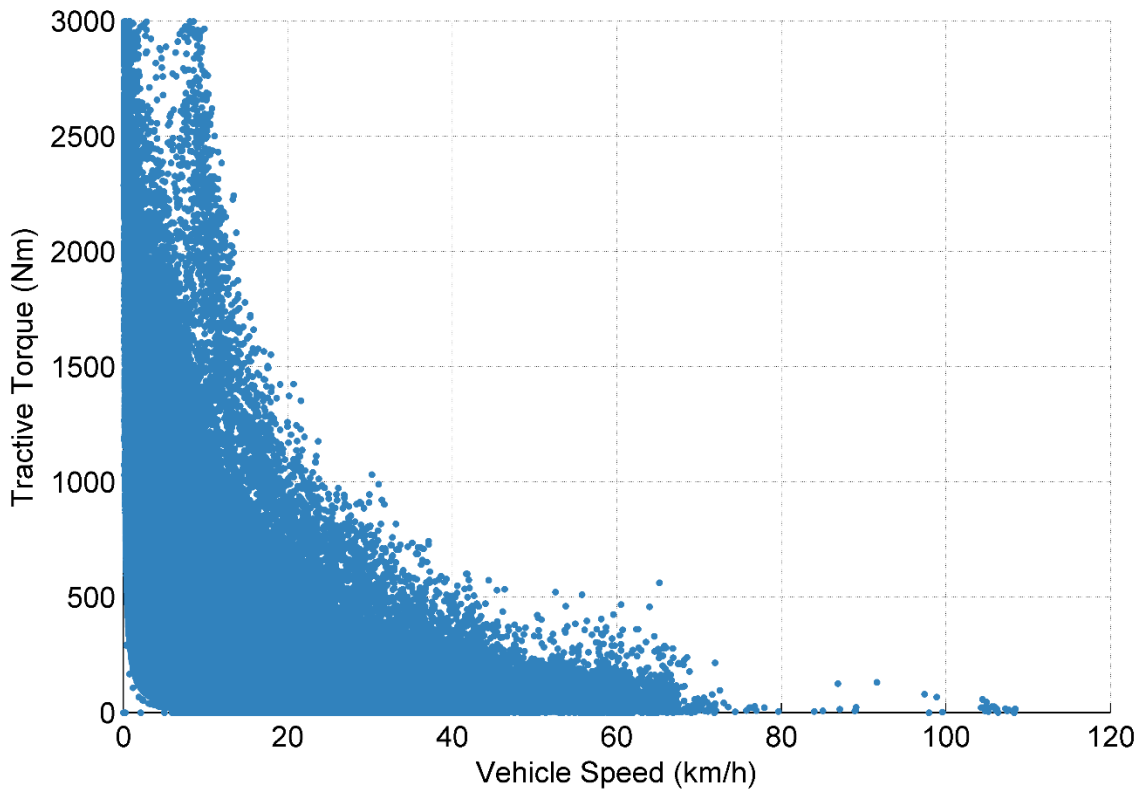


Figure 4.5: Vehicle speed against tractive torque when the Prius is operating in pure electric mode

4.3.2 Vehicle Control

4.3.2.1 Overview of Power Flow Paths

The simple power flow paths discussed in Section 4.2.2.1 describe the power flow under most vehicle operating conditions (Arata et al., 2011), but the Toyota Prius architecture is one of the most flexible powertrains on the market today. This means a more detailed analysis is needed to cover all the power paths used by the vehicle.

Figure 4.6 provides a simplified overview of all the power flow options available in the Toyota Prius powertrain architecture. The blue lines show mechanical connections and the red lines electrical connections. When the engine is off power only flows along the path 1, 5, 7 from the battery to the wheels, through the motor. Power can flow both ways along this connection allowing the battery to drive the vehicle and for power to be regenerated as the vehicle slows down.

When the engine turns on many other combinations of power flow paths are possible. If the engine turns on when the vehicle is stationary all the power passes along path 4, 8 and recharges the battery. The battery can provide power to the wheels through paths 7, 5, 1 or 8, 3, 1. The battery can also provide power to the engine through path 8, 4, this allows the generator to be used as a starter motor and as a means of controlling engine speed. If the engine is turned on while the vehicle is moving, then the battery is powering both the motor and generator as motors, one to drive the vehicle and one to start the engine.

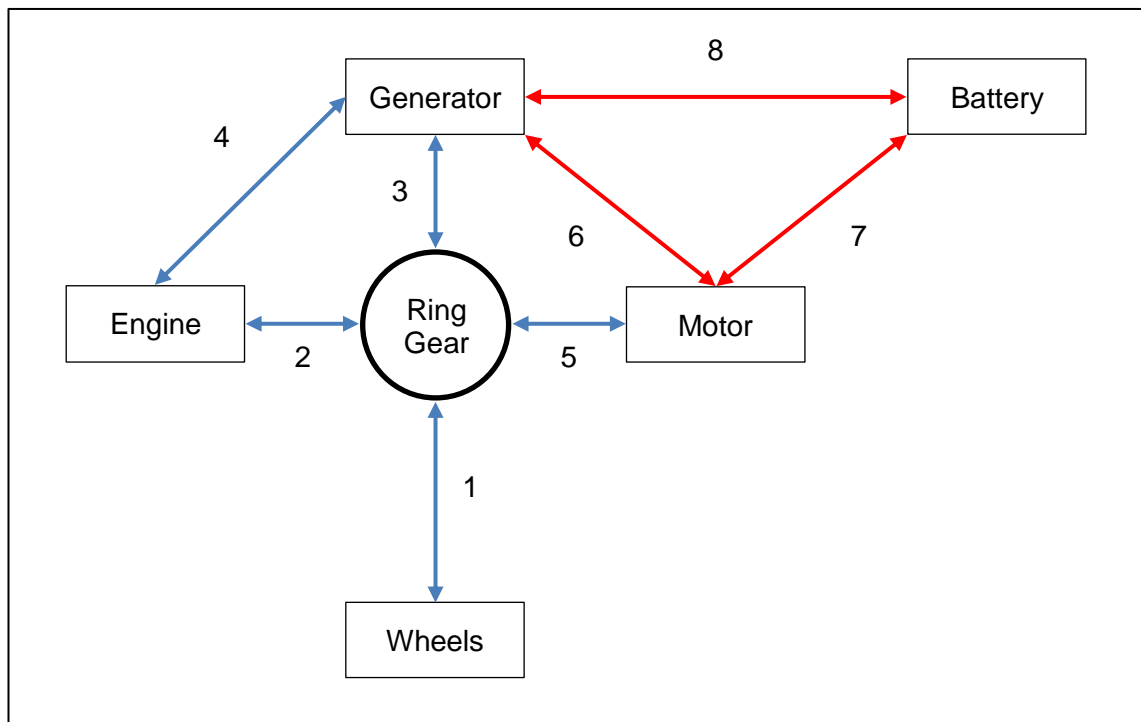


Figure 4.6: Power flow diagram for the Toyota Prius powertrain. Red lines, electrical path. Blue lines, mechanical path

If the vehicle is moving, a fraction of the engine power passes through path 4 and the rest through path 2. The split of power along these two paths depends on the vehicle speed, engine speed and engine torque. At low vehicle speeds, and at high vehicle speeds with high tractive power, the generator spins in reverse and generates power, under these conditions, there are three power paths. If the vehicle tractive power demand

is positive, then all engine power that passes along path 2 goes along path 1 and powers the wheels. If the battery is being charged then the power that passes along path 4 splits, some goes along path 8 and recharges the battery, but most passes along path 6, 5, 1 and powers the wheels. If the battery is discharging then all the power that passes along path 4 goes along path 6 and is supported by battery power from path 7, this power combines and then passes to the wheels.

During harsh braking the tractive power drops very low or below zero faster than the engine can react, so for a short period the engine is on but it is not needed. Under these conditions, all engine power passing along path 4 is routed along path 8 and charges the battery. If tractive power is low positive then some engine power from path 2 goes along path 1 to the wheels, the rest passes along path 5, 7 and recharges the battery. If the tractive power is negative then regeneration power from path 1 joins with engine power from path 2 and the combined power passes along path 5, 7 to the battery. Under these conditions both the generator and the motor act as generators.

If the vehicle is travelling at higher speeds and the tractive power is low, then the generator speed can reverse and the generator acts as a motor. The generator is then controlled to match the power of the engine from path 4, along path 3, and all the engine power passes along path 2. The motor then acts as a generator, receiving power from the engine along path 2, 5. If the battery is charging then the motor generates enough power to cover the battery and generator demand. If the battery is discharging, then the motor is controlled to supply enough power to cover the generator demands minus the battery power.

The generator only acts as a motor when the engine power is very low. If the tractive power rises suddenly then the battery support power can be larger than the engine power. When this occurs both the motor and the generator act as motors powered by the battery. This configuration can only be maintained for very short periods of time as it puts a high demand on the battery.

4.3.2.2 Overarching Control

The tractive power at *engine on* is difficult to pinpoint as the tractive power is rising rapidly and the exact threshold occurs between readings that can be a long way apart. However, it is clear that *engine on* is a function of tractive power and battery SOC, as demonstrated by (Namwook Kim et al., 2012).

The simple view given in the literature that battery power is a function of battery SOC, and engine power is a function of tractive power and battery power (Namwook. Kim & Rousseau, 2015), is not quite the full picture. Figure 4.7, a short section of data that is representative of the trends seen in the overall dataset, shows tractive power, battery power and engine power, alongside these are the predicted battery power based on battery SOC, and the predicted engine power based on tractive power, predicted battery power and efficiency losses. There appears to be a delay in engine power response which becomes more pronounced with higher rates of change in tractive power. This means over a spike in tractive power the engine first under supplies power and then over supplies power. Figure 4.7 shows an example of this, as tractive power is rising the engine power is lower than the predicted engine power, the shortfall in power is made up by the battery power, which exceeds the predicted battery power based on battery SOC alone. Conversely when the tractive power is falling the engine over supplies power and the battery value becomes more negative as it recharges. As Figure 4.7 demonstrates this effect does not reduce the maximum power the engine has to meet, nor does it reduce the number or rate of engine transients. In fact, this observed trend does not seem to benefit the vehicle efficiency, instead, it considered to be a result of

the slow engine response times needed to keep the engine operation close to the optimum path.

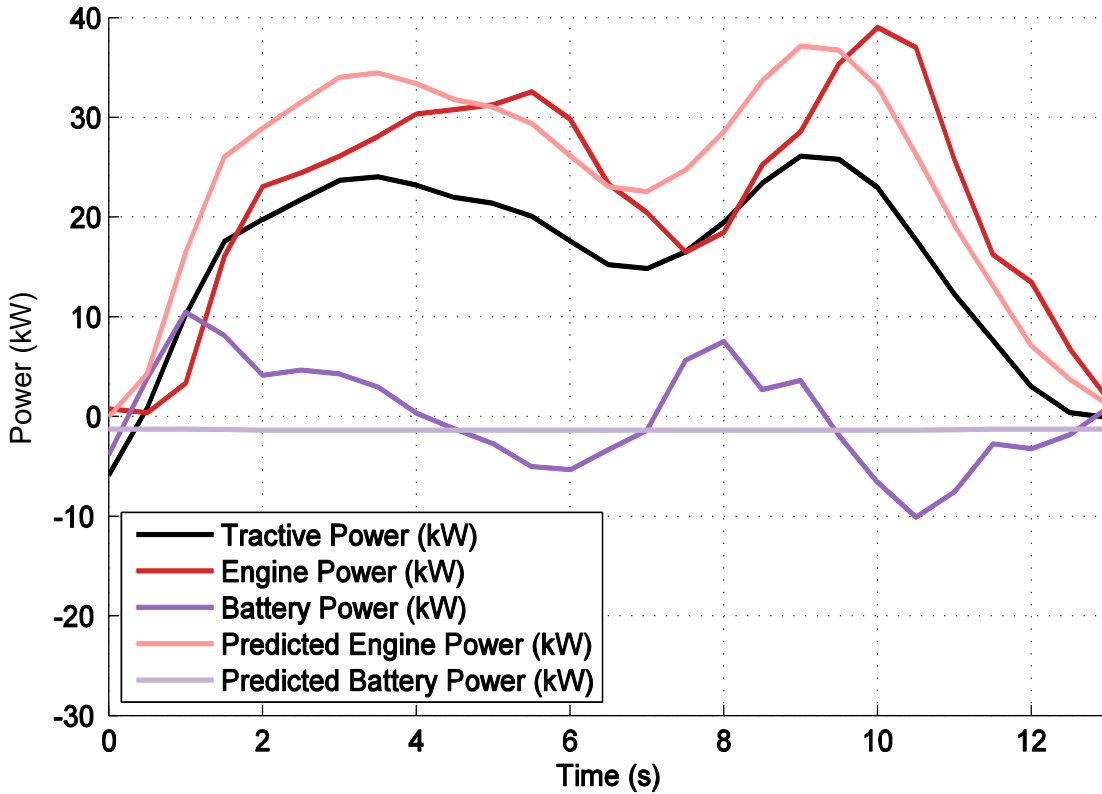


Figure 4.7: Prius tractive power, engine power, battery power, predicted engine power and predicted battery power during transient driving

Figure 4.8 presents the battery power as a function of battery SOC, colour coded by rate of change of tractive power. The underlying control can be seen as the central green band which rises to higher battery powers as the battery SOC increases, but there is a bigger shift in battery power with rate of change of tractive power. It appears that the discrepancy between actual engine power and the control systems desired engine power is balanced by the battery. This is important because it significantly increases battery use, and therefore, battery wear and power losses in the system.

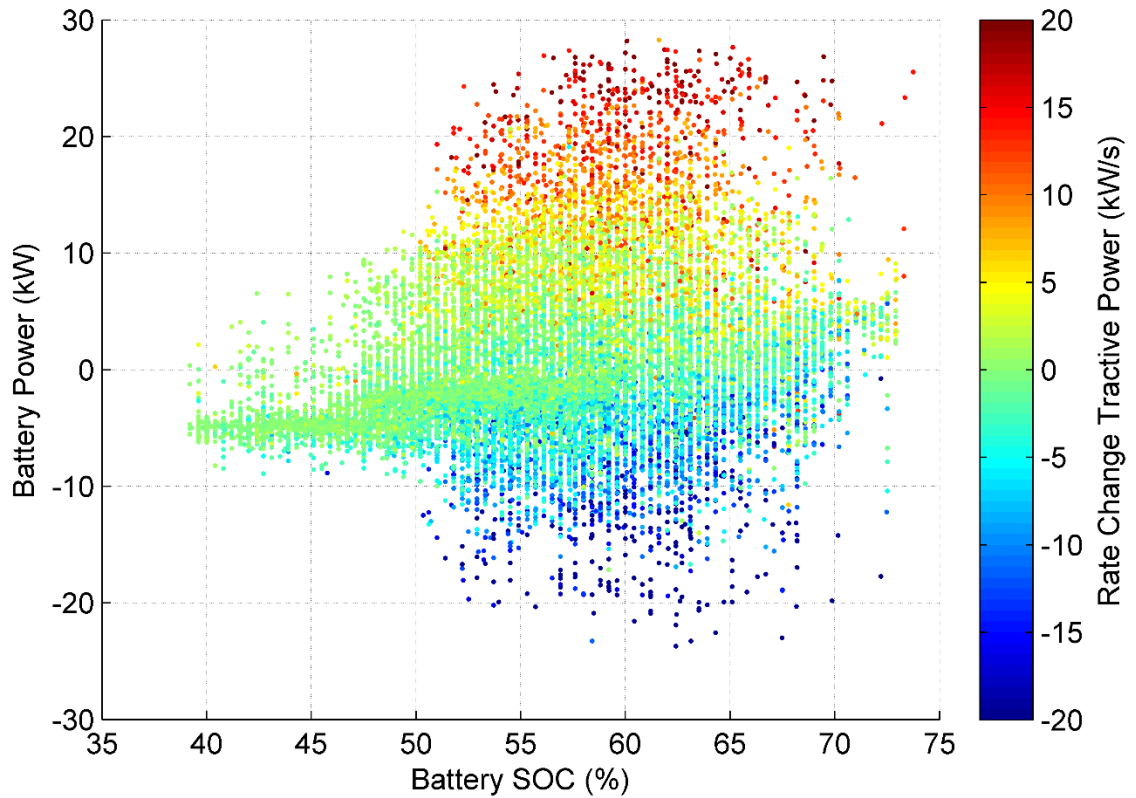


Figure 4.8: Battery power as a function of battery SOC and rate of change of tractive power

Very little evidence for full acceleration mode as described in the literature is found in the test data (Toyota, 2015a). Figure 4.9 displays three separate sections of time series data where the tractive power rises very sharply due to a strong acceleration up an incline. In each case the plot compares the observed engine power and change in engine power, shown in red, and the predicted engine power, based on the tractive power and battery SOC, and change in predicted engine power, shown in blue. In each case, the engine response is delayed but the minimum and maximum engine powers before and after the increase in tractive power are very similar for the observed and predicted engine powers. This is expected because in full acceleration mode the battery is supposed to help the engine transition power rather than helping the engine meet high powers. As there is no indication in any of three separate harsh acceleration events displayed in Figure 4.9 that the battery supports the engine, even when the engine reaches maximum power (73kW),

it can be concluded that the battery supporting the engine at high powers is not a Prius mode.

The plots also show very little difference in the rate of change of engine power, shown in light red and blue. If the battery was supporting the engine during transients then the magnitude of the light red line peaks would be lower than the magnitude of the light blue line peaks, as the engine would slowly ramp up power and the battery would meet the deficit. This is not the case, the maximum rate of change in engine power is similar for observed and predicted data, and the length of the peaks in engine power are comparable. There is, therefore, no clear evidence that the battery is supporting the engine to reduce engine transients or maximum engine power. This indicates that the battery power support seen during increasing traction power may only be used to allow the engine time to track across the engine map, close to the optimum operating line, and is not used to reduce the engine work.

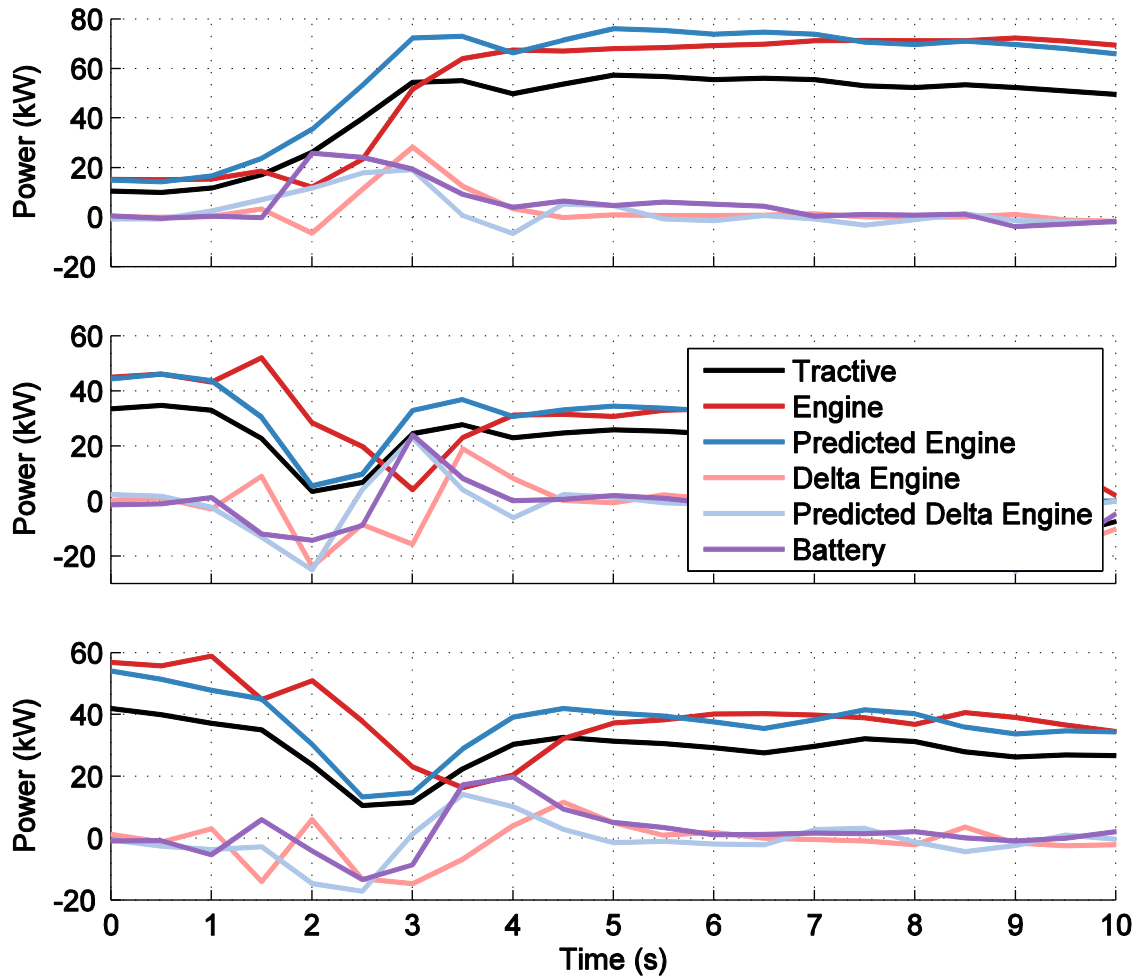


Figure 4.9: Prius powertrain response to three separate harsh acceleration events

The *engine off* threshold is incredibly difficult to extract from the data as the tractive power drops very quickly once no pedal input is given. This is exacerbated by the motor starting to regenerate power with no pedal input at vehicle speeds greater than 16 km/h. Part of the difficulty in obtaining this variable from the PAMS test data may have something to do with the difference in driving styles between chassis dynamometer testing and testing on the road. In chassis dynamometer testing there is likely to be more careful feathering of the accelerator and brake pedals to keep the vehicle speed in the allowable range. Whereas, on the road driving controls are likely to be used in a more certain and positive manner. This means that in the PAMS test data the tractive power

never fluctuates in the low positive region, but drops quickly from high positive to negative where the engine turns off.

4.3.2.3 Component Control

4.3.2.3.1 Engine

4.3.2.3.1.1 Engine Speed and Torque Operation

One of the main benefits of the Toyota hybrid architecture is that the engine speed and torque are partially disconnected from the vehicle operation. Figure 4.10 shows the engine speed and torque operating point, not including the *engine on* and *off* transitions. The engine tries to operate along an optimised path, shown in red, which aims to maximise fuel efficiency. The general shape of the red curve in Figure 4.10 is known to be correct because the maximum fuel efficiency curve for the Prius engine has been published by Toyota (Kawamoto et al., 2009), the actual curve has been fitted to the data using the 'Fit' function in Matlab which fits a best fit (defined as minimising the sum of the squared residuals) line, curve or surface.

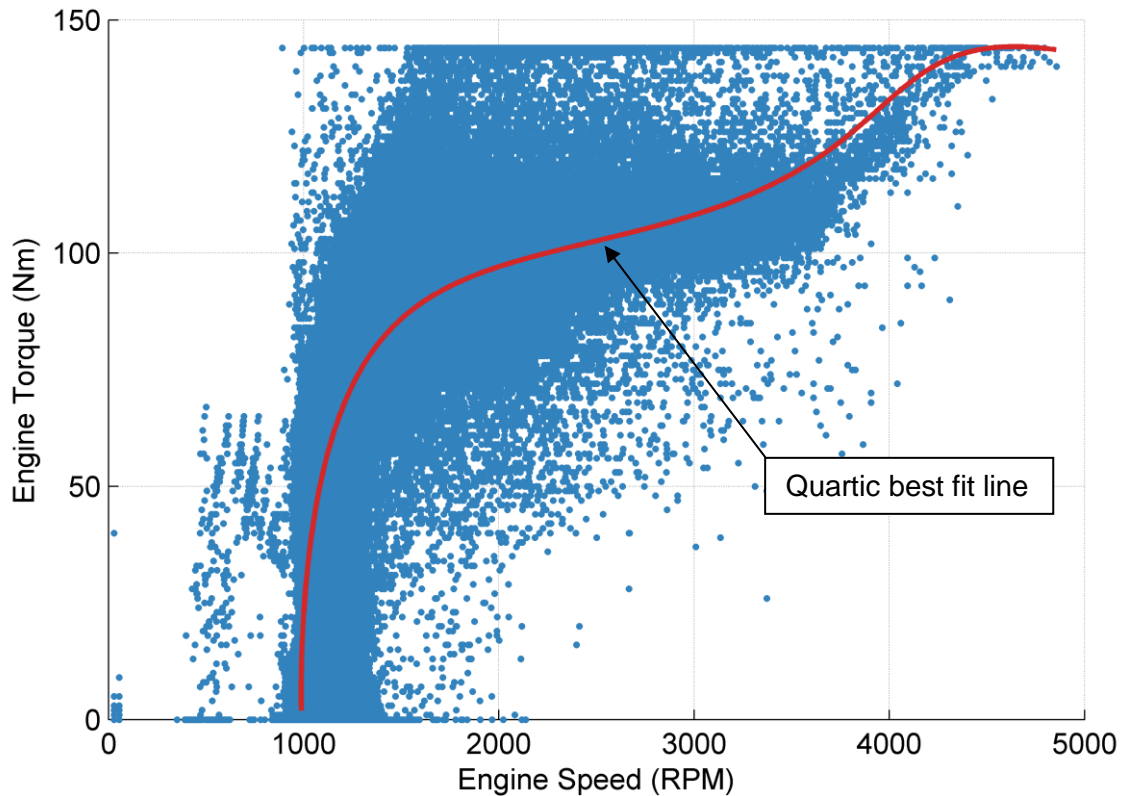


Figure 4.10: Prius engine speed and torque operating points with engine target operating line in red

While the engine aims to operate along the red line, it is impossible for the engine to quickly track changes in demand power while following the line closely. Figure 4.11 displays a short *engine on* event, subplot A presents the tractive power demand, while B shows the engine map. When the engine turns on it tracks a roughly straight line up to the point where the red line matches the desired engine power, at point A. Once the engine is fully on it matches desired power by changing speed, to change the engine speed the Prius uses the generator to speed up or slow down the engine. The engine fuelling cannot change as rapidly as the generator can change the engine speed, this results in a drop in engine torque when the engine is sped up and a rise in engine torque when the engine is slowed down.

When the tractive power peaks and troughs, at points B, C, D and E, the change in tractive power is close to zero and the engine manages to control the speed and torque

to match the engine operating line. The two rises in tractive power from A to B and from C to D clearly show a drop in engine torque, followed by a fast rise in engine speed and then a rise in engine torque back to the optimum operating line. Conversely, the two decreases in tractive power from B to C and D to E display a rise in engine torque, followed by a rapid reduction in engine speed and then a drop in engine torque back to the red line. The second peak C, D, E has a faster rate of change of tractive power and this results in a larger engine torque deviation from the line and a quicker change in engine speed to meet the new power demands.

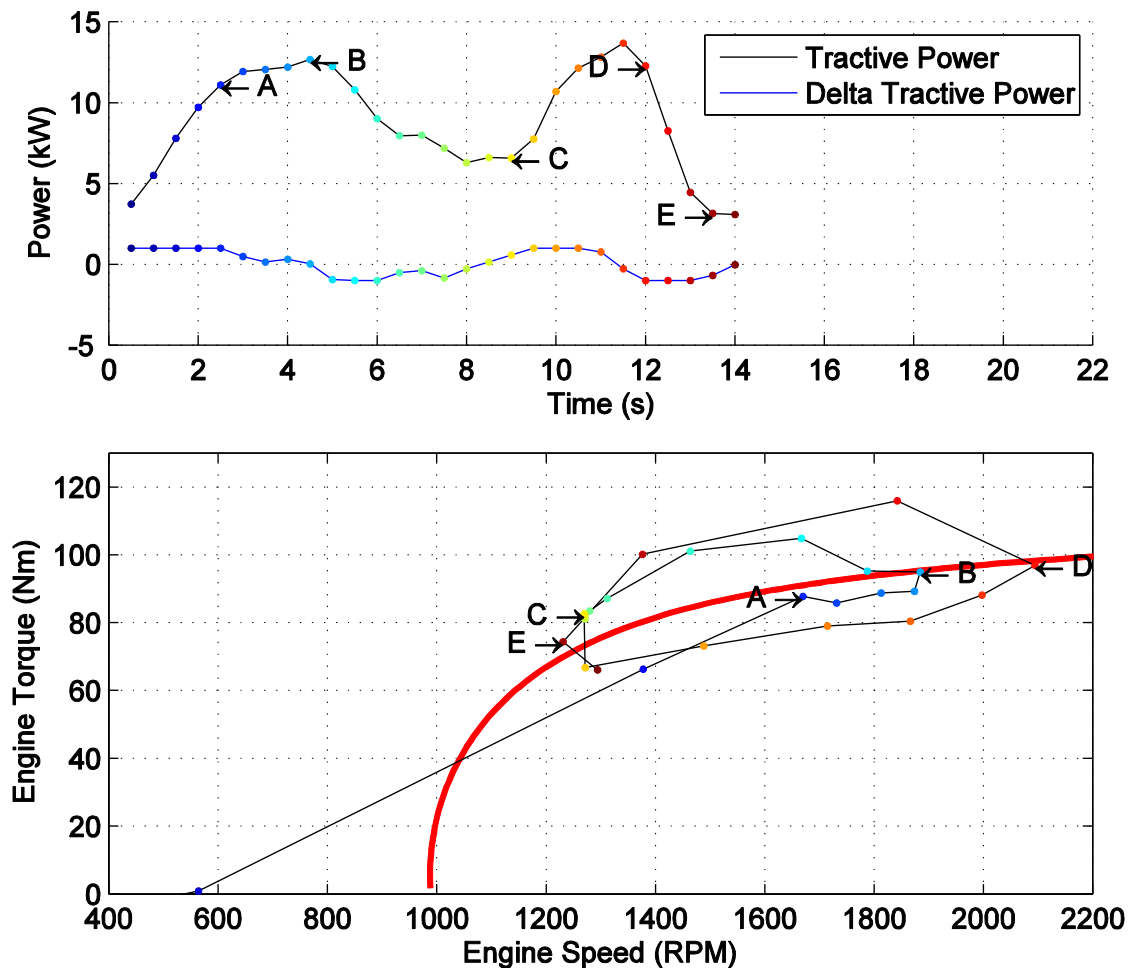


Figure 4.11: Prius engine operation during transient driving. A, tractive power and change in tractive power colour coded by run time. B, engine speed against engine torque colour coded by run time. Red line, engine optimum path

Figure 4.12 plots engine speed against engine torque at 40 km/h (25 mph), colour coded by vehicle traction torque and battery power. Plot A shows that from 1000 RPM to 3000 RPM increased vehicle power demand is only met by increasing engine speed and not increasing engine torque, although at the highest engine speeds engine torque is also used to deliver higher engine powers. Plot B explains how the discrepancy in engine power caused by the engine torque being above or below the target line is managed by the system, with high torque resulting in battery charging and low torque in battery discharging.

Figure 4.12 B can be explained by the findings in Figure 4.8. The red and orange dots with high battery support occur during *engine on*. The blue and green dots, at engine speeds less than 1,000 RPM, occur during engine off. The reason torque is not used to help deliver vehicle power demand is that high torque occurs when the engine is transitioning to lower power and therefore the additional power delivered by the higher torque is not needed. Conversely, low torque occurs when the engine is transitioning to higher power and battery support is needed to make up for the shortfall in engine power. These results support the findings of Figure 4.8, if the battery was being used to reduce the rate of engine power transitions, rather than just helping the engine track the optimised path during transitions, then battery support would occur across the engine map rather than correlated to engine torque as is seen in the data.

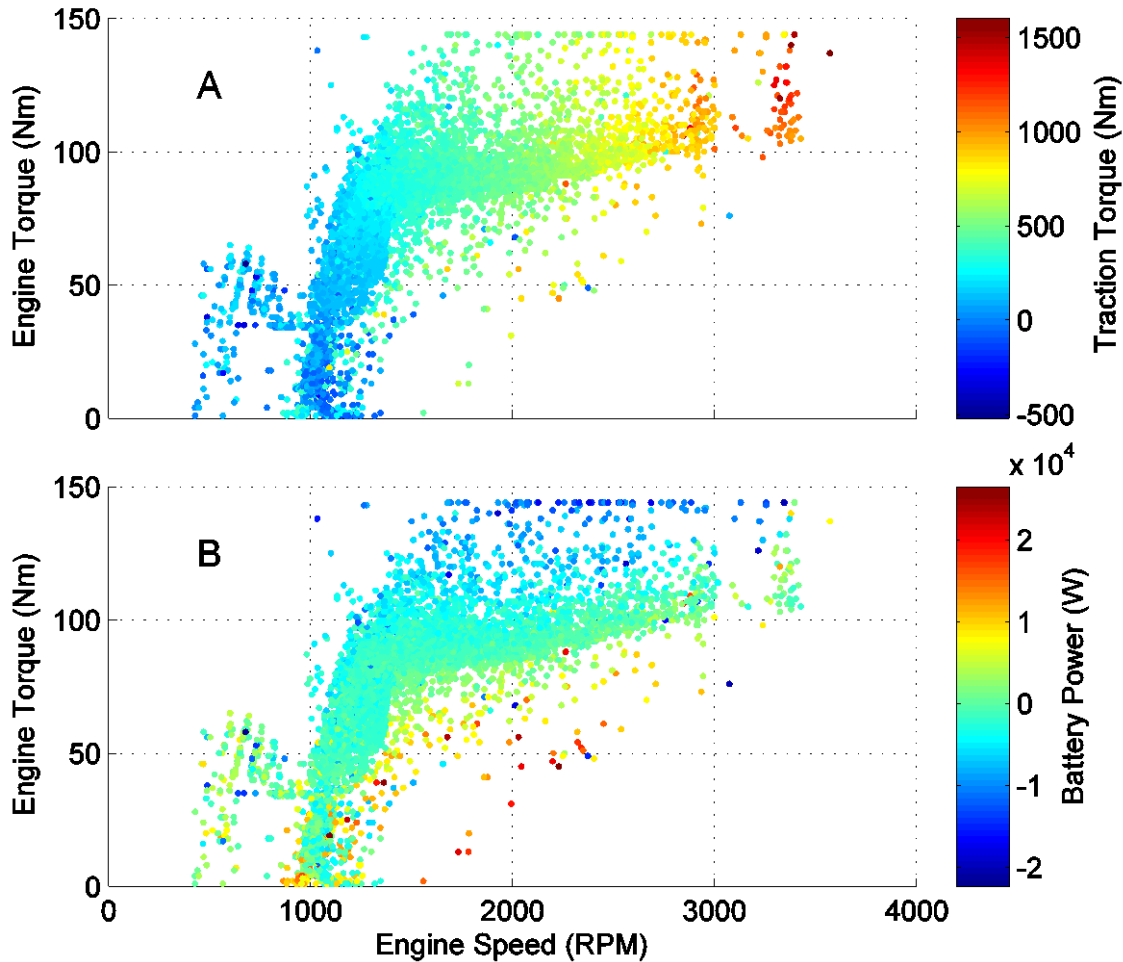


Figure 4.12: Prius engine operation at 40 km/h. A, engine speed against engine torque, colour coded by vehicle traction torque. B, engine speed against engine torque, colour coded by battery power

4.3.2.3.1.2 Engine Fuel Consumption

Creating a conventional engine map that displays brake specific fuel consumption over the engine speed and torque range is very difficult for the Prius engine because the engine only operates over a limited range. Figure 4.13 displays a fuel consumption map rather than an engine efficiency map but this still provides a good indication of how the Prius engine operates. The area between the two black lines on the Figure 4.13 indicate where 95% of the engine data falls. With high engine torque occurring during a transition to lower engine power and vice versa, it is not surprising that the fuel consumption is relatively independent of engine torque. This begins to change at higher engine powers

where engine torque is used to deliver higher power. This can be seen in the shift in the contour bands away from vertical at the highest engine speeds.

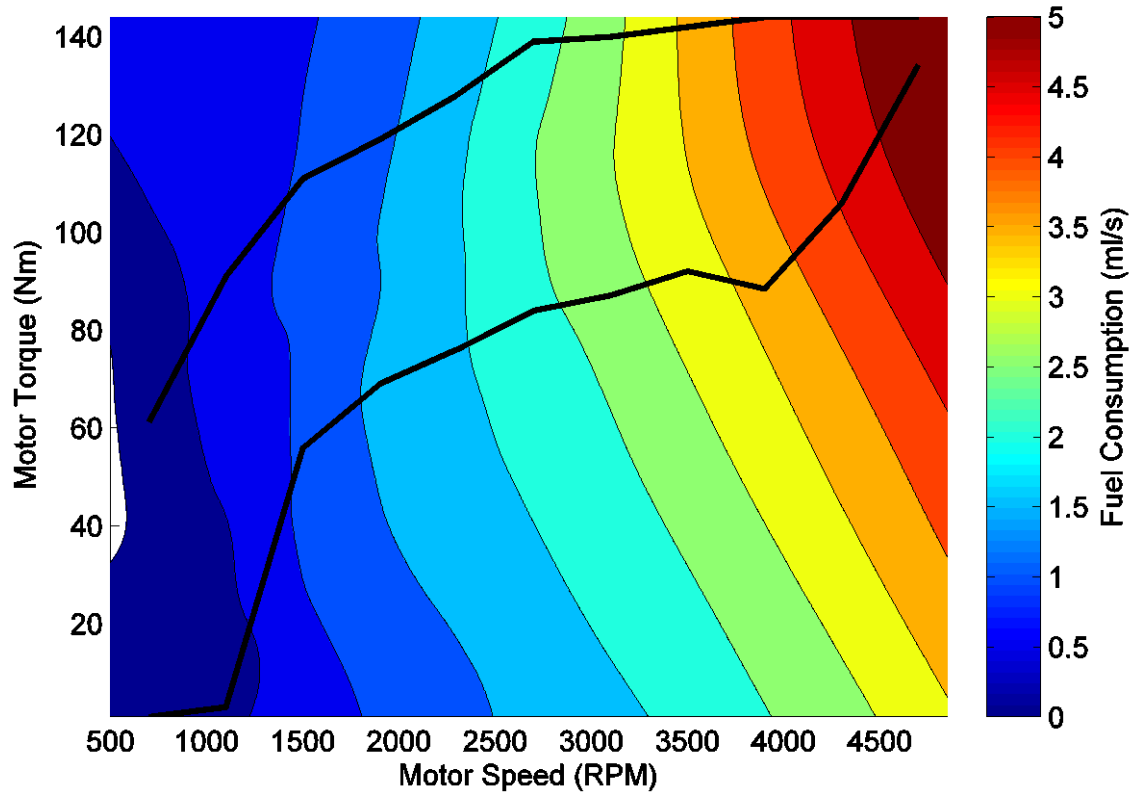


Figure 4.13: Prius engine fuel consumption map

4.3.2.3.2 Generator

The amount of engine power that is transmitted to the sun gear demands on several factors. The speed of the sun gear is dependent on vehicle and engine speed. The torque transmitted to the sun gear is a fixed proportion of the engine torque. Not all the power delivered to the sun gear turns into generator power. Figure 4.14 presents the sun gear power against the generator power. The cyan data represents points where the engine speed is stable. The difference between sun gear power and generator power for this data is only drivetrain efficiency losses. The red and blue data either side of the cyan denotes data points with rapidly increasing or decreasing engine speed. The generator can increase or decrease its power to control the engine speed, and this is how the

engine speed is maintained close to the optimum operating line even while the vehicle speed and power demand are changing.

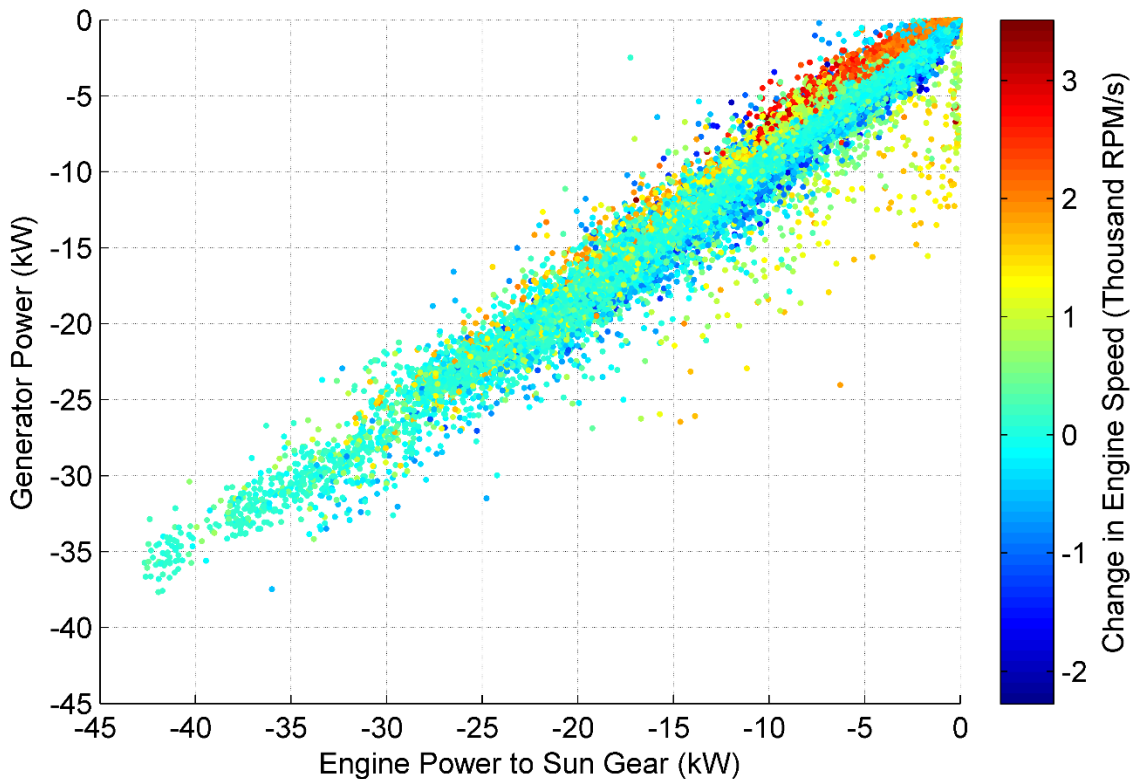


Figure 4.14: Engine power delivered to the sun gear against generator power, colour coded by change in engine speed

4.3.2.4 Additional Operating Modes

These additional operating modes are the most difficult area to study. This is because it takes a long time to prepare a car for these modes and then they only last a short period of time. For example, it takes 12 hours soak time for a car to be ready for a completely cold start test and then the car only operates in cold start mode for a few minutes. The large time gap between tests and the number of tests required, makes chassis dynamometer and PEMS testing of limited use for studying these areas. By comparison, if PAMS is fitted to a private individual's car, it is easily possible to record many repeats of the vehicle operating under these conditions.

The difficulties associated with collecting test data for these modes means that they are the least well documented in the literature. There are even disagreements between different sources in the literature as to why the vehicles operates in a particular manner while in these modes because the analysis is often based on too few runs (Barrieu, 2011; N. Kim et al., 2012; Namwook. Kim & Rousseau, 2015).

4.3.2.4.1 Cold Start

The engine operates in a different region of the engine map during cold start. Figure 4.15 shows how the engine operating range changes as the engine warms up. At low temperatures, the engine speed is higher, but the range of engine speeds is low. As the engine warms up the engine idle speed drops and the engine speed under higher loads increase rapidly. Engine torque at low engine temperature is mostly less than 50 Nm. As the engine temperature rises less engine idling occurs and the engine torque shifts upwards until most engine torque occurs between 75 and 100 Nm.

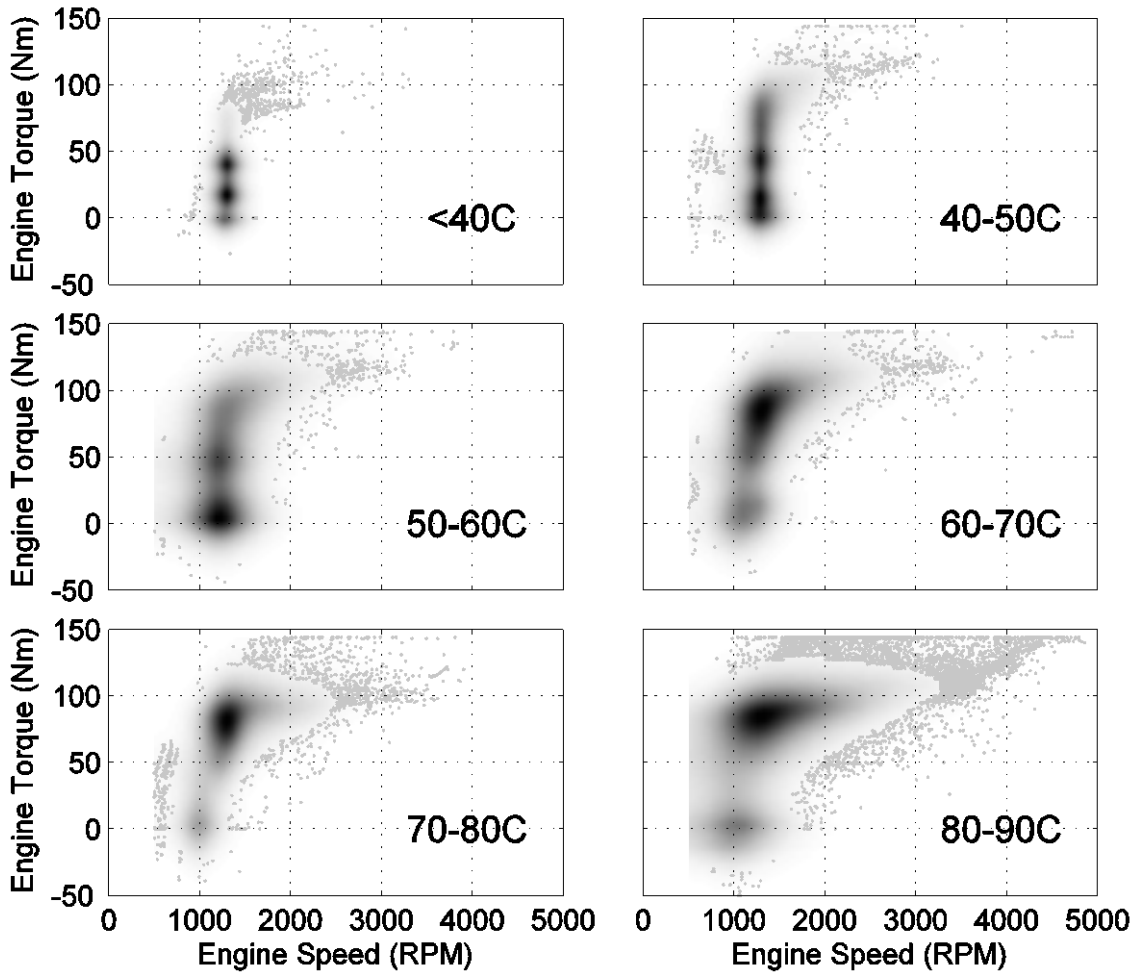


Figure 4.15: Prius engine speed and torque under different engine coolant temperatures

Engine fuel consumption and therefore efficiency is a function of engine coolant temperature. The blue data in Figure 4.16 is normal engine operation, it is clear that there is a strong correlation between coolant temperature and engine efficiency. The data highlighted in red is engine operation during catalyst warm-up mode. In this mode, the engine does not drive the vehicle, but instead follows a specially designed control path that warms up the catalyst without producing very high pollutant emissions. As Figure 4.16 indicates this may be very beneficial for pollutant emissions, but the efficiency is very low, and therefore this mode has a fuel consumption penalty associated with it.

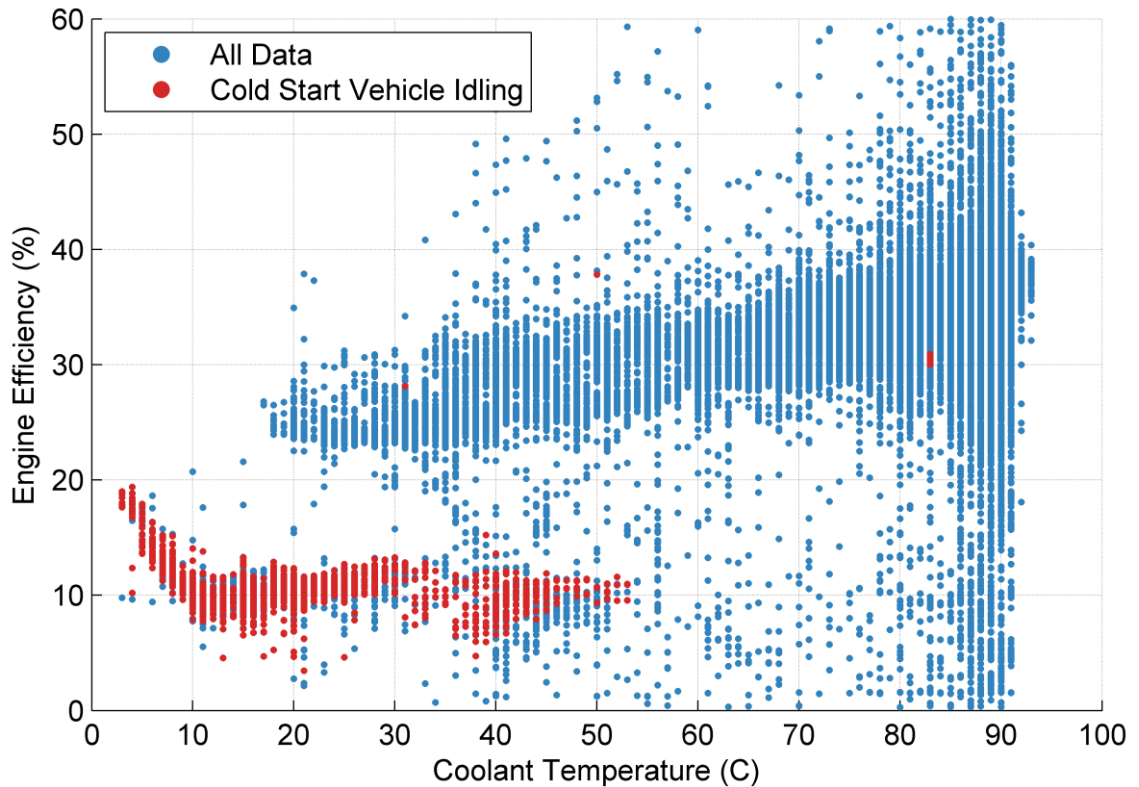


Figure 4.16: Prius engine coolant temperature against engine efficiency. Blue, all data. Red, cold start engine idling data

4.3.2.4.1.1 Cabin Heating Off

When the vehicle first turns on the engine control depends on the coolant and catalyst temperatures. The data set contains 114 vehicle on events with starting coolant temperatures ranging from 3°C to 88°C and no cabin heating. As indicated in the literature the engine warm up appears to be broken down into two phases, an initial phase aimed at heating up the catalyst and a secondary phase designed to heat up the engine.

Figure 4.17 shows the general trend for all files with a starting coolant temperature between 3°C and 26°C. The engine turns on around 15 seconds after the ignition is turned on. The first *engine on* phase, is the catalyst warm-up phase, this is defined as the initial section, normally lasting around 60 seconds, which can be characterised by low engine torque, and ending at around 73 seconds. This first phase ends when the

catalyst temperature reaches the control limit which is around 200°C to 220°C. In the second phase which immediately follows the first, the focus changes from warming up the catalyst and reducing pollutant emissions, to warming up the engine. The start of this phase can be determined by the step up in engine torque. This phase continues until the coolant temperature reaches 40°C when the engine turns off.

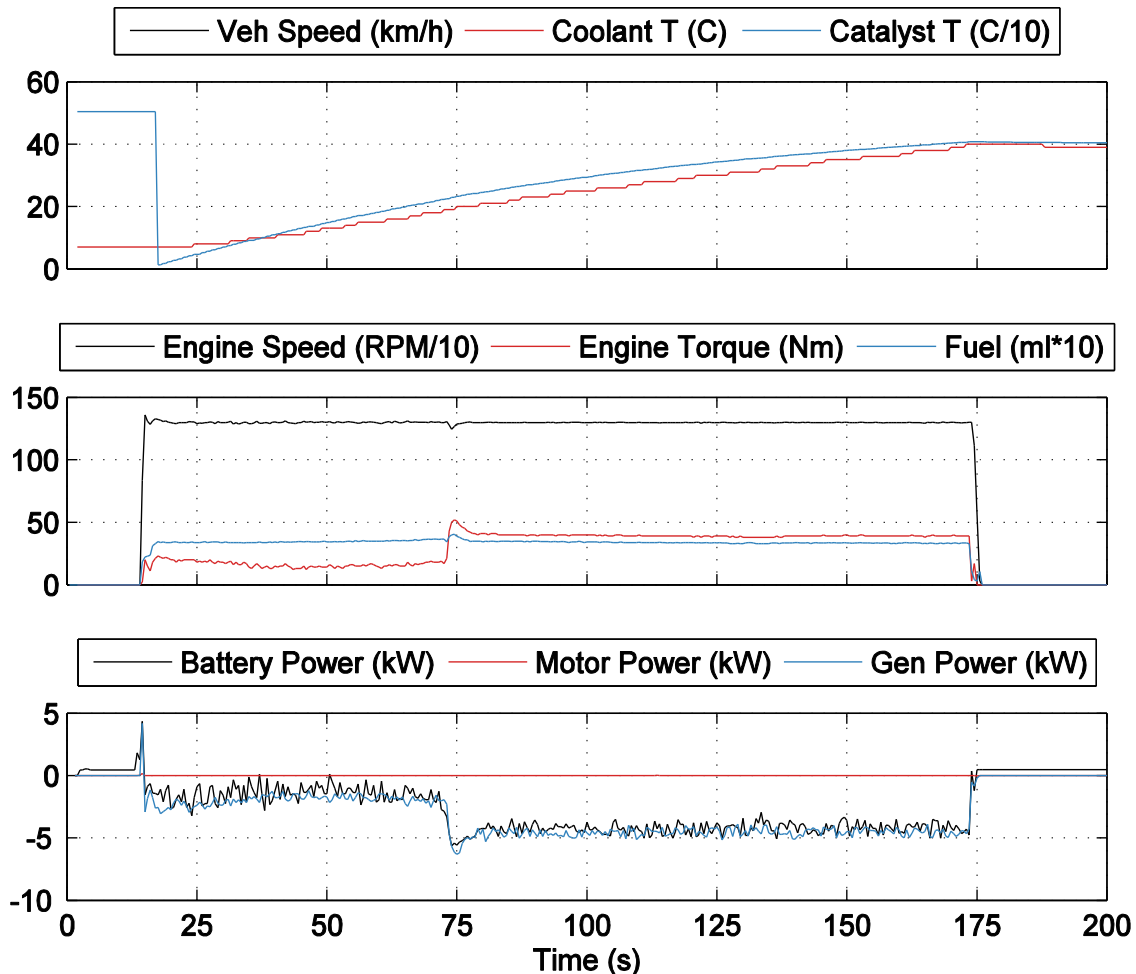


Figure 4.17: Prius cold powertrain operation at the start of a run with cabin heating off

The catalyst warm-up phase results in around a 10°C rise in engine coolant temperatures. This means that runs that start with a temperature between 30°C and 40°C will have an engine coolant temperature greater than 40°C by the time the catalyst warm-up phase is complete. Runs that start in this temperature band still complete the catalyst warm-up phase as discussed above, but at the end of the catalyst warm-up

phase the coolant temperature is greater than 40°C and the engine can immediately turn off.

Runs with a starting coolant temperature between 40°C and 48°C don't have an *engine on* after 15 seconds. Instead, the engine turns on when a hot *engine on* event occurs. Once the engine has turned on it completes a catalyst warm-up phase then turns off again.

Unfortunately, no survey data was available that started with a temperature between 48°C and 61°C, so it is not possible to define at what temperature cold start no longer has any effect on engine operations. At temperatures over 61°C no engine, or catalyst, warm-up phase is seen.

After the initial cold start phase, the engine does not appear to turn on again due to low coolant temperatures. The minimum coolant temperature in the data set after the engine cold start phase is 29°C. At these low temperatures the engine turns on due to a normal *engine on* event, or because the SOC has dropped too low. Extended periods of time without an *engine on* event result in falling coolant temperatures and battery SOC. In the case of this dataset, the SOC always reaches the bottom limit and triggers an *engine on* event, before *engine on* due to low coolant temperatures is seen. It is, therefore, unclear whether low coolant temperatures in the middle of a run can cause a second cold start event. While the engine may not turn on due to low coolant temperatures, after the first cold start, if the engine is on and the coolant temperature is below 40°C then the engine will stay on and behaves as it does during a cold start.

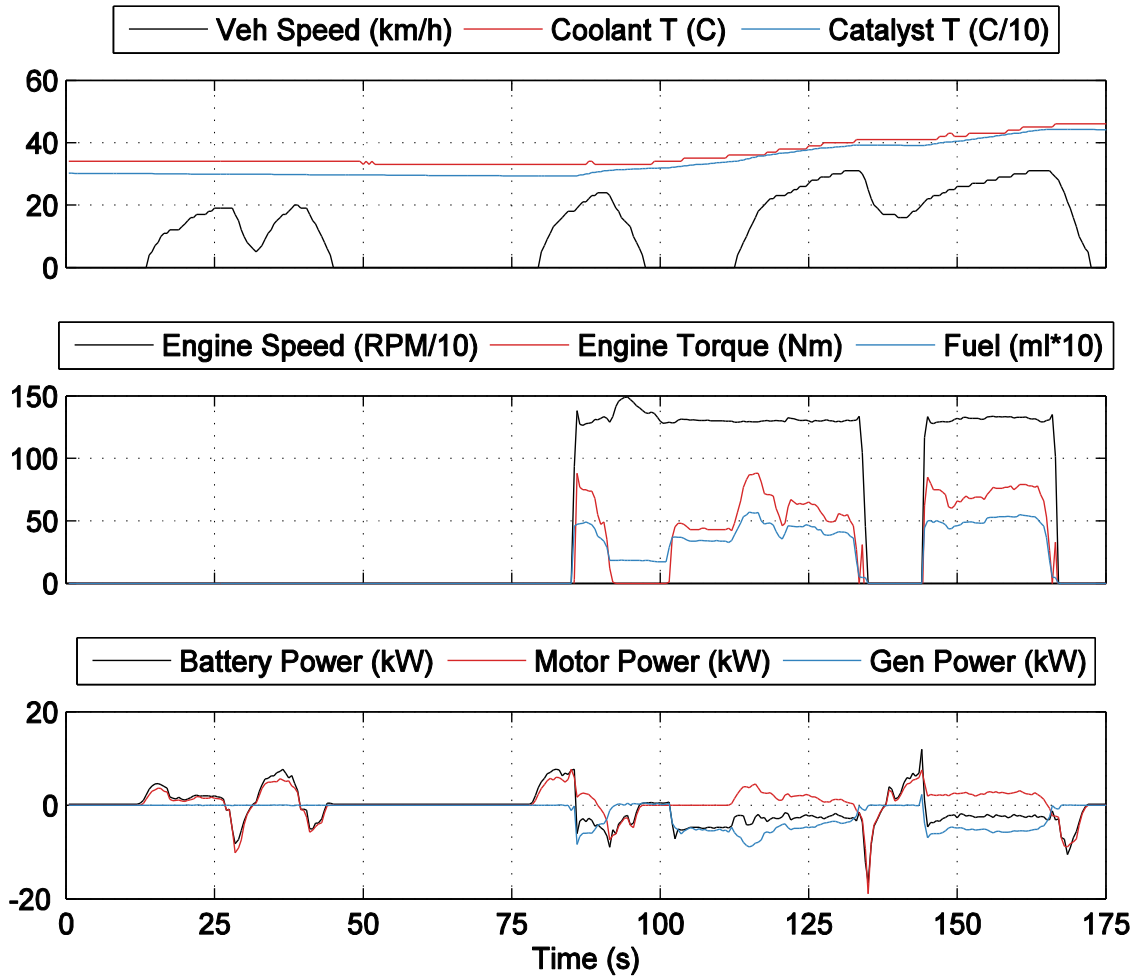


Figure 4.18: Prius cold powertrain operation in the middle of a run with cabin heating off

Figure 4.19 displays a number of engine controls which are specific to cold start. During the catalyst warm-up phase the engine speed and torque do not track vehicle power demand. The engine provides the battery with a very small amount of charge, but the battery and motor provide almost all the power required to drive the vehicle. After the catalyst warm up has finished and the engine is just warming the coolant, the engine speed and torque track the tractive power demand. When the tractive power demand goes negative and the engine would normally turn off, as it does at 128 seconds, the engine speed drops to idle and the engine torque drops to zero. If the tractive power then goes positive again the engine torque jumps up to meet the tractive power demand. If the vehicle speed drops to zero, as is the case at 140 seconds and no tractive power

demand occurs for four to five seconds, then the engine torque jumps up again to provide engine power to charge the battery, this occurs from 144 seconds till the end of the engine on.

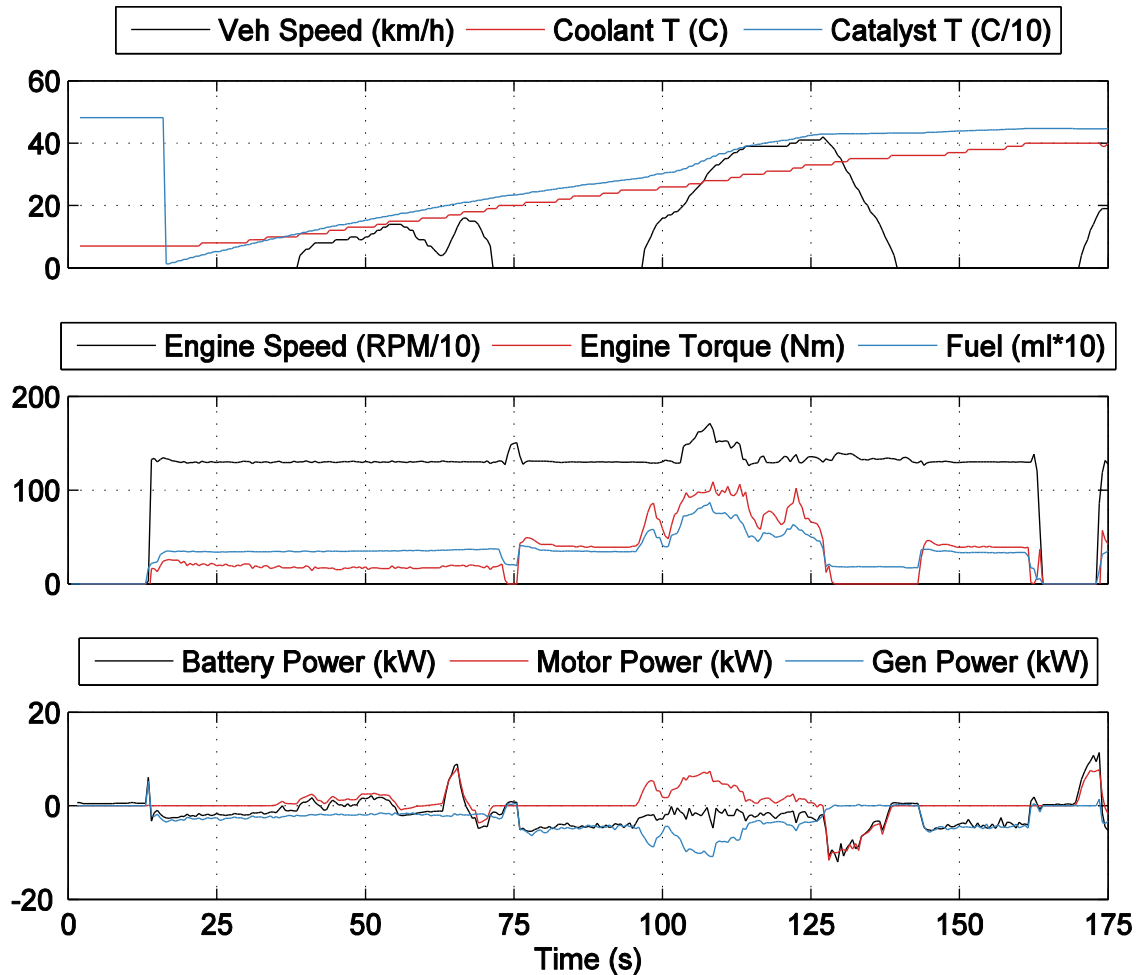


Figure 4.19: Prius powertrain response to vehicle driving demand during cold start at the beginning of a run with cabin heating off

4.3.2.4.1.2 Cabin Heating On

The cabin heating on dataset contains 43 vehicle on events with starting temperatures ranging from -2 to 82°C. With cabin heating on the vehicle performs an engine warm up similar to the procedure discussed in Section 3.4.2.4.1.1. The main difference is that the *engine off* temperature limit is increased from 40°C to 63-65°C. This results in a much

longer warm up time, Figure 4.20 reaches 40°C after 200 seconds and 65°C after 750 seconds.

The vehicle performs a full cold start, including the catalyst warm-up phase, on runs with starting temperatures between -2 and 55°C. The vehicle will also perform the cold start if there is a long idle period at the beginning of the run, and the coolant temperature starts high but drops down to 55°C before the first *engine on* occurs due to driving demand.

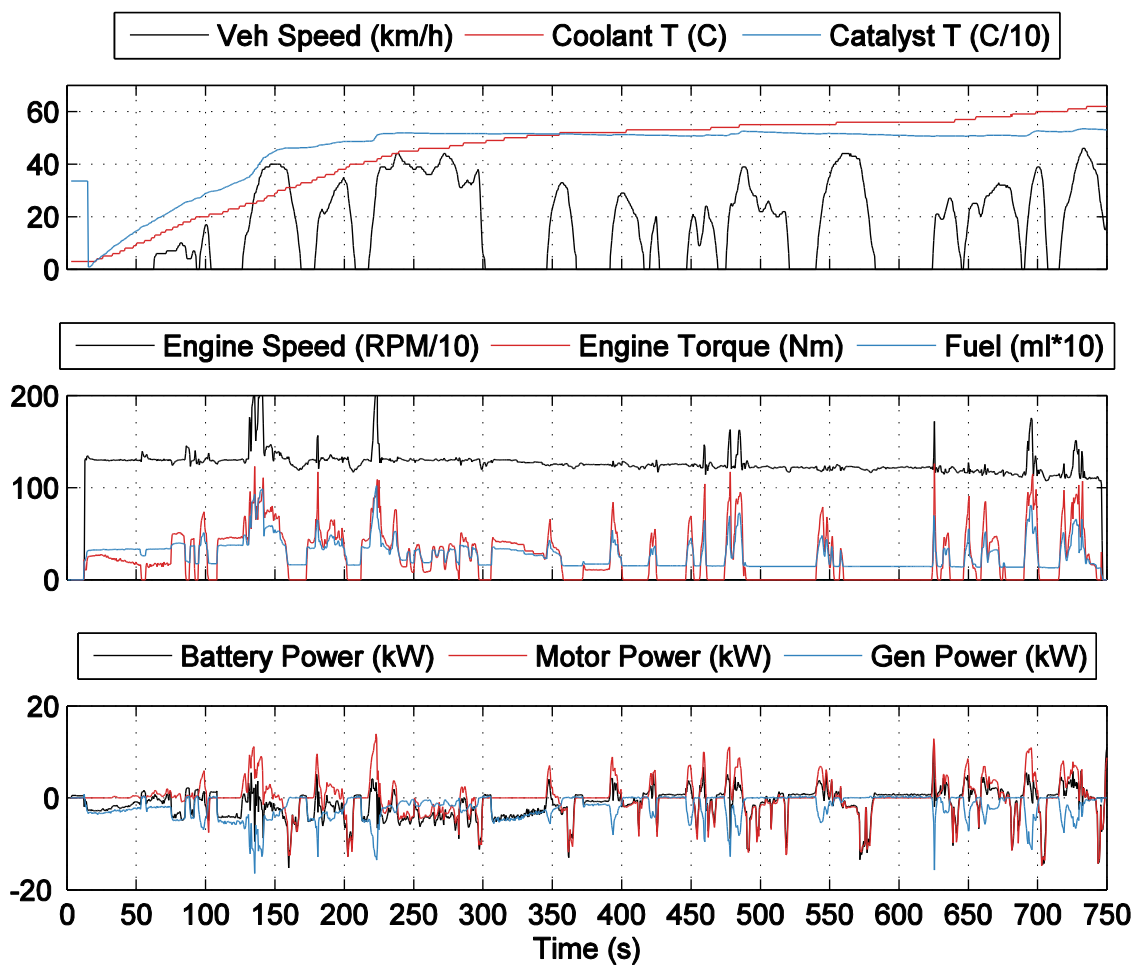


Figure 4.20: Prius cold powertrain operation at the start of a run with cabin heating on

Starting coolant temperatures between 55 and 65°C do not result in an immediate *engine on* at the beginning of the file. Instead, the engine remains off until turned on during a normal *engine on* event, in this case after 11 seconds. After turning on, the engine

operates under the high idle speed, low torque conditions seen in the catalyst warm-up phase, but unlike under cabin heating off conditions, where the catalyst warm-up phase runs until the catalyst temperature reaches its control limit, here the engine is free to turn off as soon as the coolant temperature reaches 65°C. Another difference compared to the catalyst warm-up phase used at lower coolant temperatures is that, while most of the time the motor and battery power the vehicle, under high power events the engine will power the vehicle, see 31 to 35 seconds.

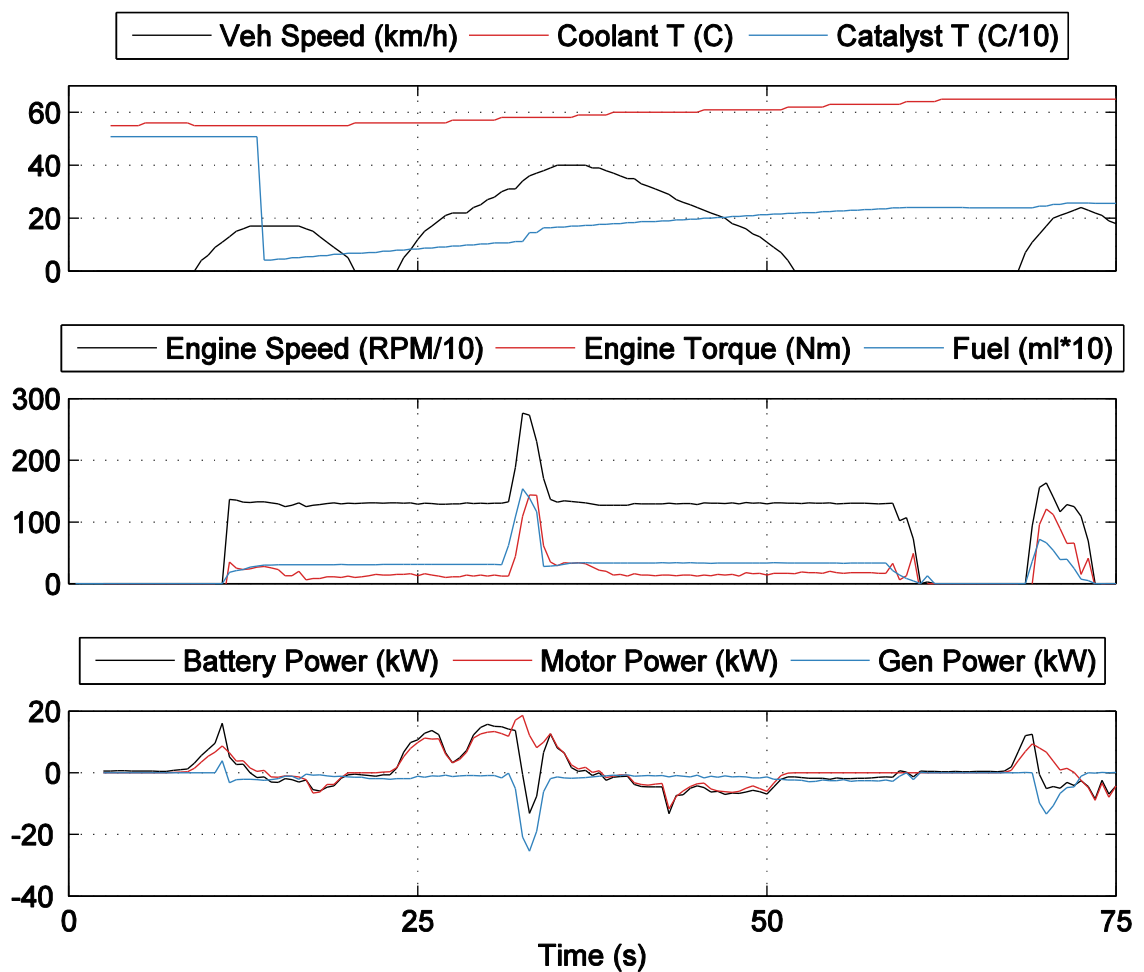


Figure 4.21: Prius warm powertrain operation at the start of a run with cabin heating on

The minimum temperature recorded after the initial cold start phase was 44°C. Several *engine on* events at temperatures well below 55°C have been recorded, this indicates that 55°C is only the coolant temperature limit for *engine on* during the initial warm up

phase. The coolant temperature at which the engine turns on and off in the middle of a run is very variable, it is thought that this is likely dependent on the cabin temperature rather than the coolant temperature. Unfortunately, cabin temperature was not recorded so this control mechanism can't be discussed further here.

4.3.2.4.1.3 Effect of Battery SOC on Cold Engine Operation

Due to the long length of the engine warm up phase with cabin heating on, excessive battery charging can occur. Figure 4.22 is a focussed section from 300 to 750 seconds of Figure 4.20, simplified and enlarged to highlight this point. There are two points at the beginning of the plot where the vehicle comes to a rest (302 and 368 seconds). Soon after these points, the engine torque rises again and starts to charge the battery. After this point, although there is an opportunity at 426, 520, and 585 seconds, the engine torque does not rise while the vehicle is stationary and no more engine to battery charging occurs during the rest of the plot. This is because the SOC limit has been met. Figure 4.22 indicates that this limit lies between 68 and 69% SOC.

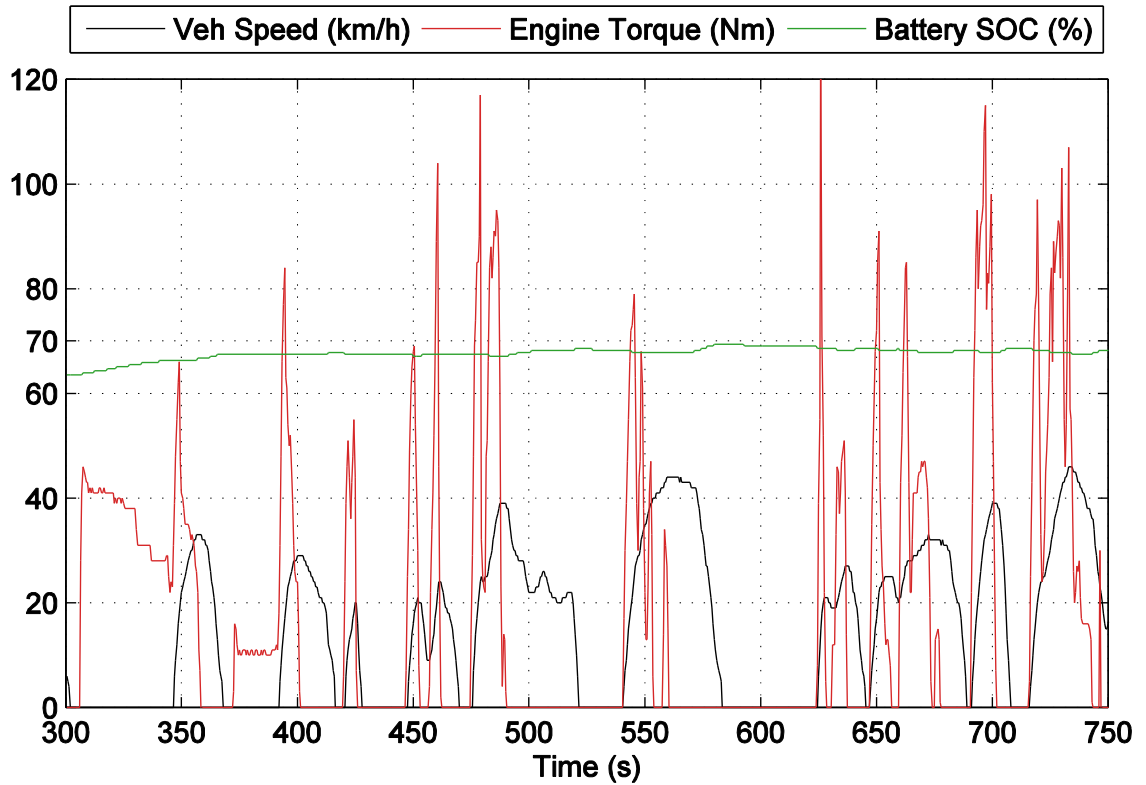


Figure 4.22: Effect of battery SOC on cold powertrain operation at the start of a run with cabin heating on

4.3.2.4.2 Low Battery SOC

During low speed congested driving the battery SOC can hit the lower limit which causes the engine to switch on and recharge the battery. Figure 4.23 shows a recharge event, the engine starts when the battery SOC drops below 40% and only turns off when the engine is not needed to power the vehicle and the SOC is above 50%. During recharge, the engine meets the power requirements of the vehicle, when tractive power drops below zero the engine continues to idle at a speed that is related to engine coolant temperature. As is the case with engine warm up the engine torque drops to zero when the engine receives the signal for a normal *engine off* event and rises again due to tractive power demand or if the vehicle has been stationary for several seconds, to recharge the battery.

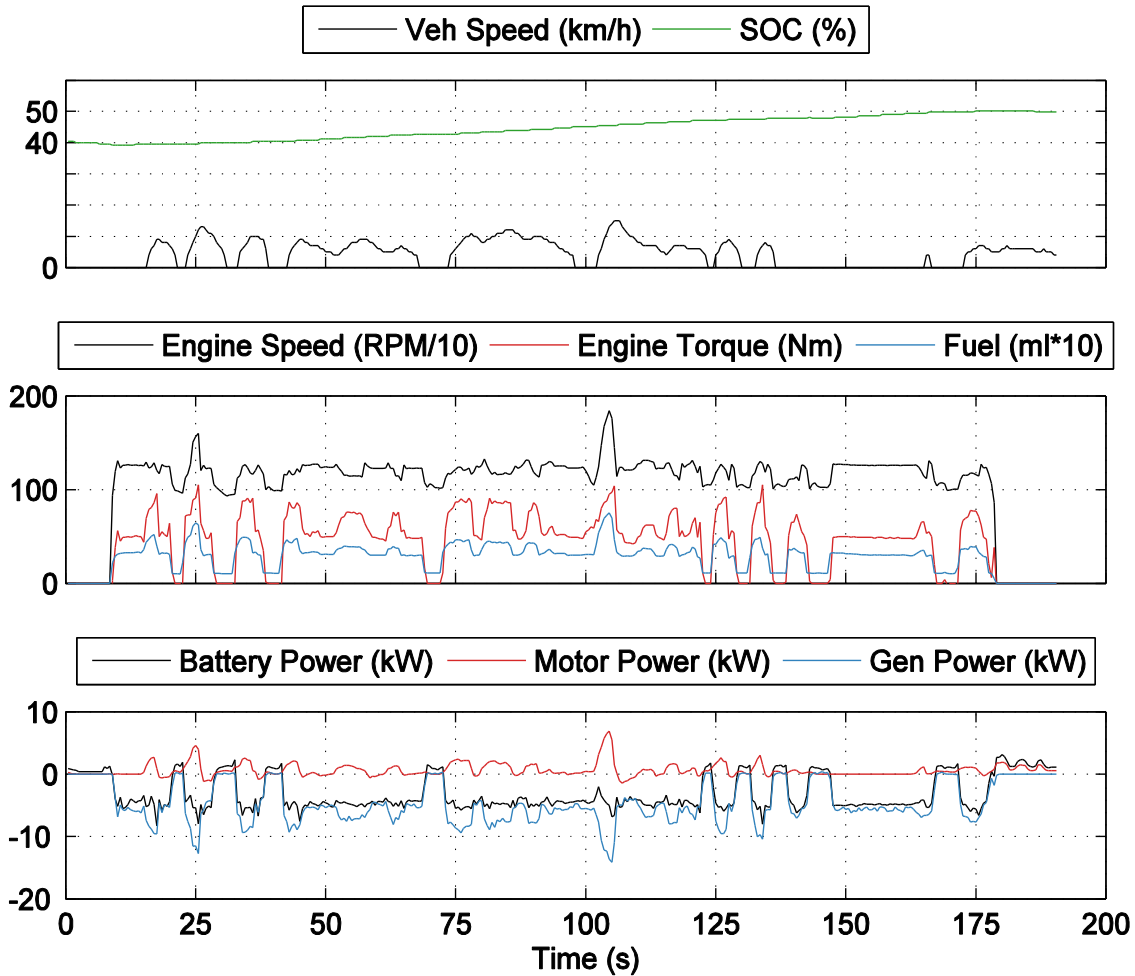


Figure 4.23: Prius powertrain operation during a low battery SOC event

4.3.2.4.3 Fuel Cut

The literature states that if the tractive power drops below the *engine off* threshold and the vehicle speed is greater than 72 km/h (45 mph) then the vehicle goes into fuel cut mode where the engine keeps spinning but the fuel flow to the engine is cut (N. Kim et al., 2012). Figure 4.24 and 4.25 show the same fuel cut event. The engine turns off at around five seconds, the engine speed drops to 993 RPM or idle speed, and the engine torque drops to -14 Nm which means the engine is being spun by an external source. Both fuel consumption parameters measured using the HEM equipment record fuel being consumed during the engine fuel cut mode. This is understandable for the MAF measurement as air is still flowing into and out of the engine as it is being spun, but the

injection measurement should be able to record the drop in fuel consumption during fuel cut. The fuel cut ends on the dotted line at eleven seconds when the vehicle speed drops below the threshold. At the end of fuel cut the engine turns on for a very short period and then turns off.

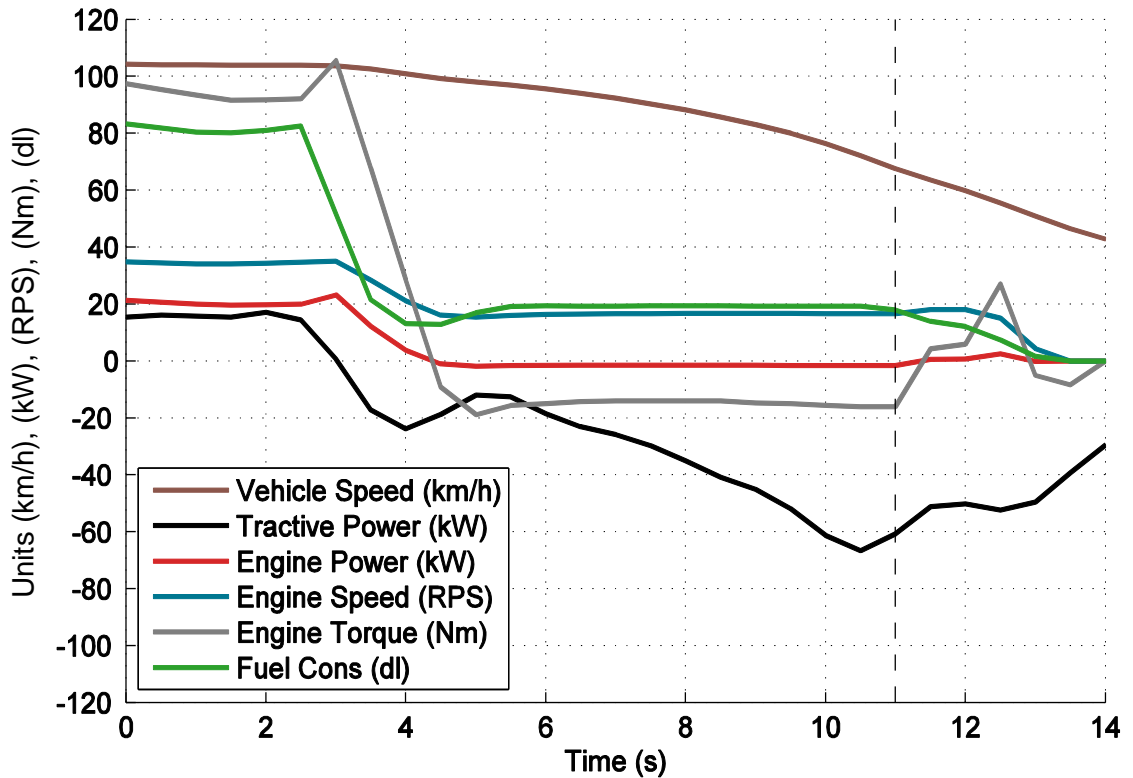


Figure 4.24: Prius vehicle speed, tractive power, engine power, engine speed, engine torque and fuel consumption during fuel cut

Figure 4.25 provides more detail about how fuel cut is achieved. Just before the fuel cut starts at five seconds the motor is being powered by the engine and regeneration power. Some of the motor power is going to the generator, which is motoring and the remaining is fed to the battery. Between five and eleven seconds the engine, generator, motor and battery power are all roughly similar negative values. This means that the vehicle is not regenerating power during fuel cut and the battery and generator are not spinning the engine as they would during an engine start. Instead, the vehicle is using the regeneration power to spin the engine during fuel cut. At eleven seconds the generator switches to motoring and restarts the engine.

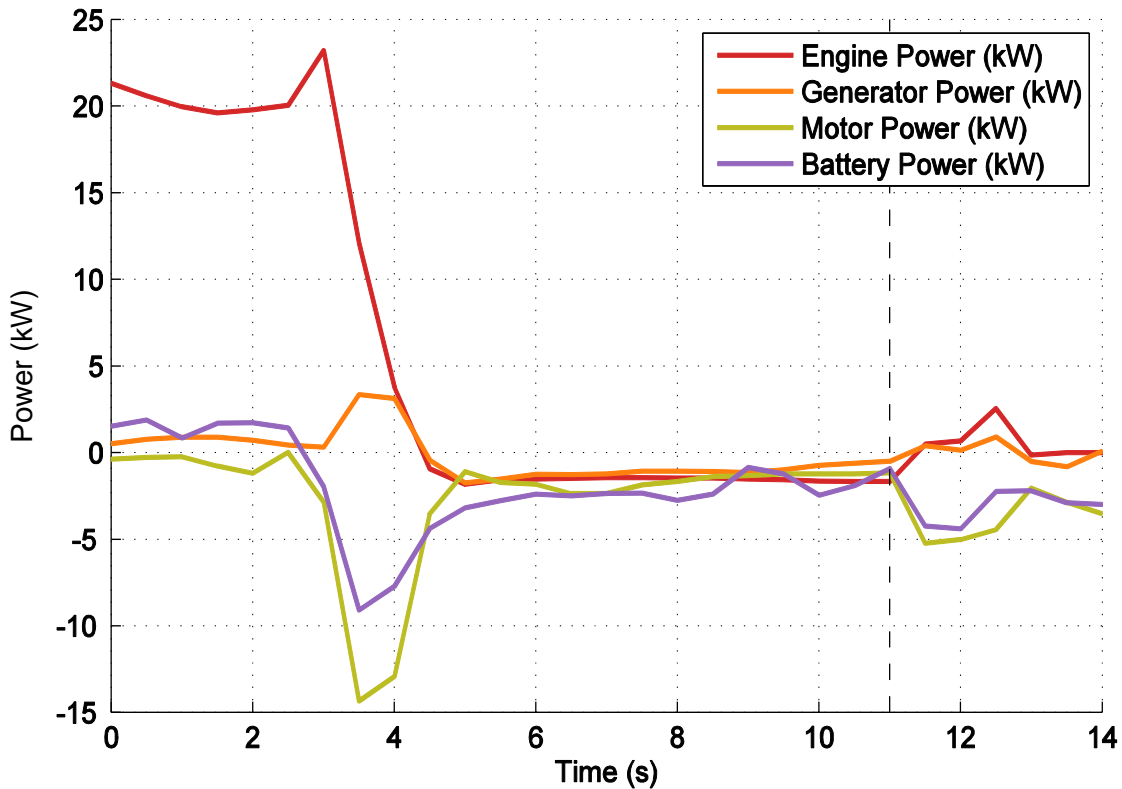


Figure 4.25: Prius engine power, generator power, motor power and battery power during fuel cut

4.3.3 Effect of SOC and coolant temperature on fuel consumption

There are a few key parameters that affect the whole Prius powertrain control, because these parameters have such a strong effect on the Prius control algorithm they also have several direct and indirect effects on fuel consumption. This analysis looks at the two most important of these parameters battery SOC and engine coolant temperature.

Figure 4.26 shows the percentage time, percentage time with the engine off and fuel consumption broken down by tractive power. The 14 tractive power bands used are displayed in Table 4.1. The percentage time is dominated by mode 3 because there is a high proportion of idling within the database, the other modes show decreased time spent in the mode as the tractive power increases. This is expected as it is hard to maintain very high power demands on public roads due to the other road users. This means that mode 13 and 14 only have tens of readings in each mode. For a hybrid vehicle the percentage time without the engine on is a good indicator of the fuel consumption within

a mode. The Prius is capable of driving in PE mode up to tractive power mode 7, data points with the engine off at higher modes are in the process of turning the engine on. The fuel consumption presented in Figure 4.26 is the mean fuel consumption for engine on data within each mode. The result is a roughly exponential growth in fuel consumption with power mode. The trends presented in Figure 4.26 provide a baseline for the analysis of the battery SOC and coolant temperature in the next two sections.

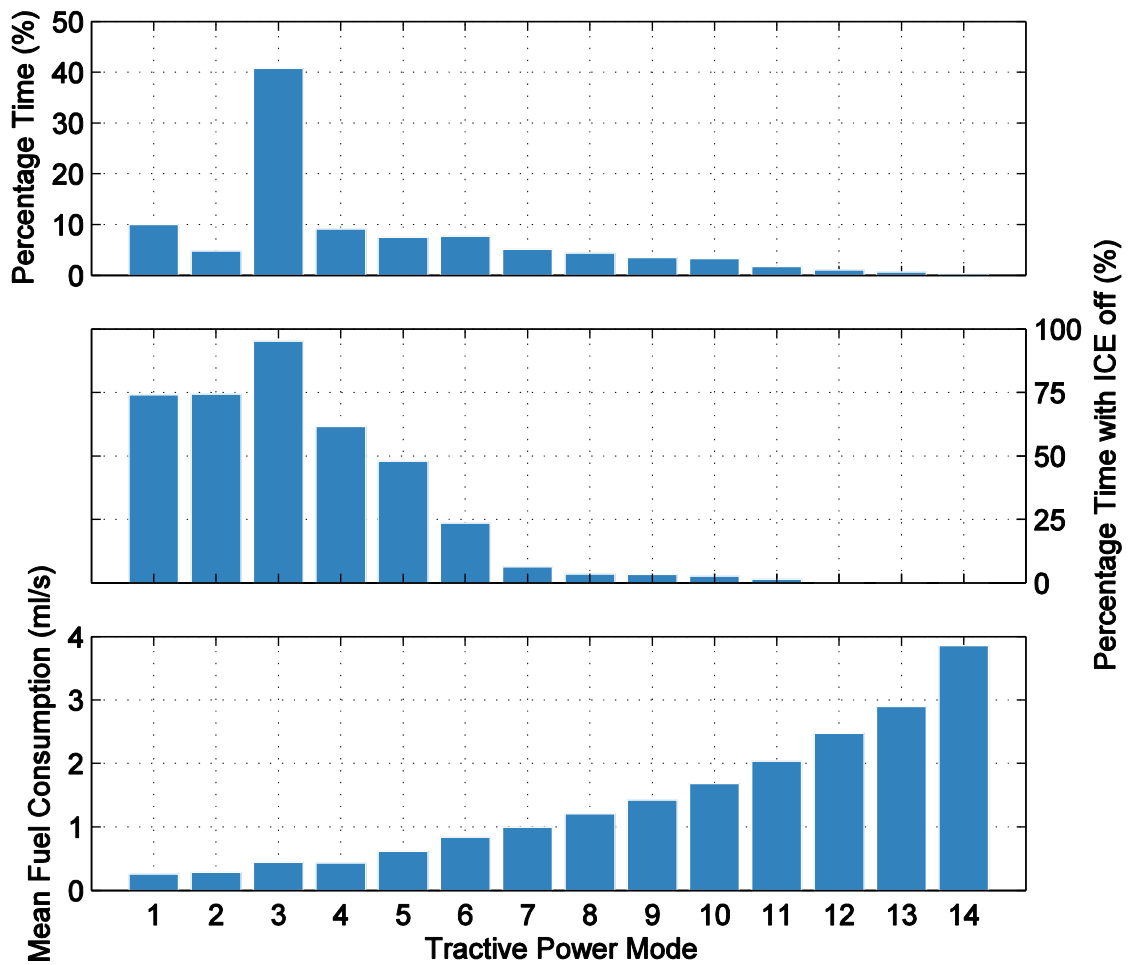


Figure 4.26: Prius percentage time, percentage time with the engine off and fuel consumption by tractive power mode

Table 4.1: EPA vehicle specific power modes (US Environmental Protection Agency, 2002)

Tractive Power Mode	Tractive Power (kW)
1	Power < -2
2	-2 <= Power < 0
3	0 <= Power < 1
4	1 <= Power < 4
5	4 <= Power < 7
6	7 <= Power < 10
7	10 <= Power < 13
8	13 <= Power < 16
9	16 <= Power < 19
10	19 <= Power < 23
11	23 <= Power < 28
12	28 <= Power < 33
13	33 <= Power < 39
14	39 <= Power

4.3.3.1 Battery SOC Effect on Fuel Consumption

Figure 4.27 presents the same data as Figure 4.26, but broken down by battery SOC. The low power modes are dominated by low SOC because the vehicle can drive in PE mode in these modes and this decreases the SOC. Also, the engine on time is very low so there is little opportunity for the battery to be recharged. Higher SOC occurs in power mode 1 where the battery receives lots of power from regeneration and in the high power modes where PE mode never occurs and so the drain on the battery is much lower. The percentage time with the engine off is not a function of SOC in the low power modes, but as the power modes near the engine on power threshold, SOC is the key determinant of whether the engine turns on or not. In power mode 6 where the engine normally turns on

the fraction of engine off data is a linear function of SOC. In power mode 7 only the very highest SOC data exhibits a significant amount of engine off data. In the positive power modes SOC has an increasing effect on fuel consumption. In power mode 3 fuel consumption decreases by 0.25 ml/s between the lowest and the highest SOC, this increases to 0.5 ml/s in mode power 8 and 1 ml/s by mode 13. The additional engine load caused by low SOC is the same for all power modes, but the additional load has a much stronger effect on fuel consumption at higher engine powers. By changing fuel consumption by 1 ml/s in mode 13 the SOC is changing fuel consumption by around a third of the fuel consumption change caused by tractive power, this demonstrates the importance of recording SOC while testing hybrid vehicles as it is a key controller of fuel consumption at any given instance.

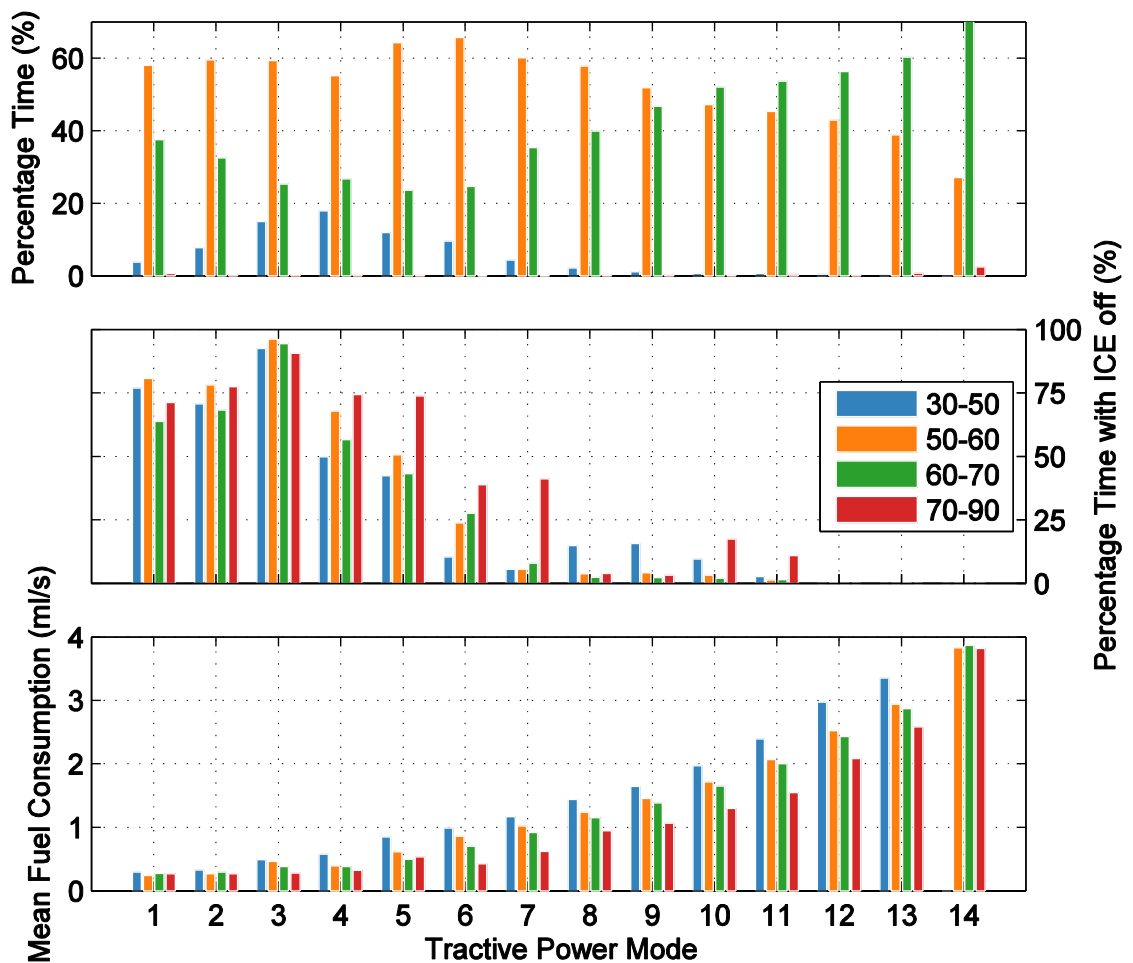


Figure 4.27: Prius percentage time, percentage time with the engine off and fuel consumption by tractive power mode, split by batter SOC

4.3.3.2 Engine Coolant Temperature Effect on Fuel Consumption

Figure 4.28 presents the same data as Figure 4.26, but broken down by engine coolant temperature. The percentage time in every power mode is dominated by high engine temperatures. The engine warm up takes a few minutes and most test runs took between 30 minutes and 2 hours. With only a few minutes of cold start data each day it takes a lot of testing to build up a comprehensive cold start database. The only cold start data exists in power mode 4 which covers the first few acceleration phases of each cycle. The engine never turns off if the coolant temperature is very low, but between 20 and 40°C, some engine off data exists where the engine turns off close to 40°C and the engine then cools down. Engine off increases with engine temperature up to power mode 5, for power modes above this SOC will dominate *engine on/off*. Increased coolant temperature results in decreased fuel consumption for power mode 1 to 4, for power modes 5 to 10 the coldest coolant temperature bin has lower fuel consumption, this could indicate that the control is limiting the demand on the engine while it is cold. For power modes 12 to 14 the fuel consumption is also lower for the second lowest temperature bin, implying that as power demand goes up the control reduces power demand on the engine up to higher coolant temperatures to prevent very high emissions. The difference in fuel computation across the coolant temperature bins is lower than the difference across the SOC bins. This shows that SOC, not coolant temperature, is the second most important predictor of fuel consumption after tractive power.

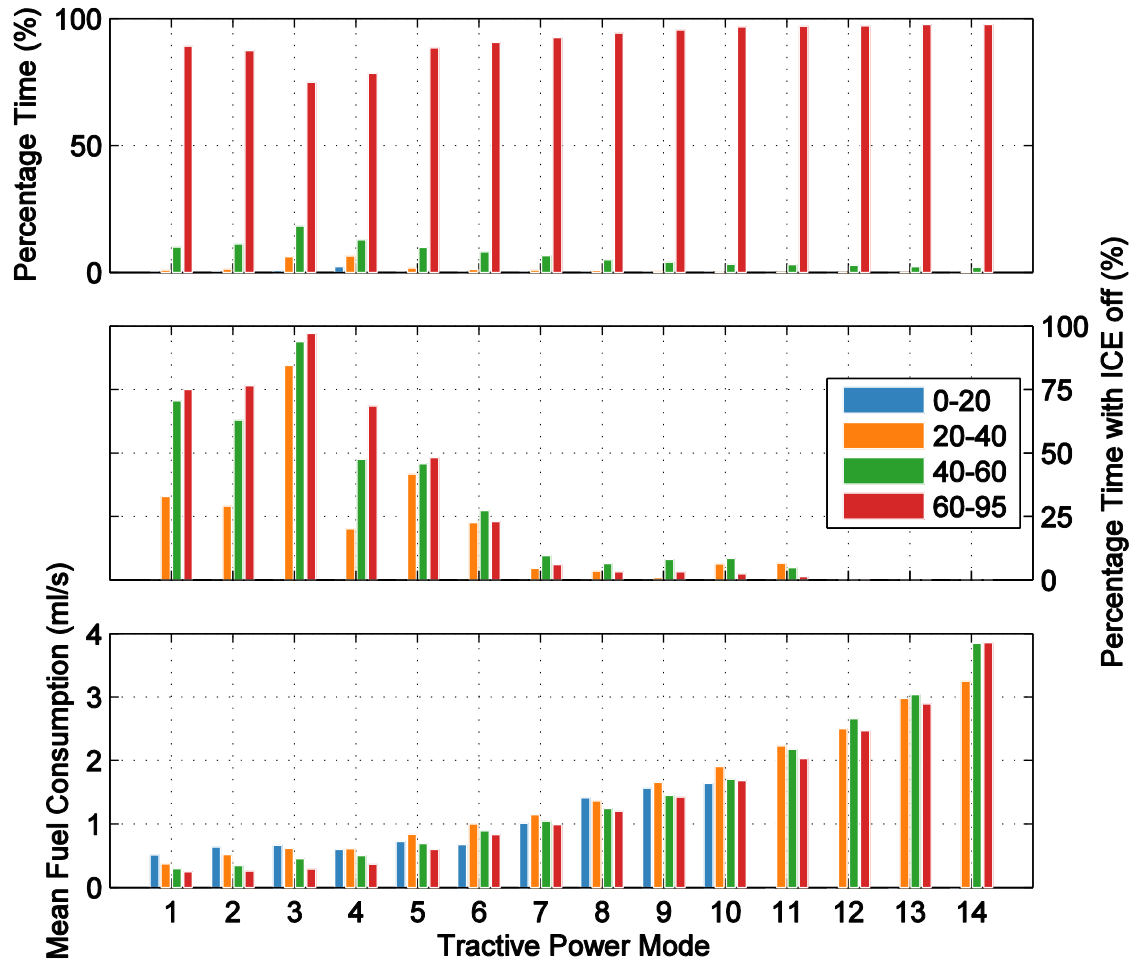


Figure 4.28: Prius percentage time, percentage time with the engine off and fuel consumption by tractive power mode, split by engine coolant temperature

4.4 Conclusions

The Toyota Prius has been very well documented in the literature through component testing and whole vehicle testing on both chassis dynamometers and on the road using PEMS. The large number of internal vehicle parameters available through PAMS testing has allowed this data collection campaign to add to the already detailed body of literature on the Prius operation and control. This chapter has demonstrated that PAMS is a successful method for analysing new vehicle technologies as they enter the vehicle fleet.

The PAMS data has provided further insight into the flexibility of the Prius architecture and how the sizing and control of the powertrain maximises the potential of each component to reduce fuel consumption. This is particularly true in the way PE mode is

used to avoid the worst efficiency regions of both the engine and the powertrain. To achieve this requires a well optimised design that considers the planetary gear ratios, the power limit of PE mode and the engine sizing.

PAMS data has also proved to be very useful for studying very transient data that is more difficult to replicate on a chassis dynamometer. The data shows that for the engine to meet the desired operating path even during strong power transients requires the support of the battery. This significantly increase battery charging and discharging, while the engine is on, which will have a knock-on effect on battery ageing. The benefit of using the battery in this way is that the engine operation is kept in the high efficiency region even during the most transient changes in engine power demand.

The areas where the PAMS data has provided the most insight is vehicle control under cold ambient conditions. This area is less well documented in the literature, probably because it is difficult to study on a chassis dynamometer, but it is none the less very important because it can have such a strong effect on real world emissions. Cold starts are made up of two phases, a catalyst warm-up phase that is characterised by low engine efficiencies, constant engine power output, irrespective of vehicle demand, high engine speeds and low engine torques. The second phase is the engine coolant warm-up phase which is typified by decreasing engine idle speed, increasing engine torque, increasing engine efficiency and *engine off* based on coolant temperature, not vehicle driving demand. In 2014 56% of all car trips in the UK were less than 8 km (5 miles), many of these trips will be for commuting where the car has stood all night or all day and the engine will be cold (Department for Transport, 2014). For these short trips cold starts have a large effect on overall trip emissions, and so understanding how cars perform during cold starts is very important. While this study has increased our understanding of the controls used in cold starts, further work is required to study how cold starts and cabin heating effect the efficiency of the Prius during real world trips.

PAMS has been shown to be an effective vehicle testing technique that can help to significantly improve our understanding of the most complex vehicle architectures on the road today. As PAMS becomes a more widely used technique in academic research it could provide a cost effective method for analysing the many new hybrid and electric powertrains entering the market, which lack the detailed information that has been collected on the Toyota Prius. By allowing this detailed analysis of the vehicle, PAMS data improves vehicle activity and emission studies, like the one carried out in Chapter 5 on taxis, by providing an explanation for the different vehicle performances in different situations. Analysing PAMS data also provides modellers with the vehicle control patterns that they need to build the structure of a vehicle model. This is the case in Chapter 6 where the analysis of the Prius conducted in the current chapter is used to build the model structure and then the PAMS data is used again to populate the model. It is expected that in the future PAMS data could play an important role in informing both local and national emission policy. The most important role of PAMS data in the near future is to provide large quantities of real-world data that can be used to highlight loopholes in type approval testing. While PAMS data collection does not record emissions data, it can none the less help to improve emission testing by recording variables such as catalyst temperature, wide band oxygen sensor and urea injection in SCR systems, that can be used to screen for and understand irregularities in real world emission figures.

Chapter 5

Potential of Hybrid Vehicles to Reduce Emissions from Taxi Fleets

5.1 Introduction

To demonstrate the potential of PAMS to inform local policy makers and consumers through situation-specific data, database B presented in Chapter 3 has been used to appraise the benefits of using hybrid vehicles as taxis. A project between Leeds City Council and Leeds University has been set up with the aim of quantifying the CO₂, air quality pollution and economic benefits of switching the predominantly diesel taxi fleet of Leeds to petrol hybrid vehicles. The PAMS testing was used to inform the CO₂ and business case sections of the project. This chapter includes:

1. A review of the current literature on the CO₂ benefits of hybrid vehicles in taxi fleets.
2. An overview of the makeup (size of the fleet, vehicle type, engine size, fuel used) and usage patterns (distance driven, time of day of operation) of the current Leeds taxi fleet.
3. A test methodology including dates and times of testing, how test routes were chosen, which test routes were used and a description of the driving styles the driver was asked to follow.
4. A detailed results and discussion section analysing the taxi driving pattern, the three driving styles the driver was asked to follow, fuel consumption, CO₂ emissions, NO_x emissions and the business case for hybrid taxis.
5. A review of policies that have been used in other cities to encourage the uptake of hybrid taxis and an assessment of how these policies could perform in Leeds.

Situation specific data is especially important for analysing taxi driving demand because the taxi driving pattern, with its long stops and city centre focus, is likely to be very different from the average driver on the road. Even without the current problems in type approval figures, it is unlikely that type-approval numbers would give an accurate picture about the advantages and disadvantages of different powertrain choices for taxi vehicles.

The specific nature of taxi driving makes it well suited to PAMS data collection. The long stops and sometimes aggressive driving style that are expected in taxi driving are difficult to replicate on a chassis dynamometer, where the cycle length and acceleration rates are limited. The long stop times also significantly increases testing time, which would have made PEMS testing very expensive. PAMS testing, by comparison, can easily record the full range of real-world vehicle operations and is cheap enough to run the long testing campaigns needed to characterise taxi usage patterns.

Hybrid vehicles have considerable potential in the taxi market for several reasons. Firstly, taxis are covered by more regulation than conventional vehicles, such as driver and vehicle licensing (Leeds City Council, 2016b). There are, therefore, more policy levers that local policy makers can use to encourage the uptake of hybrid vehicles in the taxi market. Secondly, while in 2013 there were only around 78,000 taxi vehicles in the UK, making up just 0.27% of the total fleet (UK Department for Transport, 2013), their impact is likely to be far larger than their numbers would indicate. Interviews with taxi drivers in Leeds suggests that a taxi will be driven 48,280 km (30,000 miles) a year (*Interview Head of Streamline Cabs, 2015, Unpublished Data*)(*Interview Hybrid Taxi Driver, 2015, Unpublished Data*), considerably higher than the average UK mileage of 12,713 km (7,900 miles) a year (Department for Transport, 2014). This means that switching to vehicles with lower emissions will have a greater fuel saving, and emissions benefit, for taxis than private cars. As a result, taxis benefit from shorter payback times on the high initial cost of low emission vehicles.

Thirdly, hybrid taxis provide far greater exposure of the new technology to the public than private vehicles. While a secondary benefit this could still be important for the uptake of the technology by other users. With around 15 customers a day in Leeds each hybrid taxi could make a real difference to public opinion of hybrid vehicle technologies.

Fourthly, taxi fleets in the UK are dominated by larger engine, diesel vehicles, and their numbers are focused around urban areas, where they likely do most of their driving. This combination of circumstances suggests there could be great benefits from a switch to hybrid vehicles. Leeds has 536 taxis; this fleet is dominated by 2L (41%) and 1.6L (29%) diesel saloons and MPV's (*Leeds City Council, Unpublished Data*). London by far the UK largest city has a taxi fleet of 22,200 vehicles, making up 28% of all taxis in the UK (UK Department for Transport, 2013). London is unusual in having very strict guidelines for taxis, meaning few vehicles are eligible (Transport for London, 2007). The London fleet is dominated by vehicles from the London Taxi Company and the Mercedes-Benz Vito, with 2.5L and 2.1L diesel engines respectively (Mercedes-Benz, 2008; The London Taxi Company, n.d.). London is now realising the damaging effect these polluting vehicles are having on the city air quality and has specified that all newly licenced taxis from 2018 will have to be zero emission capable, which with current technology means plug-in hybrids (Transport for London, 2015b).

Taxi use and operation is centred around urban areas, from the source data of the PCO Cenex London Taxi drive cycle, it is estimated that a typical London taxi day has an average speed of 16.33km/h, an average speed excluding stationary data of 25.49 km/h and spends 29% of the day idling, 28.9% accelerating, 4.7% cruising and 30.5% decelerating (*Millbrook Proving Ground Ltd. Unpublished Data*). These statistics suggests the driving is predominantly stop, start urban driving. The combination of these factors, low speeds and large diesel engines causes two major problems. Firstly, large engines are very inefficient at low speeds resulting in very high fuel consumption. Secondly, diesel engines, even those having met recent emission limits such as Euro 5

and Euro 6, have been shown to have very high levels of NO_x emissions in the real world (M. Weiss et al., 2012).

Hybrid vehicles, by comparison, have been shown in several studies to outperform conventional vehicles on fuel consumption and emissions, especially in urban areas. Costagliola et al. 2015 compared a Euro 4 diesel against a comparable petrol hybrid. For CO₂ g/km the diesel was 6, 91, 13, 56% higher than the hybrid over the Urban Drive Cycle (UDC) cold, UDC hot, Extra Urban Drive Cycle (EUDC) and Artemis urban drive cycles respectively (Costagliola, Prati, Mariani, Unich, & Morrone, 2015). Lenaers 2009 tested a petrol, diesel and hybrid vehicle in the real world with PEMS equipment. In urban driving the CO₂ emissions from the petrol and diesel were 70, 39% higher than the hybrid, respectively (Lenaers, 2009). Lutsey 2011 looks at the potential of hybrid and diesel technology to meet future US vehicle emission targets. When comparing hybrid and diesel CO₂ figures, taken from consumer labels, with comparable petrol vehicles, they found diesel technology could offer a 15% reduction and hybrids a 30% reduction (Lutsey, 2011). It is clear from the literature that hybrids offer great potential benefit both in the reduction of fuel use and emissions even when compared to modern conventional vehicle technology.

To provide an exact comparison between the three vehicles the hybrid vehicle was tested on the road over common taxi routes and the petrol and diesel vehicles were modelled over the driving trace created by the hybrid. The two conventional vehicles were modelled in the Passenger car and Heavy duty vehicle Emission Model (PHEM), described in Section 2.4.2.1. PHEM has been chosen for the vehicle modelling because it is considered to be the leading microscale emission model in Europe (CH2M Hill, 2013).

5.2 Literature Review

Very little academic work has been conducted on the benefits of using hybrid vehicles to reduce emissions from taxis. Wu et al. 2015 tracked a Toyota Prius and a comparable petrol and diesel vehicle, with PEMS, over a 36 km route in Macao, including freeways, arterial and residential roads. The Prius reduced CO₂ emissions by 35% and 15% compared to the petrol and diesel vehicles respectively and reduced NO_x emissions by two orders of magnitude compared to the diesel vehicle. The study clearly shows the potential of hybrids as taxis, but the routes used were not specifically taxi routes and the data does not include driving through taxi ranks. This could be because it is not part of taxi driving in Macao, the study is looking at vehicles akin to Private Hire Vehicles (PHV) in the UK or the researchers did not have permission to do so (Wu et al., 2015). Either way, in the UK the taxi rank is a key area of interest when studying taxis as it is one of the areas that differentiates taxis driving demand from any other driving demand. AbuHijleh & Nik 2013 used US Department of Energy city fuel consumption figures to estimate the benefit of switching from petrol to hybrid taxis in Dubai. They found the switch to a hybrid taxi reduced CO₂ emissions by 30% and the additional upfront cost could be paid back by fuel savings in less than one year (Abuhijleh & Nik, 2013).

Several trials and pilot schemes of hybrid taxis in North America have been recorded and they provide better evidence for the fuel saving potential of hybrid taxis. The 'Hail a Hybrid Program' run by Climate Change Central in Calgary, Alberta between 2006 and 2008 collected odometer reading, litres of fuel purchased, cost of fuel and total spent on refuelling, for six taxi vehicles, a 2006 Toyota Prius, a 2007 Toyota Camry, three 2006 Ford Escape Hybrids and a 2006 Ford Crown Victoria. The results indicate that switching to a hybrid could reduce GHG emissions by 52 to 70% and the higher cost of a hybrid could be repaid within four to nineteen months, depending on if new or second-hand vehicle was purchased (Transport Canada, 2008). The 'Toronto Hybrid Taxi Pilot' tracked ten Toyota Camry Hybrids, one Toyota Prius and five Toyota Camry, collecting

750,000 km of data over an 18-month period. Switching to the Camry hybrid reduced fuel consumption by 24%, while switching to the Toyota Prius reduced fuel consumption by 37%. Assuming a fuel cost of \$1/L the Toyota Prius saved \$2,440 over a standard seven year taxi life, this increased rapidly with increasing fuel costs. At \$1.50/L the lifetime saving increased to \$10,000 (Toronto Atmospheric Fund, 2009).

The academic studies do not use realistic UK taxi driving demand and the North American test programs do not test hybrids against diesel vehicles. There is, therefore, a need for a study to compare representative European petrol, diesel and petrol hybrid vehicles over representative European taxi drive cycles.

5.3 Leeds Taxi Fleet Overview

The Leeds taxi fleet is made up of 4387 vehicles, 536 of which are hackney carriages and 3851 of which are PHV. The two groups operate under different licencing laws, a hackney carriage licence allows drivers to pick customers up on the street without a reservation, whereas a PHV licence only allows drivers to fulfil pre-booked journeys (Leeds City Council, 2016a). This work will focus on hackney carriages as their driving pattern, which includes the taxi rank, is quite unique. Whereas, PHV have a driving pattern that is more comparable to other city centre drivers. PHV will still be discussed within this analysis as they form a larger proportion of the taxi fleet and the results for hackney carries are so conclusive that the trends will still apply to PHV.

Figure 5.1 and 5.2 show the breakdown of the two fleets by vehicle type and engine size. It is clear that the fleet is dominated by large engine, diesel saloons and MPV's, making up 86% of the Hackney carriage fleet and 89% of the PHV fleet. There is a larger proportion of MPV's in the hackney carriage fleet because they have been encouraged to increase the number of Wheelchair Accessible Vehicles (WAV) in the fleet. Only the saloon vehicles can be replaced by hybrid vehicles at this time, as there are no hybrid

WAV on the market. Even so, there are still 3576 vehicles in the fleet that could currently be replaced by hybrid vehicles (*Leeds City Council, 2016. Unpublished Data*).

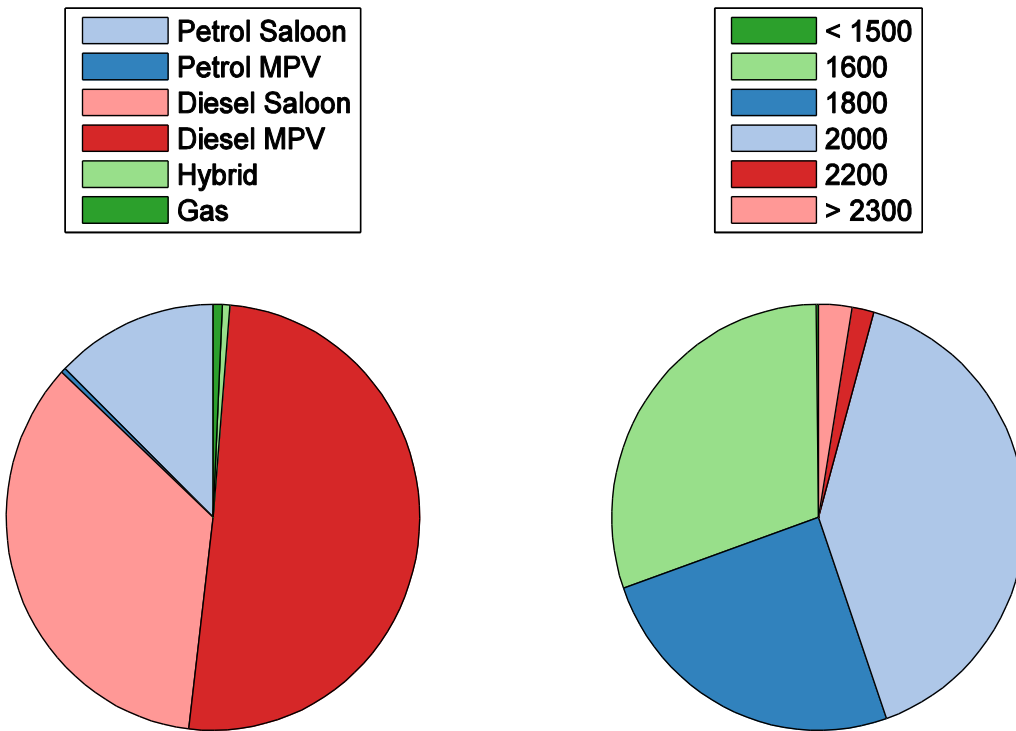


Figure 5.1: Leeds hackney carriage fleet makeup, broken down by powertrain, body type and engine size

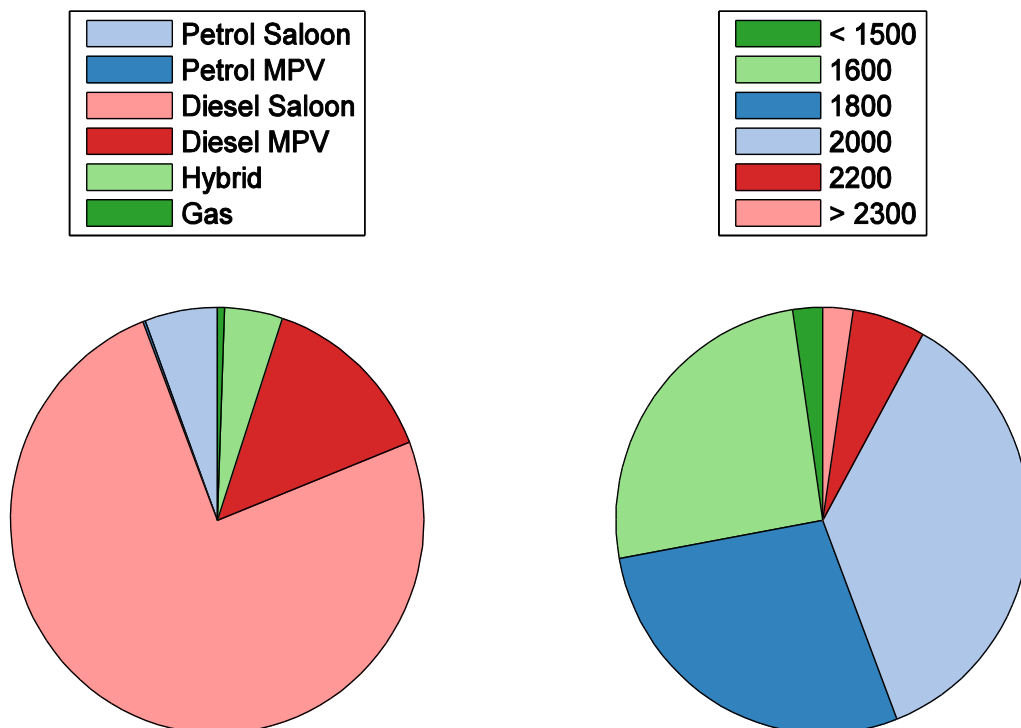


Figure 5.2: Leeds private hire fleet makeup, broken down by powertrain, body type and engine size

Taxis are only a small proportion of the 337,779 (Department for Transport, 2016b) vehicle registered in Leeds, but the very high mileage they cover, their concentration around the city centre and the unusual times of day that they work, mean that taxis can account for a significant proportion of the vehicle emissions in the city centre. A hackney carriage in Leeds covers around 30,000 miles a year and a PHV, which can have two drivers completing 12 hour shifts back to back, covers around 60,000 miles a year (*Interview Head of Streamline Cabs, 2015, Unpublished Data*)(*Interview Hybrid Taxi Driver, 2015, Unpublished Data*), this is a significantly higher mileage than the UK average which is just 7,900 miles a year (Department for Transport, 2014). This means that while taxis only account for 1.3% of the registered vehicles in Leeds, they are likely to account for closer to 10% of the distance driven across the city and a higher proportion in the city centre.

Figure 5.3 shows the number of vehicles travelling along the A660, a major road from Leeds suburbs into the city centre, in a 24 hour period, and what proportion of those vehicles were taxis. At peak times the number of taxis is at its peak, around 1,300 vehicles per hour, but because of the greater increase in other traffic, the proportion of taxis in the fleet drops to its minimum, around 4%. Whereas at night, taxis continue to run when most other traffic has stopped, so that, even though the number of taxis is much lower, around 100 vehicles per hour, taxis become the predominant vehicle group on the road, reaching nearly 50% of hourly traffic (*Leeds City Council, 2016. Unpublished Data*).

The taxi drivers operating times is important for local air quality because diesel vehicles emit high levels of NO_x and particulates. Inversion of the temperature profile of the troposphere at night, traps pollution close to the ground. This means that diesel taxis operating through the night should be targeted by the council in their efforts to meet EU air quality targets.

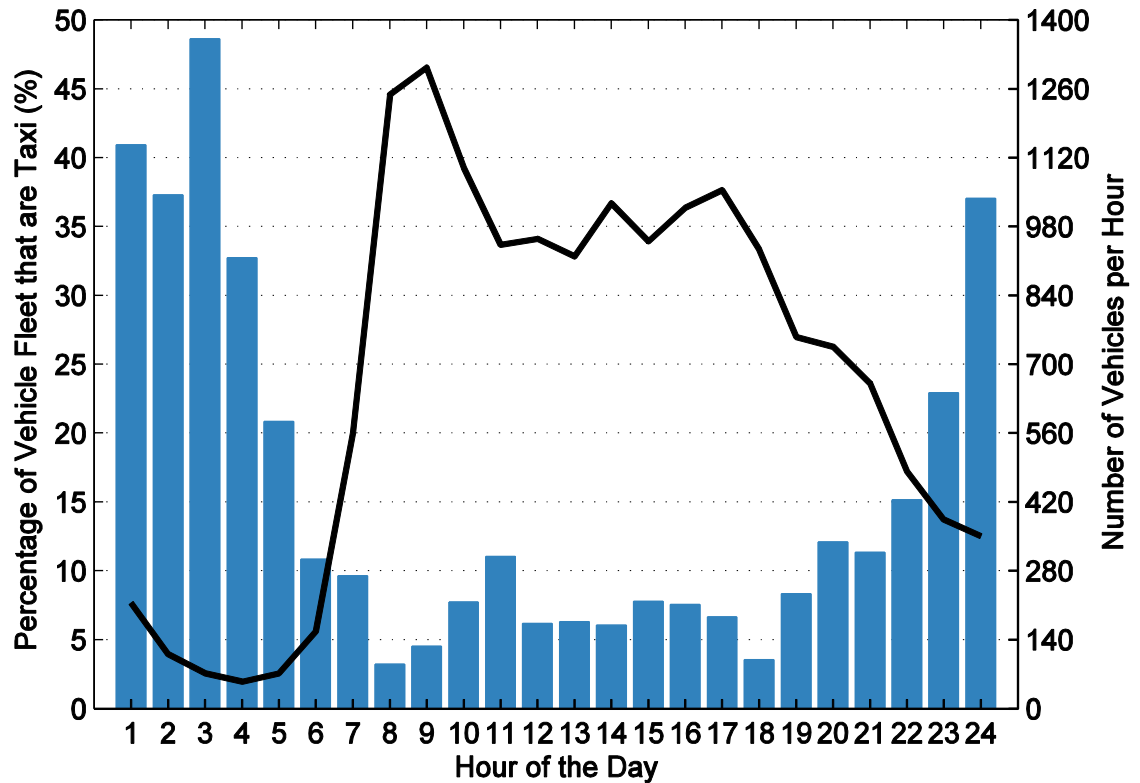


Figure 5.3: Number and proportion of taxi vehicles on the A660 in a 24 hour period. Bar chart, percentage of vehicle fleet. Line chart, number of taxi vehicles

Taxi vehicles in Leeds are mostly bought second hand. This reduces the vehicle cost which is an important factor to the drivers who can find it difficult to amass the large amounts of money needed to buy a car. Figure 5.4 shows the age of the hackney carriage and PHV fleets. Vehicles up to five years old can be licenced as a taxi which is why the number of vehicles peaks around 2010 – 2011 as many drivers will buy vehicles just less than five years old to minimise the vehicle price (*Leeds City Council, 2016. Unpublished Data*).

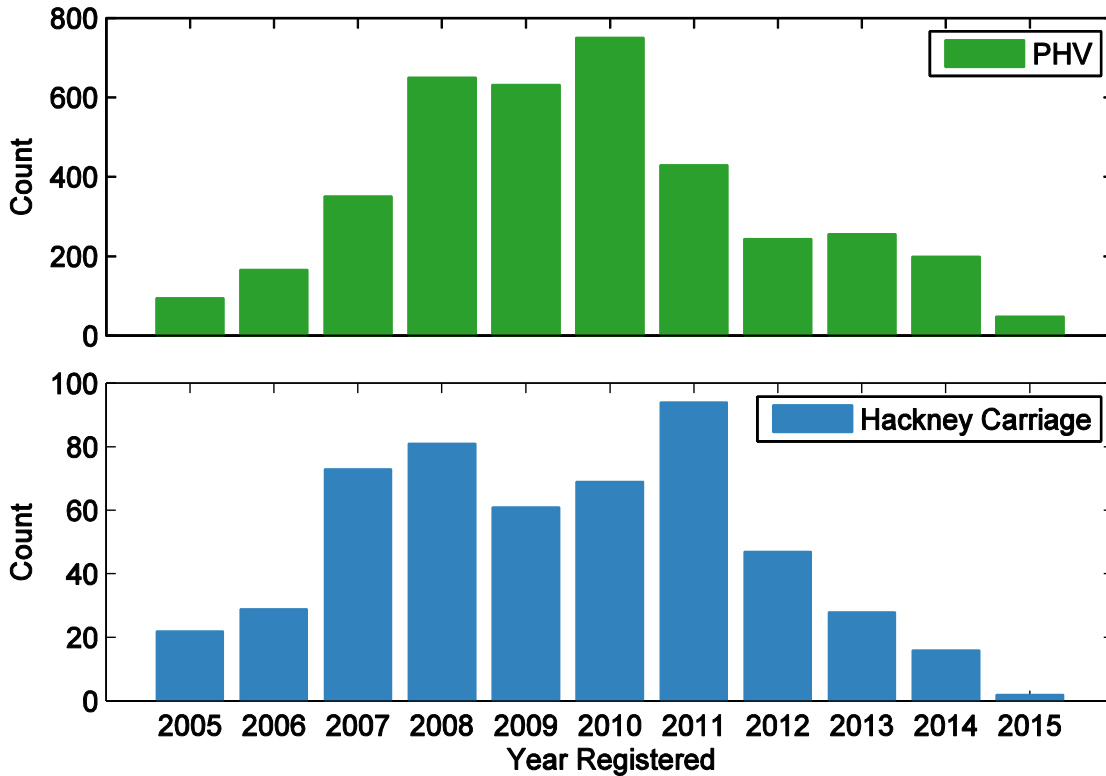


Figure 5.4: Leeds hackney carriage and PHV fleet, year of vehicle first registration

The hackney carriage and PHV fleets are made up of 32 and 133 different makes and models respectively. However, both fleets are dominated by a few models that have gained widespread popularity. This could suggest that taxi drivers choose their vehicles based on the recommendations given by other drivers, or that there is a good sales structure for these vehicles within the city. Either way, it will be important for the council to replicate this if they want hybrid vehicles to replace the current best sellers. In both fleets the Toyota Prius is the only hybrid vehicle; it is the 22nd and 7th most popular vehicle in each fleet, and makes up 0.6% and 3.2% of the Hackney carriage and PHV fleets respectively. The greater success of the Prius in the PHV fleet probably comes down to the greater number of fleet operators, who have the buying power and capital to purchase the more expensive hybrid vehicle. Also PHV higher mileage decreases the payback time of the hybrid vehicle (*Leeds City Council, 2016. Unpublished Data*).

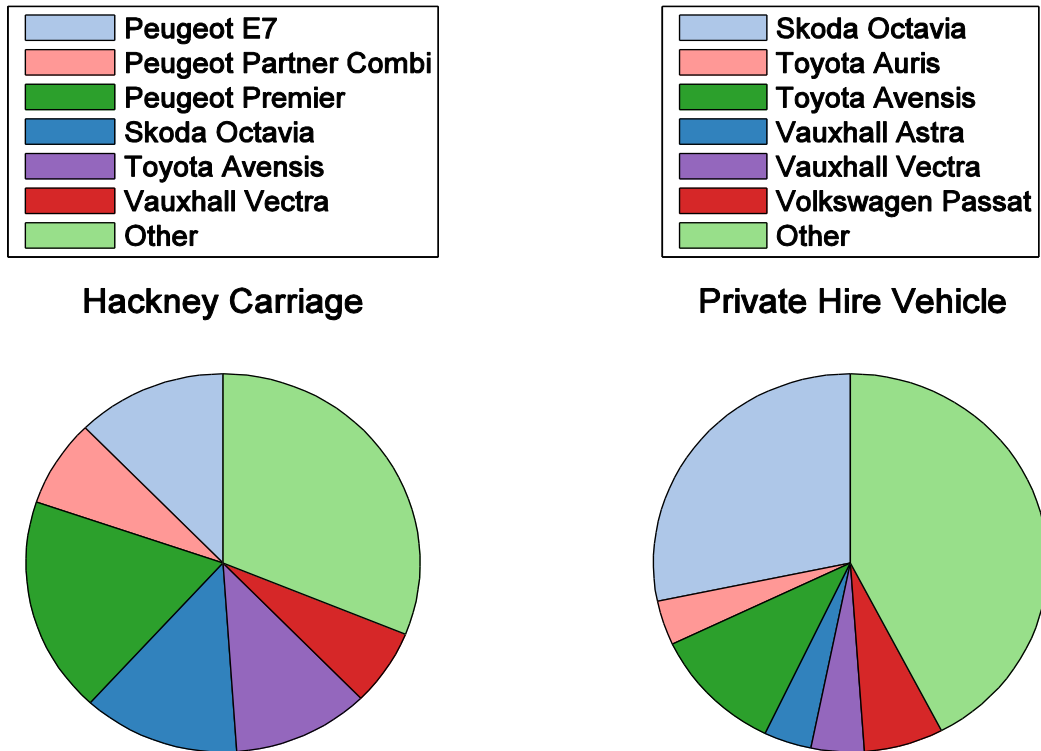


Figure 5.5: Leeds hackney carriage and PHV fleet makeup, by vehicle make and model

5.4 Results and Discussion

5.4.1 Taxi Driving Pattern

At the beginning of this research, we decided that no legislative CO₂ or fuel consumption data could be used to inform which vehicle would perform best as a taxi in Leeds. This was for two reasons. Firstly, the growing gap between legislative and real word emission figures is not evenly distributed across make, segment or technology, making the use of this data for comparison between vehicles very difficult. Secondly, as shown in Figure 5.6 the driving style of a taxi is very different to legislative test cycles.

Figure 5.6 a, b, c, d, e, f shows the Toyota Prius test data collected during this project, with and without the taxi rank data included, the PCO Cenex London taxi driving cycle, the UDDS cycle, the NEDC, and the WLTC respectively. The PCO Cenex cycle was

created based on over 500 hours of taxi vehicle tracking data in London and is, therefore, a good, representative benchmark of taxi driving in London and possibly the UK (*Millbrook Proving Ground Ltd. Unpublished Data*).

The test data and PCO Cenex cycle show very similar speeds, but the test data exhibits higher VSP (Jiménez-Palacios, 1999), this could be because London is more congested than Leeds or the high acceleration could have been lost in the cycle building process. The closest legislative cycle is the UDDS, which is not surprising considering the central urban data set from which the cycle was created. The UDDS, however, is not the only drive cycle that goes into creating vehicle fuel consumption test figures in the USA; the other more aggressive and highway focused cycles make the test figures more representative of the rest of the fleet, but will make the figures less informative for taxis. The European drive cycles, both the NEDC currently and the WLTC in the future, lack the low-speed power demand and include too much high speed driving to provide fuel consumption figures that are useful when comparing technologies for taxis.

Another major difference between taxi data and legislative drive cycles is the idle time. Queuing through the taxi rank adds a significant amount of idling and *engine off* phases to urban driving, which already has a very high idling percentage. When the test data was collected the engine was kept on for the whole route, but when the speed profile was modelled, all stops in the taxi rank longer than one minute were counted as *engine off* phases for the conventional vehicles. This was done because the data for how often taxi drivers turn off their engines in the taxi rank was not available, and this method will result in a conservative, rather than an optimistic estimate of the fuel consumption benefits of hybrid vehicles. The test data has 10.7% vehicle off and 27.7% idle data, this is in good agreement with the PCO Cenex source data, which has 6.9% vehicle off and 29% idling (*Millbrook Proving Ground Ltd. Unpublished Data*).

These figures are much higher than most of the test cycles 19.3% UDDS, 27.3% NEDC, and 13% WLTC. This means that cars used by taxi drivers, but developed for the test

cycles do not prioritise the use of technology that could reduce the effect of idling on emissions. These technologies could include, engine stop-start, electric engine coolant water pumps, exhaust heat recovery systems, catalyst heaters and electric cabin heaters. The problem with trying to solve idling emissions with stop-start technology is that many taxi drivers will use some cabin heating in the winter and AC in the summer. The engine is required to run these systems in both conventional and hybrid vehicles. To try and overcome this problem the City of New York funded a \$10 million project that, among other things, aimed to design and retrofit a system to taxis that provided cabin heating while the engine was turned off (City of New York Taxi & Limousine Commission, 2007).

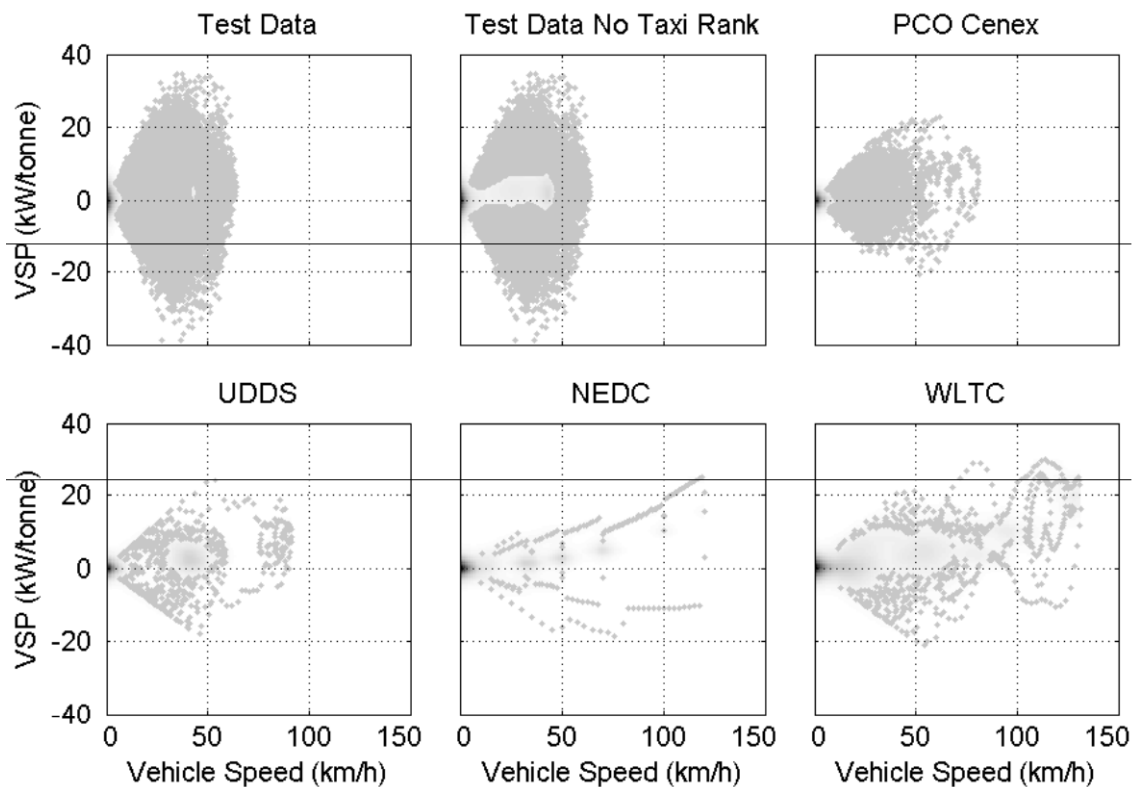


Figure 5.6: Vehicle Speed against VSP for six data sets. Top-panel (a) Toyota Prius test data, (b) Toyota Prius test data with taxi rank data removed, (c) PCO Cenex London taxi driving cycle. Bottom-panel (d) Urban Dynamometer Driving Schedule (UDDS), (e) New European Drive Cycle (NEDC), (f) Worldwide harmonized Light-duty Test Cycle (WLTC)

5.4.2 Driving Styles

In testing, three different drive styles were used; calm, normal, and aggressive. Figure 5.7 shows the distribution of speed and acceleration for the three driving styles, excluding stationary data. These driving styles represent the full range of driving possible in urban conditions. The calm driving accelerated as smoothly as possible and tried to avoid excessive power, but still had to keep up with the flow of traffic. The aggressive driving accelerated as fast as possible, but was limited by the Prius performance, the traffic flow and speed limits.

The 0.05, 0.25, 0.5, 0.75, 0.95 quantiles, shown in red, clearly show the shift between each driving style. Calm driving has slow acceleration up to the speed limit with a lot of data existing in the acceleration phase. As the driving becomes more aggressive, the low-speed acceleration increases, the vehicles moves through the low speeds quickly and ends up cruising at the speed or traffic limit. The ranked nonparametric Wilcoxon Mann Whitney test was applied to the test data to check for statistical significant difference between the three driving styles. At 95% confidence level, the three driving styles were found to be significantly different from each other for vehicle speed, vehicle acceleration and fuel consumption.

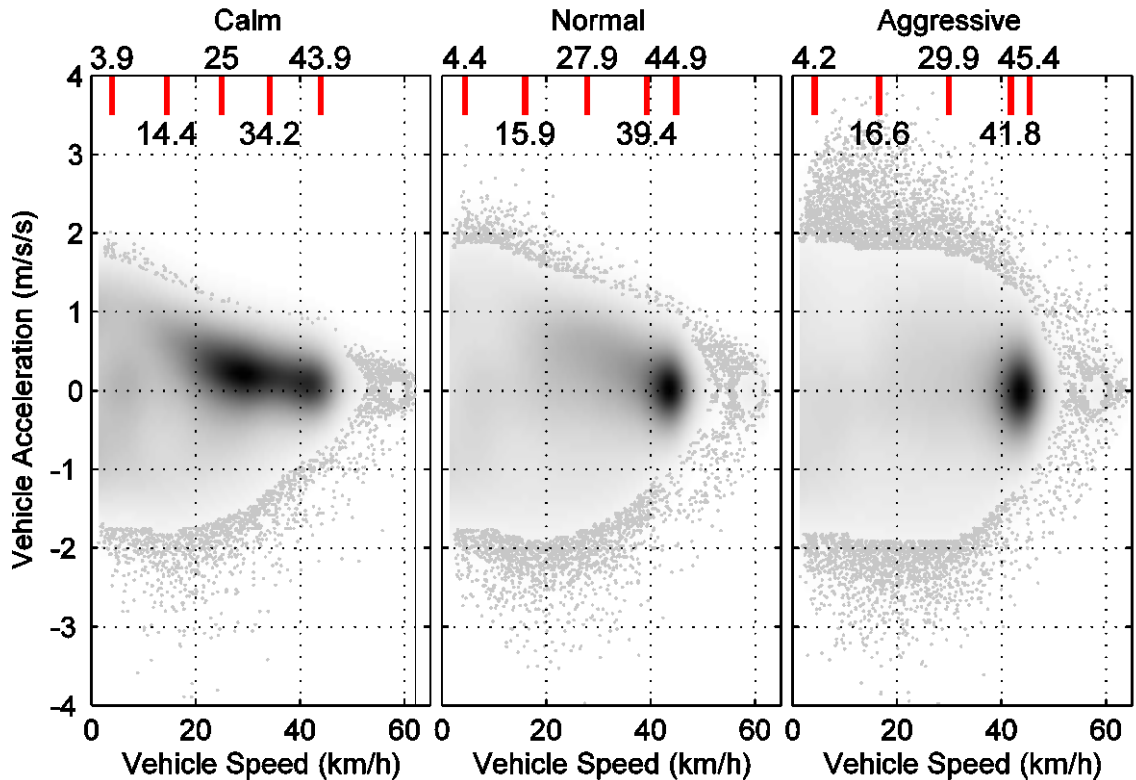


Figure 5.7: Vehicle speed against vehicle acceleration, for the three taxi driving styles

5.4.3 Fuel Consumption and CO₂ Emissions

Table 5.1 compares the fuel consumption of the three vehicles tested, for the three driving styles. The Prius has the lowest fuel consumption under all three driving conditions, with the lowest fuel consumption in calm driving and the highest fuel consumption during aggressive driving. The Prius also exhibits the widest range of fuel consumptions, with calm driving saving over 1 l/100km compared to aggressive driving. The Prius switches the *engine on* for two reasons, because the tractive power demand is too high or because the battery SOC is too low. During calm driving the vehicle can travel much further before the battery power limit is met and the engine often turns on due to low battery SOC. Whereas, during aggressive driving the battery power limit is met soon after the vehicle moves away from a stop, this means that the car cannot utilise the full energy available in the battery. By driving with a calm driving style the percentage time in PE mode increases by 20%, over aggressive driving. This shift in PE mode usage

is the main reason why driving style has a greater effect on the Prius than the conventional vehicles. Both of the conventional vehicles are most efficient under normal driving. This is because calm driving forces the engine to operate at low torques, where the engine efficiency is low and aggressive driving significantly increases the power demand for the cycle.

Table 5.1: Fuel economy, fuel consumption and CO₂ emissions for the three vehicle technologies and three driving styles

	Fuel Economy (MPG)	Fuel Consumption (l/100km)	Carbon Dioxide Emissions (g/km)
Hybrid Calm	59.41	4.75	111.11
Hybrid Normal	56.31	5.02	117.24
Hybrid Aggressive	47.94	5.89	137.71
Hybrid All	54.10	5.22	122.02
Petrol Calm	21.10	13.39	312.87
Petrol Normal	21.84	12.93	302.28
Petrol Aggressive	21.21	13.32	311.18
Petrol All	21.38	13.21	308.78
Diesel Calm	32.87	8.59	230.64
Diesel Normal	33.04	8.55	229.49
Diesel Aggressive	31.43	8.99	241.23
Diesel All	32.43	8.71	233.79

The Toyota Prius has lower fuel consumption than conventional vehicles because the hybrid powertrain gives greater flexibility and control over when and how the engine is operated. To understand these differences the Prius operation has been split up into three main modes and eight sub-modes, described in Table 5.2.

Table 5.2: Toyota Prius operating modes

Mode Number	Mode Colour	Main Mode	Sub Mode
1	Clear	Vehicle Stationary	None
2	NA	Pure Electric Mode	All PE mode data
2a	Light Blue		Full micro trip with no engine on. Positive tractive power
2b	Dark Blue		Full micro trip with no engine on. Negative tractive power
2c	Light Green		PE mode operation between sections of HE mode operation in the same micro trip. Positive tractive power
2d	Dark Green		PE mode operation between sections of HE mode operation in the same micro trip. Negative tractive power
3	NA	Hybrid Electric Mode	All HE mode data
3a	Purple		Engine start up
3b	Dark Red		Engine charging traction battery
3c	Light Red		Traction battery assisting engine
3d	Yellow		Engine on standby

Table 5.3: Fuel saving achieved by Prius in each operating mode

Mode Number	Percentage Time (%)	Percentage Fuel Saving Petrol (%)	Percentage Fuel Saving Diesel (%)
1	40.6	13.4	16.6
2	31.9	54.6	73.1
2a	4.30	8.23	12.2
2b	4.27	5.37	6.50
2c	7.94	19.5	30.2
2d	15.4	21.5	24.2
3	27.5	32.0	10.3
3a	2.92	4.75	4.48
3b	17.4	17.4	-1.29
3c	2.84	3.85	2.14
3d	3.93	5.39	4.37

Figure 5.8 shows a section of driving data with all the modes colour coded. The top plot, with axes on the left, presents vehicles speed and engine power for the three vehicles, while the bottom plot, with axes on the right, presents fuel consumption for the three vehicles. The colour of each mode is given in Table 5.2. The following three subsections will explain in more detail how the efficiency benefits of the Prius, presented in Table 5.3, are achieved through an in-depth analysis of the drivetrain operation in each of the three main modes defined in Table 5.2.

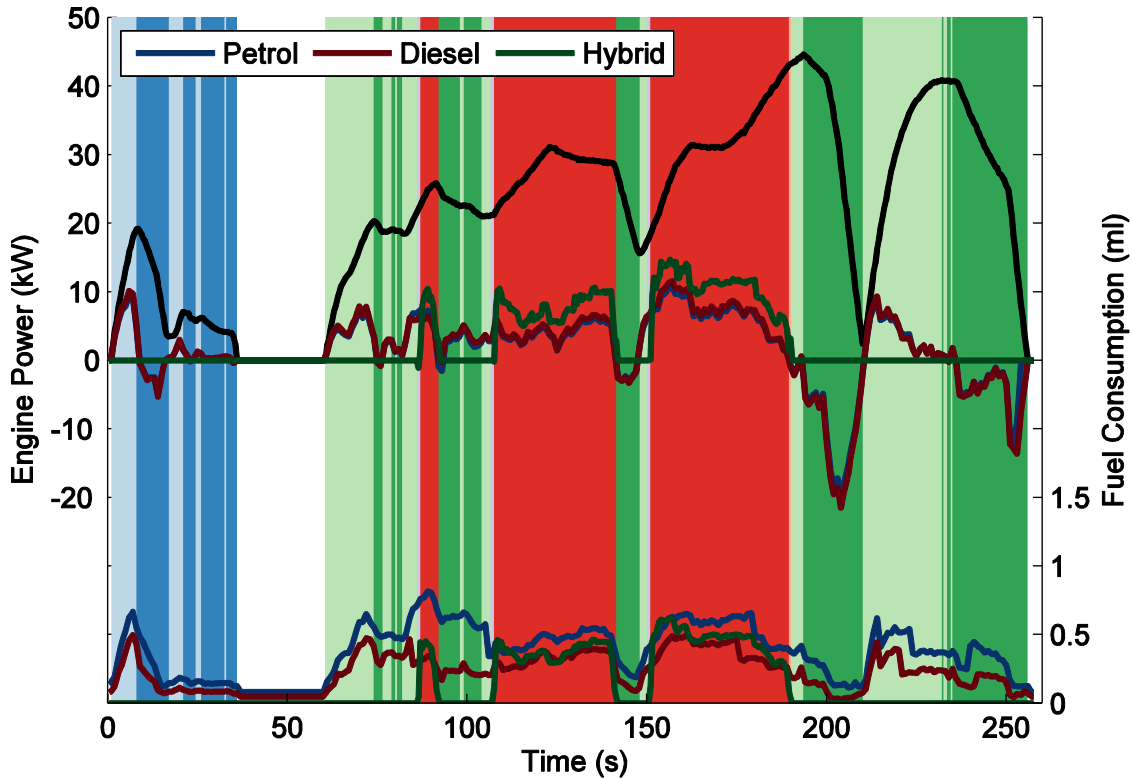


Figure 5.8: Engine power and fuel consumption for the hybrid, petrol and diesel vehicles, colour coded by Prius operating mode

5.4.3.1 Mode 1, Vehicle Stationary Mode

Taxi driving demand combines city centre driving with regular queuing in the taxi rank, it, therefore, has significantly more stationary data than most ordinary vehicle users. Because of this, it may be expected that stop-start technology could achieve most of the fuel consumption benefits of a hybrid vehicle in taxi driving. Instead, Table 5.3 shows that even with stationary data taking up 40% of the test time, stopping the engine when the vehicle is stationary only achieves around 15% of the fuel consumption benefit of full hybrid technology.

5.4.3.2 Mode 2, Pure Electric Mode

Even hybrid vehicle with relatively small battery packs like the third generation Toyota Prius can achieve significant fuel consumption benefits by operating in PE mode. In fact, as Table 5.3 shows operating in PE mode is the main way the hybrid saves fuel in city

driving. There are two main reasons for this; firstly, the hybrid vehicle operates in PE mode during low power events when the conventional engine is forced to operate in the low speed, low torque region of the engine map where it is particularly inefficient. Figure 5.9 and 5.10 show the conventional vehicle engine speed and torque when the hybrid is operating in PE mode. The Figures displays a lot of low engine torque operation, at these low torques, the engine efficiency may be half the peak engine efficiency, doubling the benefit of using PE mode for the hybrid vehicle (Treiber & Kesting, 2013).

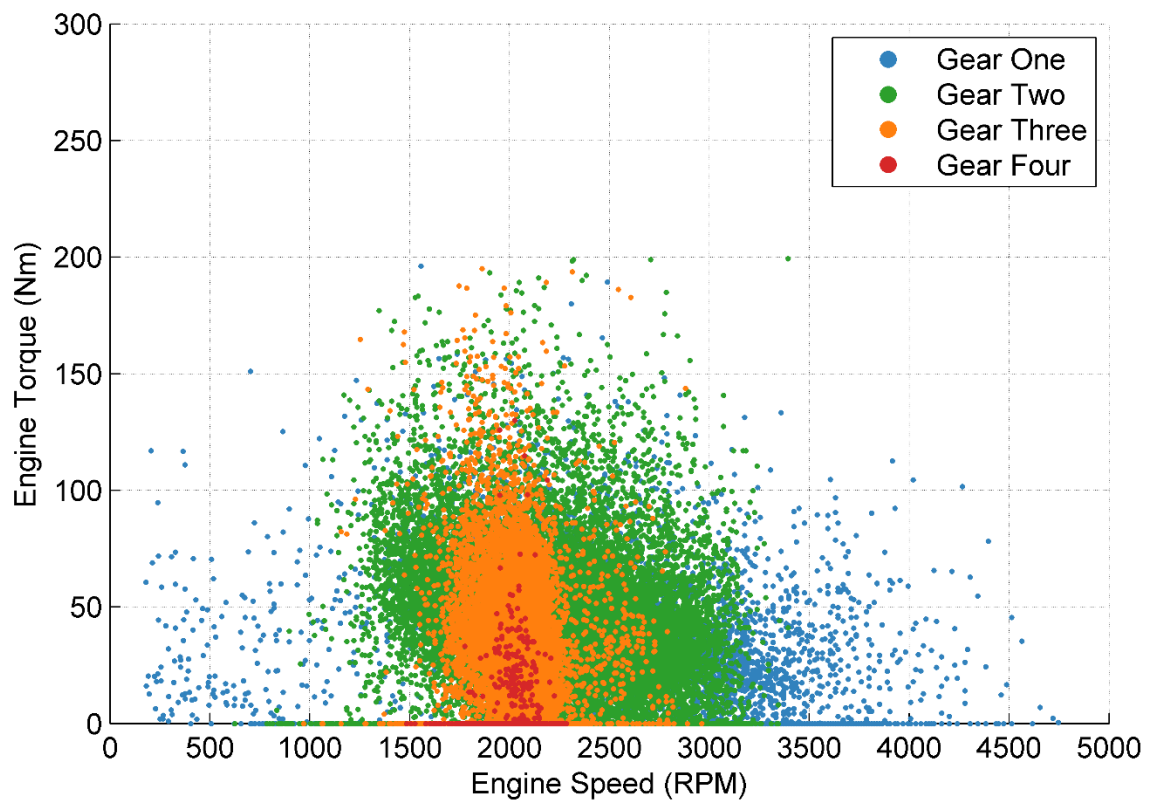


Figure 5.9: Petrol engine speed versus torque, at each gear ratio, when the Prius is in pure electric mode

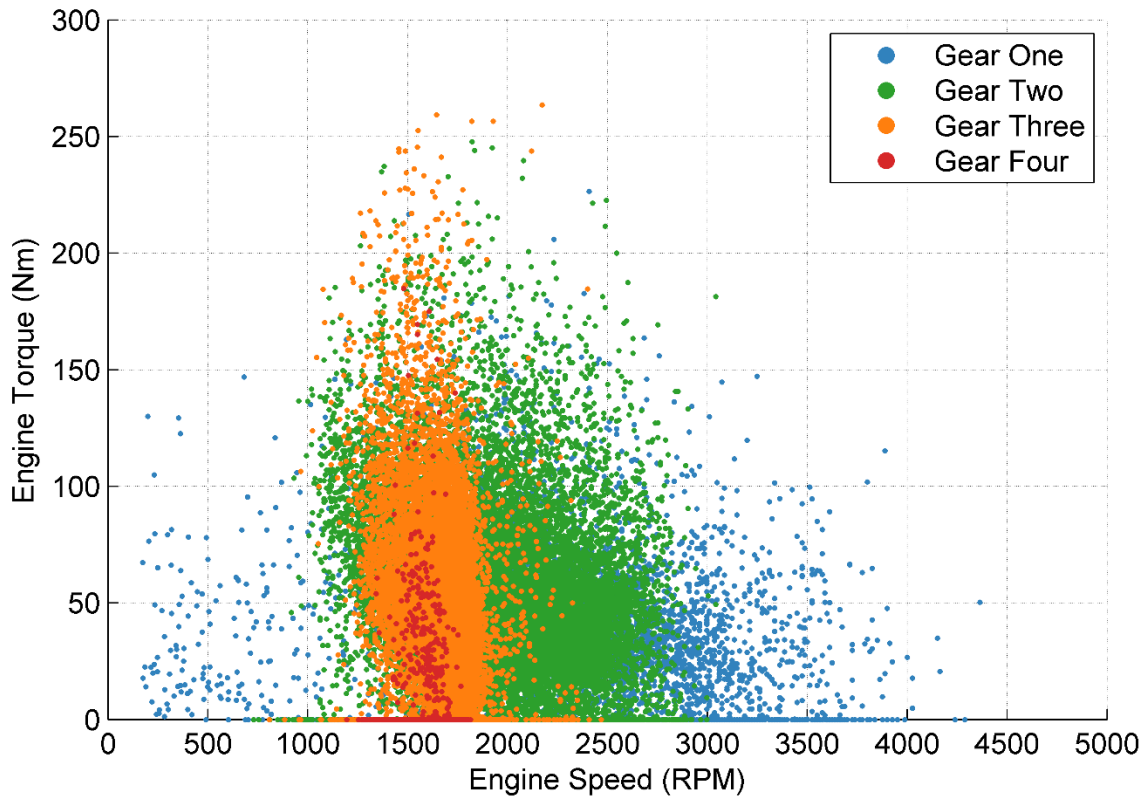


Figure 5.10: Diesel engine speed versus torque, at each gear ratio, when the Prius is in pure electric mode

Secondly, while it is sometimes assumed that most of the power used during PE mode has come from the engine and been stored in the battery, in a fairly inefficient power path. Actually during all the taxi testing 196kW of engine power went to charge the battery, whereas 277kW of power regenerated from the vehicle slowing down also charged the battery. The success of PE mode is a combination of these factors, the inefficiency of the conventional vehicle in this mode and the fact that around 60% of the energy used by the hybrid in this mode did not come from the engine and therefore had no associated emissions.

As shown from the first micro trip in Figure 5.8, the Toyota Prius can drive low-speed trips completely in PE mode. However, the battery SOC drops quickly and only very short distances can be covered before the engine comes on. Sub-mode 2a and 2b still

constitutes quite a large proportion of the fuel saving in PE mode, especially during slow stop start traffic, at peak times and queuing in the taxi rank.

Far more of the fuel saving in PE mode occurs in sub-mode 2c and 2d. With the large battery and generator, the Prius can very quickly and smoothly turn the *engine on* in the middle of a micro trip. This allows the engine to be regularly turned on and off, switching the vehicle from HE mode to PE mode and back again, without the driver noticing. In most micro-trips the engine comes on early because the power required to accelerate the vehicle up to speed is greater than the power the battery can deliver. However, once the vehicle is up to speed, far less power is required to cruise at a constant speed and so the battery can take over driving again.

5.4.3.3 Mode 3, Hybrid Electric Mode

The clear advantages of the hybrid powertrain in PE mode are no longer so obvious in HE mode. Now the engine has to pull the additional mass of the battery and motors, some of the engine power passes to the wheels through an electric power path which is far more inefficient than the mechanical power path used in a conventional vehicle and the engine must meet the power demands of driving the vehicle and recharging the battery. However, as Table 5.3 shows the Toyota Prius fuel consumption is still lower than that of the conventional vehicles in HE mode, even when it has to overcome these draw backs. This is achieved in three ways; firstly, in sub-mode 3a, 3c and 3d the battery is supporting the engine, thus reducing the power demand on the engine.

Secondly, the Toyota Prius engine has been decoupled from the vehicle wheels; this means that the engine speed is no longer directly dependent on vehicle speed. This flexibility allows the engine to operate along an optimised speed, torque path that maximises the engine efficiency for the power demand.

Thirdly, the Toyota Prius uses a large Atkinson cycle engine, with cooled EGR at all loads. This design allows the engine to operate with very little throttling which increases engine efficiency at low loads. The engine also has a much higher compression ratio

than other petrol engines providing higher engine efficiency at high loads (Kawamoto et al., 2009).

For 63% of the engine on time the vehicle operates in sub-mode 3b, where the Prius engine meets the full power demand of the vehicle and provides charge to the battery in proportion to its SOC. As can be seen from Figure 5.8, in this sub-mode the Prius engine power is substantially higher than the conventional vehicle engine power, while the fuel consumption is lower than the petrol engine and matches that of the diesel engine. The Prius achieves this by decoupling the vehicle speed from the engine speed, thus allowing the engine to operate in a higher efficiency zone.

Figure 5.11, 5.12 and 5.13 presents the speed and torque of the three engines, it is clear that the conventional vehicles, with a manual gear box, are forced to operate the engine over a wider range of speeds and torques, to meet the vehicle power demand. The extremes of engine speed and torque that the conventional engine experiences results in high emissions of CO₂ and many air quality pollutants (Schäfer & Basshuysen, 1995).

By contrast, the Toyota Prius controls engine speed and torque to avoid areas of the engine map which are particularly detrimental to emissions. The low and high torque regions of an engine fuel consumption efficiency map are very steep giving large benefits if the powertrain can be designed to avoid these regions. The Toyota Prius manages this reasonably well avoiding engine operation at low torque, above the engine idle speed of 1000 RPM, while at the same time limiting the engine torque to below 150 Nm.

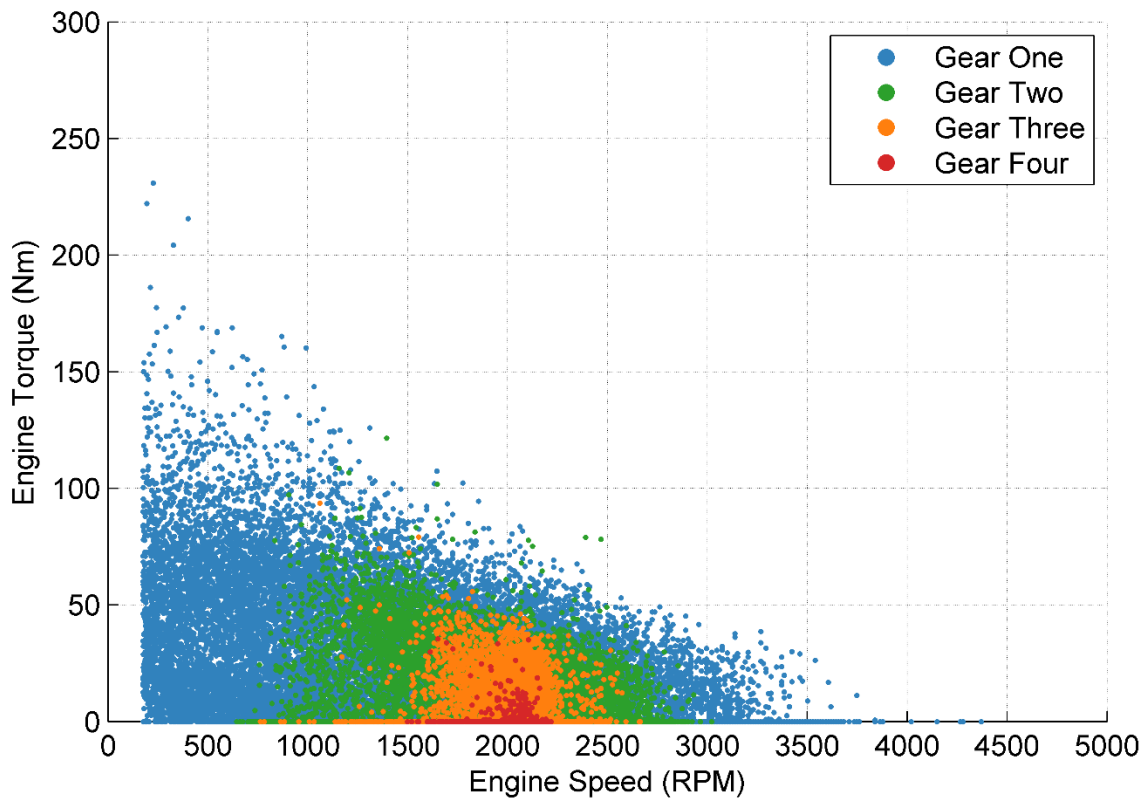


Figure 5.11: Petrol engine speed versus torque, at each gear ratio, when the Prius is in hybrid electric mode

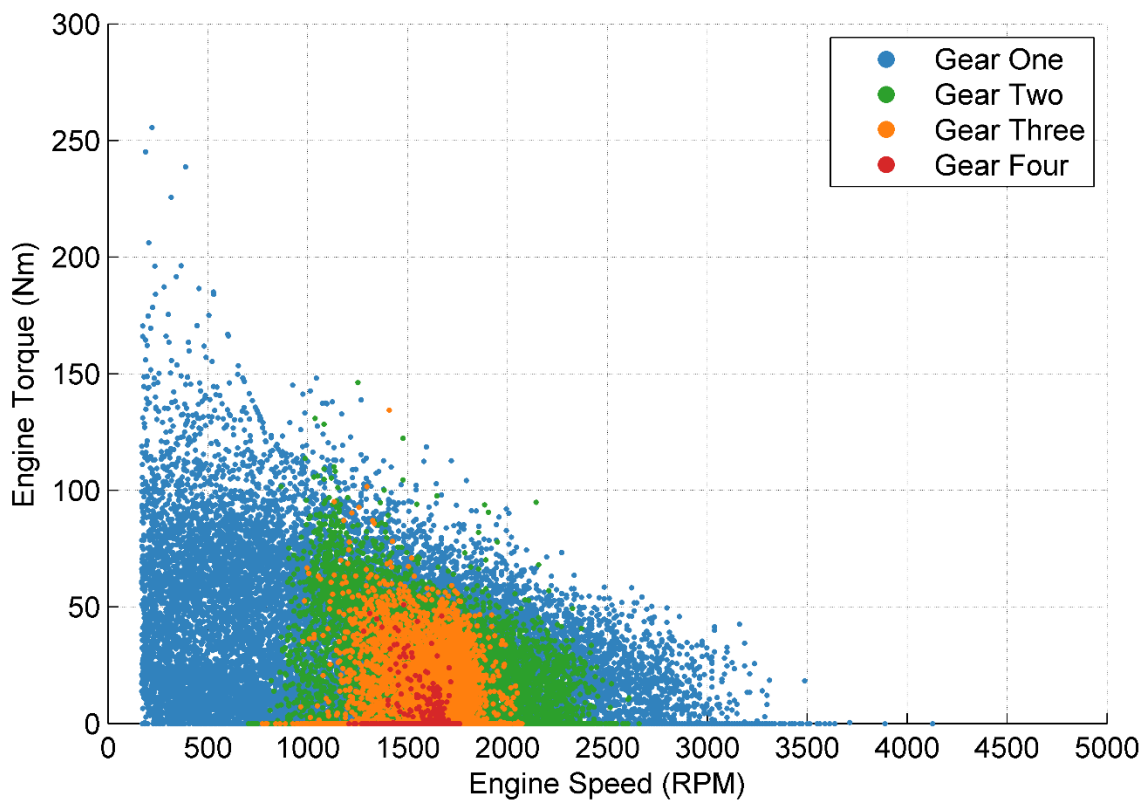


Figure 5.12: Diesel engine speed versus torque, at each gear ratio, when the Prius is in hybrid electric mode

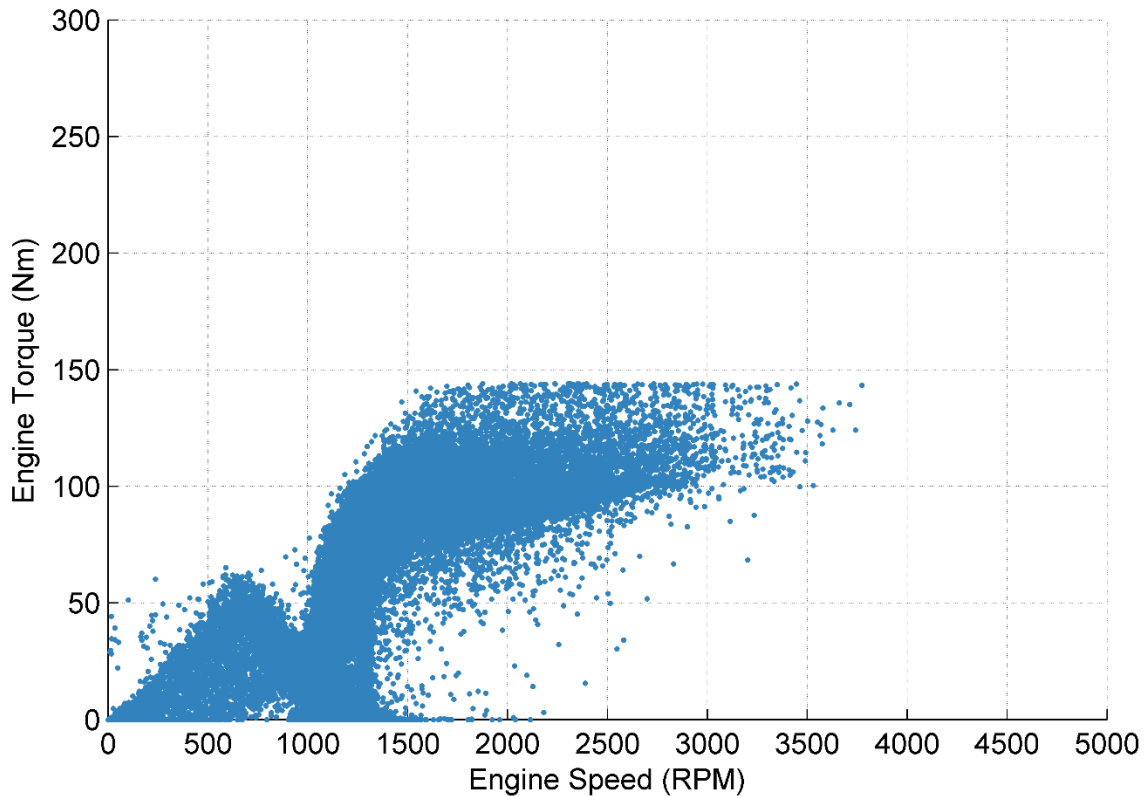


Figure 5.13: Prius engine speed versus torque, at each gear ratio, when the Prius is in hybrid electric mode

To understand how the conventional engine operation points shown in Figure 5.11 and 5.12 are shifted to other areas of the engine map in the hybrid engine, Figure 5.14 and 5.15 splits the conventional vehicle engine map up into a grid, each one shown as a subplot. Each subplot presents a small area of conventional engine operating points, alongside the hybrid engine operating points at the same moment in time. A power curve matching the average power of the conventional vehicle points has been added to each subplot to demonstrate how the hybrid vehicle can meet the same power demand, while using a different region of the engine map.

What is clear from Figure 5.14 and 5.15 is that the hybrid engine uses the same region of the engine map in all the subplot, no matter where the conventional vehicle data lies along the power curve, the hybrid engine control meets the same power demand by

shifting the engine operation along the power curve to the higher efficiency region of the engine map.

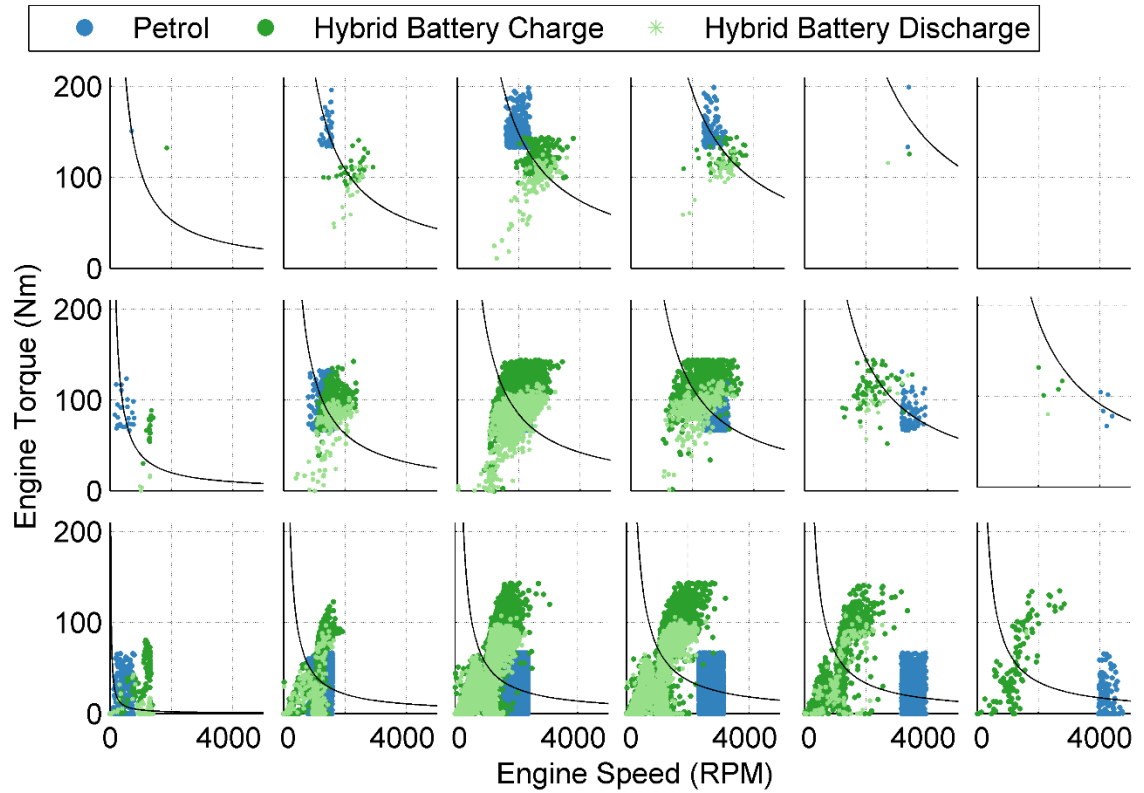


Figure 5.14: Comparing petrol and hybrid engine speed versus torque, by segment, over the engine map

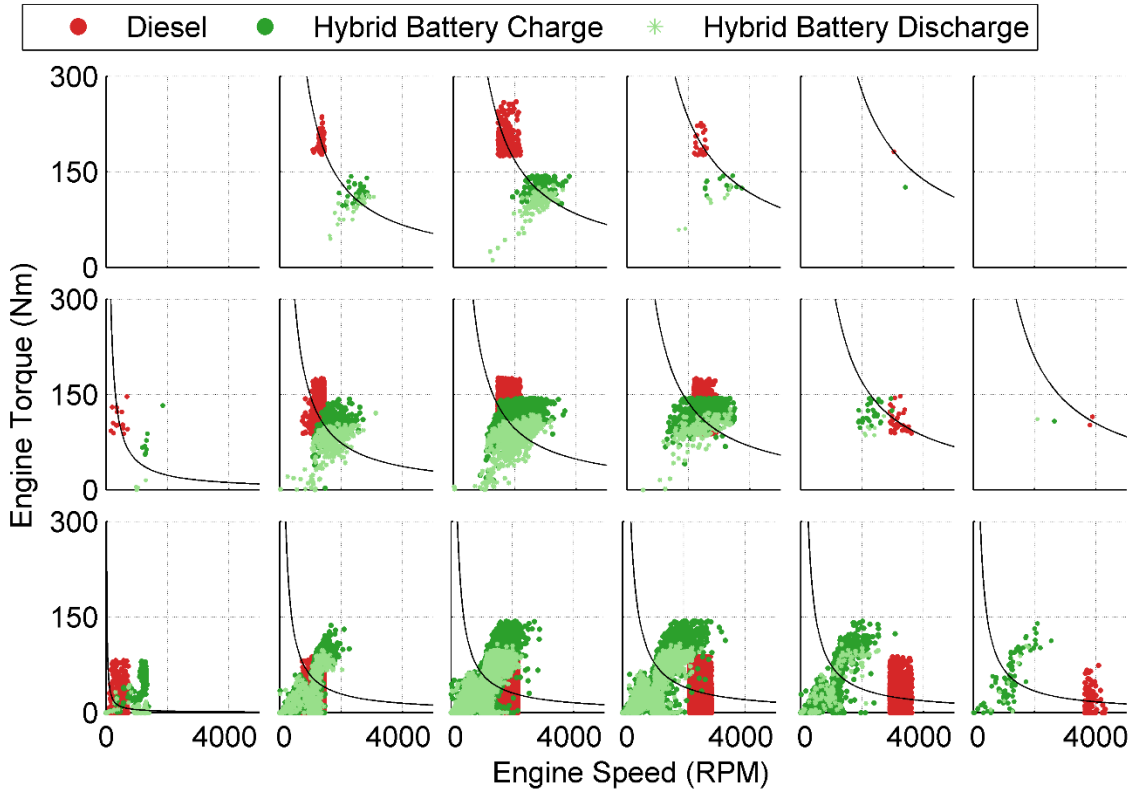


Figure 5.15: Comparing diesel and hybrid engine speed versus torque, by segment, over the engine map

By using the efficiency benefits of the Atkinson cycle and by operating the engine in a higher efficiency zone, the Prius can match the fuel consumption of the conventional vehicles, see Table 5.3, even though the Prius engine is operating under a higher load. However, if the hybrid and conventional vehicles were compared in rural or motorway driving, the proportion of sub-mode 3b would increase and the conventional engine operation would shift to a more efficient region of the engine map, resulting in the overall fuel consumption gap between hybrid and conventional vehicles decreasing.

Sub-mode 3d, standby mode, is when the engine power drops to zero and the battery and motor take over driving the vehicle, but the engine is still being fuelled at a low rate. This mode occurs very occasionally under calm and normal driving, and is normally due to the engine not turning off because it has still not reached full temperature. By contrast during aggressive driving, the engine often uses standby mode; it is postulated that this

is because the power mode has been switched on in the car during aggressive driving. With power mode on the vehicle expects sudden accelerations so it goes to standby mode instead of turning the *engine off* to better react to sudden throttle demand.

5.4.4 NOx Emissions

Although this project focuses on CO₂ emissions it is important to mention other emission benefits of switching from a predominantly diesel, to a petrol hybrid taxi fleet. Evidence has been mounting for some time that diesel vehicles which pass the Euro standard tests still emit very high levels of NOx emissions in the real world. Chassis dynamometer testing of 32 Euro 6 vehicles, over the WLTC, found that vehicles fitted with EGR, SCR and LNT exceed the Euro 6 NOx limit by 2.3, 2.8 and 8 times respectively (Yang, Franco, Campestrini, German, & Mock, 2015). This suggests that NOx control technologies are being designed to meet the low power demands of the NEDC and are unable to cope with the high power demands of the WLTC. This trend is even worse in the real world where the power demands often exceed those found in either test cycle.

Local authorities must improve the air quality in UK cities to meet EU air quality targets. The air quality improvements that should have been achieved, by the tightening of consecutive Euro standards, were a key part of the range of policies designed to meet the EU targets. With the Euro standards not delivering in the real world and the European Commission in the middle of legal proceedings against the UK government for infringement of air quality standards, reducing NOx emissions is now high on many local and national political agendas (House of Commons, 2014).

Taxis high mileage, predominantly city centre driving and diesel dominated fleet make them a key source of air quality pollutants. This alongside the higher level of policy influence that local authorities have over taxi fleets makes them the obvious starting place when developing new policies to tackle air quality.

The drawback of using PAMS, instead of PEMS, is that no air quality emission data was collected as part of this project. To give an indication of the effect of switching taxis to petrol hybrid vehicles, on NO_x, three vehicles, a petrol hybrid (Toyota Prius), a petrol (Ford Focus) and a diesel (Ford Fiesta) will be compared over the London Drive Cycles (LDC). This data was collected by the Department for Transport (DfT) and all three vehicles were tested under the same conditions on a chassis dynamometer.

Table 5.4 compares the taxi driving data collected during this project with the LDC. As would be expected the taxi data is most similar to the LDC Urban drive cycles. The PAMS data collected is a bit faster and more aggressive during accelerations and decelerations than the LDC Urban cycle, but these kinds of differences are expected when comparing real world data and chassis dynamometer test cycles. The key difference between the PAMS data and the LDC Urban cycle is the proportion of stop time which is much higher in the collected data. Overall LDC Urban is similar enough to the taxi data collected to give a good indication of the magnitude of NO_x savings that petrol hybrid taxis could achieve.

Table 5.4: Comparison between PAMS taxi data and the London Urban, Suburban and motorway drive cycles

	Taxi Normal Driving Style	LDC Urban	LDC Suburban	LDC Motorway
Percentage Stop Time (%)	40.8	28.4	16.2	4.98
Vehicle Speed 2.5% Quantile (km/h)	2.85	1.16	1.83	4.89
Vehicle Speed 25% Quantile (km/h)	15.9	12.4	21.9	32.0
Vehicle Speed 50% Quantile (km/h)	27.9	24.7	41.0	89.2
Vehicle Speed 75% Quantile (km/h)	39.3	36.1	51.2	106.2
Vehicle Speed 97.5% Quantile (km/h)	46.3	47.6	77.5	111
Vehicle Acceleration 2.5% Quantile (km/h)	-1.72	-1.57	-1.46	-1.05
Vehicle Acceleration 25% Quantile (km/h)	-0.344	-0.328	-0.259	-0.163
Vehicle Acceleration 50% Quantile (km/h)	0.0556	0.0183	-0.00514	0.00111
Vehicle Acceleration 75% Quantile (km/h)	0.472	0.368	0.263	0.168
Vehicle Acceleration 97.5% Quantile (km/h)	1.447	1.32	1.34	0.954

Table 5.5 presents the NOx emissions saving by switching from a diesel to a petrol, a diesel to a petrol hybrid or a petrol to a petrol hybrid, over the LDC urban, rural and motorway drive cycles. It is well documented that diesel vehicle have much higher NOx emissions than petrol vehicles because petrol vehicles use TWC, which are very effective at treating NOx emissions in the exhaust pipe (OECD, 2011). A petrol hybrid has the NOx benefits of a conventional petrol vehicle, but also has the added benefit of being able to operate in PE mode. It is clear that switching from diesel to petrol or petrol hybrid taxi vehicles could have a significant impact on the air quality of many cities.

Table 5.5: NOx saving achieved, by road type, through switching from diesel to petrol, or conventional vehicles to petrol hybrid

Road Type	Percentage reduction in NOx, diesel to petrol (%)	Percentage reduction in NOx, diesel to hybrid (%)	Percentage reduction in NOx, petrol to hybrid (%)
Urban	97.8	99.8	89.1
Suburban	97.6	99.8	93.0
Motorway	95.7	97.8	48.3

Table 5.6 shows how much time the Toyota Prius spends in stationary, PE and HE mode, as well as the percentage of the total NOx saving, compared to the petrol and diesel vehicle, in each mode. Stationary mode makes up 3.10% and 14.0% of the total urban NOx emissions for the petrol and diesel vehicles respectively. The TWC appears to do a very good job at cutting NOx emission when the engine is idling and so the petrol emissions are very low in stationary mode. The diesel engine without exhaust after-treatment is producing a lot of NOx emissions in the stationary mode, this problem would be even worse in taxi driving where stationary mode is a higher proportion of the time. These results highlight how big an effect diesel engine idling has on city air quality, this is an area city councils could act on in the short term, and have fast, positive effect.

Table 5.6: Percentage time and percentage NOx saving, by switching from conventional to hybrid vehicles, split by Prius stationary, Prius pure electric mode and Prius hybrid electric mode

Mode / Drive Cycle	Percentage Time (%)	Percentage NOx Saving Petrol (%)	Percentage NOx Saving Diesel (%)
S Urban	28.4	2.26	14.1
PE Urban	44.9	31.1	36.1
HE Urban	26.8	66.6	49.4
S Suburban	16.2	2.69	7.25
PE Suburban	40.1	16.6	25.4
HE Suburban	43.7	80.7	67.4
S Motorway	5.00	0.131	0.884
PE Motorway	25.5	4.95	7.35
HE Motorway	69.6	94.9	91.8

Figure 5.16 shows the hybrid and petrol NOx emissions over a short section of the LDC Urban cycle. The figure is colour coded with stationary data in clear, PE mode in Blue and HE mode in Red. From the Figure and the results in Table 5.6 it is clear that PE mode is far less effective at reducing NOx, than it is at reducing CO₂. This is because NOx emissions tend to occur during high engine power events. If one of these occurs and the Prius is operating in PE it will immediately switch into HE mode to meet the power demand. This means that high NOx events for the conventional vehicles rarely occur when the Prius is in PE mode, so PE mode does not contain much of the NOx saving.

Figure 5.16 displays one of the few spikes in Prius NO_x that occurs during urban driving. Most of the time the Prius manages to keep its NO_x emissions at very low levels as illustrated by Figure 5.16. By contrast, the petrol vehicle has regular spikes that are 100 times the background level. It is these spikes that make the difference between the petrol and the hybrid NO_x emissions, as the emissions between the spike are relatively similar. As both vehicles have TWC it seems likely that the difference in emissions is a result of engine out emissions rather than the effectiveness of the after-treatment systems, although NO_x slippage in the catalyst may cause some spikes for both cars. The difference in engine out NO_x emissions is likely to be caused by the Prius use of cooled EGR across all engine powers. The EGR in the Prius has been fitted to help improve fuel consumption, but a side effect of the EGR will be to reduce combustion temperatures, and therefore NO_x emissions. EGR is used in this manner in conventional diesel engines to reduce NO_x, but because the diesel engines are not oversized they cannot use EGR at high loads when the NO_x emissions peak. The Prius, on the other hand, uses EGR at all engine powers providing NO_x reductions at high engine loads where it is most needed (Kawamoto et al., 2009).

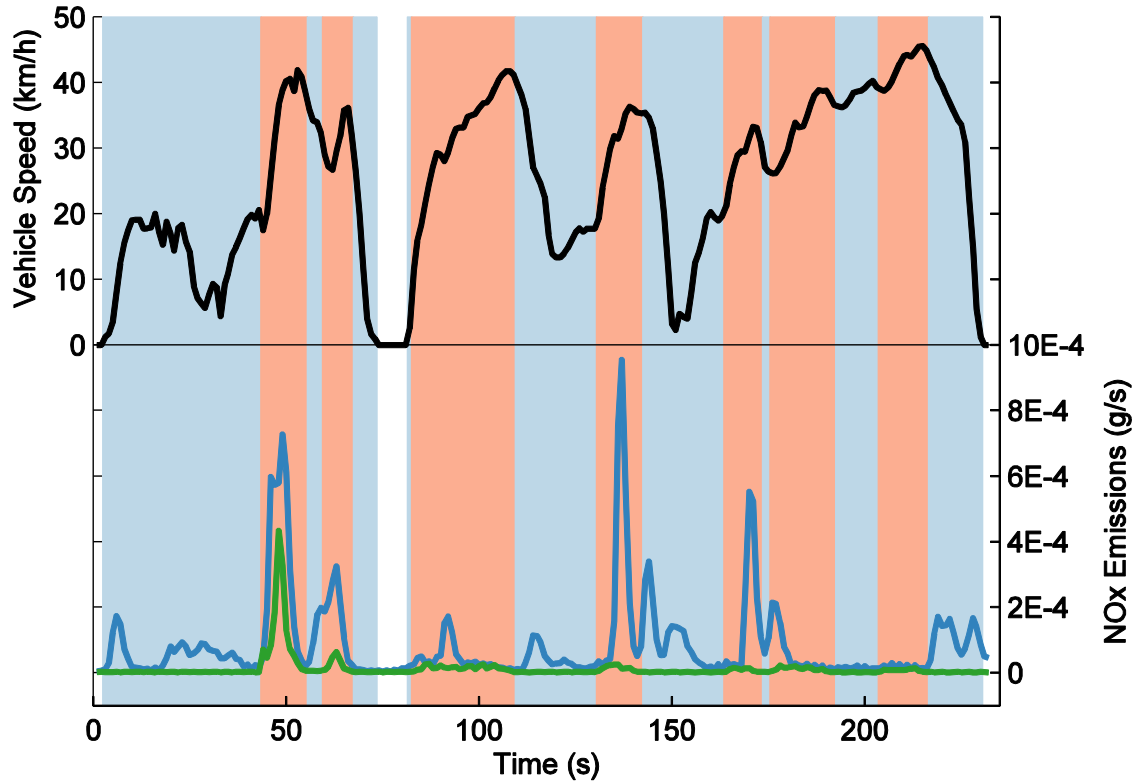


Figure 5.16: Petrol and petrol hybrid NOx emissions, colour coded by Prius mode. Clear, vehicle stationary. Blue, pure electric mode. Red, hybrid electric mode

5.4.5 Business Case

In the hackney carriage fleet, most vehicles are bought and owned by the drivers. The only exception to this is WAV's which are leased, but as no hybrid WAV are available on the market, they will be left out of this analysis. In the PHV fleet, there is a mixture of drivers who own their vehicles, but drive for a company, and drivers who rent a fleet vehicle from a company. The vehicles owned by individuals are normally bought second hand to reduce the purchase cost. The maximum age limit for a vehicle to first enter the fleet is five years, as a result of this many of the vehicles first registered are over four and a half years old. The vehicles bought in bulk for a fleet are purchased new. As the oldest a vehicle can be before it has to be retired is ten years, the individually owned vehicles have a five year life, while fleet vehicles could have a ten year life, if they can

be kept in good running order over such a high mileage (*Leeds City Council, 2016. Unpublished Data*).

5.4.5.1 New Vehicle Business Case

Table 5.7 presents the fuel saving and payback time for the higher upfront cost of buying a new hybrid fleet vehicle. The figures are based on a bottom of the range Toyota Prius costing £23,295 (Toyota, 2016), and a new bottom of the range Skoda Octavia diesel costing £16,515 (Skoda, 2016), giving a purchase premium for the hybrid of £6,780. Table 5.7 shows the payback time assuming an annual mileage of 96,560 km (60,000 miles) a year (*Interview Head of Streamline Cabs, 2015, Unpublished Data*)(*Interview Hybrid Taxi Driver, 2015, Unpublished Data*). The calculations use the current fuel price, for the Yorkshire region, of 104 p/L for petrol and 107.3 p/L for diesel (AA, 2015), a 3% discount rate and the fuel consumption figures from Table 5.1.

Table 5.7: Fuel saving and payback times for purchasing a new hybrid taxi

	Switch Diesel to Hybrid		Switch Petrol to Hybrid	
	Annual Fuel Saving (£)	Payback Time (Years)	Annual Fuel Saving (£)	Payback Time (Years)
Calm	4,005	1.6	8,410	0.8
Normal	3,706	1.8	7,713	0.9
Aggressive	3,293	2.0	7,231	0.9

5.4.5.2 Second Hand Vehicles Business Case

A second-hand conventional vehicle similar to those used as taxis in Leeds costs around £5,000, based on a review of Skoda Octavia's sold second hand on auto trader, January to June 2015. A second hand Toyota Prius costs around £10,700, based on the price paid for a second hand Prius by a taxi driver in Leeds (*Interview Hybrid Taxi Driver, 2015, Unpublished Data*). Table 5.8 shows annual fuel saving and payback time, assuming an annual mileage of 48,280 km (30,000 miles) and the same fuel prices, discount rate and

vehicle fuel consumption figures used in the previous section (*Interview Head of Streamline Cabs, 2015, Unpublished Data*)(*Interview Hybrid Taxi Driver, 2015, Unpublished Data*).

There are only three hybrids in the Leeds hackney carriage fleet, so it is difficult to make generalisation about how the fleet might operate if it were larger. However, it is expected that the higher price of hybrid vehicles will encourage drivers to buy them as old as possible to reduce the price. This means it is very unlikely for a hybrid vehicle to have a hackney carriage life longer than five years, so it is important for the Prius to have a payback time shorter than this for it to be successful in the taxi fleet. Table 5.8 shows that the payback time is substantially lower than five years for all the driving styles. The key selling point for the Prius is that having paid back the higher upfront cost it will save drivers, over the lifetime of the vehicle, £3,343 or £13,122 when compared to buying and running a diesel or petrol equivalent respectively.

Table 5.8: Fuel saving and payback times for purchasing a second-hand hybrid taxi

	Switch Diesel to Hybrid		Switch Petrol to Hybrid	
	Annual Fuel Saving (£)	Payback Time (Years)	Annual Fuel Saving (£)	Payback Time (Years)
Calm	2,002	2.8	4,205	1.4
Normal	1,853	3.0	3,857	1.5
Aggressive	1,647	3.5	3,615	1.6

5.4.5.3 Sensitivity of Payback Time to Vehicle Mileage

Payback time is very sensitive to mileage and this obviously depends on each driver's situation. Figure 5.17 shows the payback times for switching from a petrol or diesel vehicle to a hybrid, depending on driving style and annual mileage. Even under the worst case scenario of low mileage and aggressive driving, the payback matches the five year lifetime of a taxi. There is a clear payback benefit from a higher mileage which explains

the higher uptake of hybrid vehicles in the PHV fleet (4.5%) when compared to the HC fleet (0.6 %) (*Leeds City Council, 2016. Unpublished Data*).

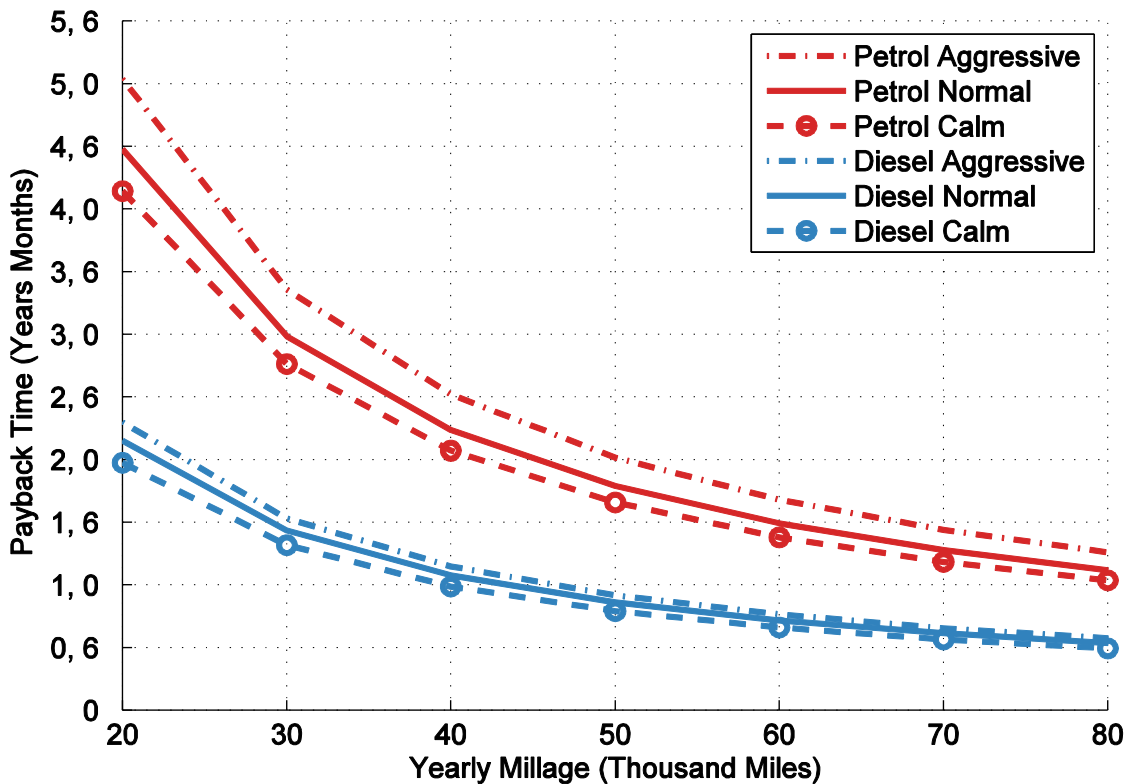


Figure 5.17: Change in payback time with changing mileage for switching from a petrol or diesel taxi to a hybrid taxi

5.4.5.4 Sensitivity of Payback Time to Fuel Price

Payback time is also very sensitive to fuel price which as we have seen over the last year can fluctuate rapidly in both directions. Figure 5.18 shows how petrol fuel price effects the payback time when shifting from a petrol vehicle to a hybrid. The drop in petrol fuel price since its maximum in spring 2012 has increased payback time by around four months, but the substantial difference in fuel consumption between the two vehicles means the payback time, even with a low mileage of 20,000 miles a year and a low fuel price of 0.80£/L, never exceeds two and a half years.

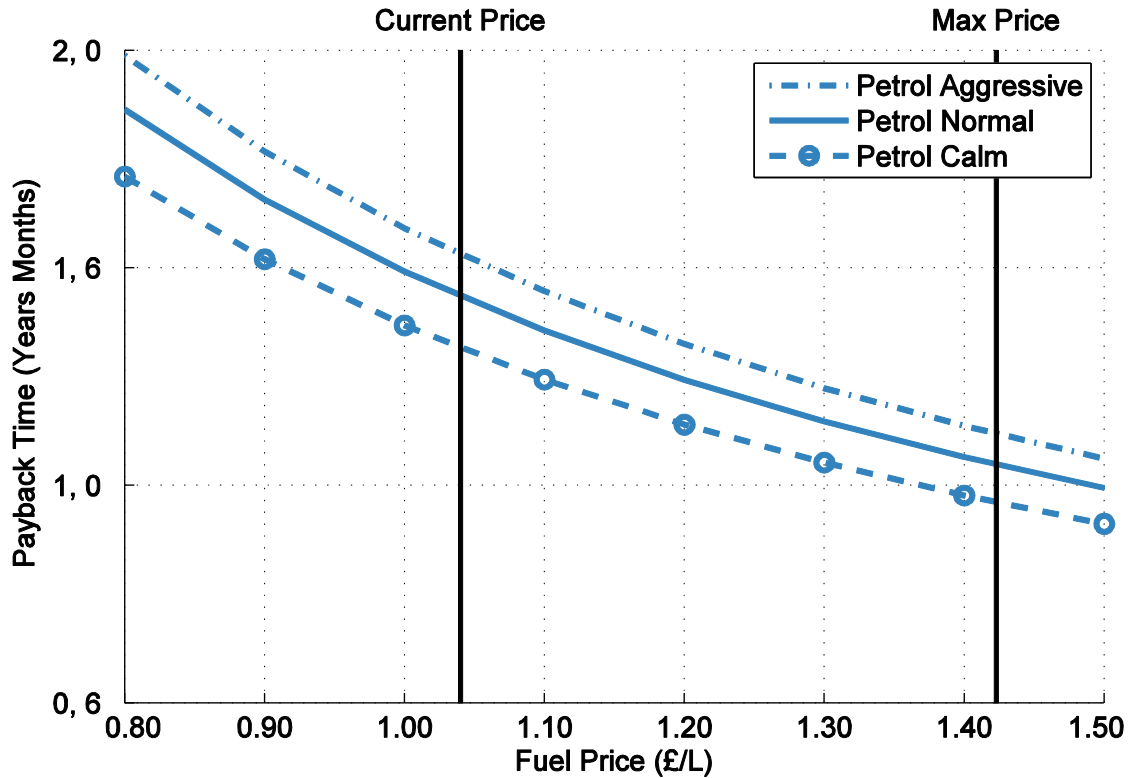


Figure 5.18: Change in payback time with change in petrol fuel price for switching from a petrol taxi to a petrol hybrid taxi

Figure 5.19 shows how payback time changes with petrol and diesel price, assuming normal driving and an annual mileage of 30,000 miles. When fuel prices peaked in spring 2012 the payback time was over nine months shorter than at current fuel prices, helped by a 5p gap in price between diesel and petrol that has shrunk to just 3.3p today. It is clear that increased diesel fuel tax could play an important role in encouraging the switch to hybrid vehicles, a 10p increase in diesel price above today's value would decrease payback time by six months. Even under a worst case scenario where petrol prices were 5p higher than diesel prices, payback times do not exceed the five year lifetime of the taxi.

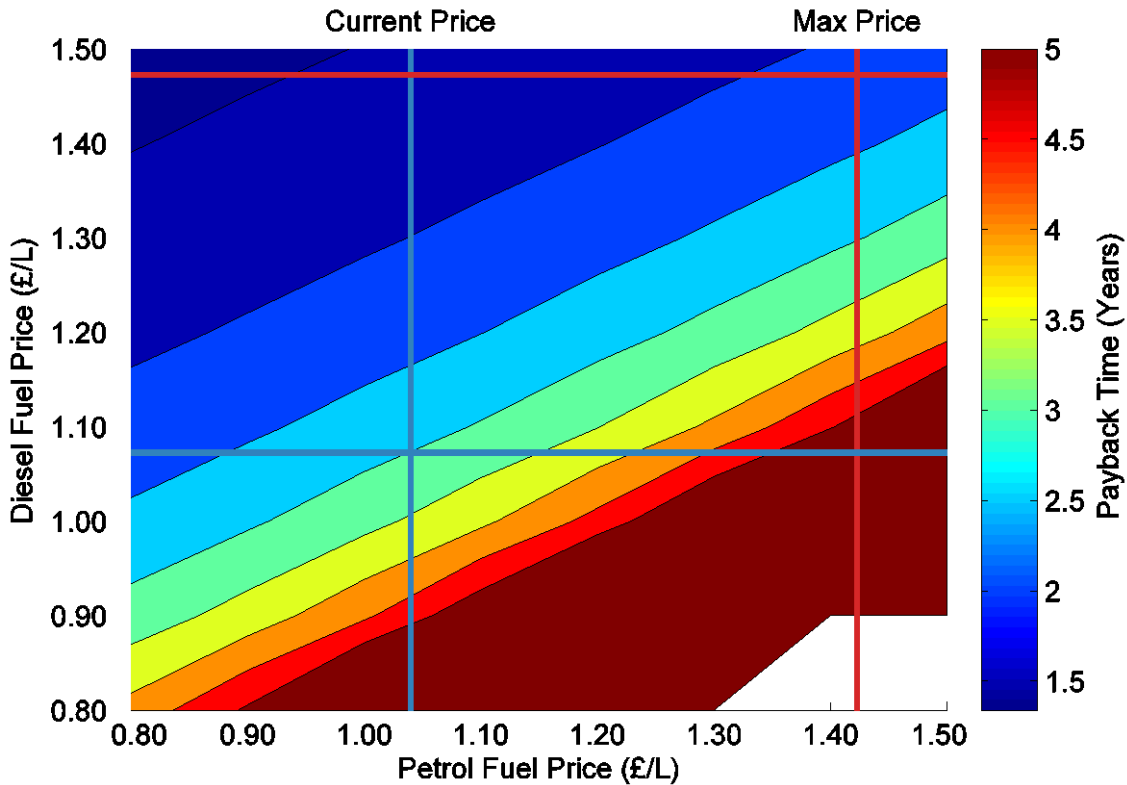


Figure 5.19: Change in payback time with changing petrol and diesel prices for switching from a diesel taxi to a petrol hybrid taxi

5.4.5.5 Anecdotal Evidence from Taxi Driver Interview

To validate these results, one of the three hybrid taxi drivers in Leeds was interviewed by Leeds City Council. He calculated that he spent on average £10.50 for every 100 miles travelled in his Toyota Prius and £17.50 per 100 miles in his previous diesel taxi. Using the average fuel price over the period that the two cars were owned, this converts to 5.52 L/100km for the hybrid and 8.20 L/100km for the diesel, giving a payback time of 3 years, 10 months (*Interview Hybrid Taxi Driver, 2015, Unpublished Data*). While these numbers are not strong evidence, because it is only one driver and he did not make an accurate log of his mileage and fuel costs, none the less the good agreement, especially with the data collected on the Prius, provides greater confidence that the routes chosen and the driving styles used were a good match to real taxi usage.

Fuel saving is not the only monetary benefit from switching to hybrid vehicles. The taxi driver interviewed, stated, higher reliability, lower maintenance costs and fewer days of work lost, while the vehicle was being repaired, as key factors in his choice to buy a hybrid vehicle. The driver interviewed also saved £150 on his car insurance when he switched vehicles (*Interview Hybrid Taxi Driver, 2015, Unpublished Data*). However, quotes given by several online insurance comparison sites suggests that insurance for a hackney carriage is around £1,200 and there is little difference in costs between a Skoda Octavia diesel and a Toyota Prius (insuremytaxi4less, 2016).

5.5 Policy Options to Encourage the Uptake of Hybrid Taxis

5.5.1 Vehicle Licencing, Emission Limits, or Technology

Requirements

Taxis are one of the most heavily regulated light-duty vehicles on the road. With local councils providing licenses for the drivers and the cars, there is an opportunity to control the vehicles in the taxi fleet through licencing laws.

San Francisco was one of the first cities to do this by setting a target to reduce emissions from the taxi fleet by 20% between 1990 and 2012. To achieve this it was mandated that all new taxis from 2008 should emit less than 38 tons CO₂e a year and the taxi commission was given the power to suspend or revoke taxi permits for noncompliance (City & County of San Francisco Office of the Mayor, 2012; San Francisco Municipal Transportation Agency, 2008).

Boston MA tried to introduce a scheme in 2008 that would have required all taxis to be AFV by 2015 (City of Boston, 2008). However, this was blocked by a federal court ruling in 2009, when only 15% of the taxi fleet had switched over to hybrids (City of Boston, 2009). One of the main sources of complaint from taxi drivers about the scheme was that

only new AFV were eligible for financial support and so the program was very expensive for taxi drivers (Valencia, 2009).

In 2005 – 2006 New York made over 200 of its taxi medallions AFV only (City of New York, 2006). This was backed up in early 2008 when the city agreed that all taxis entering the fleet after October 2008 must achieve a minimum of 25 mpg and after October 2009 30 mpg (City of New York Taxi & Limousine Commission, 2007). These policies were again blocked by a federal judge in 2008 when only 12% of the taxi fleet had switched over to hybrids (City of New York, 2008).

As part of the Ultra-Low Emission Zone (ULEZ) in London, all hackney carriages licenced for the first time in 2018 must be Zero Emission Capable (ZEC). ZEC is defined as emitting less than 50 gCO₂/km, with an all-electric range of 30 miles and a petrol engine, if an engine is used. The scheme also covers PHV. All PHV licenced for the first time in 2018 must be Euro 6 standard or better, unless the vehicle is a petrol hybrid in which case it must be Euro 4 or better. These standards are raised over time so that, all new vehicles applying for a PHV licence for the first time in 2020 must be ZEC and all PHV licenced for the first time in 2023 must be ZEC. For PHV ZEC is defined as emitting less than 50 gCO₂/km, with an all-electric range of 10 miles or emitting less than 75 gCO₂/km, with an all-electric range of 20 miles (Transport for London, 2015c).

The literature presented in this section shows that setting green standards for new taxis joining the fleet can very quickly shift the fleet towards hybrid vehicles, without forcing drivers to buy new cars before the investment they have made in their current car has provided its maximum benefit. However, the lessons of Boston and New York show that forcing hybrid vehicles into the fleet can backfire if a range of other supporting policies do not get the taxi drivers on-board with the scheme.

5.5.2 Financial Incentives

All cities that have put green taxi licencing laws in place have also offered financial support to taxi drivers to help them buy the more expensive hybrid vehicles. San Francisco offered \$2,000 off the purchase cost of the first 250 AFV to enter the fleet (San Francisco Municipal Transportation Agency, 2008). Boston MA offered \$3,000 in tax credits to help pay for new hybrid taxis (National Renewable Energy Laboratory, 2009). Chicago set aside \$1,000,000 to subsidise the upfront costs of AFV, the amount reimbursed depended on the technology of the vehicle, with hybrids eligible for \$2,000 off the purchase price (City of Chicago, 2011). New York made AFV, sales tax exempt for taxi drivers (City of New York Taxi & Limousine Commission, 2007). The UK offers 35% off the cost of a new plug-in vehicle up to a maximum of £4,500 (Department for Transport, 2016a), and taxi drivers are to be offered an additional £3,000 off the purchase cost between 2017 and 2020 (Transport for London, 2015c).

This financial support is a key part of getting new technology into the market, but there is a clear trend in the financial support given, the money is always a grant that only applies to new vehicles and the technology must be new to the mass market not just to the taxi market. For hybrid technology, which has become mainstream, to dominate taxi fleets requires a different kind of financial support that offers short term, low interest loans to buy second-hand hybrid vehicles.

5.5.3 Vehicle Licencing

Other areas of taxi vehicle licencing can be used to encourage the uptake of hybrid vehicles without setting hard limits. In some American cities, most of the taxis are owned by fleet managers who charge drivers a fee to use the vehicle and the taxi licence for a shift. In San Francisco fleet managers are allowed to charge drivers \$7.50 more a shift for using an AFV. This encourages the fleet managers to buy AFV and is considered fair for the drivers as they pay lower fuel costs when they use AFV, which offsets the higher charges (San Francisco Municipal Transportation Agency, 2008). In Boston a similar

policy allowed fleet managers to charge an extra \$15 a shift for drivers leasing AFV (National Renewable Energy Laboratory, 2009). In New York, the shift fee was increased by \$3 for AFV and decreased by \$12 for conventional vehicles, although this policy was again blocked by legal proceeding (City of New York, 2008, 2011).

Another area of taxi licencing that has a big effect on the business model of both individual taxi drivers and taxi fleets is taxi licencing age. Different cities have different limits on how old a vehicle can be before it must be retired and some cities also limit how old a vehicle can be to enter the taxi fleet for the first time. In Chicago conventional taxis may be licenced as taxis until they are four years old, AFV and WAV until they are five years old and vehicles that are both AFV and WAV until they are six years old (City of Chicago Department of Business Affairs and Consumer Protection, 2012). New York explored the option of decreasing the retirement age of the most polluting vehicles and increasing the retirement age of AFV, but it was never enacted. In the consultation for the London ULEZ it was proposed that the taxi age limit should be brought down from 15 to 10 years for conventional vehicles (Transport for London, 2015a). However, through the consultation period, this was changed to a voluntary decommissioning scheme that offered drivers of vehicles over 10 years old, up to £5,000, depending on the age of the vehicle, to retire the vehicle early (Transport for London, 2015c).

5.5.4 Taxi Rank

A large proportion of a taxi driver's day is spent queueing in the taxi rank, if the queueing time for AFV can be reduced it can make a big difference to a drivers profits. As part of the Boston Clean Air program, that got scrapped, AFV drivers got two "front of the line" passes, per shift, at the airport taxi rank, giving two extra journeys a day (National Renewable Energy Laboratory, 2009). After this policy was gone the airport introduced a dedicated AFV taxi rank to encourage further uptake of AFV (Nelson\Nygaard, 2013).

5.5.5 Restricted Zone or Lane Access

As is the case with London's ULEZ, cities can use Low Emission Zone (LEZ) to specify a particular taxi technology or emission standard for specific areas of a city (Transport for London, 2015c). This can be a big advantage for low emission taxis which can operate in the busiest parts of the city where there are the most jobs, while high emitting vehicles are pushed to the outskirts where the business is not as good. Taxis in Leeds currently have access to bus lanes, which can cut travel times during peak periods (*Leeds City Council, Unpublished Data*). Benefits like these could be provided only to Low Emission Vehicles (LEV). This would encourage taxi drivers to buy LEV for two reasons. Firstly, they could complete more jobs per shift and secondly, once consumers realised they would pay less to travel at peak times in a LEV, consumers would choose to use LEV taxis.

5.5.6 Green Taxi Image

Currently, vehicles have to be white to be eligible to be taxis in Leeds. Black stickers are added to the bonnet and the boot, and a taxi number is stuck on each of the front doors (*Leeds City Council, Unpublished Data*). This gives taxis a memorable image, like a yellow taxi in New York, that customers recognise and know they can hail on the street. This, however, reduces the already limited number of second-hand hybrid vehicles that taxi drivers can purchase. This pushes up the price and means there are not the available vehicles, in the local area, if Leeds City Council wanted a rapid shift in the fleets towards hybrid vehicles. A possible solution to this is to create a new set of taxi badges for low emission taxis, which could not only identify hybrid taxis to conscientious consumers, but make the vehicles immediately recognisable without all the vehicles having to be the same colour.

5.5.7 Taxi Community Engagement

Consumer awareness is a primary factor in hybrid vehicle fleet penetration rates. There is no reason why taxi drivers are very different to general car buyers, and so it seems reasonable that greater consumer awareness within the taxi community will encourage hybrid vehicle uptake (H. O. Gao & Kitiratragarn, 2008).

Alberta ran a test scheme, called Hail a Hybrid, in which four taxi firms were given hybrid vehicles to test. At the end of the test period, all four firms went on to buy hybrid vehicles for their fleets, while firms not part of the scheme did not. The report author highlighted first-hand experience of hybrid vehicles as a key step to successful uptake (Transport Canada, 2008).

This finding seems to have been supported by the hybrid taxi experience in New York. Gao et al. 2008 used surveys to study taxi drivers buying preferences in New York. The study predicted that without strong policies the percentage of hybrid vehicles in the taxi fleet would only reach 10% by 2011. This was because taxi drivers buying preference was based on vehicle purchase cost, vehicle maintenance cost, fuel price, passenger space and environment, in that order. Hybrid vehicles cost more to buy and many drivers claimed the batteries would have to be replaced at regular intervals, making maintenance cost very high, even though Toyota and Ford have never replaced a battery in either the Prius or the Escape (H. O. Gao & Kitiratragarn, 2008).

In reality the number of hybrid taxis in New York reached 12% in 2008 (City of New York, 2008) because of strong policies, but even after both of New York's taxi policies were blocked by federal judges, the number of hybrid taxis continued to rise, reaching 60% in 2014 (City of New York Taxi & Limousine Commission, 2014). It appears that even though the taxi community were initially sceptical of the introduction of hybrid taxis, once hybrids had reached a certain proportion of the fleet, the experience of the hybrid taxi drivers has spread to other drivers, and their fears about cost and reliability have been

assuaged, resulting in the number of hybrids in the fleet continuing to rise without strong policy to drive the uptake.

New York should be a clear lesson to other cities. A strong information campaign to ensure taxi drivers are well informed about hybrid vehicles and schemes to allow taxi drivers to try hybrid vehicles for themselves, can avoid expensive legal challenges to hybrid taxi policies and speed up hybrid vehicle uptake.

5.5.8 Consumer Engagement

Consumers both private and business could drive the uptake of hybrid taxis if they were aware of the emission and air quality benefits and were free to make a choice. A consumer information campaign about the need to improve the air quality within the city could be targeted at taxi users at the big city taxi ranks, and at businesses in the city centre that often book PHV. In parts of Scotland, green taxi companies are winning NHS contracts because of their use of hybrid vehicles (The Scottish Government, 2010). Other companies with strong corporate social responsibility could drive hybrid vehicle uptake in the PHV fleet by always requesting hybrid vehicles from the fleet operators.

Councils also have to allow the consumer to choose. Currently, a consumer has to pick the taxi at the front of the taxi rank or the PHV which is closest. Councils must make it clear to taxi drivers, PHV fleet operators, Uber and customers that the customers must be provided with information on whether a low emission taxi is available and then have the right to choose that taxi over any other. This will be made easier if all low emission taxis have a clearly recognisable livery.

5.5.9 Reducing the Price of Second Hand Hybrid Vehicles

There are a limited number of second-hand hybrid vehicles on the market, when compared to conventional vehicles, especially when taxi drivers can only choose white vehicles. This means that drivers must be prepared to search for a new hybrid vehicle, for an extended period of time, over the entire country, to get a good deal. Increasing the

number of hybrid vehicles available on the second-hand market across the country could bring the price down and make buying a hybrid vehicle more convenient.

In the UK cars enter the market as either company cars or privately owned cars, with a split of around 55%, 45% (Department for Transport, 2016c). Company cars are usually sold on after two to three years, with a good maintenance record and a high mileage. This could make them attractive purchases for taxi drivers who want a reliable vehicle, but could be less concerned about the high mileage because their own use will make the car unsalable, so vehicle mileage and resale value are less of a concern.

In the UK company cars used for private use are taxed as a benefit in kind, this tax depends on, the value of the car, its rated CO₂ emissions and what type of fuel it uses. The difference in tax between a diesel 3 series BMW and a Toyota Prius, is around £500 a year (HM Revenue & Customs, 2016; United Kingdom Government, 2016). This has driven the emissions in the company car sector down meaning it is now cleaner on average than the private car sector, with 25% of new company cars having a type approval CO₂ figure less than 109 g/km (The Society of Motor Manufacturers and Traders Limited, 2015).

The private car sector could also be a good source of vehicles for the taxi fleet. However, there is no strong policy to encourage the uptake of clean vehicles in the private sector. A registration tax, as used in the Netherland, has been shown to be effective at creating a consumer market for low emission vehicles. The difference in registration tax between a diesel 3 series BMW and a Toyota Prius, is around £5,000 (Netherlands Government, 2016), resulting in the Netherland having the lowest average fleet emissions of any country in Europe (Transport & Environment, 2014).

If the UK were to strengthen the company car tax scheme and introduce a registration tax then the number of hybrid vehicles in the new car fleet would increase. This would provide taxi drivers with a much larger range of hybrid vehicles in the second-hand fleet, making the option of switching to a hybrid vehicle, cheaper and more convenient.

5.6 Conclusions

This chapter has successfully demonstrated the use of PAMS data to inform local policy makers about a new policy and to educate consumers to encourage the purchase of low emission vehicles. The research presented here has formed the basis of a report for Leeds City Council which will feed directly into their policy making decisions. Leeds City Council will distribute the business case to the Leeds taxi driving community and it is hoped that these results alongside the City Councils new policies will encourage taxi drivers to choose hybrid vehicles when they buy their next taxi.

The Leeds taxi fleet is made up of large diesel vehicles that are inefficient in city centre driving and emit very high levels of NOx and particulates. While the fleet is small they drive very high mileage which makes them a high proportion of the vehicles on the road, especially at night. Unlike the London taxi fleet, in Leeds, the taxi fleet is predominantly made up of mass market saloon vehicles. This means there is already a new and second-hand hybrid vehicle market, though a larger second-hand market could be helpful in getting more hybrid vehicles into the taxi fleet. This means the challenges in hybrid vehicle uptake are cultural and financial, not technical, and so these are the areas policy makers need to focus on.

Taxi drivers driving pattern is unlike any other driving group. This makes it difficult for the taxi drivers to find fuel consumption data that is accurate for them. Without taxi driver specific data that clearly demonstrated a good payback for switching to hybrid vehicles, it will always be very difficult to persuade drives to take an unknown risk that would impact the profitability of their business for the next five years.

To create taxi driver specific fuel consumption data, a testing method was needed that provided real world figures, for the varied conditions experienced in taxi driving. PAMS testing performed very well for this chosen task, providing a cost effective way to conduct nine days of testing, and provided a rich data source, that not only showed the magnitude

of the fuel saving potential of switching over to hybrid vehicles, but disclosed how the hybrid architecture achieved these savings. PAMS data collection has great potential in the future, as cost come down and reliability improves these systems will be able to track large numbers of vehicle, driven on the road, under normal everyday operation.

Switching over to a petrol hybrid fleet from the current conventional fleet has several major advantages. These include, reducing fuel consumption by 7.91 l/100km and 3.53 l/100km compared to a petrol and diesel vehicle respectively. Reducing NOx emissions by 99.8% and 89.1% compared to a petrol and diesel vehicle respectively. The higher upfront cost of a hybrid vehicle can be paid off by fuel savings in 1.4 and 3 years, and the fuel savings can go on to save the drivers £13,122 and £3,343 compared to a petrol and diesel vehicle respectively, over the life of the vehicle. This study has found that switching from a petrol or diesel to a hybrid taxi reduces fuel consumption by 60% and 40% respectively. This is a much larger saving than the 30 – 35% compared to petrol and 15% compared to diesel found in the literature (Abuhijleh & Nik, 2013; Wu et al., 2015). This could be because the taxi driving patterns in Macao and Dubai are very different to Leeds. Higher levels of motorway driving in these areas would result in a decreased benefit from hybrid vehicles. These studies also omit the taxi rank from their driving routes and this alone may make up 5 to 10% of the total saving made by the hybrid vehicle.

There are a wide range of policies that have been shown to work at encouraging hybrid vehicle uptake in taxi fleets. Over the period of a decade these policies have converted the taxi fleets of San Francisco and New York to 97%, 60% of AFV respectively (City of New York Taxi & Limousine Commission, 2014; San Francisco Municipal Transportation Agency, 2015) and it is expected that by 2030 London will have achieved a similar switch. It is clear that for Leeds to switch to a hybrid taxi fleet the initial driving force needs to be strong licencing policy, coupled with taxi driver and consumer education, but once the change has started less involved policies can complete the switch.

Chapter 6

Hybrid Vehicle Model Creation and Validation

6.1 Introduction

This chapter presents the building, validating and use, of a backward facing (the model starts with vehicle speed and back calculates to find the engine operating conditions and the fuel consumption), microscale (runs at 1Hz), fuel consumption model, of the third generation Toyota Prius. This chapter includes:

1. A description of the modelling environment and the model inputs.
2. A detailed description of all the model components and how they were developed using the test data from database A presented in Chapter 3.
3. Model validation against a completely independent data set collected at Argonne National Laboratory on a chassis dynamometer (Argonne National Laboratory, 2015).
4. The model is demonstrated by testing a new policy application to show the capability and flexibility of the model architecture.

The model is built based on empirical relationships found in the PAMS test data described in Chapter 3. The model is designed to be as simple and as computationally efficient as possible. This is important because the input data for this kind of model is likely to be vehicle tracking data or traffic simulation data. Both data sources produce very large quantities of vehicle speed data. It is, therefore, important that the model can process these data inputs in a reasonable time.

The modelling process has several key differences to much of the modelling work presented in the literature review, Section 2.4. Firstly, the mix of first principle and empirical methods used, results in a fast running model that can incorporate complex vehicle architectures and controls, and can be adapted to test changes in vehicle design.

This method has proved very successful at modelling the Toyota Prius, which has one of the most complex powertrain architectures and control algorithms of any light duty vehicle on the market. Having proved this method for the most difficult case, applying the method to other vehicles should prove faster and more accurate. To compile and run the model presented here, over 24 hours of data at 1 Hz, the common modelling frequency for models such as PHEM (CH2M Hill, 2013), takes just over nine seconds. This shows how powerful a modelling tool such as this can be if large quantities of vehicle speed data is available from vehicle tracking or traffic simulation.

Secondly, the model has been created from on-road test measurements taken from the vehicle CAN. This method of data collection for model building has several advantages and disadvantages. Large amounts of data can be collected from many vehicles under real-world conditions at relatively low cost, providing an underlying database which includes a wide range of vehicle operating conditions not normally experienced during chassis dynamometer, or short sections of PEMS testing. The difficulty of using this testing method for modelling is that the conditions of testing are far less controllable, meaning more variables need to be recorded and control patterns identified within the data.

Thirdly, the model has been validated against an independent database created by a different institution, using a different vehicle testing method and different testing equipment. This last point is very important as many models in the literature present very little independent validation (Rakha, Ahn, & Trani, 2004; Smit et al., 2006) and without this the model can become over fitted.

6.2 Model Creation

This model has been created in the Matlab/Simulink environment. Matlab is a numerical computing environment with its own programming language that allows users to perform complex data analysis and visualisation. Simulink is visual computing environment

(models are created by joining function blocks such as addition or integration together to form hierarchical models). Matlab/Simulink was chosen because Matlab has a wide range of built in functions that made data analysis and presentation easy and efficient, Simulink's graphical modelling environment makes modelling systems with multiple loops simpler and it's powerful inbuilt model validation functions helped to deliver an accurate model, and it is easy to transfer data between the two allowing raw data analysis in Matlab, model creation and execution in Simulink and results analysis and plotting in Matlab.

One of Matlab key functions for building sub-models based on real world data is the 'Fit' function which fits best fit lines, curves or surfaces to raw data. The curve fitting application of the function used in this thesis works by constructing a Vandermonde matrix of linear equation which are solved using QR factorisation, a method commonly used to solve linear least squares problems. The 'Fit' function has been used anywhere in this chapter where a red best fit line has been added to raw PAMS data, this includes Figure 6.7-9, 6.12, 6.14, 6.16-17, 6.22, 6.27, 6.32-34.

The rest of this section describes the fitting of each model component. The description of each sub-model is structured:

1. Table of sub-model inputs and outputs.
2. A description of how the sub-model operates.
3. An outline of the experimental data used to fit the sub-model.
4. Analysis of the sub-model errors.

The error discussed is the error between the model and the database used to create it. It was not possible to validate the sub-models against the validation database as this does not contain many of the internal vehicle parameters needed.

6.2.1 Model Input

The model requires three inputs vehicle speed, ambient temperature and road gradient. Vehicle speed and ambient temperature are both collected from the vehicle CAN, while road gradient is calculated during post processing of the GPS data using the DSM method as outlined in Section 3.3.2.

6.2.2 Model Components

Figure 6.1 shows the structure of the Toyota Prius powertrain as it exists in a car, with each component that has been included in the model underlined and parameters calculated by each sub-model highlighted in red. Figure 6.2 shows the inputs and outputs to each sub-model as well as the hierarchy of each sub-model where it is made up of several sub-sub-models.

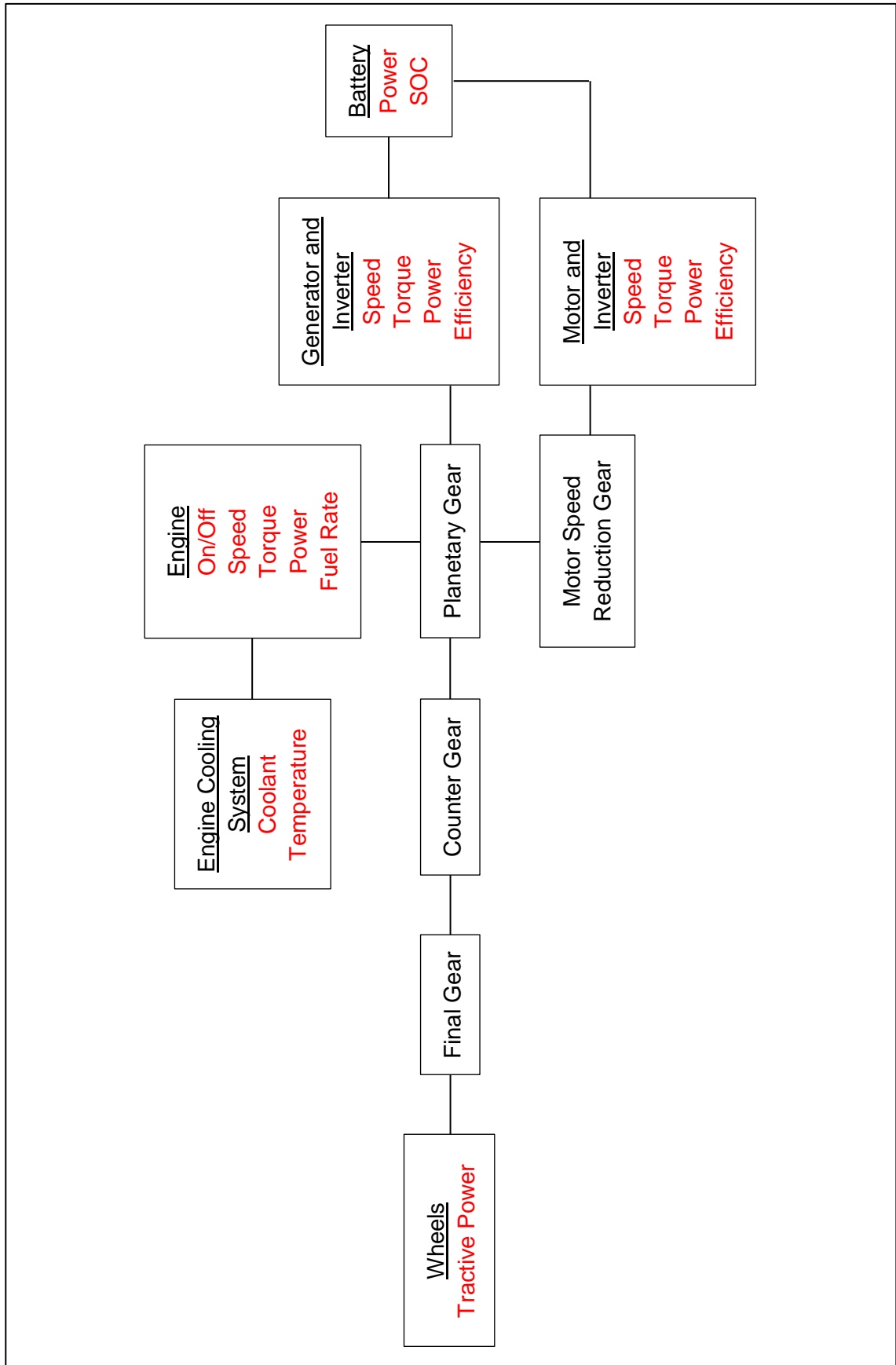
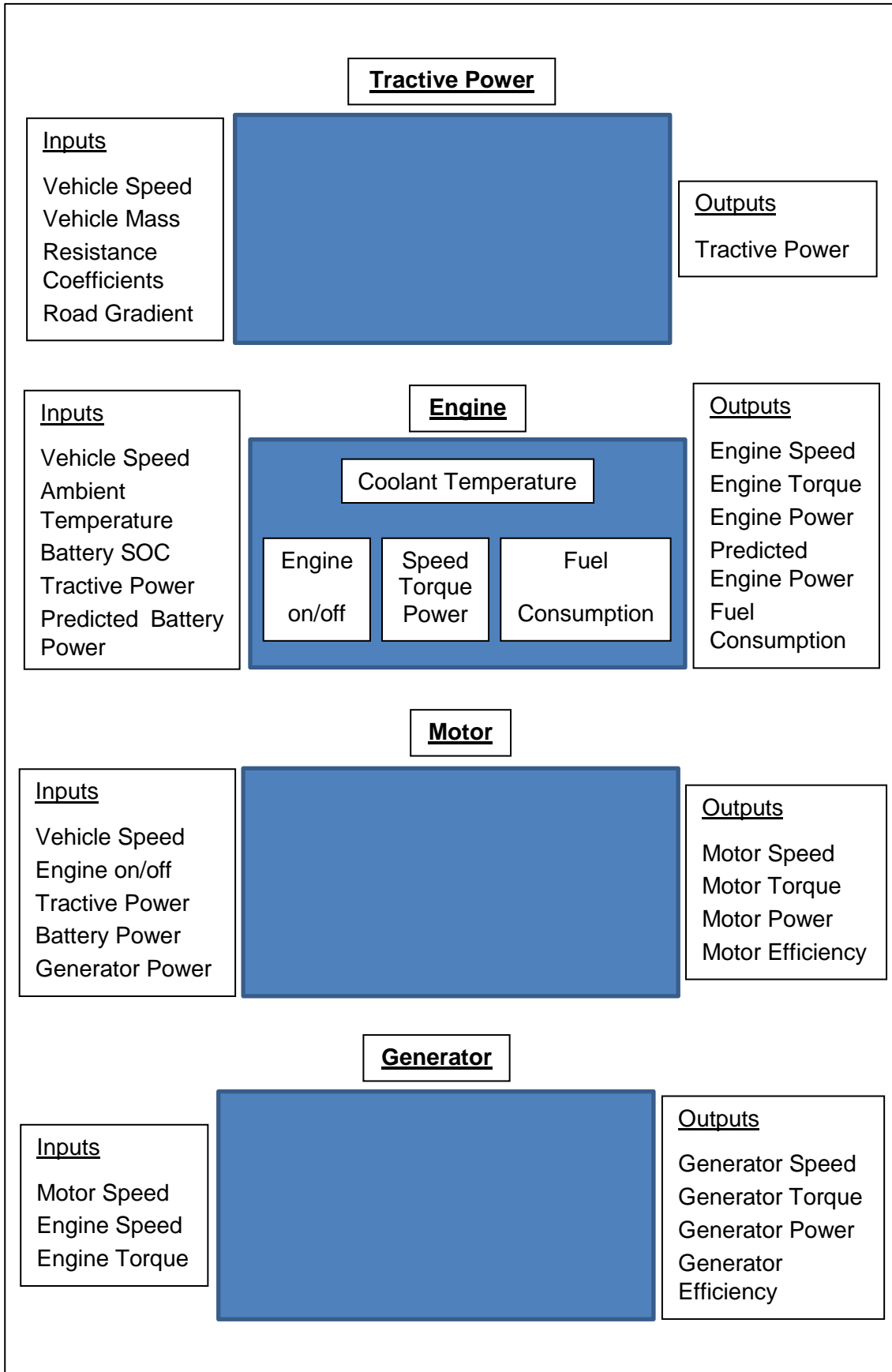


Figure 6.1: Toyota Prius powertrain overview. Sub-models underlined. Parameters calculated within each model in Red



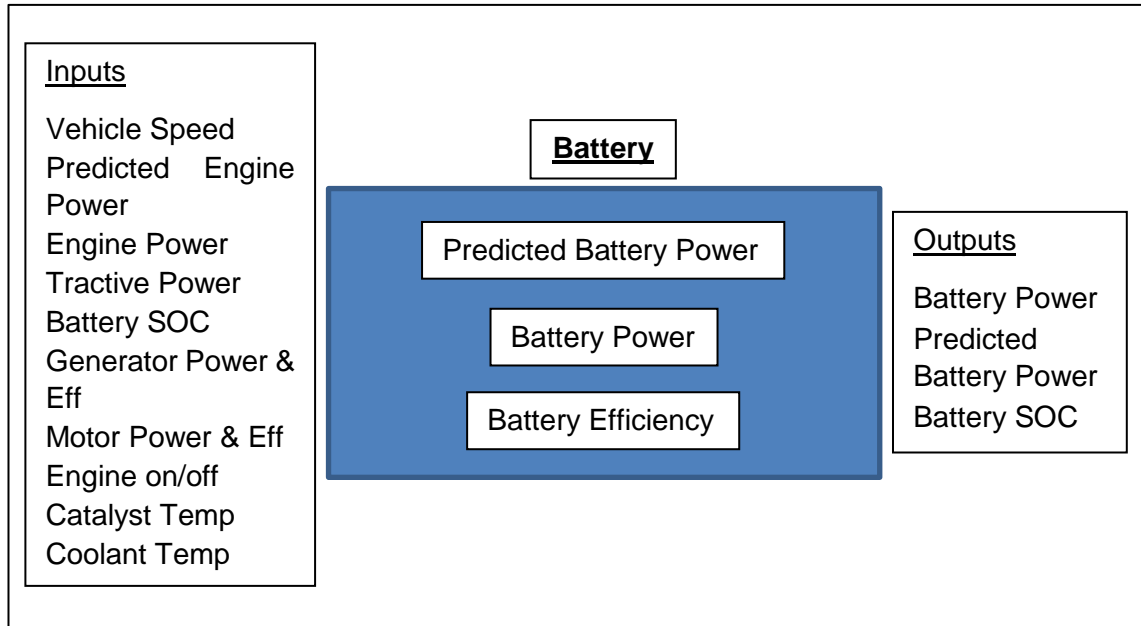


Figure 6.2: Sub-model inputs and outputs

6.2.2.1 Tractive Power

Table 6.1: Tractive power model: inputs and outputs

	Parameter	Symbol	Value	Units
Inputs	Vehicle Speed	v	Changes	m/s
	Vehicle Acceleration	a	Changes	m/s/s
	Vehicle Mass	m	1370	kg
	Gravitational Acceleration	g	9.80665	m/s/s
	Road Gradient	θ	Changes	Degree
	Rolling Resistance Coefficient	A	90.00	(N)
	Speed Correction to Rolling Resistance Coefficient	B	0.1983	(N/(m/s))
Air Resistance Coefficient	C	0.4171	(N/(m/s) ²)	
Outputs	Tractive Power	Tp	Changes	W

Tractive power is the power demand needed, at the wheels, to drive the car at the specified speed and acceleration, over a particular road gradient. Tractive power is the main parameter in the model as it sets motor power output in pure electric mode and engine power in hybrid electric mode. Tractive power is calculated at every time step, using Equation 6.1. The fitted coefficients used to calculate tractive power have been calculated from coast down tests conducted by the EPA in America, as part of the type approval procedure (United States Environmental Protection Agency, 2016). It is difficult to calculate the accuracy of these coefficients without independent testing, but unlike in the EU where the results of the coast down tests are privately held data, in the USA this data is freely available and is subjected to rigorous checking procedures by the EPA, see Section 2.2.1.3. It is therefore expected that these coefficients are reasonably robust.

$$T_p = A \cdot v + B \cdot v^2 + C \cdot v^3 + m \cdot v \cdot (a + g \cdot \sin\theta) \quad Eq. 6.1$$

(Cappiello et al., 2002)

6.2.2.2 Engine

The engine sub-model is itself made up of five sub-models: engine coolant temperature, *engine on/off*, engine power, engine speed and torque, and engine fuel consumption.

6.2.2.2.1 Engine Cooling Sub-Model

Table 6.2: Engine coolant sub-model: inputs and outputs

	Parameter	Symbol	Value	Units
Inputs	Initial Engine Coolant Temperature	T_{Ci}	Changes	$^{\circ}\text{C}$
	Ambient Temperature	T_a	Changes	$^{\circ}\text{C}$
	Engine On Off	E_{OnOff}	Changes	NA
	Model Run Frequency	F	2 or 10	Hz
Outputs	Engine Coolant Temperature	T_c	Changes	$^{\circ}\text{C}$

The engine coolant model is split into two models. One models the coolant temperature when the engine is off and the coolant temperature is falling. The second models the coolant temperature when the engine is on and the coolant temperature is rising.

The cooling model has been developed using data when the cabin heating is switched off, so as not to include data affected by recirculation of heat from the exhaust, see Section 4.2.1.3. The data contains over 6,000 section of data between *engine off* and *engine on* events, when the coolant temperature is cooling. This dataset was filtered to remove sections of data shorter than 25 seconds and this left around 1,300 sections of data, totalling 300,000 readings, for analysis. Finally, the data files were corrected, by deducting the ambient temperature from the engine cooling temperature, to give coolant temperature above ambient, rather than coolant temperature above 0°C .

Figure 6.3 shows the data sections after they have been time aligned to produce a single temperature curve with the full range of engine coolant temperatures. A logarithmic curve, shown in red, has been fitted to the data. To model this relationship, the drop in

temperature per second is calculated for every value of coolant temperature minus ambient temperature. This temperature drop is denoted by T_d and calculation of the current coolant temperature at each time step of the model is given by Equation 6.2.

$$T_{c_i} = \left((T_{c_{i-1}} - T_a) + \frac{T_d}{F} \right) + T_a \quad \text{Eq. 6.2}$$

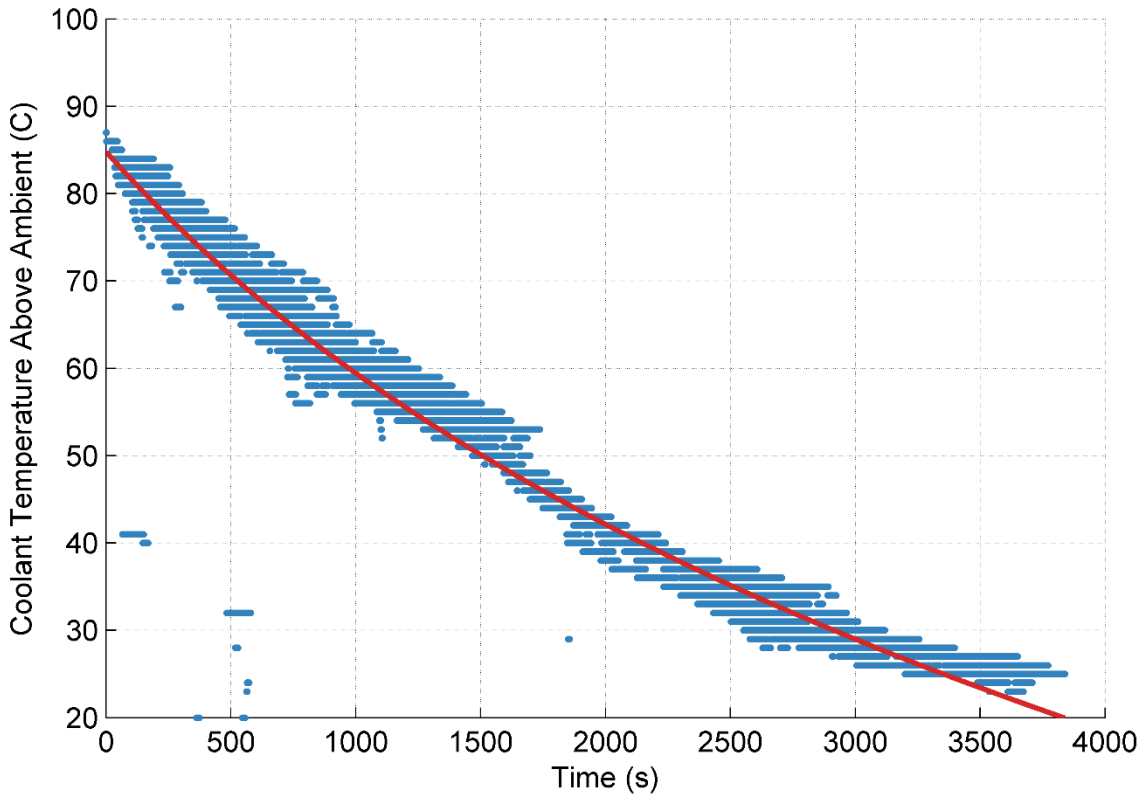


Figure 6.3: Prius engine coolant temperature, cooling over time

The coolant heating sub-model is based on the same dataset as the coolant cooling sub-model, the same filtering process leaves around 1,500 *engine on* sections of data, totalling 85,000 readings. Using the same time alignment process as before Figure 6.4 is created. This time the data does not follow a standard curve shape so the fitted line is a smoothed moving average. Again the system is modelled by calculating the rise in temperature per second at every value of coolant temperature, the temperature rise is denoted T_r , and the calculation of the current coolant temperature is given by Equation 6.3.

$$Tc_i = Tc_{i-1} + \frac{Tr}{F}$$

Eq. 6.3

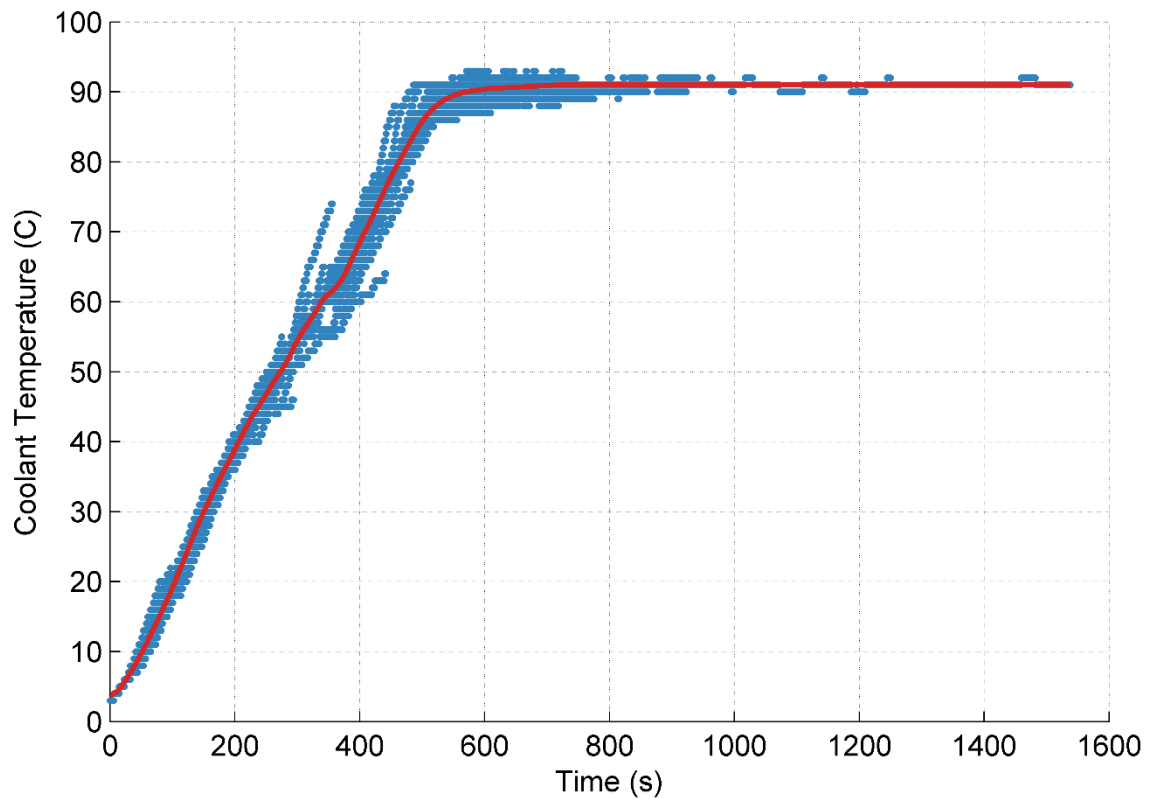


Figure 6.4: Prius engine coolant temperature, heating over time

Engine coolant temperature is a difficult parameter to model as each value depends on the previous value, and so errors grow the longer the model runs. Figure 6.5 shows a time series plot of the tested and modelled coolant temperature. This simple model is not accurate enough to model trips where the coolant temperature repeated drops very low due to vehicle inactivity, but it does a good job of modelling the initial engine warm-up, which sets the duration for the first *engine on*. For any test cycle and for most real world trips the initial cold start is the only time the coolant temperature will affect the engine operation, this means that for this work the simple approach shown here is satisfactory.

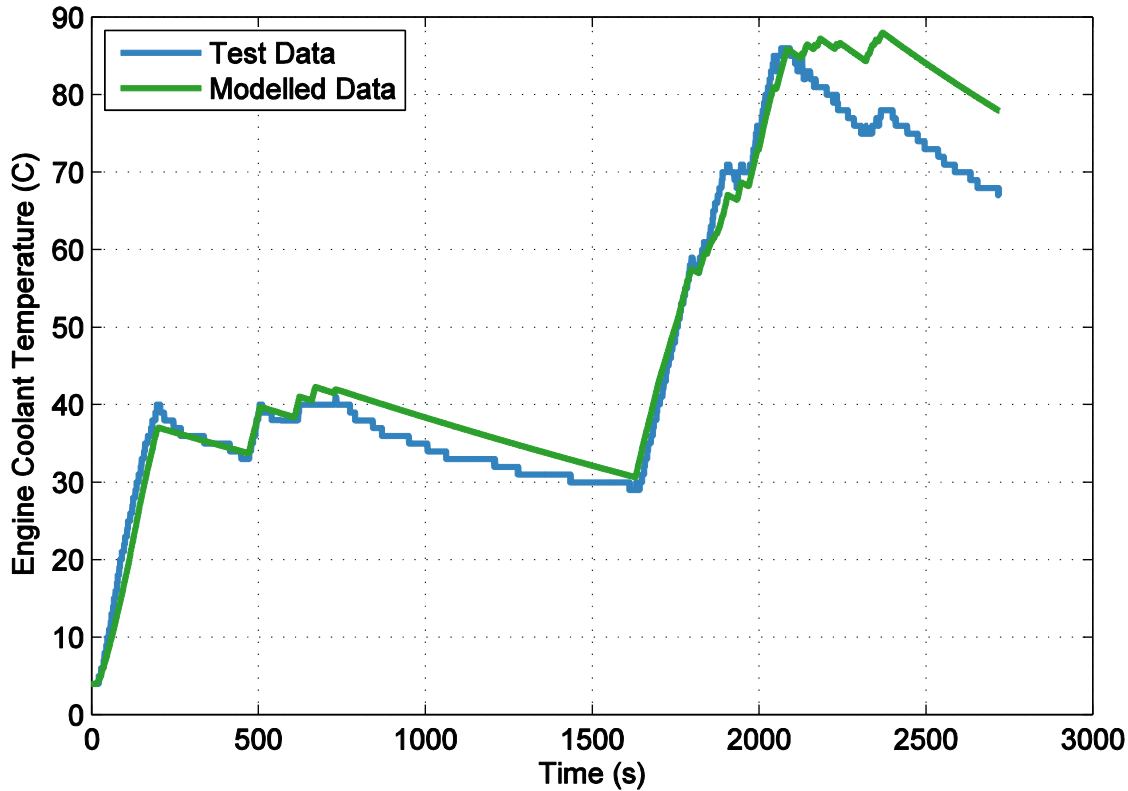


Figure 6.5: Test data and modelled engine coolant temperature

6.2.2.2.2 Engine On Sub-Model

Engine on can occur for three different reasons. Most commonly the engine turns on because the tractive power demand has exceeded the battery power limit at the current SOC. However, the engine can also turn on because the battery SOC or coolant temperature is too low.

If neither the battery SOC nor the coolant temperature limits are breached, then the vehicle will drive in PE mode until the driving demand exceeds the tractive power limit. Figure 6.6 shows how, as the tractive power demand reaches the limit value the engine turns on to help meet the power demand. Correlating tractive power with *engine on* occurrences is problematic because tractive power is dependent on road gradient which is difficult to measure accurately. However, at *engine on*, motor power is a good proxy for tractive power and can be measured far more accurately. *Engine on* will, therefore, be modelled as a function of motor power, which provides a clear peak at the point where

engine power steps in and starts to power the vehicle. Battery power also peaks at *engine on*, but will not be used because it is more difficult to correlate battery power and SOC to *engine on*. This is because at *engine on* the battery powers the vehicle through the motor, but also drives the engine through the generator, as indicated by the trough in engine power at *engine on*, seen in Figure 6.6 at five seconds.

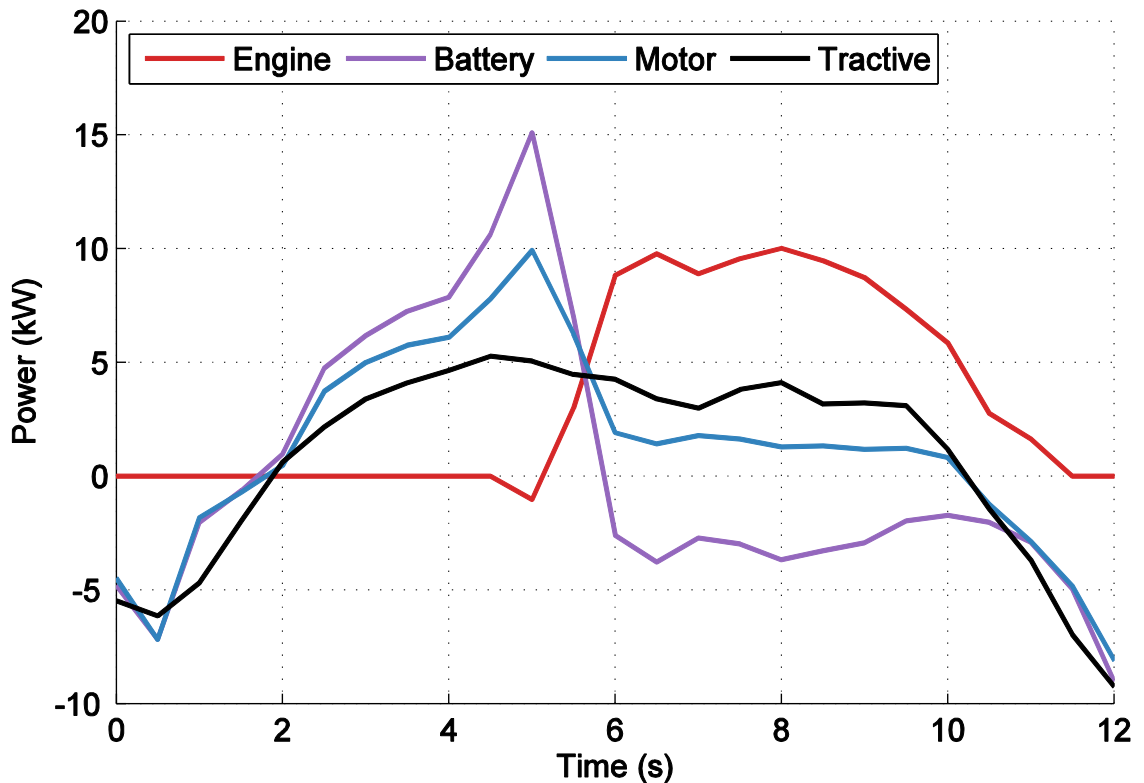


Figure 6.6: Prius engine, battery, motor and tractive power at engine on

Figure 6.7 presents the correlation between motor power, at *engine on*, and battery SOC. All recorded *engine on* events will occur above the *engine on* threshold, so a line has been fitted under the data that follows the trend of the data points. The threshold line has been fitted in two steps. In the first step a line was fitted to the raw data, using the method presented in Section 6.2, this step gave the line gradient. In the second step the y intercept of the fitted line was reduced until 95% (selected to allow for outliers) of the data fell above the line. *Engine on* due to tractive power is modelled by switching the *engine on* if the motor power, in PE mode, exceeds the red line. The *engine on* control

threshold is one of the key controls in the vehicle as it acts to protect the battery, manage the battery SOC close to the desired optimum and allows much greater utilisation of PE mode if the battery SOC is high. The database for *engine on* is very small, with only 710 readings. This is because *engine on* does not occur very often, especially in rural and motorway driving where the engine is continually operating to meet the tractive power demand. The data also had to be filtered to remove *engine on* events due to cold start, low battery SOC or very high motor power transients.

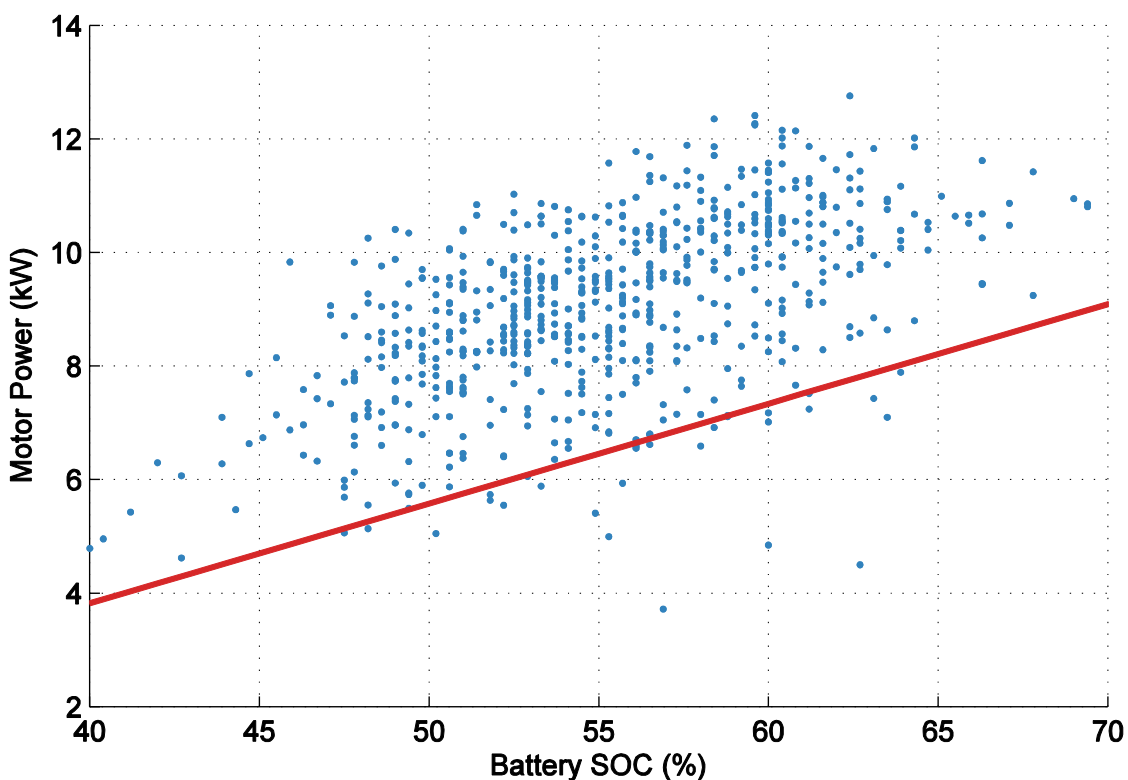


Figure 6.7: Prius battery SOC against motor power, at engine on. Blue dots represent raw data. Red line is a corrected linear best fit

6.2.2.2.3 Engine Off Sub-Model

Engine off events occur when the tractive power demand drops below a lower limit. Like *engine on* this is a function of battery SOC, allowing the engine to turn off earlier if the battery SOC is high. However, the control limit for *engine off* is difficult to observe. This is because the tractive power drops very quickly, from positive when the throttle pedal is

pushed, to negative when no input is given or the brake pedal is pushed. This results in the tractive power jumping from above to below the control limit, without providing much information to define where the control limit lies. The *engine off* control signal is also more difficult to define than the *engine on* control signal. At *engine on* the engine speed begins to rise from zero, but the *engine off* signal can be given at any engine speed and the time between the *engine off* signal and the engine coming to a stop is not very consistent. Instead, it has been estimated, based on the drop in fuelling rate, that if the engine speed falls below 900 RPM the engine is in an *engine off* event.

All recorded *engine off* events will occur below the *engine off* threshold, so a line has been fitted, using the method presented in Section 6.2.2.2.2, above the *engine off* points following the trend of the data. The *engine on* and off trend lines have very similar gradients and occur roughly 4.5 kW apart. The positioning of the *engine off* threshold is logical because the low SOC *engine on* threshold is 40%, it, therefore, makes sense that the *engine off* threshold drops below zero tractive power just above 40% SOC, as this will stop the engine turning off and back on again in a very short space of time. As is the case with *engine on*, *engine off* does not occur very often so limited data points are available to build the fit. Figure 6.8 is based on a filtered database that does not include *engine off* events during cold starts, low battery SOC events or very sharp drops in tractive power, leaving 500 data points to build the model fit.

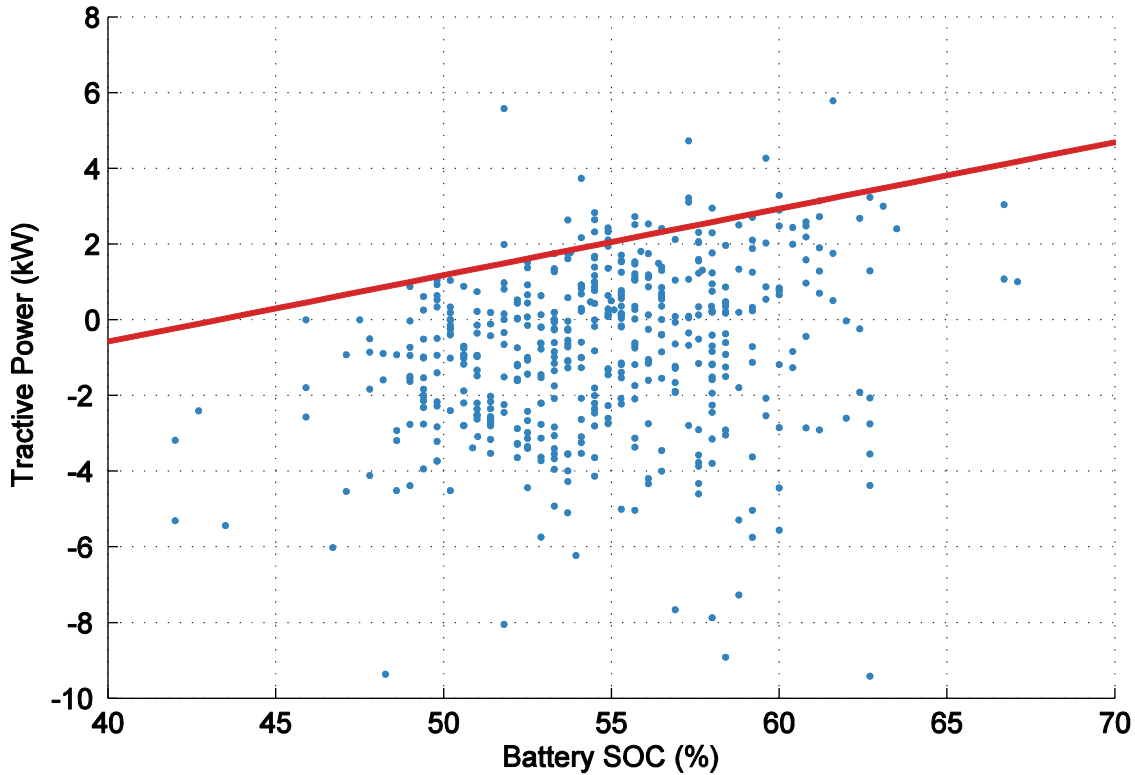


Figure 6.8: Prius battery SOC against tractive power, at engine off. Blue dots represent raw data. Red line is a corrected linear best fit

Engine off events can occur at high vehicles speeds as the vehicle decelerates or due to downhill gradients. When the *engine off* signal is given and the vehicle speed is greater than 72 km/h (45 mph) fuel cut mode is activated. When this occurs engine speed drops to idle, engine torque drops to -14 Nm, which forces the generator to drive the engine, and the fuel consumption is ramped down to zero over the period of half a second. If the engine turns back on again, during fuel cut, then the engine speed and torque rise to meet the power demand and the fuel consumption is ramped back up again over a period of one second.

6.2.2.2.4 Engine Power Sub-Model

Table 6.3: Engine power sub-model: inputs and outputs

	Parameter	Symbol	Value	Units
Inputs	Tractive Power	T _p	Changes	W
	Battery SOC	SOC	Changes	%
	Predicted Battery Power Demand	B _{p_p}	Changes	W
Outputs	Predicted Engine Power	E _{p_p}	Changes	W
	Engine Power	E _p	Changes	W

When the engine is running it must meet the power demand for the whole vehicle, this means producing enough power to meet the tractive power, battery recharging power and efficiency losses in both the mechanical and electrical paths. Engine power is based on the required battery power needed to keep the battery SOC in the permissible range. During engine transients, the engine power does not track the engine power demand perfectly and the difference must be made up by the battery. This means it is necessary to calculate a predicted battery and engine power based only on steady state numbers and then corrected this to the actual engine and battery power once transients have been considered. Equation 6.4 is used to calculate a first estimate of engine power.

$$E_{p_p} = \frac{(T_p - B_{p_p})}{\eta_a} \quad \text{Eq. 6.4}$$

Figure 6.9 is used to calculate η_a , to create the figure the tractive power database is filtered to remove cold starts, power regeneration, low battery SOC recharge and engine off data, leaving just over 50,000 data points. The data to the left of x equal zero is the engine in the process of turning off. The data to the right of x equals zero is normal engine operation. The efficiency losses at low tractive powers are very high because a high proportion of the power is passing through the electrical path, but as the power

demand increases so does the vehicle speed, this allows better optimisation of the mechanical path and therefore inefficiencies in the powertrain decrease.

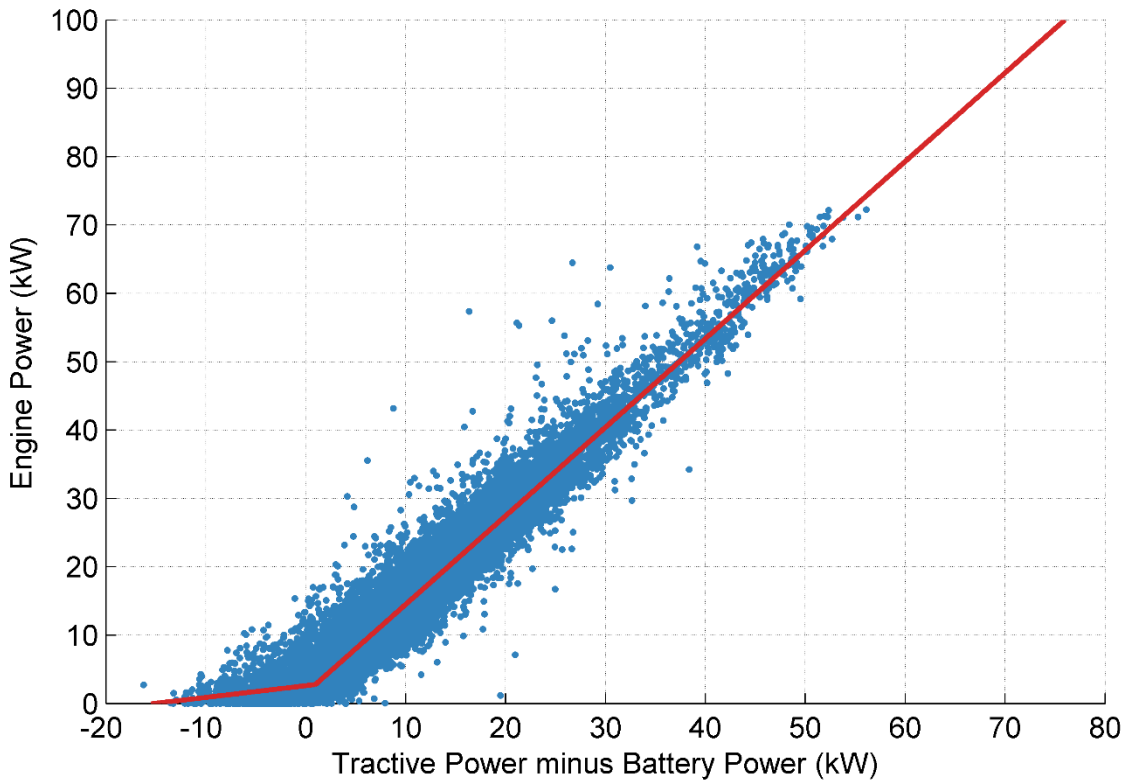


Figure 6.9: Calculating engine power from tractive and battery power. Blue dots represent raw data. Red line is a linear best fit fitted over two power ranges (-20-0kW, 0-80kW)

To convert predicted engine power into engine power two corrections are made. The first area corrected is *engine on*, for the first 0.5 seconds, after the *engine on* signal is given, engine speed starts to climb linearly from zero to predicted engine speed, while engine power drops linearly from zero to -1500 W. From 0.5 to 1 seconds after the *engine on* signal is given both engine speed and power climb linearly up match the predicted values. This control stops the engine from jumping from off to on in a single time step and matches the way tested engine speed and torque cut linearly across the engine map to the desired power during *engine on*, rather than following the optimised engine path. The negative drop in engine power at the start of *engine on* is caused by the generator acting on the engine to turn it on.

The second area corrected is *engine off*, this is done in a similar way to *engine on*, for the last second of *engine on* the engine power and speed drop linearly from the predicted value down to zero.

A third correction for engine power delay should be included in the model to improve the prediction of battery power, but it was found that the addition added more complexity to the model without significantly improving the fuel consumption prediction over a drive cycle. Future work should develop an engine power delay sub-model as this will improve the model accuracy over long runs and will be vital for people wishing to study battery degradation.

The engine power limit is 73kW, which the engine does meet at maximum torque under harsh accelerations at high speed. Figure 6.10 shows the engine operating points, the engine torque appears to be limited between -144 and 144 Nm, and the engine speed has a maximum between 5000 and 6000 RPM. These hard limits have been added to the model with no contingency for if they are met. It has been assumed that as long as the vehicle speed data has been collected on a Prius then the model will be able to drive the speed trace without meeting these limits.

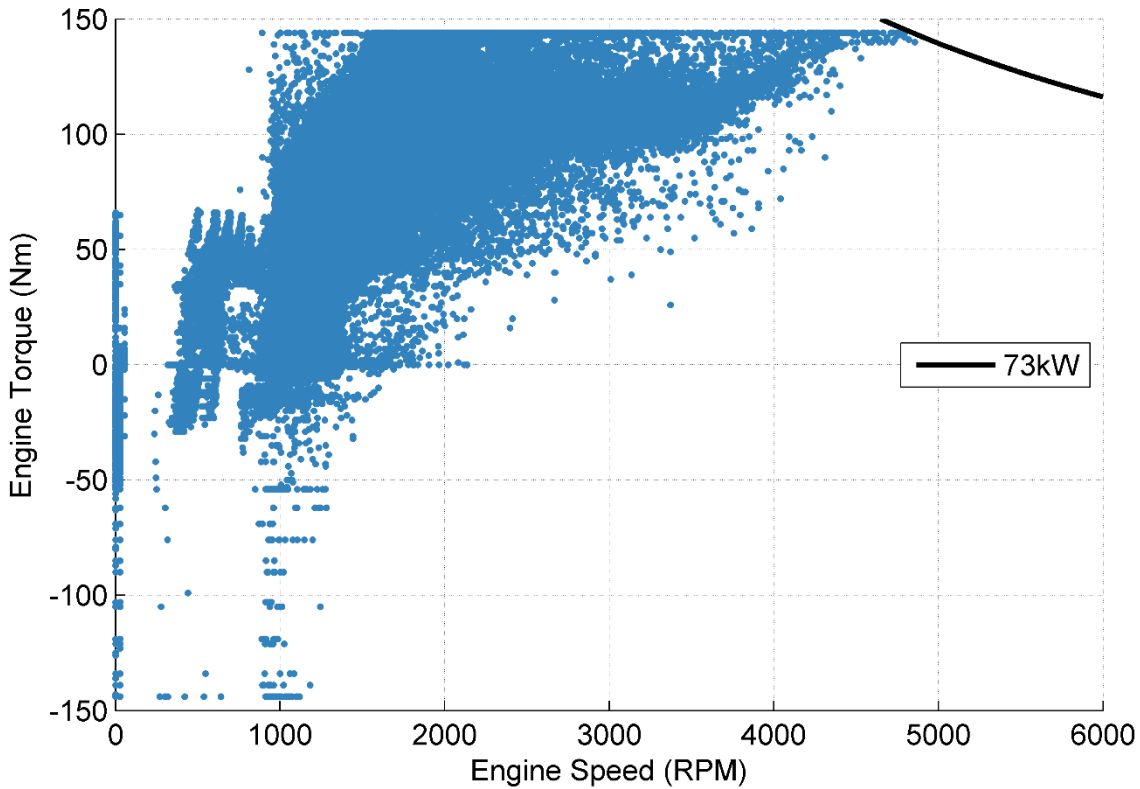


Figure 6.10: Prius engine operational area and power limit

Figure 6.11 displays the error in modelling engine power against the two main sub-model inputs. The error is calculated as model data minus test data. The model predicts engine power well under negative tractive power conditions, but the error, when the tractive power is positive, is skewed towards the negative. This indicates that the model is under predicting engine power.

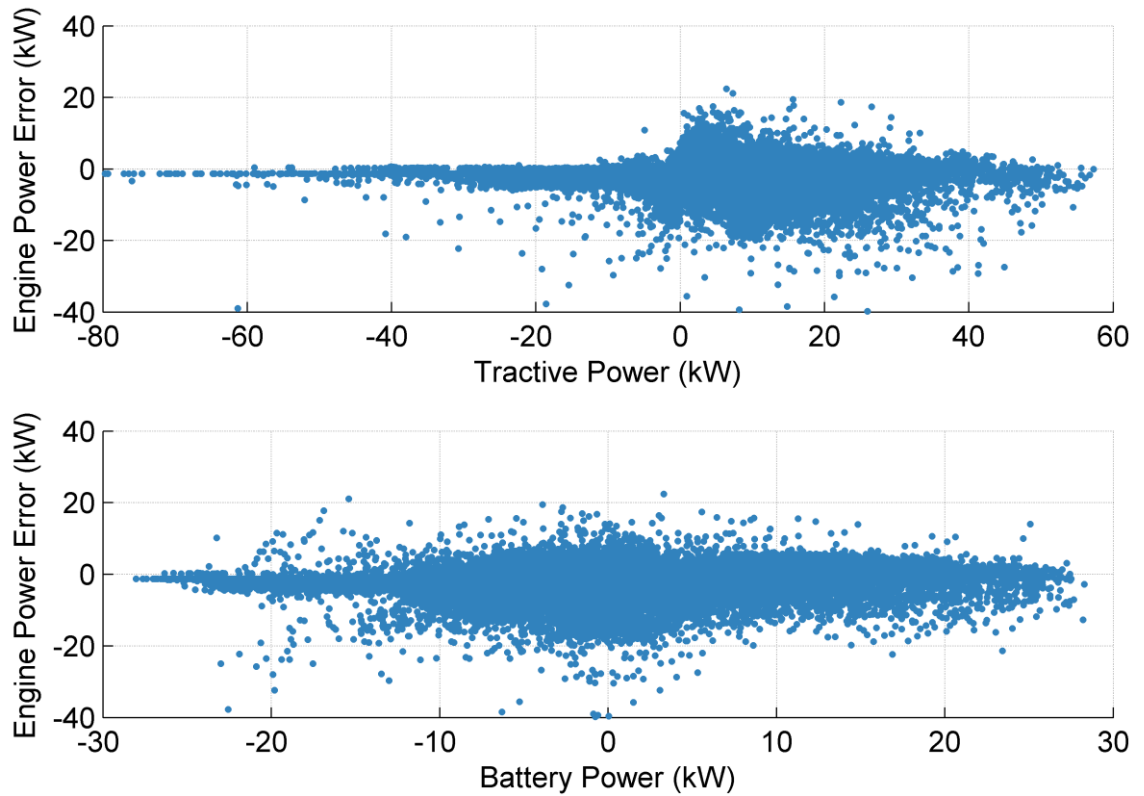


Figure 6.11: Engine power error against sub-model inputs, tractive power and battery power

6.2.2.2.5 Engine Speed and Torque Sub-Model

Table 6.4: Engine speed and torque sub-model: inputs and outputs

	Parameter	Symbol	Value	Units
Inputs	Engine Power	E_p	Changes	W
	Engine Coolant Temperature	T_c	Changes	$^{\circ}\text{C}$
Outputs	Engine Speed	E_s	Changes	Radian/s
	Engine Torque	E_t	Changes	Nm

The Prius engine tracks an optimised path across the engine map, this means that under steady state conditions there is only one set of engine speed and torque values for each

engine power. In this model engine speed is estimated as a function of engine power and engine torque is calculated from the result using Equation 6.5.

$$Et = \frac{Ep}{Es} \quad Eq. 6.5$$

Figure 6.12 displays the relationship between engine power and speed, the dataset has been filtered to remove engine off, and cold engine data, leaving 190,000 reading for the analysis. A fourth order polynomial has been fitted to the data as this most closely follows the optimised engine path when the data is plotted as engine speed against torque.

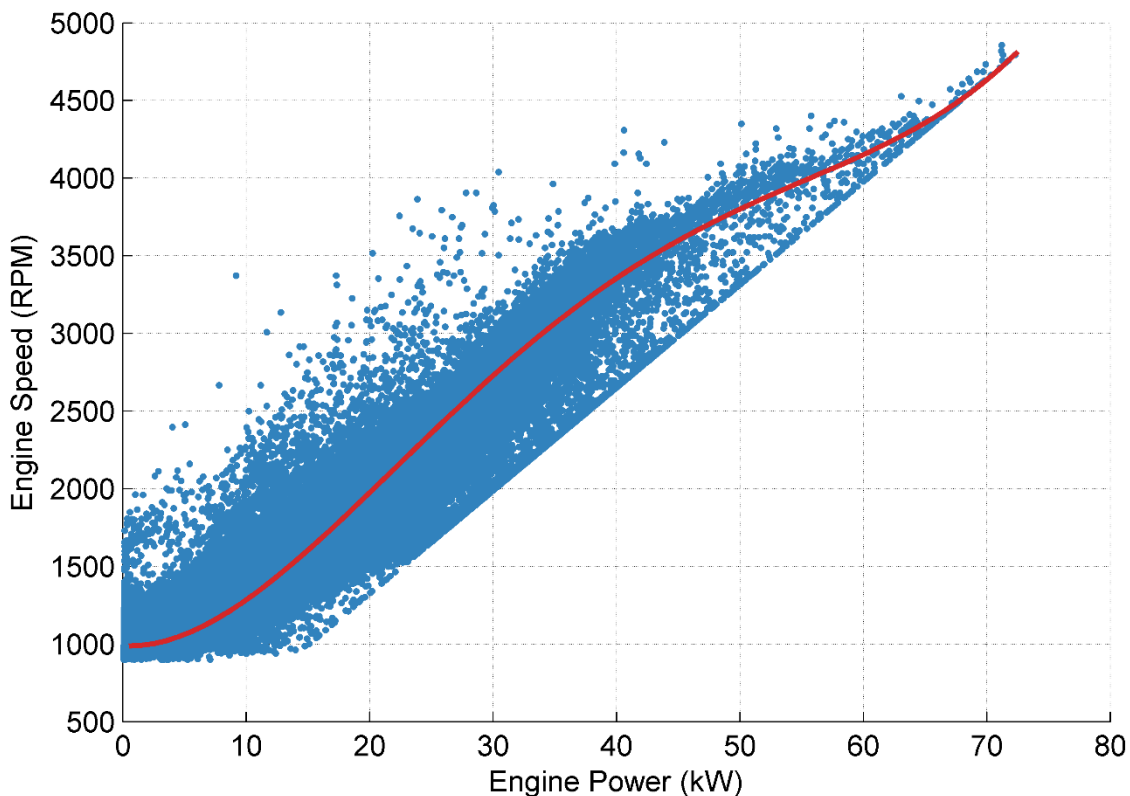


Figure 6.12: Calculating engine speed from engine power. Blue dots represent raw data. Red line is a quartic best fit curve

The engine idle speed is related to the engine coolant temperature. Figure 6.13 shows the engine coolant temperature against engine speed for a data set that has been filtered to remove engine off data and positive driving demand data. The Figure shows that engine idle speed is set to 1300 RPM for all coolant temperatures up to 50°C. The idle

speed drops from 1300 RPM to 1000 RPM in a linear trend between 50°C and 70°C. Engine idle speed is then independent of temperature at coolant temperatures greater than 70°C.

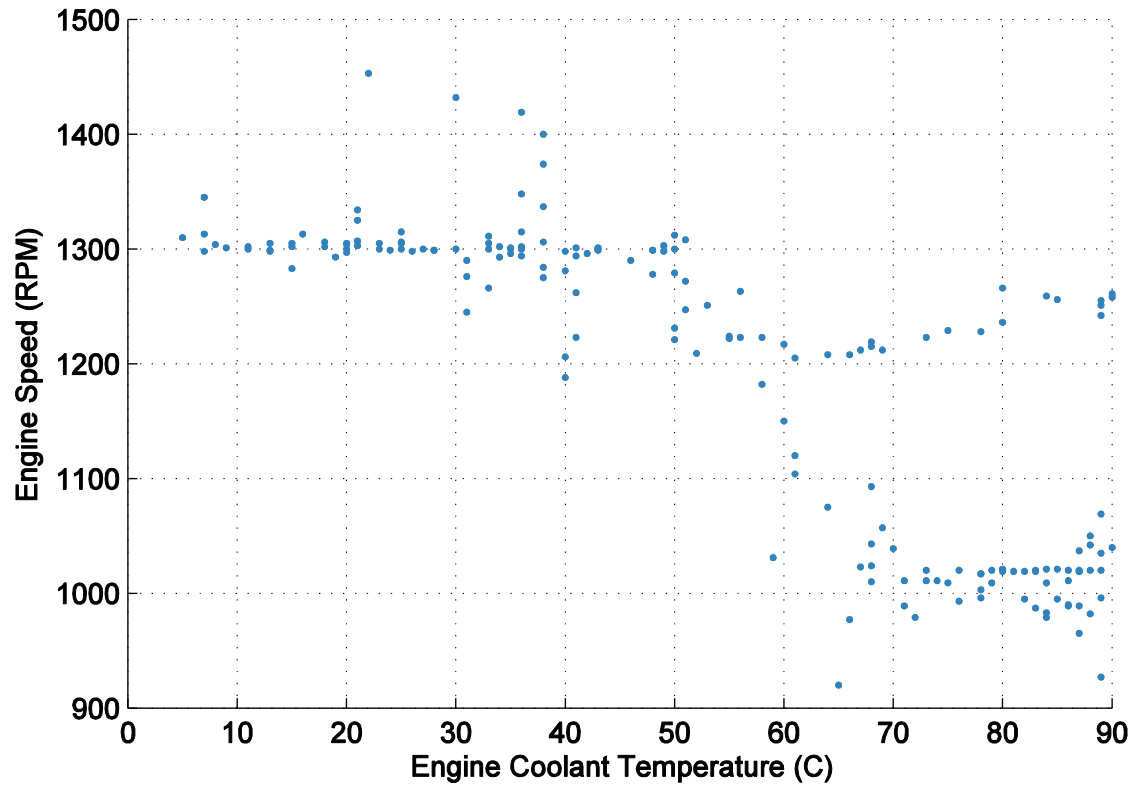


Figure 6.13: Prius engine idle speed as a function of engine coolant temperature

6.2.2.2.6 Engine Fuel Consumption Sub-Model

Table 6.5: Engine fuel consumption sub-model: inputs and outputs

	Parameter	Symbol	Value	Units
Inputs	Engine Speed	Es	Changes	Radian/s
	Engine Torque	Et	Changes	Nm
	Engine Coolant Temperature	Tc	Changes	°C
Outputs	Instantaneous Fuel Consumption	Fc	Changes	ml
	Cumulative Fuel Consumption	Fc _c	Changes	l

The engine fuel consumption is predicted using a quartic polynomial equation based on engine speed, torque, coolant temperature and transient level. The analysis uses a filtered database of over 160,000 points. The data has been filtered to remove engine off data and very short *engine on* events. The quartic equation is fitted to the data using the built in stepwise regression function in Matlab.

The stepwise fit is presented in Equation 6.6, symbols 2, 3 and 4 stand for squared, cubed and to the fourth power respectively. transSB stands for the change in engine speed between the current and previous time step, transSM stands for the change in engine speed between the previous, and next time step. transTB and transTM are the same as transSB and transSM but for torque rather than speed. The subscript e stands for transient at *engine on* and *off* only.

$$\begin{aligned}
Fc = & (Es) + (Es2) + (Es3) + (Es4) + (Et) + (Et2) + (Et3) + (Et4) + (Tc) + (Tc2) \\
& + (Tc3) + (Tc4) + (Es.Et) + (Es.Et2) + (Es.Et3) + (Es.Et4) + (Es.Tc) \\
& + (Es.Tc2) + (Es.Tc3) + (Es.Tc4) + (Et.Es2) + (Et.Es3) + (Et.Es4) \\
& + (Et.Tc) + (Et.Tc2) + (Et.Tc3) + (Et.Tc4) + (Tc.Es2) + (Tc.Es3) \\
& + (Tc.Es4) + (Tc.Et2) + (Tc.Et3) + (Tc.Et4) + (Es2.Et2) + (Es2.Tc2) \\
& + (Et2.Tc2) + (Es3.Et3) + (Es3.Tc3) + (Et3.Tc3) + (Es4.Et4) \\
& + (Es4.Tc4) + (Et4.Tc4) + (Es.Et.Tc) + (Es2.Et2.Tc2) \\
& + (Es3.Et3.Tc3) + (Es4.Et4.Tc4) + (Es2.Et.Tc) + (Es.Et2.Tc) \\
& + (Es.Et.Tc2) + (Es3.Et.Tc) + (Es.Et3.Tc) + (Es.Et.Tc3) \\
& + (Es4.Et.Tc) + (Es.Et4.Tc) + (Es.Et.Tc4) + (Es2.Et2.Tc) \\
& + (Es.Et2.Tc2) + (Es2.Et.Tc2) + (Es3.Et3.Tc) + (Es.Et3.Tc3) \\
& + (Es3.Nm.Tc3) + (Es4.Et4.Tc) + (Es.Et4.Tc4) + (Es4.Et.Tc4) \\
& + (transSB) + (transSM) + (transTB) + (transTM) + (transSB_e) \\
& + (transSM_e) + (transTB_e) + (transTM_e)
\end{aligned}
\tag{Eq. 6.6}$$

Figure 6.14 presents the test vehicle fuel consumption against the predicted fuel consumption from the stepwise model. The least squares best fit line has a y intercept of 0.04, a gradient of 0.96 and an R squared value of 0.96. The fit does a good job considering the fact that no high transient data was filtered from this analysis. However, the fit error increases with fuel consumption, this indicates that not enough very high fuel consumption data was present in the dataset for the model to prioritise a good fit at the highest fuel consumptions.

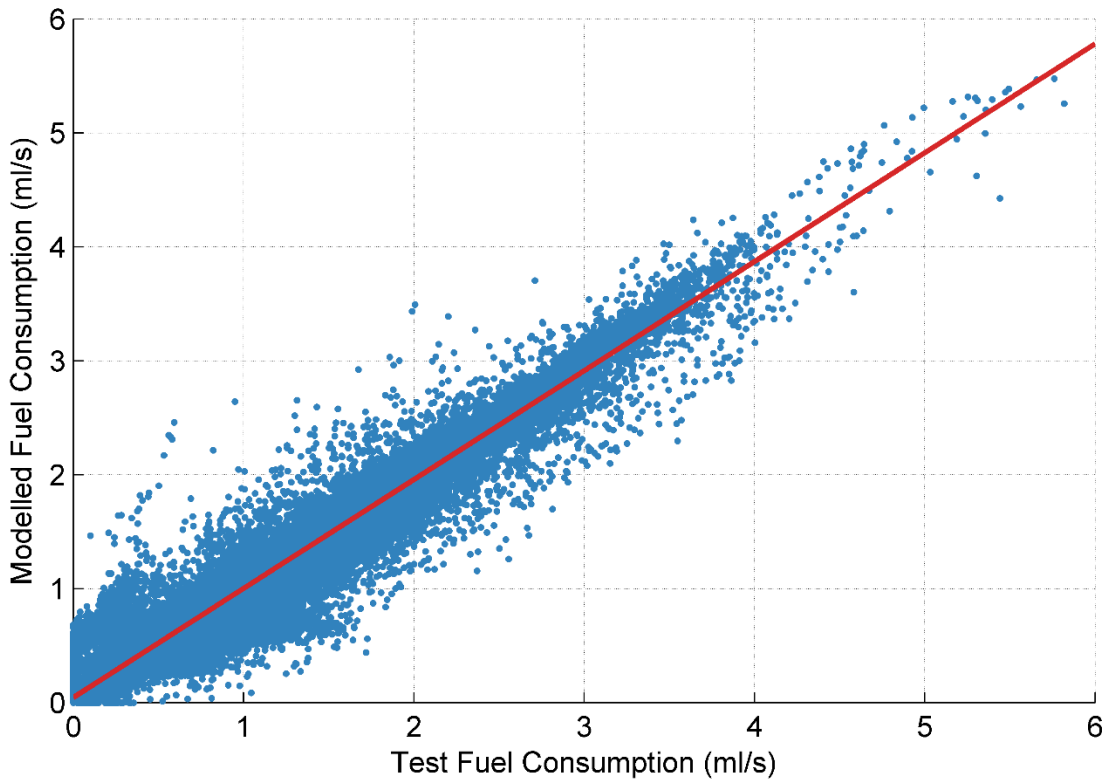


Figure 6.14: Engine fuel consumption, test data against model data. Blue dots represent raw data. Red line is a linear best fit

As Figure 6.15 shows the fuel consumption modelling error is evenly spread, with no clear trends, over the full range of sub-model inputs. This indicates the model is well balanced providing a good estimation of fuel consumption under all conditions. The widening band of error seen at higher coolant temperatures is likely caused by the increase in data available at these higher temperatures and the lower engine transients in the engine warm up stage.

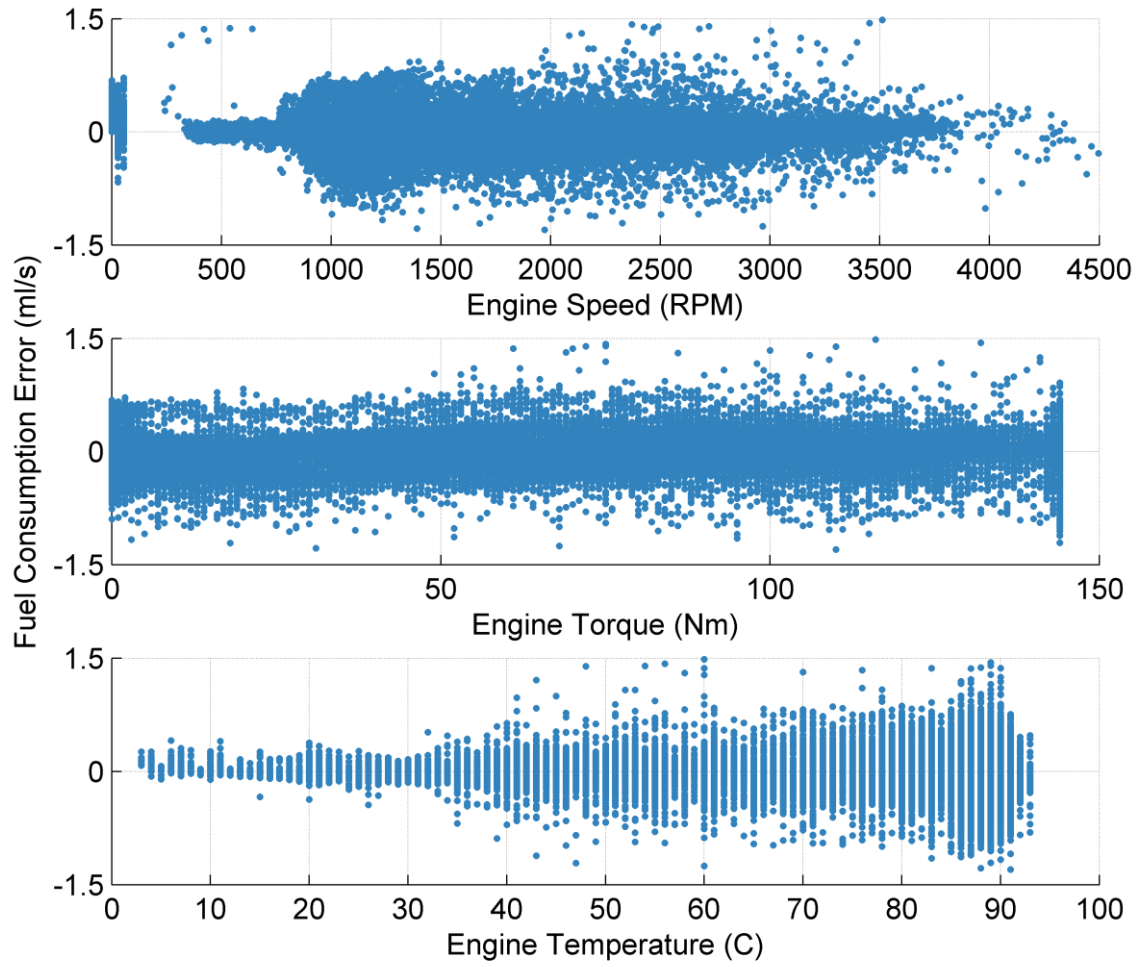


Figure 6.15: Fuel consumption error against model inputs, engine speed, torque and temperature

6.2.2.3 Motor and Inverter

Table 6.6: Motor model: inputs and outputs

	Parameter	Symbol	Value	Units
Inputs	Vehicle Speed	v	Changes	m/s
	Tractive Power	T_p	Changes	W
	Generator Power	G_p	Changes	W
	Battery Power	B_p	Changes	W
	Wheel Radius	r	0.305	m
	Number of Teeth FG Drive Gear	N_{fd}	24	NA
	Number of Teeth FG Driven Gear	N_{fn}	77	NA
	Number of Teeth CG Drive Gear	N_{gd}	54	NA
	Number of Teeth CG Driven Gear	N_{gn}	55	NA
	Number of Teeth MSRG sun gear	N_{s_2}	22	NA
Number of Teeth MSRG ring gear	N_{r_2}	58	NA	
Outputs	Motor Speed	M_s	Changes	Radian/s
	Motor Torque	M_t	Changes	Nm
	Motor Power	M_p	Changes	W

The motor is directly connected to the wheels through the motor speed reduction gear, Figure 4.2. This means motor speed can be calculated based only on vehicle speed using Equation 6.7, the first term converts vehicle speed in m/s to wheel rotations in rps, the second term convert wheel rational speed from rps to rad/s, the third, fourth and fifth terms adjust the speed of rotation due to the final gear, counter gear and motor speed reduction gear respectively.

$$M_s = \frac{v}{2.\pi.r} \times 2.\pi \times \frac{Nfn}{Nfd} \times \frac{Ngn}{Ngd} \times \frac{Nr_2}{Ns_2} \quad Eq. 6.7$$

The motor power is calculated using different methods depending on the vehicle mode. In PE mode, motor power is equal to tractive power plus PG efficiency losses and is calculated using Equation 6.8 and 6.9 for motor power during vehicle motoring and regeneration respectively. The vehicle uses the mechanical brakes alone to bring the vehicle to a stop, therefore at speeds lower than 6 km/h (3.7 mph), see Figure 6.29, Equation 6.9 is bypassed and M_p drops to zero.

$$M_p = T_p \div \eta_p \quad Eq. 6.8$$

$$M_p = T_p \times \eta_p \quad Eq. 6.9$$

When the vehicle is stationary, and for the first second of each microtrip the model uses the best fit line presented in Figure 6.16 to calculate η_p . This fit is created from the tractive power dataset, filtered to remove *engine on* data and vehicle moving data, except the first second of each microtrip, this leaves around 120,000 readings.

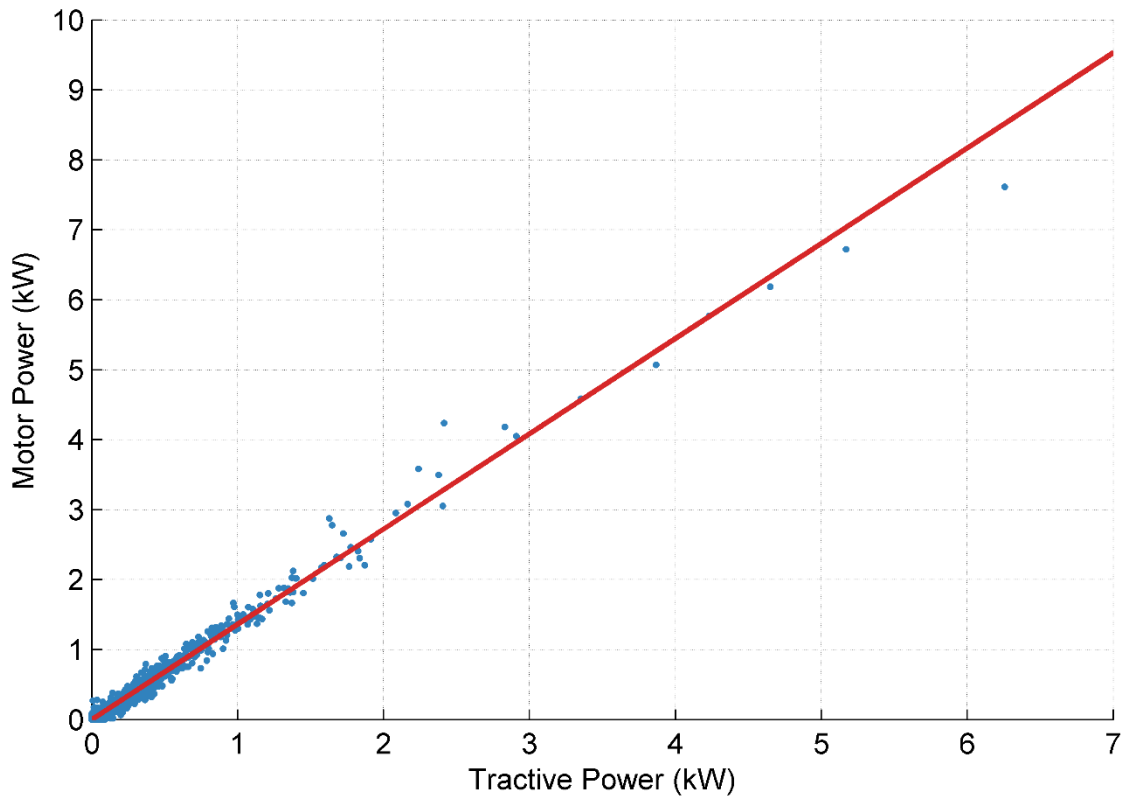


Figure 6.16: Tractive power against motor power at the start of microtrips. Blue dots represent raw data. Red line is a linear best fit

For the rest of the microtrip, after the first second, until the engine turns on, η_p is calculated based on Figure 6.17. This fit is based on the tractive power dataset filtered to remove engine on and vehicle stationary data, the filtering leaves 155,000 data points to build the fit.

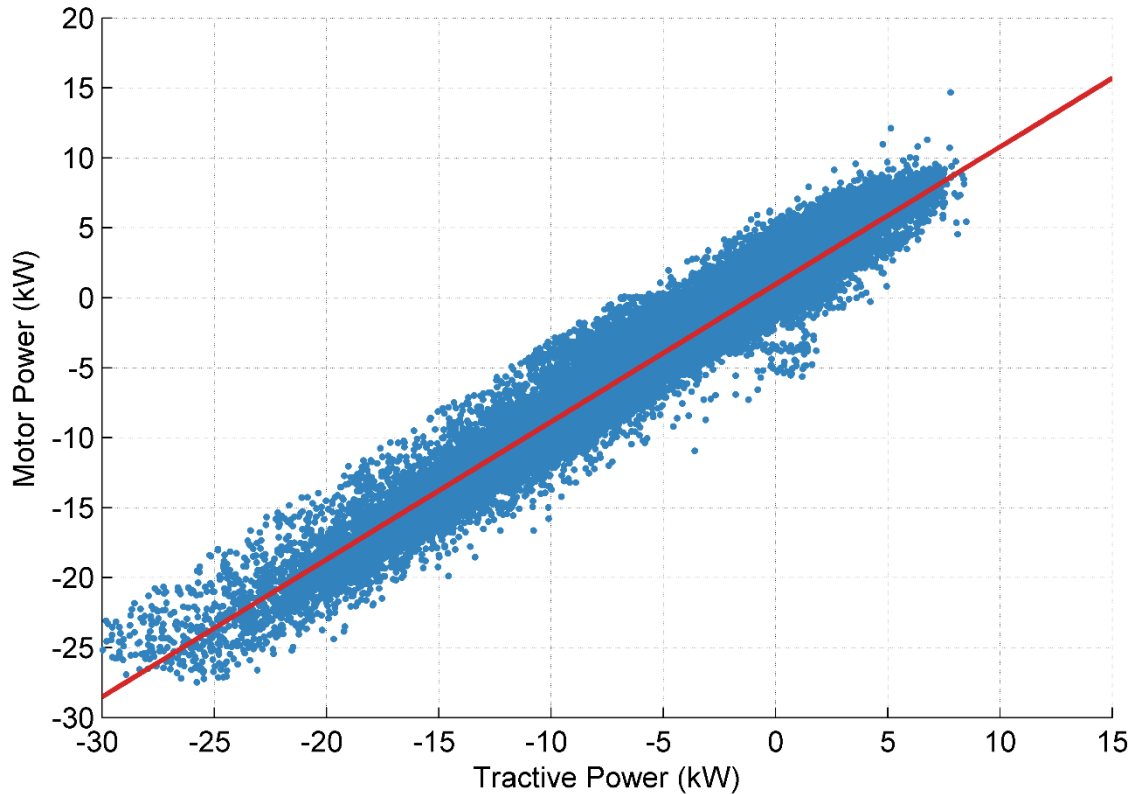


Figure 6.17: Tractive power against motor power in Prius pure electric mode. Blue dots represent raw data. Red line is a linear best fit

In HE mode, when the tractive power demand is positive, the power flow through the electrical path either goes from the generator to the motor or from the motor to the generator. In the first case, motor power is calculated using Equation 6.10 and in the second, Equation 6.11. In both cases, the motor power matches the generator and battery power plus efficiency losses. While the engine is turning on and off the equation of PE mode, not HE mode, is used as this gives a better match to test data.

$$Mp = ((Gp \times \eta_g) + Bp) \times \eta_m \times -1 \quad Eq. 6.10$$

$$Mp = \frac{\left(\left(\frac{Gp}{\eta_g} \right) + Bp \right)}{\eta_m} \times -1 \quad Eq. 6.11$$

Under some situations like engine turning off, very high traction power transients, cold start and low SOC the vehicle will operate in HE mode while the traction power is

negative. Under these conditions, Equation 6.9 for regeneration in PE mode is used and η_p is calculated based on the negative power region of Figure 6.17.

The motor maximum power is dependent on which mode the vehicle is operating in. As shown in Figure 6.18, when the vehicle is being driven, either by the engine, or battery and engine, the motor is limited to the motor maximum power of 60kW. When the vehicle is regenerating power the motor is limited depending on vehicle speed. At speeds less than 6 km/h the regeneration power is zero, from 6 to 34 km/h the allowable regen power is limited, this could be because of braking stability or motor overheating, and at speeds greater than 34 km/h the motor is limited to the maximum power of the battery which is 27kW. As the *engine on* threshold is well below the maximum battery power and motor power when the engine is on is relative low there is no need to limit the maximum motor power in the model. A minimum motor power limit is needed because regeneration power often exceeds the maximum battery power. A lower power limit line based on Figure 6.18 has been added to the model that prevents motor power from dropping below the area the motor operates in, in real life.

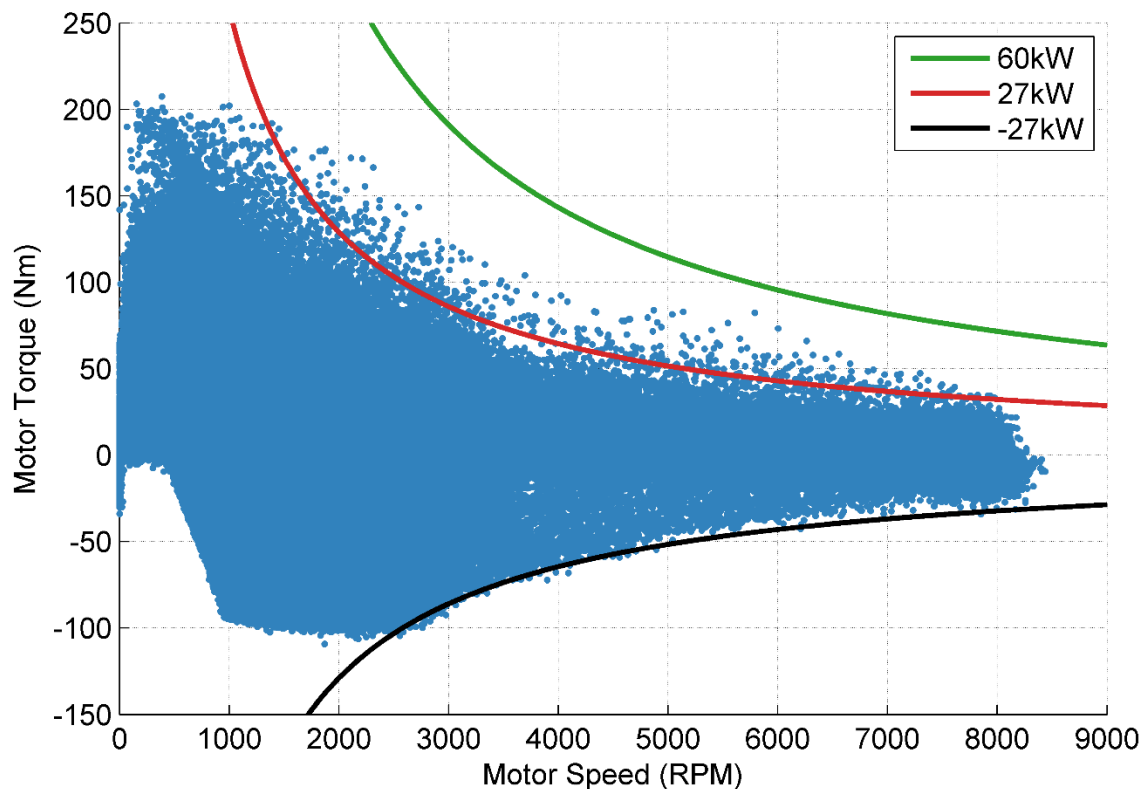


Figure 6.18: Prius motor operational area and power limit

The motor efficiency map could not be calculated using the test data because the mechanical and electric power on either side of the motor was not recorded. Burrett et al. 2011 presents the combined motor and inverter efficiency maps across the motor voltage range. These maps have been combined to produce a motor efficiency lookup table presented in Figure 6.18. The motor efficiency is used to convert the motor mechanical power to motor electrical power and vice versa, through a motor efficiency parameter, η_m .

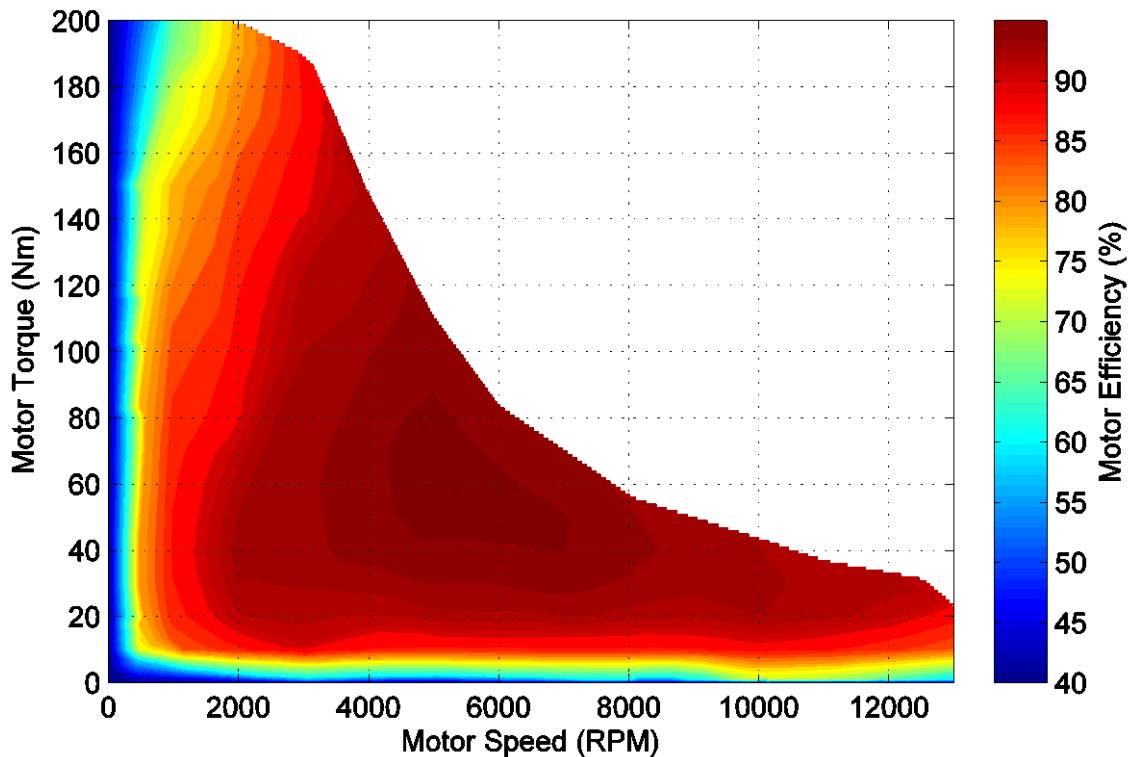


Figure 6.19: Prius Motor and inverter efficiency map. Adapted from (Burress et al., 2011)

The error in motor power has been split into two plots, the first for PE mode and the second for HE mode. In PE mode the error is computed over 250,000 points and in HE mode over 100,000 points. Overall the fit is reasonable good, the error in PE mode is lower which is to be expected as the calculations in PE mode are simpler and requires fewer assumptions. In both cases the negative error grows at low tractive power, this corresponds to the model estimating a more negative value than is seen in the test data. The reason for this is that the maximum power of the battery is 27 kW as the motor regen power nears this point, the motor regenerates less of the available power. This is not included in the model because the battery limit is included in the battery sub-model, not the motor sub-model.

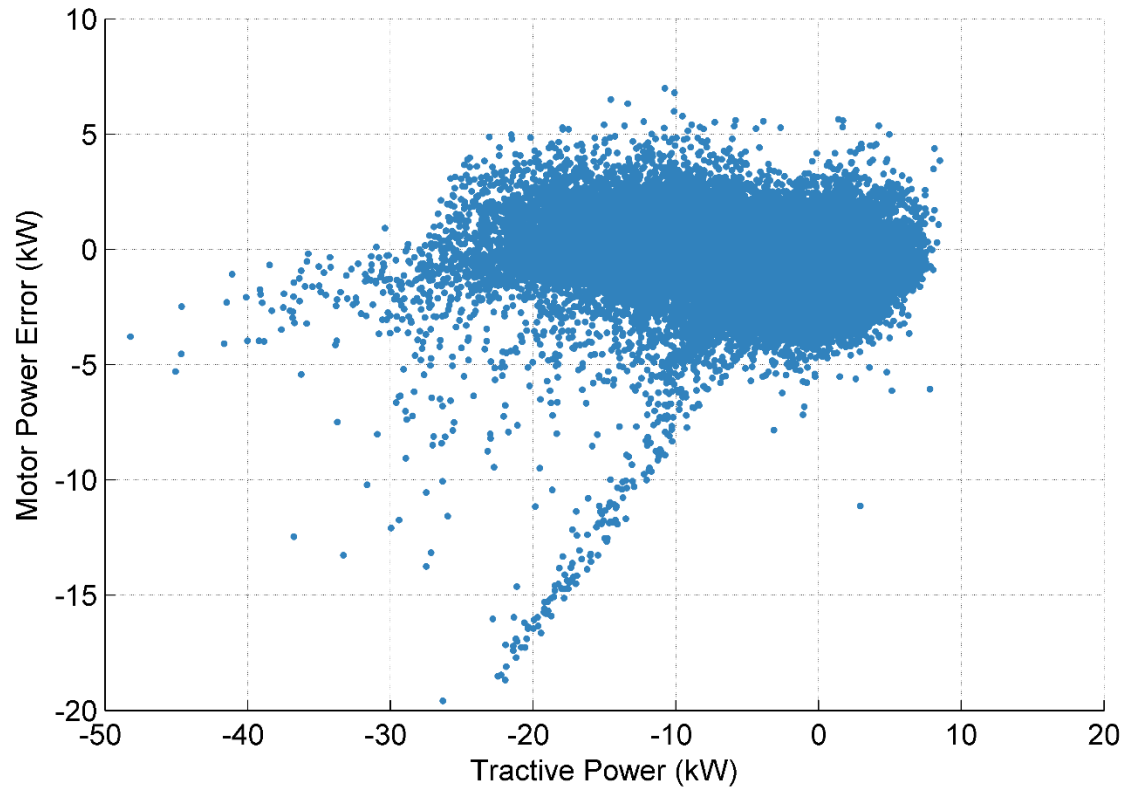


Figure 6.20: Motor power error against model input, tractive power, when the Prius is operating in pure electric mode

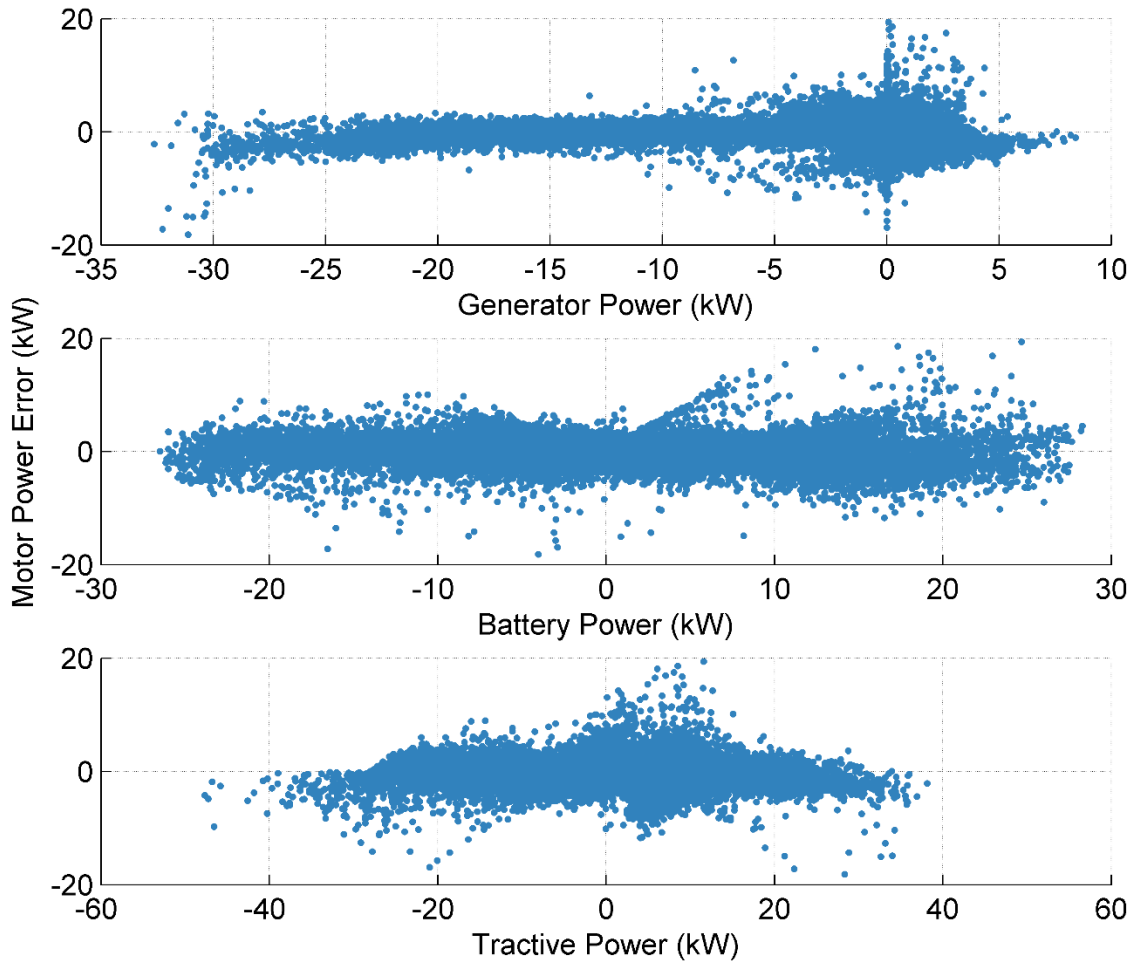


Figure 6.21: Motor power error against model inputs, generator, battery and tractive power, when the Prius is operating in hybrid electric mode

6.2.2.4 Generator and Inverter

Table 6.7: Generator model: inputs and outputs

	Parameter	Symbol	Value	Units
Inputs	Motor Speed	Ms	Changes	Radian/s
	Number of Teeth MSRG sun gear	Ns ₂	22	NA
	Number of Teeth MSRG ring gear	Nr ₂	58	NA
	Number of Teeth PG sun gear	Ns	30	NA
	Number of Teeth PG ring gear	Nr	78	NA
	Engine Speed	Es	Changes	Radian/s
	Engine Torque	Et	Changes	Nm
Outputs	Generator Speed	Gs	Changes	Radian/s
	Generator Torque	Gt	Changes	Nm
	Generator Power	Gp	Changes	W

The generator is connected through the planetary gear to the engine and the motor. The generator speed can, therefore, be calculated using Equation 6.12, which adjusts the motor speed and engine speed by the planetary gear ratios between the respective components.

$$G_s = \left(\left(M_s \times \frac{N_{s_2}}{N_{r_2}} \right) \times -\frac{N_r}{N_s} \right) + \left(\left(1 + \frac{N_r}{N_s} \right) \times E_s \right) \quad \text{Eq. 6.12}$$

When the engine is on, a fraction of the engine output torque drives the sun gear. This torque can be calculated using Equation 6.13, the ratios of the planetary gear in the third generation Prius mean that 27.78% of the engine torque goes to the sun gear.

$$Gt = -Et \times \frac{\frac{N_s}{N_r}}{1 + \frac{N_s}{N_r}} \times \eta_p \quad \text{Eq. 6.13}$$

When the generator is generating there is a power loss due to inefficiencies in the planetary gear, this is represented in Equation 6.13 as η_p . To simplify the model, the planetary gear efficiency and the generator power used to control engine speed are modelled as a single function. Figure 6.22 displays the relationship between the power at the sun gear and the generator power. The data in Figure 6.22 (blue dots) is split up into ten groups based on the rate of change in engine speed, measured as change in RPM per second. A straight-line function passing through zero (red lines) is fitted to each section of data.

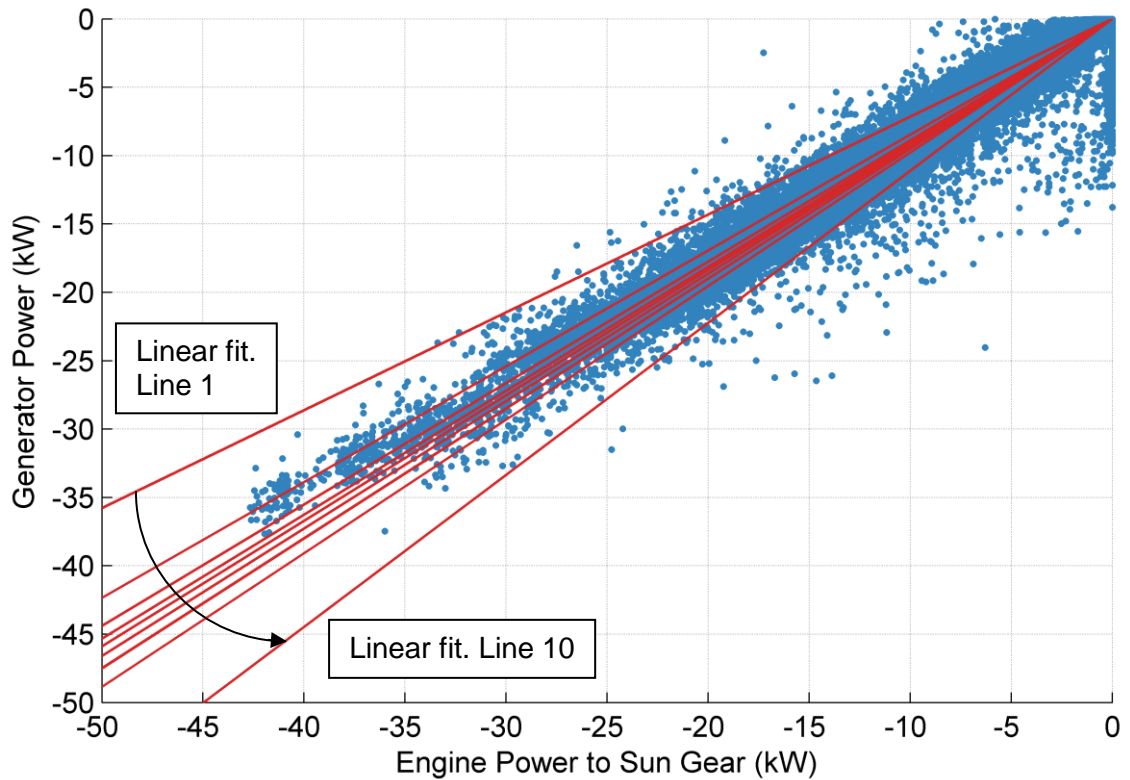


Figure 6.22: Sun gear power versus generator power with lines fitted at nine bands of rate of change of engine speed. Blue dots represent raw data. Red lines are linear best fit

Figure 6.23 shows how the gradient of each straight line is a function of the rate of change of engine speed. The relationship between sun gear power and generator power can thus be modelled by finding the gradient of the line from change in engine speed and Figure 6.23. This then provides an equation for a straight line passing through zero which converts sun gear power to generator power. The process of calculating generator power uses the full database filtered to remove sections of data where the generator acts as a motor and engine off data, this leaves 180,000 data points to build the model fit.

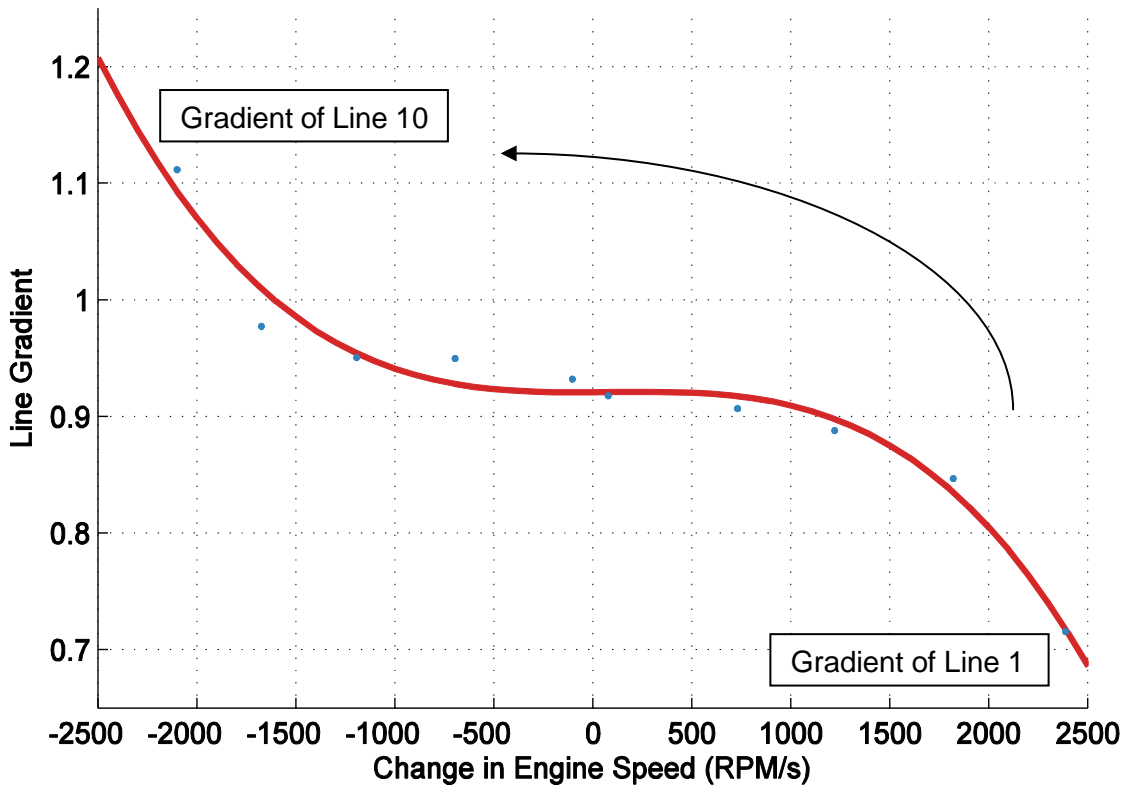


Figure 6.23: Gradient of lines fitted to generator power as a function of rate of change of engine speed. Blue dots represent raw data. Red line is a cubic curve best fit

When the generator is acting as a motor the vehicle speed is high and the engine speed is low. There is therefore very little fluctuation in engine speed while the generator is in this mode. This means there is no observable effect of change in engine speed on generator power in this mode so it is not included in the model.

Figure 6.24 presents all generator speed, torque data. The generator only appears to be limited by the maximum power limit of the device which is 43kW. As the test data never gets very close to this limit, no power limits for the generator were included in the model.

Figure 6.24 shows a lower torque limit of 41 Nm, but this only appears to be the case because the engine has a maximum torque limit of 144 Nm and the generator torque is only a function of engine torque.

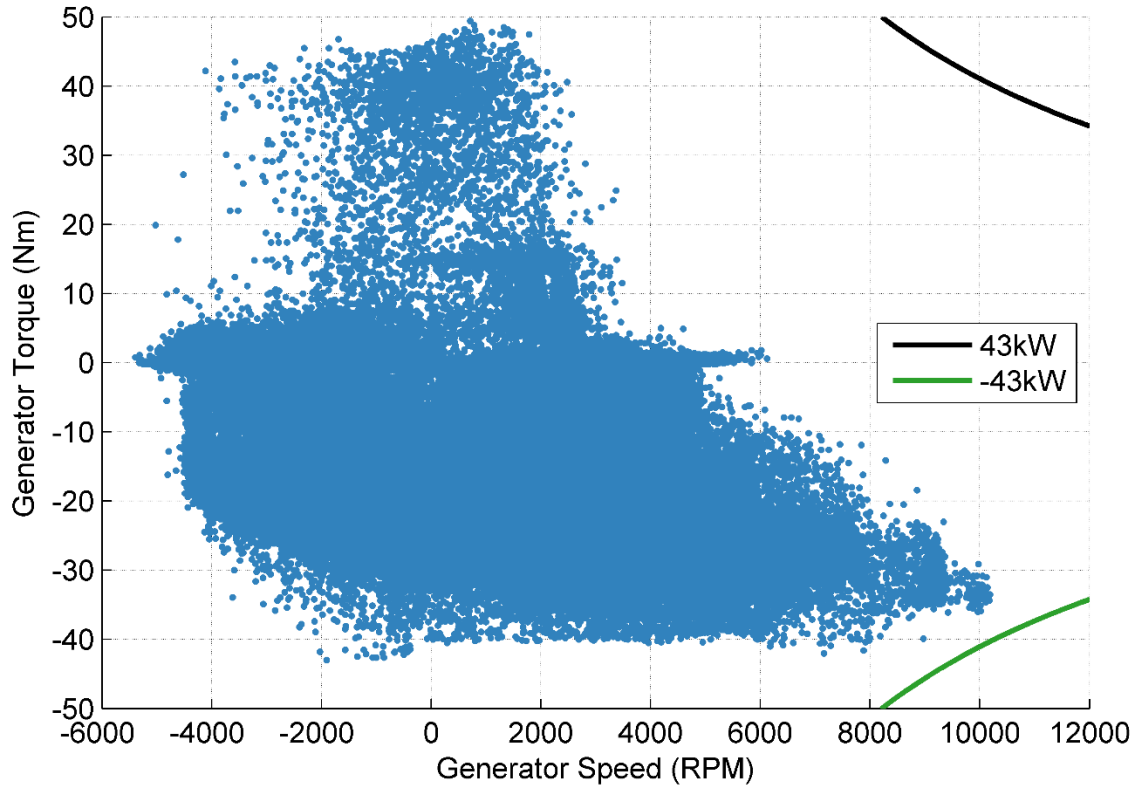


Figure 6.24: Prius generator operational area and power limit

As is the case for the motor, the generator efficiency map could not be calculated from the test data. Again data taken from Burress et al. 2011 has been used to create a combined generator inverter efficiency lookup table presented in Figure 6.25. The generator speed and torque are used to lookup the generator efficiency which is applied to the mechanical generator power to calculate the electrical generator power which is used to calculate power flows through the electrical power path.

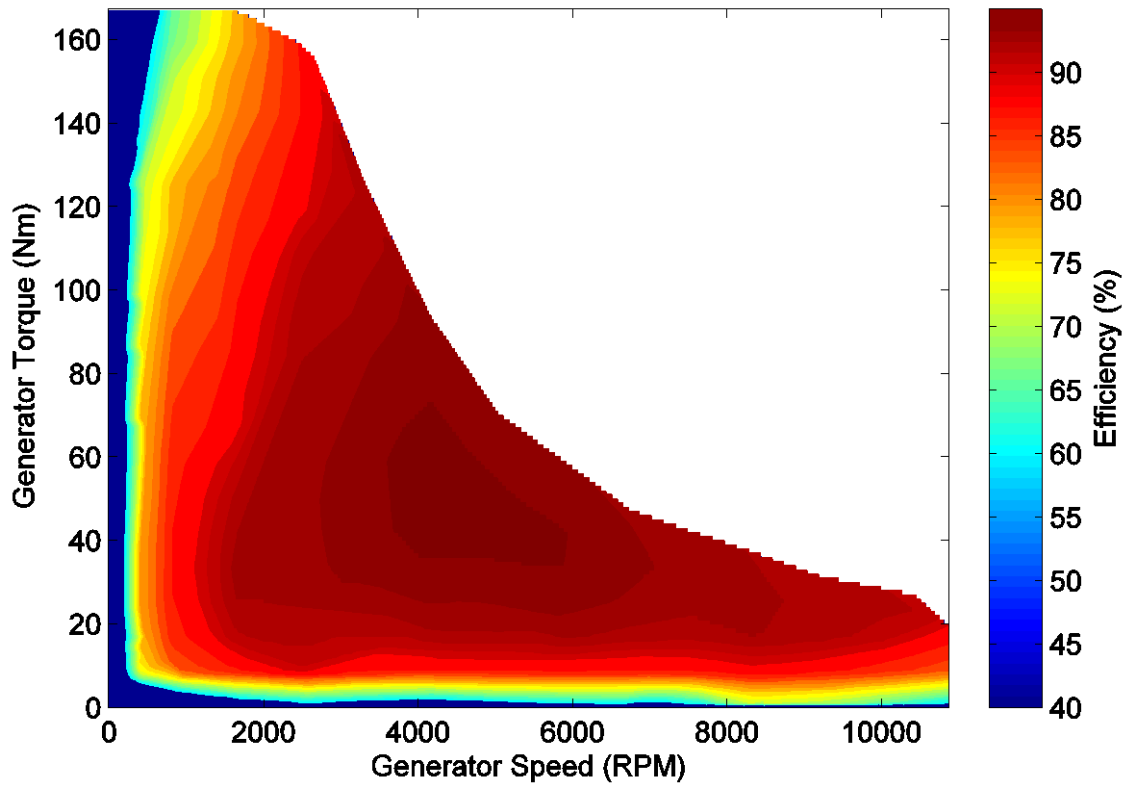


Figure 6.25: Prius generator and inverter efficiency map. Adapted from (Burruss et al., 2011)

Figure 6.26 shows the generator power error against the input parameters. The error is evenly distributed across the full range of sub-model inputs meaning the error is not caused by a problem with the modelling control.

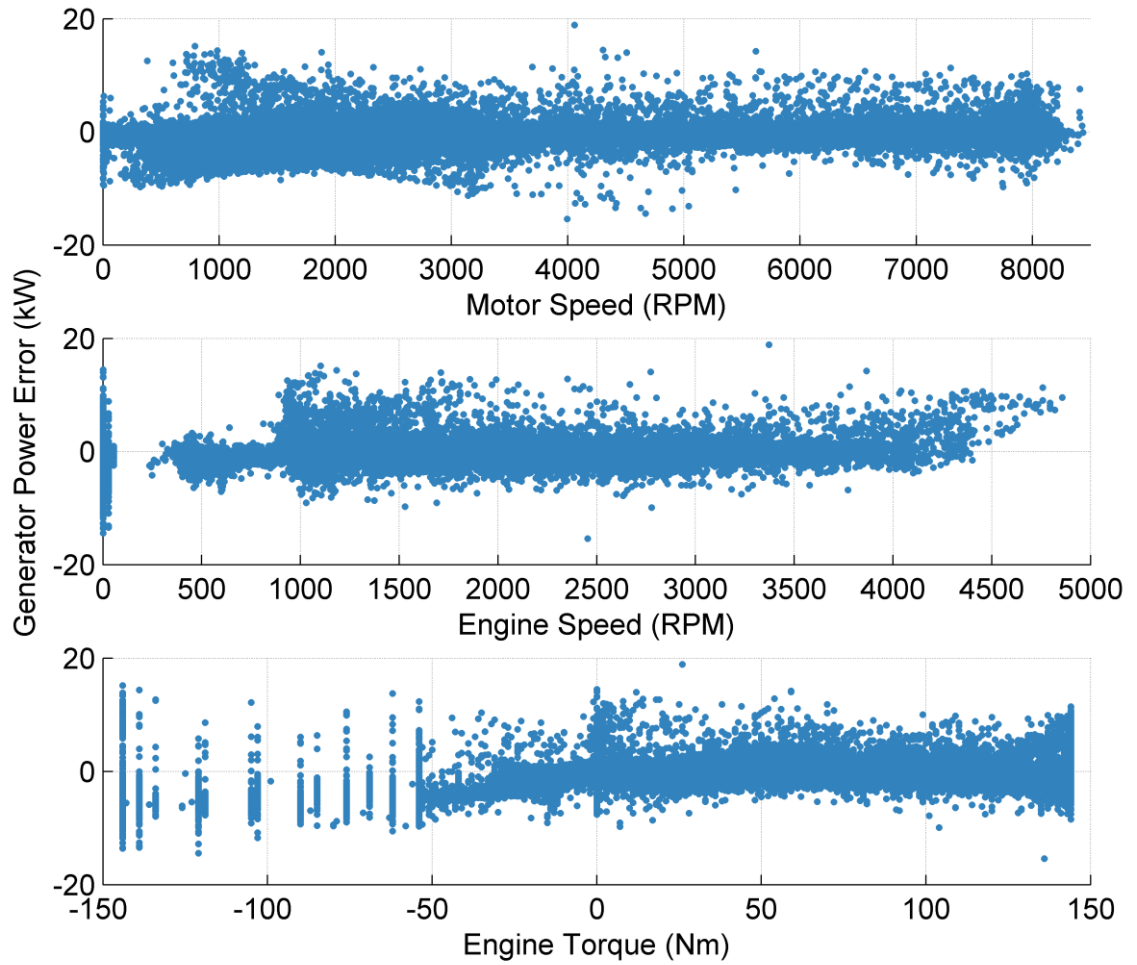


Figure 6.26: Generator model error, against model inputs, motor speed, engine speed and engine torque

6.2.2.5 Battery

The battery sub-model is made up of three sub-models, predicted battery power, actual battery power and battery SOC.

6.2.2.5.1 Predicted Battery Power Demand

Table 6.8: Predicted battery power sub-model: inputs and outputs

	Parameter	Symbol	Value	Units
Inputs	Battery SOC	SOC	Changes	%
	Catalyst Temperature	Tca	Changes	°C
	Engine Coolant Temperature	Tco	Changes	°C
	Battery Recharge Indicator	lb	0 or 1	NA
Outputs	Predicted Battery Power Demand	Bp _p	Changes	W

An estimate of battery power is only required when the engine is on. Under normal engine on operating conditions the base level battery power demand is a linear function of battery SOC, as shown in Figure 6.27. The figure is based on the full database filtered to remove engine off, cold start, battery recharge and transient data, this leaves 10,000 readings from which the model fit is created. From the red line fitted to the dataset the desired battery power is modelled.

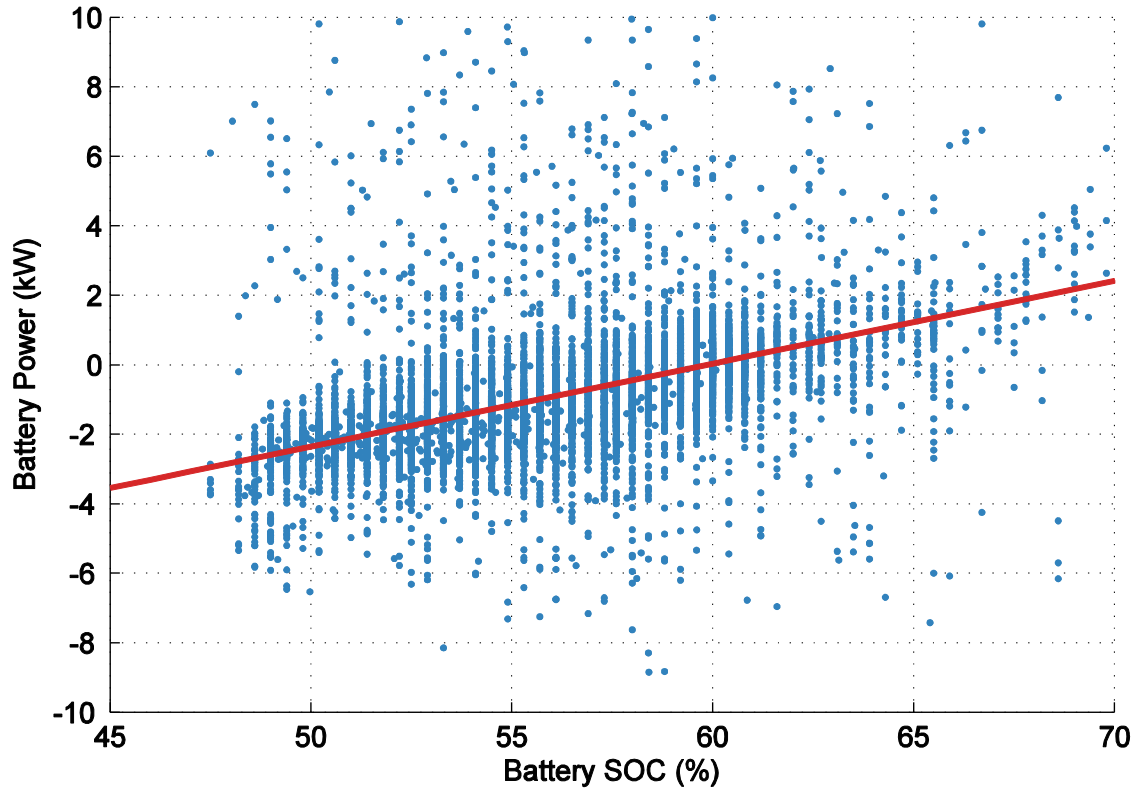


Figure 6.27: Battery SOC against battery power, under normal engine on conditions. Blue dots represent raw data. Red line is a linear best fit

6.2.2.5.2 Actual Battery Power Demand

Table 6.9: Battery power sub-model: inputs and outputs

	Parameter	Symbol	Value	Units
Inputs	Motor Power	M_p	Changes	W
	Motor Efficiency	η_m	Changes	NA
	Engine Predicted Power	E_{p_p}	Changes	W
	Engine Actual Power	E_p	Changes	W
Outputs	Battery Power	B_p	Changes	W

When the engine is off the battery power matches the motor power plus the efficiency losses in the motor. Equation 6.14 and 6.15 calculate the battery power during vehicle motoring and regenerating respectively.

$$Bp = Mp \div \eta_m \quad \text{Eq. 6.14}$$

$$Bp = Mp \times \eta_m \quad \text{Eq. 6.15}$$

When the engine is on, the battery power is calculated using Equation 6.16 or 6.17 depending on if the tractive power demand is positive or negative. When the tractive power is positive the battery power is calculated by taking the predicted battery power, based on battery SOC, and adding the difference between the estimated stable engine power and the actual transient engine power. What this means in practice is that if the engine power does not meet its target, or if it overshoots the target, the battery responds by either discharging or charging respectively to ensure the target power is met at the wheels.

$$Bp = (Ep_p - Ep) + Bp_p \quad \text{Eq. 6.16}$$

$$Bp = (Mp \times \eta_m) - Ep \quad \text{Eq. 6.17}$$

Throughout each run, there is also an observed background battery discharge power. This is a constant drain on the battery when the vehicle is stationary. This constant has a value of 0.2215 kW, which is the mean value across all the 200,000 engine off, stationary data points in the database. This parameter plays a key role in modelling urban runs especially taxi data where the vehicle is stationary for long periods of time.

Battery power is limited by the maximum rated power of the battery and during regeneration it is also limited at low vehicle speeds. Figure 6.28 shows the battery operating between the power limits of -27 and 27 kW. In the model this limit is added as a saturation to battery power before it is used to calculate battery SOC. Figure 6.3 shows the battery regeneration power from 10km/h down to vehicle stationary. At around 6 km/h the battery no longer regenerates any power from the vehicle slowing down and the

friction brake acts alone to stop the vehicle. This is done because there is very little power to be regenerated at low speeds, and the control required for a smooth vehicle stop using only the motor is very difficult to achieve.

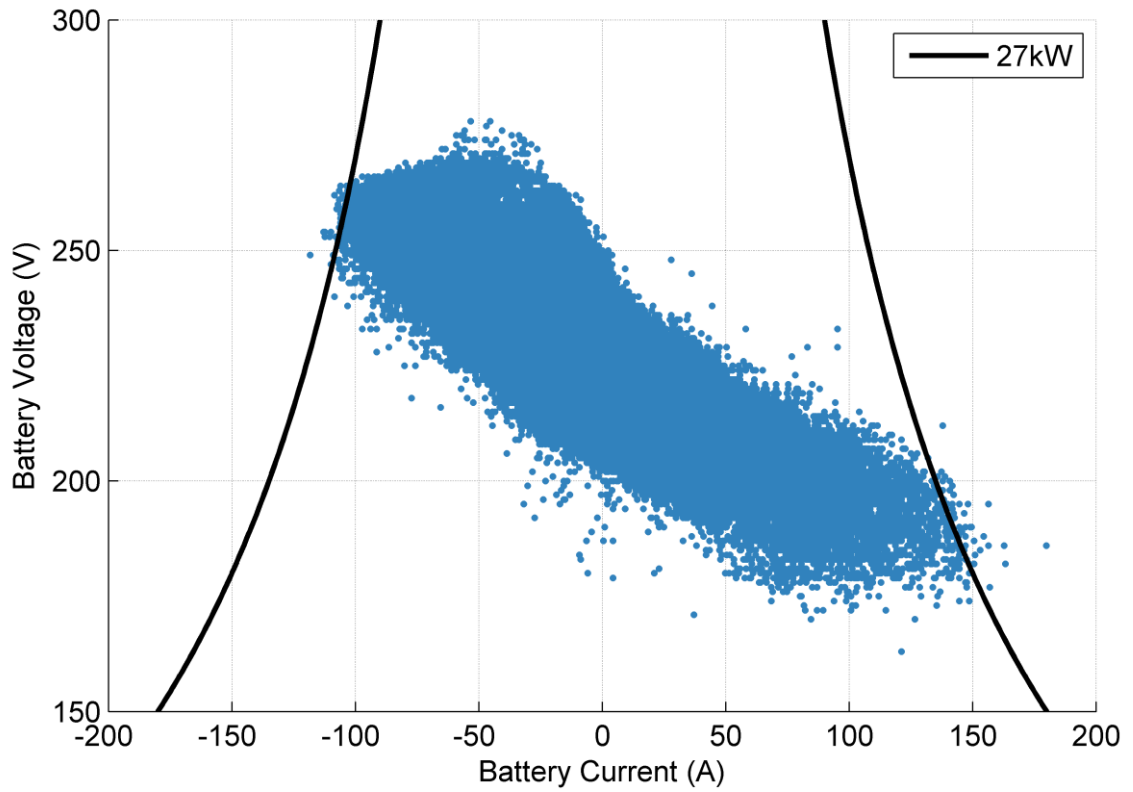


Figure 6.28: Prius battery operational area and power limit

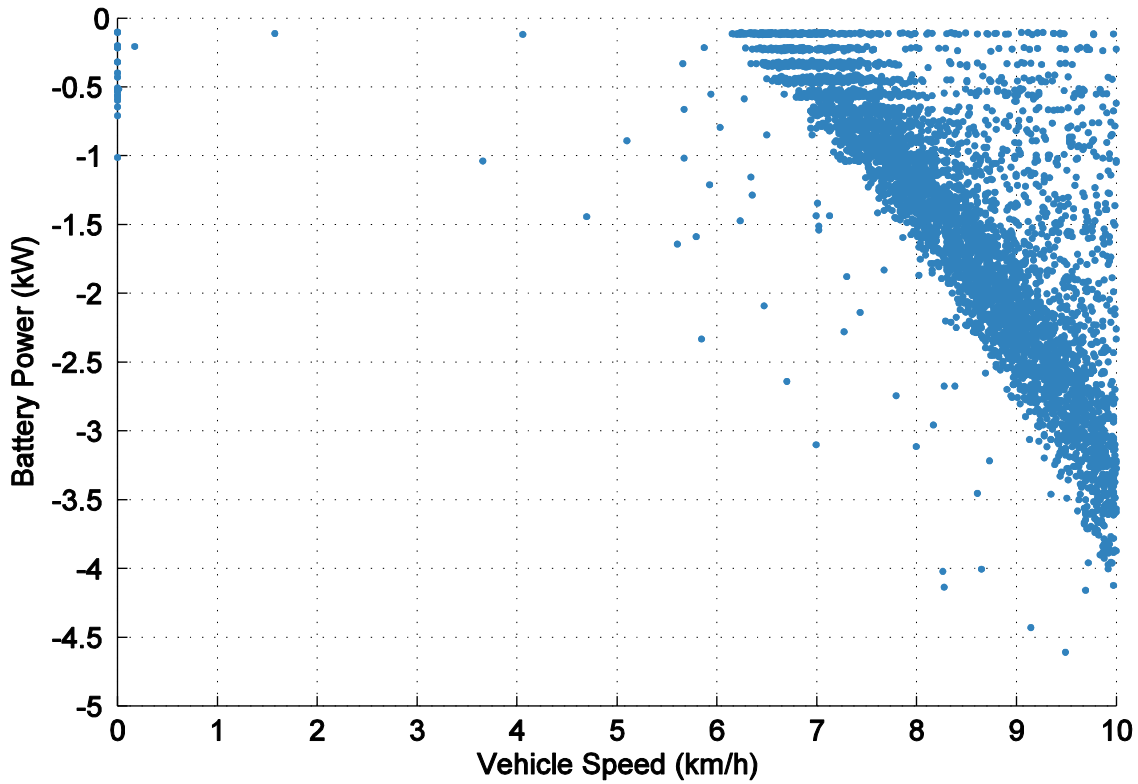


Figure 6.29: Vehicle speed against battery regeneration power

Figure 6.30 displays the error in modelled battery power over the tractive power database with 380,000 simulated points. Overall the fit is good but there is a slight negative trend in both plots that could indicate that one or several of the efficiency values in the model is not quite right. As the battery power depends on both the motor and engine powers which in turn are a function of battery SOC, it is difficult to pinpoint at which point in the loop the discrepancy in battery power occurs.

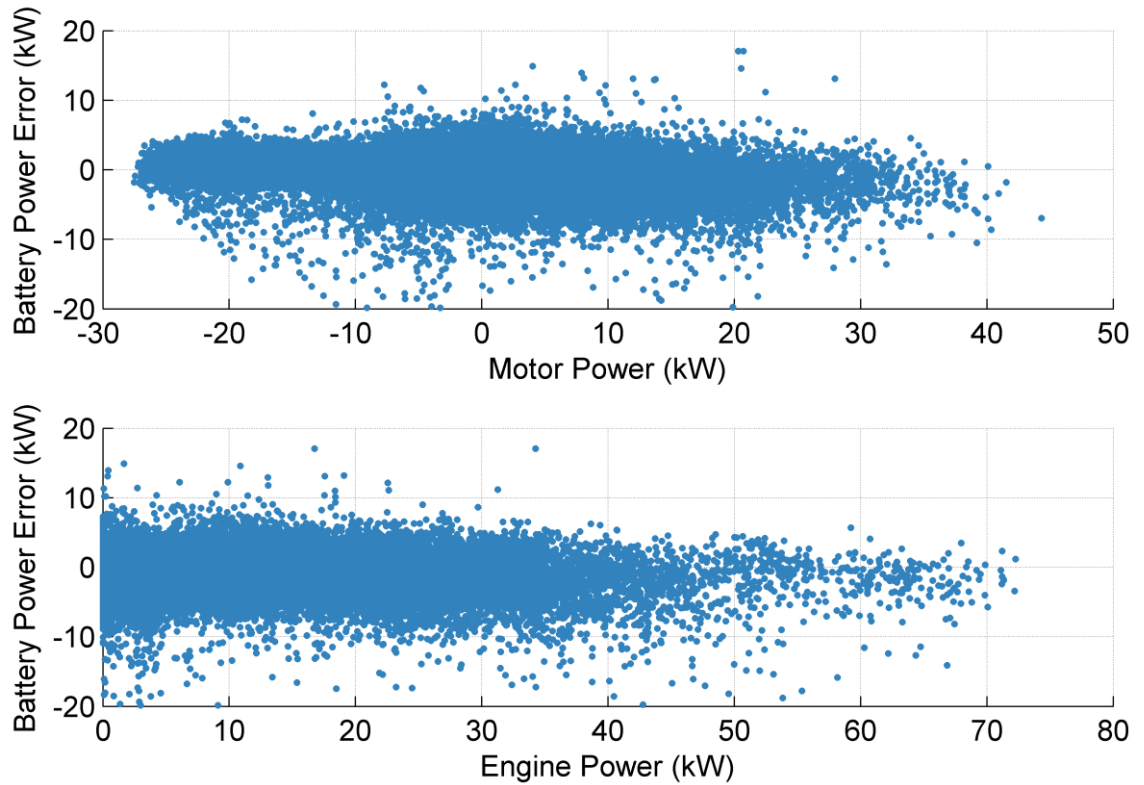


Figure 6.30: Battery power error against model inputs, motor and engine power

6.2.2.5.3 Battery SOC

Table 6.10: Battery SOC sub-model: inputs and outputs

	Parameter	Symbol	Value	Units
Inputs	Battery Power	Bp	Changes	kW
	Maximum Battery Energy	Be	4824000	J
Outputs	Battery SOC	SOC	Changes	%

Battery SOC is calculated using Equation 6.18, during battery discharge and 6.19, during battery charging. The equations calculate what percentage of the total battery energy is being transferred to or from the battery in each time step.

$$SOC = \int \frac{Bp}{Be} \times -100 \quad Eq. 6.18$$

$$SOC = \int \frac{Bp \times \eta_b}{Be} \times -100 \quad Eq. 6.19$$

The battery efficiency value η_b has been created by fitting the battery power data to the battery SOC across each run using Equation 6.18 and 6.19 and the MATLAB optimisation toolbox. Battery efficiency is commonly a function of charge and discharge rates, battery SOC and battery temperature (Dhameja, 2002). No correlation between charge and discharge rates and battery efficiency was found in the test data. Likewise, no broad correlation across the full range of battery SOC was observed, but it was discovered that battery efficiency drops rapidly at very lower battery SOC. No data on battery temperature was recorded so this parameter could not be included in the model but the work of Kim et al. 2015 shows that temperature has a strong effect on battery efficiency and this should be included in future work to improve the model (Namwook. Kim & Rousseau, 2015).

Two values of battery efficiency have been fitted one for battery SOC greater than 45%, and one for battery SOC less than 45%. The fit is based on the whole tractive power database, this provides over 370,000 data points for fitting battery efficiency when the SOC is greater than 45% and 8,000 points for SOC less than 45%. A pair of fitted efficiency values has been created for each of the 85 runs in the database. The fitted values for the data over 45% SOC, range from 0.89 to 0.97 with a mean of 0.9414. The fitted values for the data less than 45% SOC, range from 0.32 to 0.71 with a mean of 0.50.

Runs with data well above 45% SOC fit well, as shown in Figure 6.31 A. Runs where the data drops below 45% are harder to fit, because any error in the prediction of SOC before the SOC drops below 45% is magnified as the efficiency drops in the low SOC region. Figure 6.31 B illustrates a situation where the model matches the test data well as the

SOC drops below 45%, this leads to a reasonably good fit for the rest of the run. Figure 6.31 C, by comparison, shows a worst case scenario where the high error in modelling SOC before the test SOC drop below 45% means that the modelled SOC never drops into the low SOC zone and the gap between modelled and test SOC grows rapidly.

Battery SOC like engine coolant temperature is difficult to model because each value depends on the previous value, and so errors grow the longer the model runs. As a result of this, the sub-model error cannot be compared to the sub-model inputs to check for poor model fitting as has been done for the other sub-models.

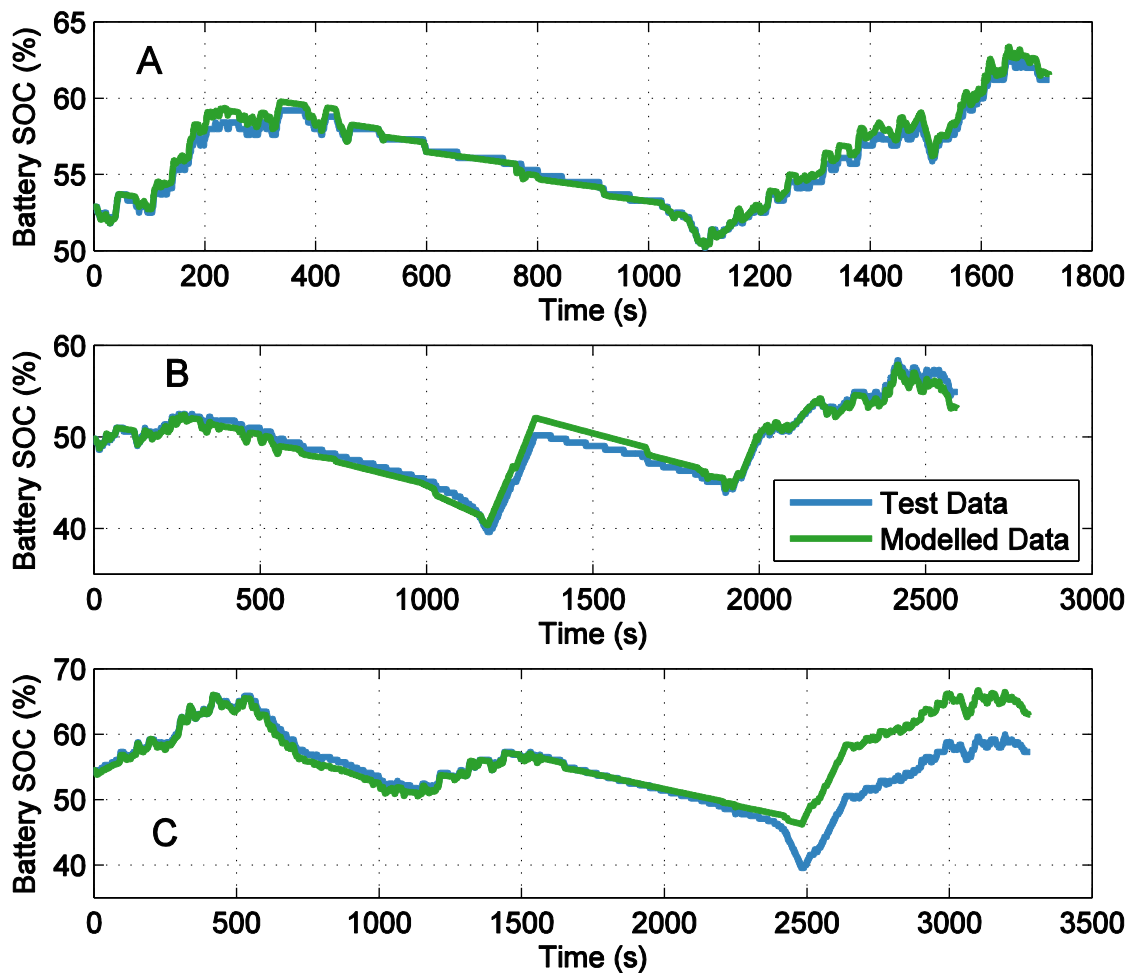


Figure 6.31: Battery SOC error, test versus modelled data

6.2.3 Additional Model Control Modes

The basic control of each component is described along with its function in the previous section. However, two situations, cold start and low battery SOC result in completely different powertrain controls.

6.2.3.1 Cold Start

Low coolant temperatures can only trigger an *engine on* at the beginning of a run, after the engine has been on once coolant temperature can affect the engine control but will not cause an *engine on* event. At the beginning of a run, the engine will turn on early if the coolant temperature is below 40°C. The dataset contains 23 cold *engine on* events when the cabin heating is off. The engine turns on between 11 and 15 seconds after the ignition is turned on, with most runs starting after 13 seconds. Once the engine has turned on in response to a cold start it will stay on until the vehicle power demand is below the *engine off* threshold and the coolant temperature reaches 40°C. If the engine turns on later in the cycle, due to tractive power demand, and the coolant temperature is below 40°C, the engine will remain on until this minimum temperature limit is reached.

Cold starts can be broken down into the catalyst warm up and the coolant warm-up phases. The catalyst warm-up phase starts as soon as the engine turns on and continues until the catalyst temperature reaches 200-220 °C. Modelling catalyst temperature for the whole run requires unnecessary extra computing so the catalyst warm-up phase is run for a set period of time. In the test data, the catalyst warm-up phase lasts for between 53 and 63 seconds with most runs having a catalyst warm-up phase of 58 seconds. During catalyst warm up the engine power only matches the battery power demand, the engine speed is defined by the coolant temperature and the engine torque can be calculated from engine power and speed. With low engine power and relatively high engine speed the catalyst warm-up phase is characterised by very low engine torque. During catalyst warm up the efficiency losses through the electric path η_a appears to remain relatively constant at 0.8

During the coolant warm up phase the engine power is calculated in the same way as under normal operating conditions using Equation 6.4. However, for the periods of the cold start where the vehicle is stationary and the engine only meets the battery power demands the efficiency losses η_a drop to match the values seen in catalyst warm up. Engine speed and torque are also calculated in the same way as under normal operating conditions but the minimum engine speed is elevated as shown in Figure 6.13.

The cold start also affects the predicted battery power. Figure 6.32 and 6.33 display the battery power against battery SOC for low catalyst temperatures and low engine coolant temperatures respectively. The battery power demand for catalyst warm-up is very low, this combined with the engine not tracking vehicle power demand ensures that the engine load is low and the engine out emissions are minimised. In each case the data has been filtered to select only cold start data when the vehicle is stationary, this leaves 1,500, 1,650 readings for each plot, from which the model fit is created. Cold coolant temperatures also affect the engine fuel consumption but this is already considered in the original fuel consumption model.

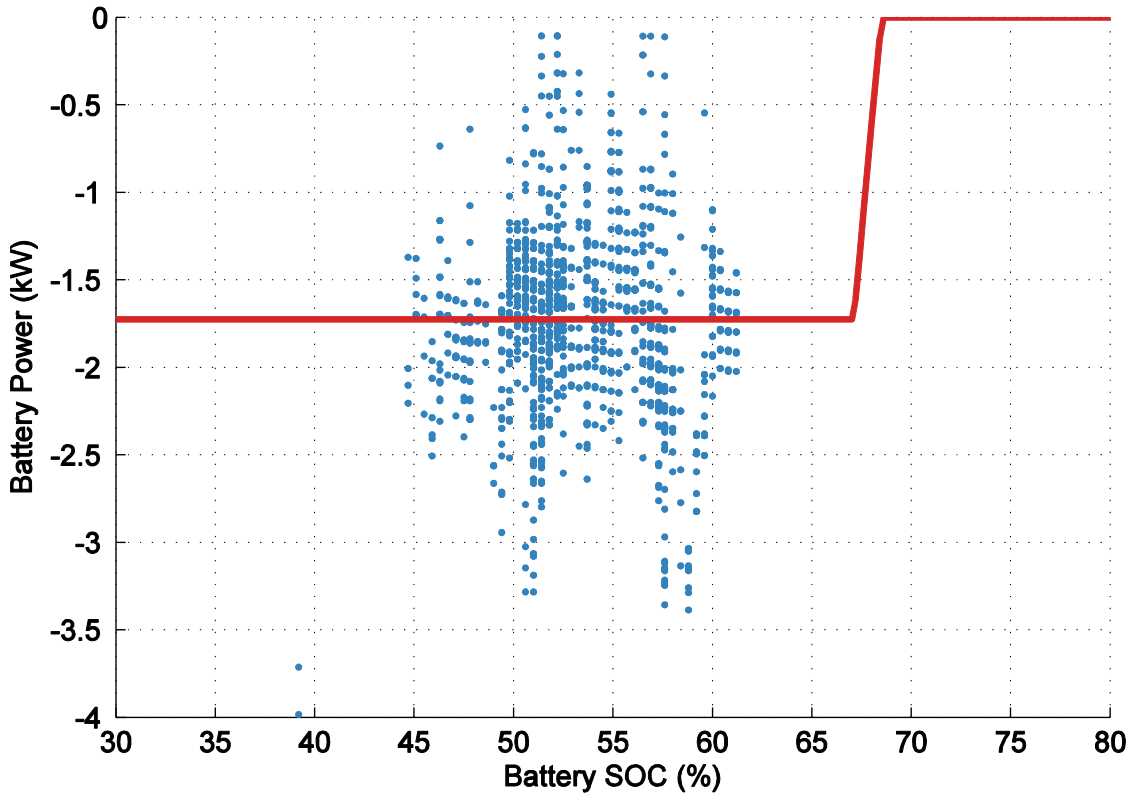


Figure 6.32: Battery power demand as a function of battery SOC at low catalyst temperatures. Blue dots represent raw data. Red line is a linear best fit over the battery SOC range from 30-65%. The range from 65-80% is assumed based on the finding in Figure 6.33

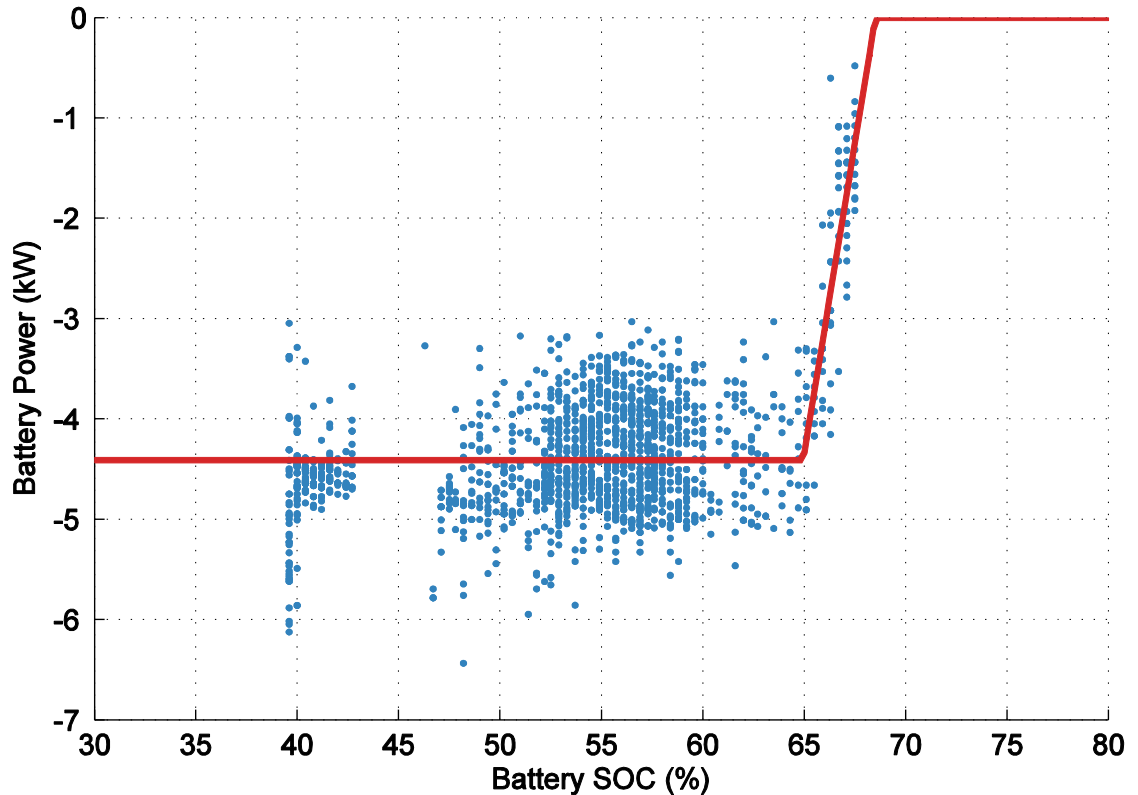


Figure 6.33: Battery power demand as a function of battery SOC at low coolant temperatures. Blue dots represent raw data. Red line is a linear best fit fitted over three battery SOC ranges (30-65%, 65-68%, 68-80%)

6.2.3.2 Low Battery SOC

The battery SOC lower limit is 40%, if the SOC drops below this limit the engine will turn on and stay on until the battery SOC has reached 50%. During battery recharge, the engine power is calculated in the same way as under normal operating conditions, as are the engine speed and torque. As is the case for cold starts when the vehicle is stationary the efficiency losses η_a remain relatively constant at 0.8.

Like cold start control, low battery SOC control also has a different predicted battery power demand. Figure 6.34 presents the battery power demand during battery recharge for a filtered database that only includes data for recharging event while the vehicle was stationary, this left 4,000 data points to create the model fit.

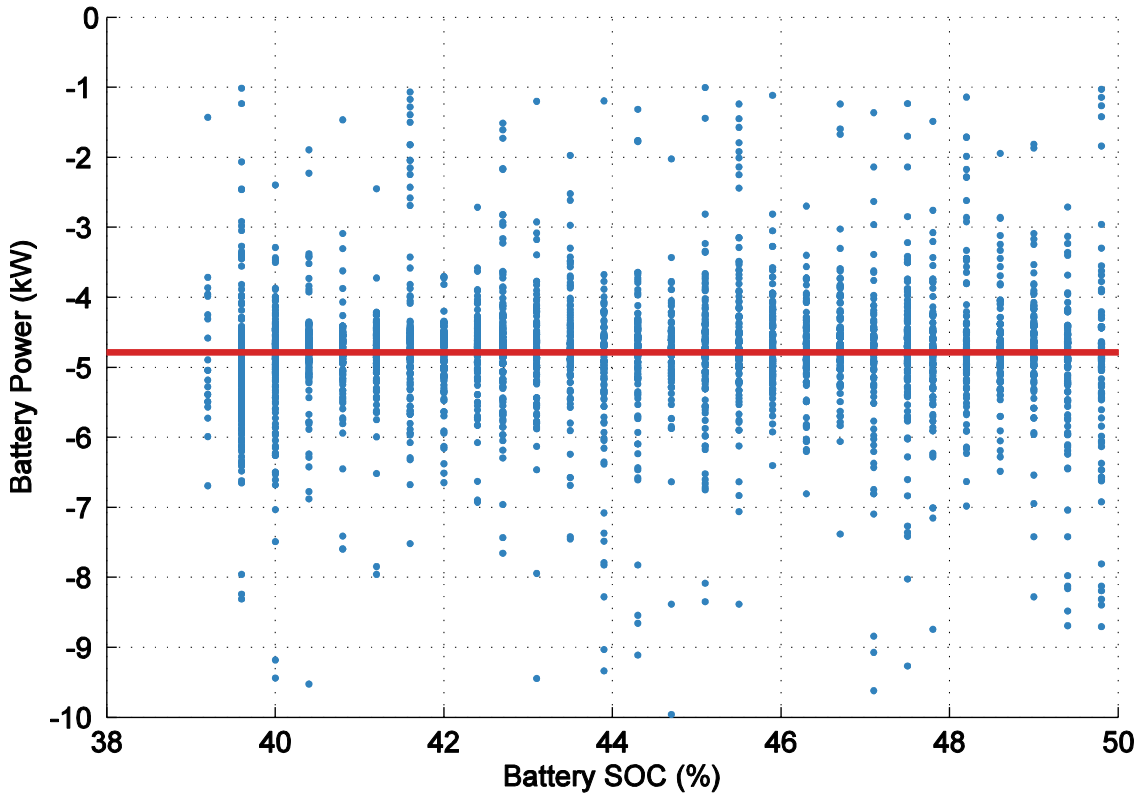


Figure 6.34: Battery power demand as a function of battery SOC during a low battery SOC event. Blue dots represent raw data. Red line is a linear best fit

6.3 Model Validation

6.3.1 Validation Database

Argonne National Laboratory has conducted extensive testing of the Toyota Prius as part of a larger project, across several national laboratories, aimed at better understanding the current best alternative vehicle technologies on the road (Burress et al., 2011; Rask et al., 2010). The testing included chassis dynamometer testing of the Prius over five cycles, shown in Figure 6.35, these were the HWFET, UDDS with hot start, UDDS cold start, US06 and a steady state speed test. These cycles comprise a wide range of testing conditions, including urban, motorway, and aggressive driving. Thirteen parameters were collected during the tests at 10Hz, these are presented in Table 6.11 (Argonne National Laboratory, 2015).

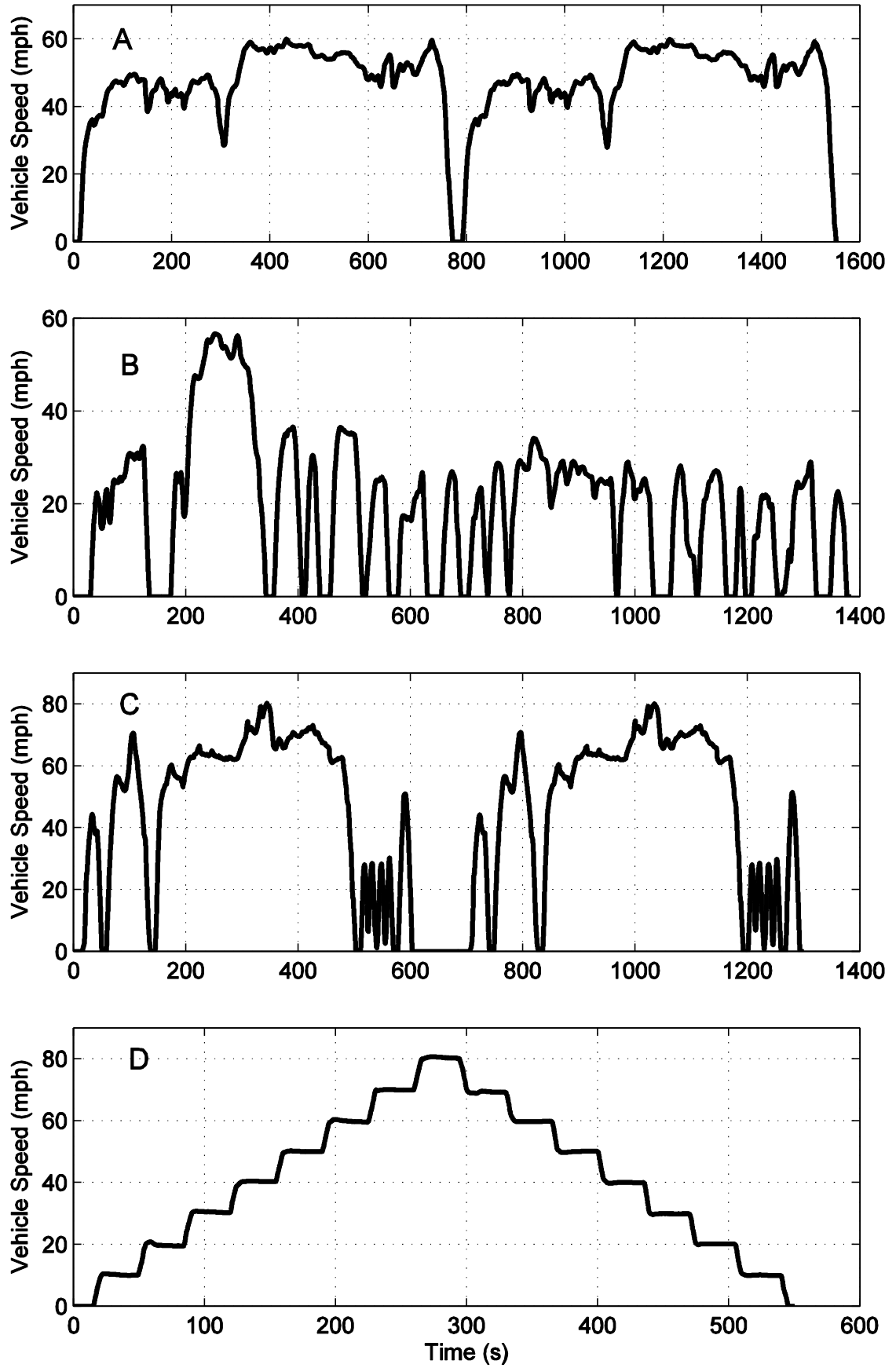


Figure 6.35: Validation drive cycles. A, HWFET. B, UDDS. C, US06. D, Steady State

Table 6.11: Validation database, parameters collected

Parameter	Units
Time	s
Vehicle Speed	mph
Dynamometer Tractive Effort	N
Cell Temperature	°C
Cell Relative Humidity	%
Phase	#
Engine Speed	RPM
High Voltage Battery Voltage	V
High Voltage Battery Current	A
Engine Coolant Temperature	°C
Engine Oil Temperature	°C
Battery SOC	%
Fuel Flow	cc/s

During the testing, each cycle except the steady speed test was conducted twice, this gives a combined test time of 1 hour, 43 minutes and a total distance of 93 km. Figure 6.36 presents the vehicle speed and acceleration distribution of the entire validation dataset. Overall the distribution of the data is very similar to the data collected during this project. The only slight differences between the datasets are the validation dataset includes slightly higher speeds and lower accelerations than those recorded on the road.

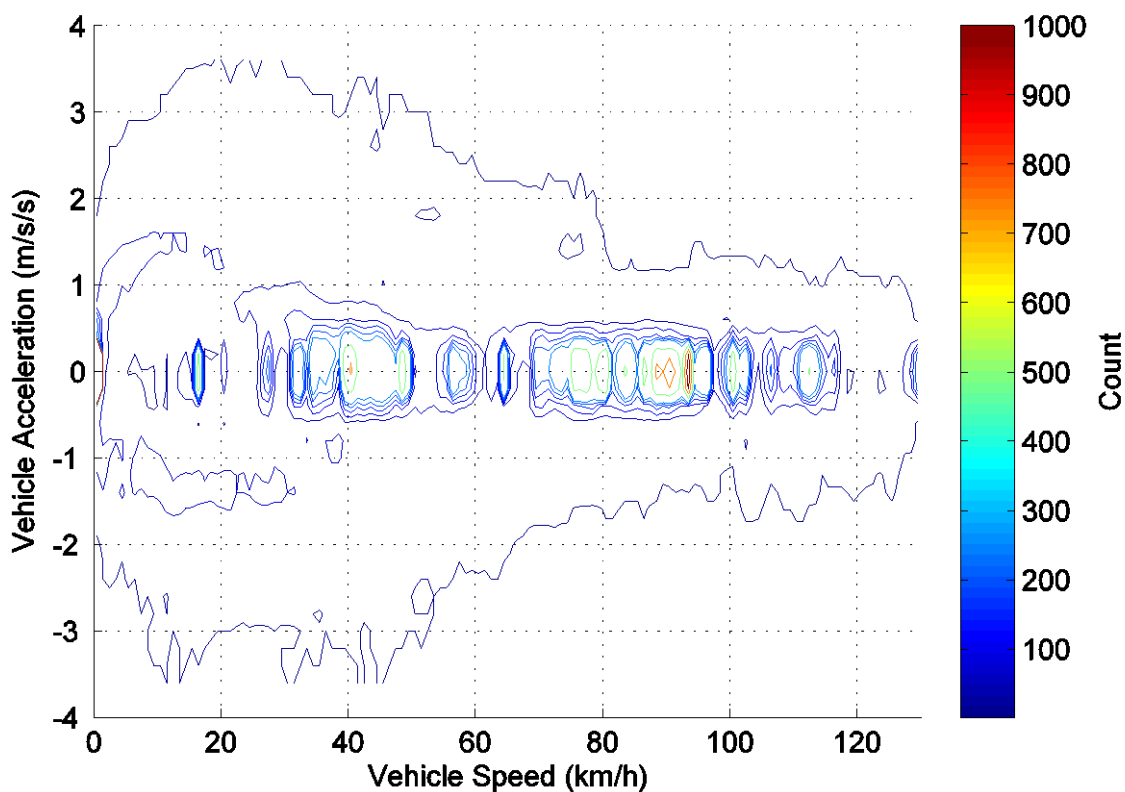


Figure 6.36: Vehicle speed and acceleration distribution for the validation database

During validation testing the tractive power demand was calculated directly from the vehicle speed and dynamometer tractive effort, as the method for calculating tractive power given in Equation 6.1 consistently predicted higher power demands than the dynamometer was forcing the car to meet. This is likely because different resistance coefficients have been used in the two cases.

Table 6.12 presents the error in modelling fuel consumption over each validation cycle. All the cycles meet the project initial aim of creating a model that can predict fuel consumption with a total error of less than 5%. The mean bias for the two UDDS cycles is very low, this shows that the error in the cycle is very well balanced above and below the test fuel consumption, this is reflected in the low total error for these two cycles. The other three cycles, which include more high speed and high speed, high acceleration data have a higher negative mean bias, indicating that the model is consistently under predicting fuel consumption under these conditions. This is unsurprising as the dataset

on which the model is based includes less high speed driving because the DSM used to calculate road gradient included few sections of motorway. Also, the US06 and steady state cycle include sections of acceleration from 113 to 129 km/h (70 to 80 mph), as the speed limit in the UK is 113 km/h (70 mph) no test data has been collected for these conditions.

The root mean square error is lowest for the least transient cycles. The steady state cycle and HWFET are the easiest cycles to follow with less *engine on/off* events and fewer sudden spikes in fuel consumption. The steady state figure is slightly distorted by a few points with a large error during peak fuel consumption. The two UDDS cycles have a slightly higher root mean squared error due to a couple of incorrect *engine on/off* events, while the US06 cycle has the highest root mean squared error, with very good *engine on/off* timing this error is all due to the model struggling to follow the very high speed, high transient cycle. The correlation for the three faster cycles, HWFET, US06 and steady state is good, the correlation for the city cycles, UDDS hot and cold is significantly lower due to *engine on/off* miss timing. Overall when the complexity of the Prius control and the difference in the vehicle testing methods are taken into consideration the model built from real world data does a good job of predicting fuel consumption over most of the conditions likely to be experienced on UK roads.

Table 6.12: Error in modelled fuel consumption over five validation cycles

Model Fit Statistics	HWFET	UDDS Hot	UDDS Cold	US06	Steady State
Total Fuel, Test Data (l)	1.13	0.372	0.447	1.36	0.363
Total Fuel, Model Data (l)	1.10	0.377	0.454	1.32	0.345
Total Fuel, Percentage Difference (%)	-2.60	1.26	1.71	-3.05	-4.71
Mean Engine On Fuel Cons (ml/s)	0.858	1.14	1.18	1.65	1.26
Mean Bias (ml/s)	-0.0188	0.00340	0.00552	-0.0319	-0.0310
Root Mean Squared Error (ml/s)	0.160	0.176	0.256	0.352	0.189
Spearman Correlation Coefficient	0.943	0.725	0.772	0.942	0.929

Figure 6.37, 6.38, 6.39, 6.40 and 6.41 show a time series comparison between chassis dynamometer and model results, for the four parameters that the two databases have in common; these are, fuel consumption, engine speed, battery SOC and engine coolant temperature.

The first cycle used in validation is HWFET, over this cycle the model slightly under predicts fuel consumption, by 2.6%, although the fuel consumption fit across the whole cycle is very good. There are seven instances, totalling 19 seconds, across the cycle

where the test or model engine speed drops to zero, while the other signal stays on, this is as a result of the difficulty in setting the *engine on/off* threshold during model creation. Overall 17 seconds of the additional *engine off* was the model turning the *engine off* when the test engine stayed on, this will have contributed to the lower modelled fuel consumption over the cycle. The battery SOC is slightly under predicted, early on in the cycle, because the model engine turned off a couple of times when the real engine stayed on. However, the model does a good job of balancing the SOC and by the middle of the cycle the SOC fit is very good. The maximum engine coolant temperature recorded in this project was 91°C, whereas the validation data often exceeds this. This is probably because Argonne National Laboratory has added a thermocouple to their test vehicle to record coolant temperature and it is in a different location to the thermocouple used by the vehicle, and recorded on CAN. The model coolant temperature is therefore limited to a maximum of 91°C which is why the model does not track the highest validation data coolant temperatures.

The second cycle used in validation is UDDS with hot start. During the first validation data *engine on* the model struggles to get the *engine on/off* controls correct. It is not understood why the validation data engine stays on between 33 and 138 seconds, as the tractive power demand during this period regularly drops well below zero. Kim et al. 2012 predicted Prius engine speed over the UDDS cycle using the Autonomie model and their results show the same *engine off* pattern at the beginning of the cycle as seen in the model presented here (Namwook Kim et al., 2012). The error in the initial *engine on*, results in an early drop in model SOC, but again the model balances SOC well and the fit improves as the cycle continues. Due to the additional *engine off* the model has to make up around 5% SOC across the cycle, this has a knock on effect on engine power, and therefore fuel consumption, as the lower SOC increases battery power demand on the engine. This increase in fuel consumption when the engine is on will balance some of the reduced fuel consumption from when the model engine turned off, early in the cycle. The model prediction of engine coolant temperature is inaccurate at the beginning

of the cycle due to the *engine off* error, but through the rest of the cycle the model fit is reasonably good.

The third cycle used in validation is UDDS with cold start. This is the hardest of the cycles to model because of the complexity of cold start control. The model turns the engine on slightly late during the cold start, but no reasons were discovered for the changes in cold start *engine on* time in the PAMS data, and it is expected that if the validation test were run again the *engine on* time would change slightly either side of the model *engine on* time. During the fourth and fifth *engine on* between 400 and 500 seconds, the model engine turns off early. In these two cases, the model follows the same pattern as seen in the hot cycle which is expected because the SOC is very similar in the two cases. However, even though by this point in the cycle the engine is hot and the SOC is high the validation engine still stays on slightly longer, the reasons for this are not well understood. The validation fuel consumption has a very large peak at cold *engine on*, this is not seen in the PAMS test data and is therefore not included in the model. The validation engine also keeps a relatively constant engine power throughout cold start, whereas, the model engine matches vehicle power demand as soon as the catalyst warm up is finished.

The model gives a good prediction of battery SOC across the cycle, considering the battery will be cold at the beginning of the cycle and battery temperature was not corrected for in the model. The model struggles to predict engine coolant temperature, but during the cold start both the validation and model engines turn off at the same time, even though the validation coolant temperature is slightly higher. This again could indicate that the validation dataset is monitoring coolant temperature at a hotter point in the cooling circuit. The difference in coolant temperatures grows during the early cycle, this suggests that the model is under predicting the rate of increase of coolant temperature when the engine is on. This will have a knock on effect on engine fuel

consumption as the engine is less efficient at lower temperatures. This could be one reason why the model over predicts fuel consumption across the cycle.

The fourth cycle used in validation is the US06. This is a challenging cycle to model because of its high speeds and aggressive driving style. The overall fit is very good with all *engine on* and *offs* matching the validation data well. At the highest peaks in engine power the model slightly under predicts fuel consumption, and the battery SOC prediction across the cycle is too high. These effects combined, result in the cumulative model fuel consumption being lower than validation data across the cycle. The SOC prediction over this cycle is worse than over the other four cycles. This could be caused by the model regenerating too much power during the rapid vehicle decelerations from high speeds or by aggressive use of the battery resulting in high battery temperatures which limit maximum battery charging and discharging or battery efficiency could change at very high battery SOC. In any case, the data on which the model was created does not contain very high speed decelerations, data on battery temperature or sufficient SOC data above 75% to identify which of these areas could be causing the SOC over prediction.

The fifth cycle is a steady speed cycle that steps up speeds in 16 km/h (10 mph) increments, up to 129 km/h (80 mph), cruising at each speed for a short time before stepping back down to stationary. The model *engine on/off* match the test data very well. The model under predicts fuel consumption because the model fuel consumption at the highest engine powers is significantly below the validation test data. This error in the model is caused by a lack of very high engine power events in the database used to build the model. This shortfall of the model is not considered a major problem as it is very unlikely that the model will ever be used to predict fuel consumption for high speed accelerations over the UK maximum speed limit. The prediction of battery SOC is very good. As with all high demand, hot start cycles the prediction of engine coolant temperature is good, but as the coolant temperature does not affect control under these conditions it is not a very important parameter for these cycles.

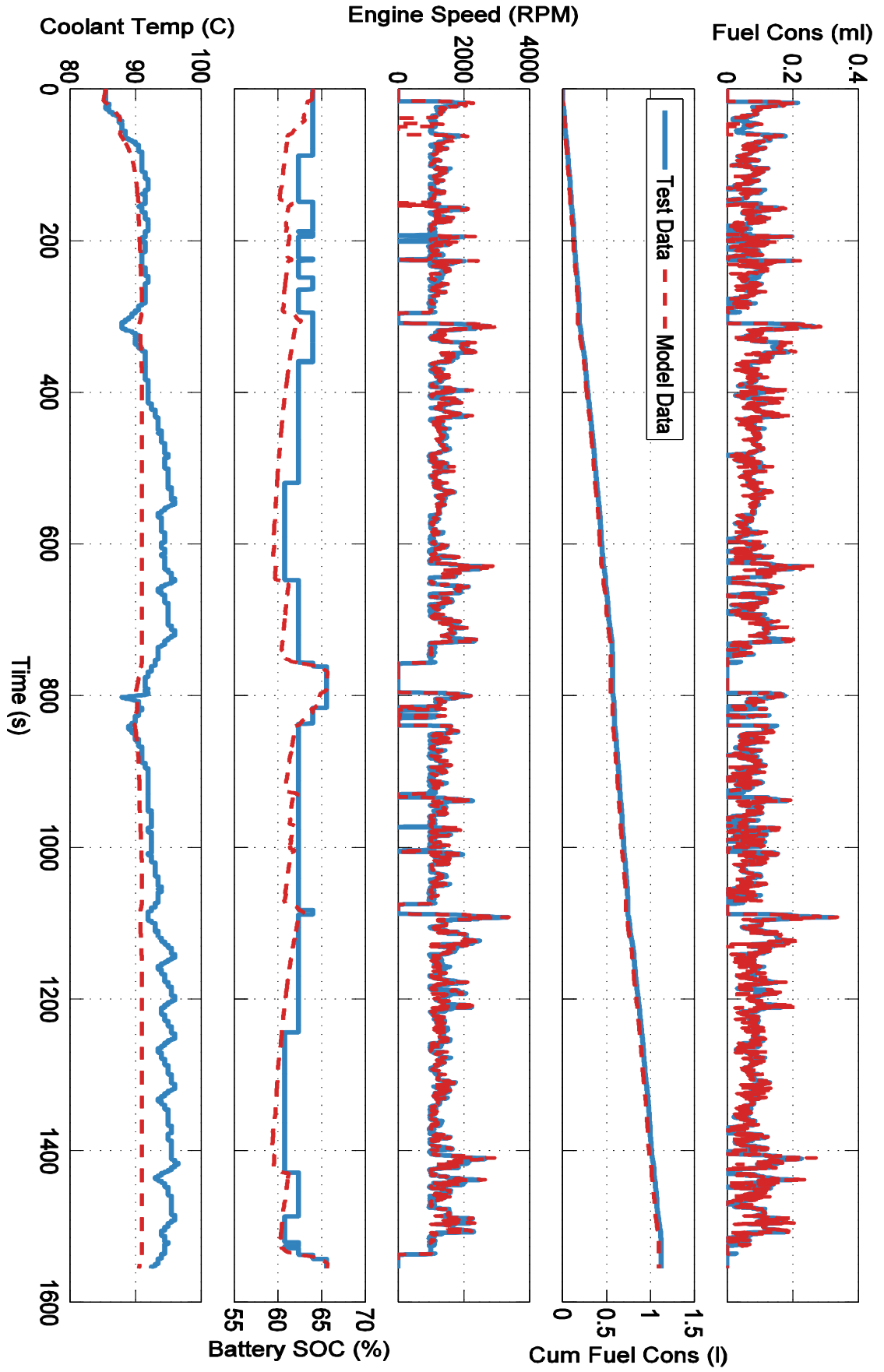


Figure 6.37: Model validated against HWFET cycle

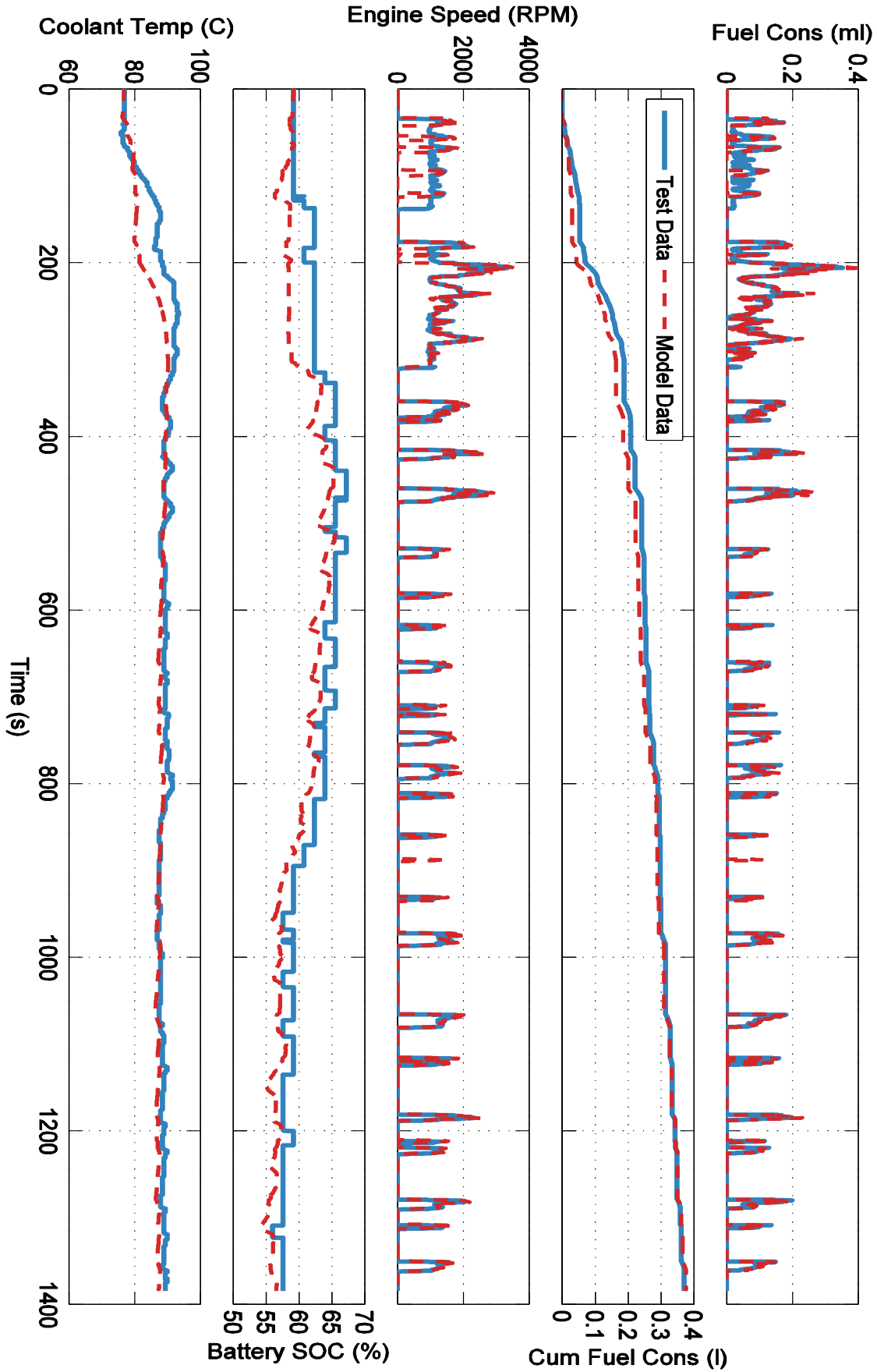


Figure 6.38: Model validated against UDDS cycle with hot start

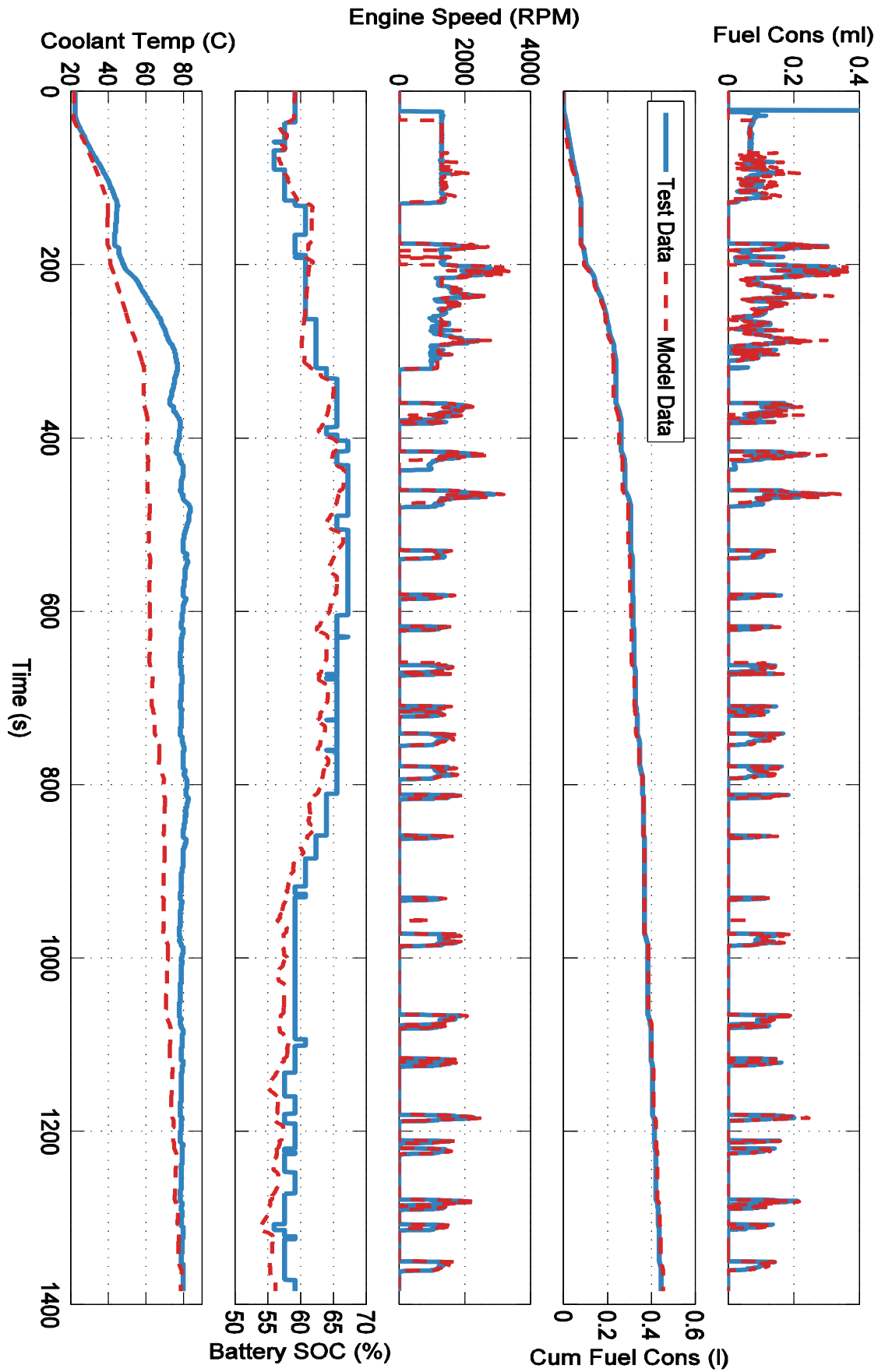


Figure 6.39: Model validated against UDDS cycle with cold start

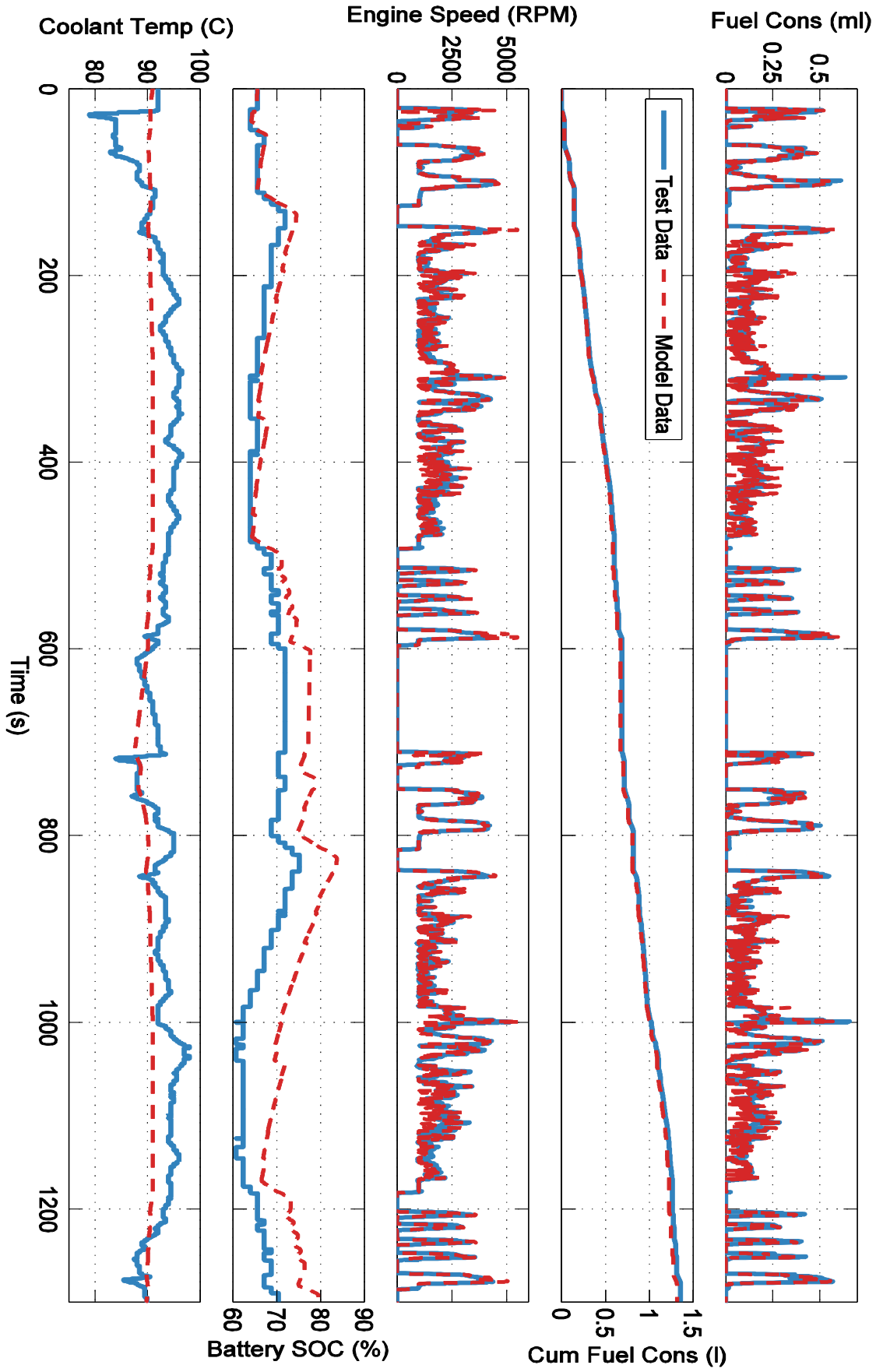


Figure 6.40: Model validated against US06 cycle

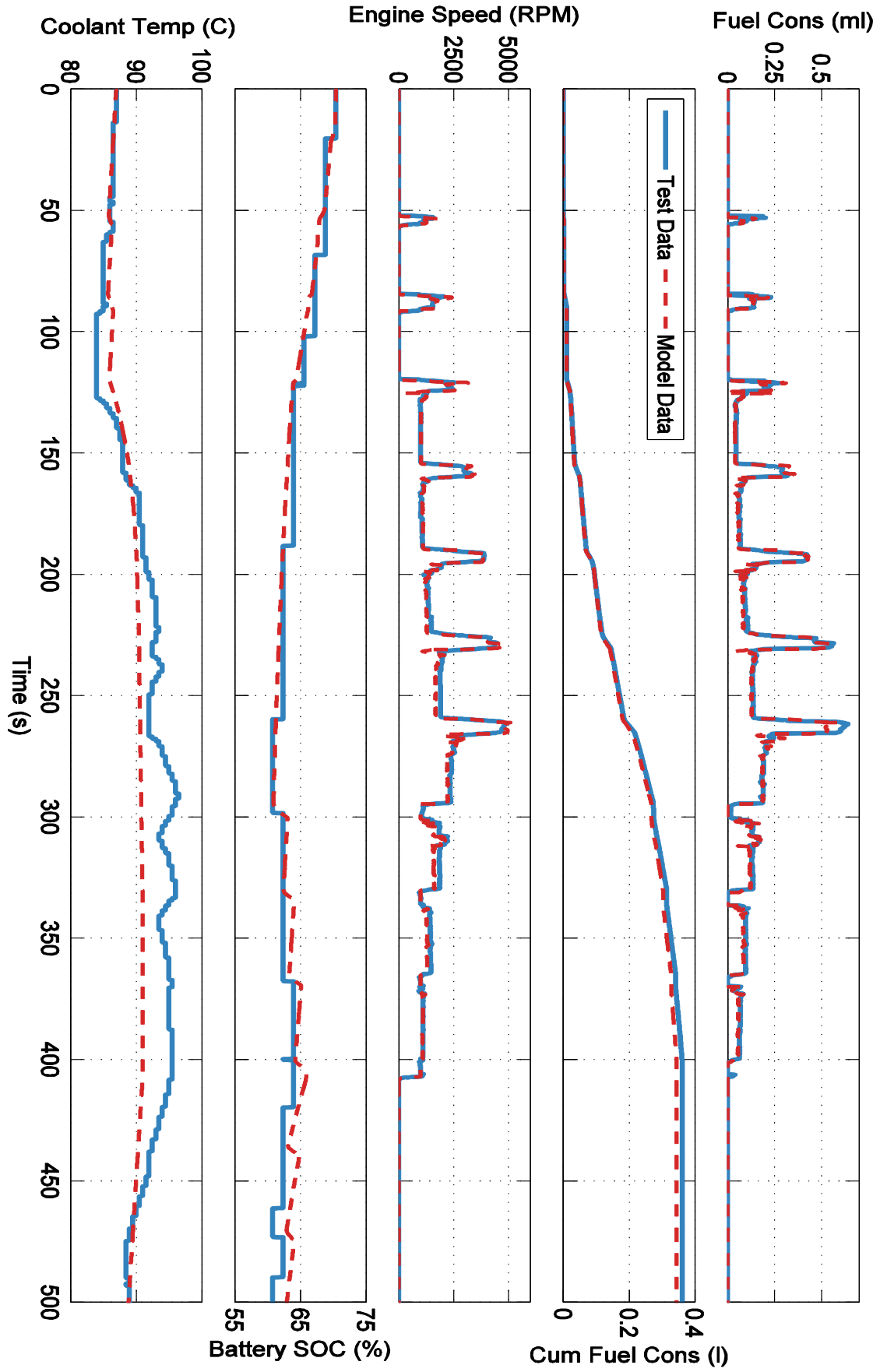


Figure 6.41: Model validated against steady state speed cycle

Figure 6.42 plots the fuel consumption from the validation testing data against model fuel consumption. The best fit line, shown in red, has a gradient of 1.00, a y intercept of 0.0143 and an R squared value of 0.94. The model data is a very good fit at very low fuel consumption, less than 1.5 ml/s. In the middle range, 1.5 – 4 ml/s, the model over predicts fuel consumption, this could be because the tractive power used to fit the model was only an estimate or because the fuel consumption sub model over emphasises the effect of engine transients in this range, which is almost entirely made up of fuel consumption peaks. At the highest fuel consumptions, the model under predicts, this is because the model source data only included fuel consumption up to 6 ml/s and the model, therefore, can't match the test data for fuel consumption between 6 and 7 ml/s.

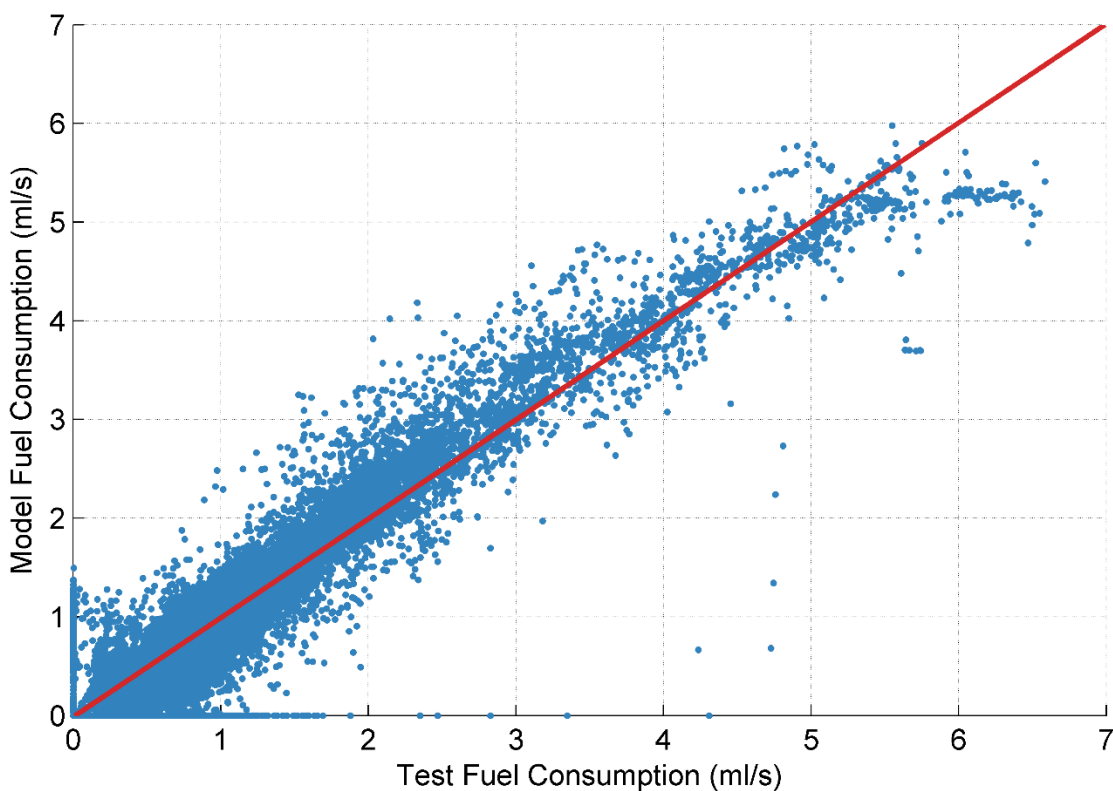


Figure 6.42: Validation fuel consumption against model fuel consumption

Figure 6.43 displays the fuel consumption error against the tractive power which represents the main model input vehicle speed. During negative tractive powers, the error is either zero where both the test and model engines are off or the error is negative

which indicates the test engine fuelling is always a little higher than the modelled. From 0 to 10 kW the error is well balanced either side of zero with a few lines of points indicating errors in *engine on/off* timing. Between 10 and 40 kW the error is dominated by more positive points indicating the model is over predicting fuel consumption in this middle range. The couple of very negative error values in this power range occur at the beginning of the cold start in cycle three where the validation test data shows a large positive spike in fuel consumption at *engine on*. No spike of this magnitude is seen at cold *engine on* in the PAMS test data so the model does not match this spike, the model also starts the engine slightly late during cold start which amplifies the error during this *engine on* event. Over 40 kW the error is more balanced apart from a few large negative errors at very high powers due to the model's inability to match the highest fuel consumption values. Overall no strong trends exist in the error data indicating that the model does a good job of estimating fuel consumption across the full range of model inputs.

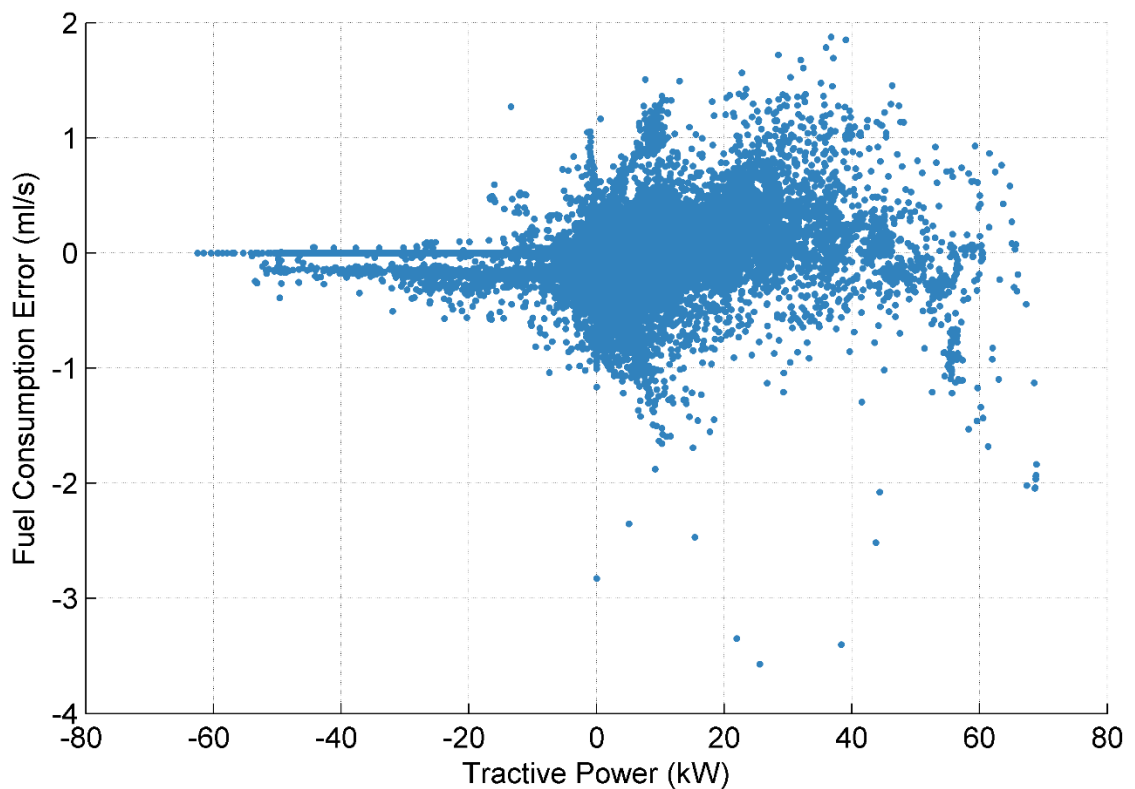


Figure 6.43: Fuel consumption error against tractive power for five validation cycles

6.4 Model Applications

6.4.1 Introduction

A microscale emission model of the type presented here has a wide range of applications for researchers and policymakers. Microscale emission models have several benefits and drawbacks. The key benefit is that the model can predict emissions that are specific to the vehicle type, vehicle operation and driving location. The drawback of this added detail is that collecting input data for the model can be time consuming and expensive. Several methods are available to collect this data including, micro-simulation traffic models, specific vehicle tracking campaigns and potentially smart phone GPS data (Barlow, Boulter, & McCrae, 2007).

With the required input data, a microscale emission model can be used to investigate a wide range of issues. These have been split into five areas discussed in more detail below.

Firstly, to answer specific policy questions. These are usually policies aimed at changing people's driving behaviour, through changes to road infrastructure, or the introduction of Intelligent Transport Systems (ITS). These changes often include changes in speed limits, better routing information, eco-driving techniques, different levels of congestion, caused by charging schemes, communications between vehicles, and between vehicles and road infrastructure, changes in lane access and many other changes to the driving experience and the road environment.

Secondly, to provide specific consumer information. This model application only really reaches its full potential with the availability of person specific GPS data from smart phones. With this data, consumers could be given realistic real world CO₂ emissions and running cost information. This may help them to weight up the benefits of switching to low carbon vehicles under their specific usage conditions.

Thirdly, to study the effect of real world conditions that are difficult to measure in a data collection campaign. These include parameters such as, a wide range of ambient temperatures, road gradient and vehicle load, as well as situations that can't always be arranged on the road such as, very high power events, very high and low speeds and varying levels of congestion.

Fourthly, to study the effects of small hardware and control changes on vehicle operation and emissions. The model allows the vehicle components sizing and efficiency to be changed, as well as permitting changes to the powertrain control strategy. This can be used to quantify the CO₂ emission benefits of optimising the powertrain design to a particular vehicle use. This could be used in a specific situation like the design of a city car similar to the Prius c.

This feature of the model could also be used more broadly to research the effects of vehicles actively selecting driving modes. It is becoming increasingly common for vehicles to be able to change modes depending on the drivers, driving style. The Toyota Prius tested had three modes activated by buttons on the dash board, the modes have been designed to be applicable in all situations, with no problems if the driving style or road type suddenly changes. However, in the future when cars have access to their location, road type, route, future traffic conditions and driver's normal driving pattern, the car could optimise its control strategy to its current situation, to a much greater extent than cars do today.

Fifth, to provide more realistic emission figures for vehicles over legislative drive cycles. As discussed in Section 2.2.1 emission factors from legislative test cycles do not match emissions in the real world. Microscale emission models can be used to see if type approval figures are reasonable, model test cycles and real world operation data to give a fair comparison, and compare test cycles with their source dataset to ensure a representative cycle has been created.

6.4.2 Geofence Model Application

Geofencing works by tracking users with GPS, when a user enters or exits a virtual fenced zone a message is sent to the user. This can be a message for a human user or it can be a signal designed to automatically change the operation of an electronic device. As part of TfL work to reduce emissions of air quality pollutants from transport in London they have outlined a range of ambitious measures that could be introduced by 2020. One of these is using geofencing to force zero emission capable buses and taxis to run in PE mode while inside pollution hotspots (Transport for London, 2014).

This application of the model has been chosen as it demonstrates a wide range of model uses, including, answering a policy question, modifying vehicle controls and providing consumer information, as well as playing to microscale emission modelling strengths by being very location specific.

Leeds like many of the major cities in the UK suffers from high air pollution levels due to road traffic. In the next section, the model will be used to study the changes required in the Toyota Prius design and control so that it can drive the taxi routes developed in Chapter 5, while only operating in PE mode in high emissions zones. The taxi routes pass through two areas that are very congested and have high numbers of pedestrians due to nearby shops. These two areas are Leeds city centre and central Headingley. Figure 6.44 shows a road map of Leeds with the two zones used for the geofence marked on by black circles.

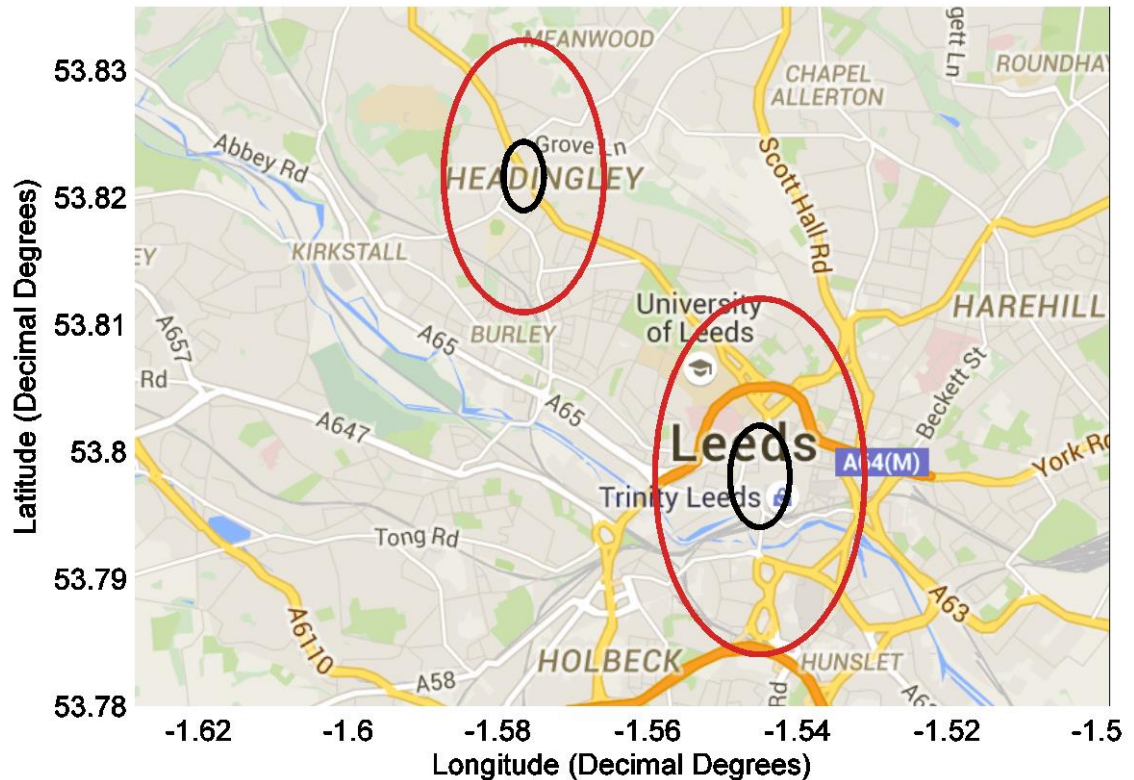


Figure 6.44: Roadmap of Leeds marked with geofence zones

For the geofencing to work, two fences are required for each zone. An outer fence, shown in red, set a given distance outside the inner fence, shown in black. The outer zone allows the vehicle to prepare for the inner zone by increasing the battery SOC. The outer zone has been designed so that, if the cars general direction, over a five minute period, is towards the inner fence then the outer zone is activated. Conversely, if the cars general direction is away from the inner fence then the outer zone is not activated. This means that taxis moving away from the inner fence do not unnecessarily emit more emissions while passing through the outer zone. The inner fence instructs the car to switch into PE mode as the car enters the zone and to switch to normal operation when the car leaves the zone.

In the outer zone, the model is modified in two ways. Firstly, the engine is turned on and set to stay on until the battery SOC reaches 90%. If the engine reaches this target the engine can turn off and stay off until it is needed to meet the tractive power demand or

the SOC drops to 80%. Secondly, while the engine is on the power demanded from the battery is increased. Figure 6.45 shows the battery power demand as a function of battery SOC for the original model, in black, and for the revised geofence model, in blue. The maximum power demanded of the engine, by the battery, occurs at 40% SOC. This has not been changed in the new model to ensure that the battery power demand can always be realistically met by the engine. The new battery power demand line has been designed to increase the battery SOC as quickly as possible without resulting in excessive engine fuel consumption. The new battery power demand hits zero at 90% SOC, at which point, if the tractive power demand is low the engine will turn off. If the engine is forced to stay on past 90% SOC due to tractive power demand the battery will only gain charge during regeneration and this alone will not increase the SOC by 10%. This control strategy, therefore, limits the SOC below 100% without the need for a hard limit.

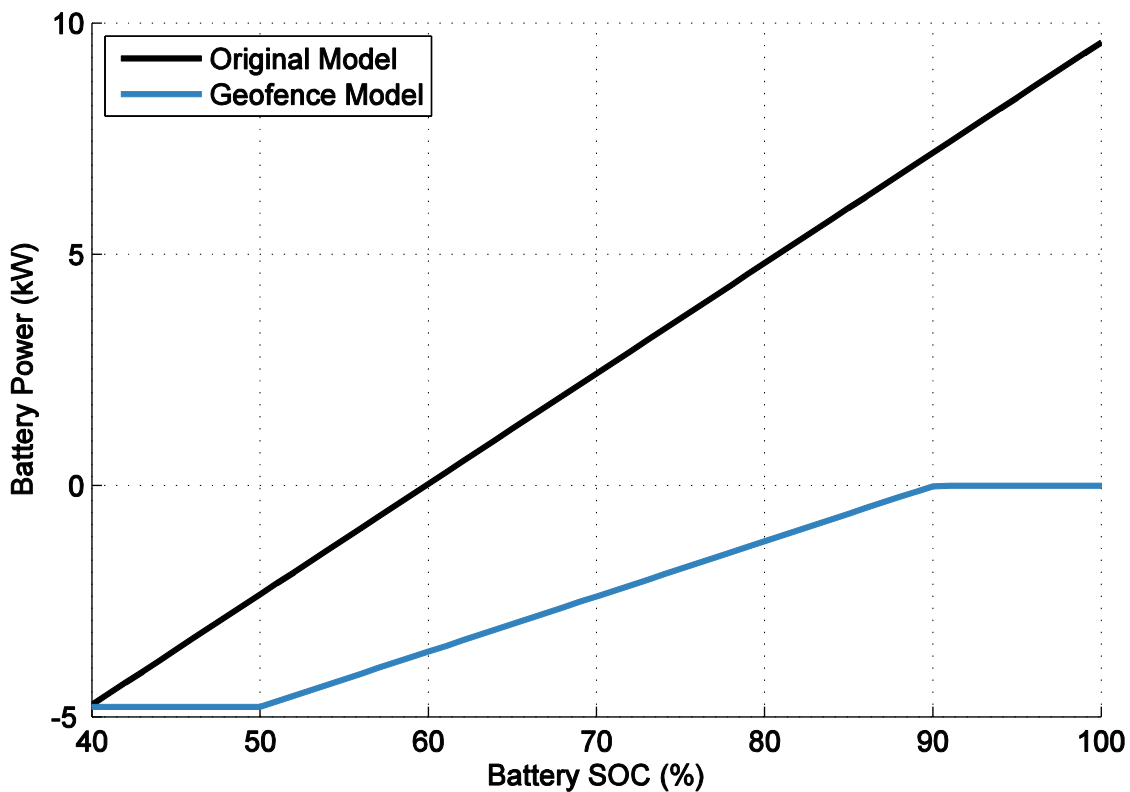


Figure 6.45: Predicted battery power as a function of battery SOC for the original and geofence model

In the inner zone the model is modified to always turn the *engine off*, with two exceptions. These are, battery SOC less than 40%, and very high tractive power demand. If the control of the outer zone is designed correctly then the battery charge should be high enough to drive through the inner zone without the battery SOC dropping too low, but if the battery SOC does drop to 40% then the engine comes on and stays on until the SOC hits 45%. The highest motor power recorded, in the taxi dataset, while the engine was off, is 19kW. Under normal operation, the motor power at *engine on* is a function of battery SOC, with the engine turning on early if the SOC is low. For the inner zone, this top motor power limit will be applied across all battery SOC uniformly, allowing the engine to turn on if this threshold is met. If the maximum power limit is met the engine stays on until the motor power drops below 6 kW. This lower limit was chosen as this is the power the engine turns on at when the battery SOC is 40%. It is therefore known that the vehicle can drive this power in PE mode under the full range of possible battery SOC.

One other adaptation was made to the geofence model that affects the model operation outside the inner zone. In the original model, the low SOC limit was 40%, and a low SOC event resulted in the engine staying on until the SOC reached 50%. These limits have been changed to 45 and 55%. This means that if the SOC drops to 40% in the inner zone, and the engine comes on and increases the SOC before the vehicle leaves the inner zone, then when the vehicle exits the inner zone the engine will immediately come on and start to recharge the battery, rather than waiting for the SOC to drop to 40% again.

One of the greatest difficulties in allowing the taxi to run in PE mode through the centre of town without hitting the lower SOC limit is the drop in SOC while driving through the taxi rank. In the 72 taxi runs the SOC drop across the taxi rank ranges from 1% to 15% with an average drop of around 6%. With only a small battery the Toyota Prius can complete the runs, in PE mode, when the stop time in the taxi rank is short, but can't afford to drop 15% battery SOC sitting still. It is therefore assumed that the introduction

of the geofencing policy is accompanied by policies to reduce taxi idling in the taxi rank. This is reflected in the model by switch the *engine off* if the vehicle is idling for more than two minutes, while in the taxi rank.

6.4.3 Geofence Model Results

While the model has been modified to ensure that the engine stays off in the inner zone, these conditions are not always met because the modifications are a compromise. The new model is designed to allow the vehicle to drive the inner zone in PE mode as much as possible, but there is little added value in designing the vehicle so that it is always able to drive the inner zone in PE mode, if it means that the battery and motor have to be much bigger, or the trip fuel consumption is much higher, or the emission problem is just shifted from the inner, to outer zone.

In the raw data collected the max power limit for operating in PE mode in the inner zone is breached 362 times, all of these occurrences were under the most aggressive driving style. These breaches resulted in 105 *engine on* events, totalling just under five minutes of engine running time.

Across all 72 runs, there is one case where the SOC drops below 40% inside the inner zone. This results in the engine turning on and staying on for one minute. All of the lowest SOC points occur in the calm driving style data and are therefore unlikely to occur often under real taxi driving. Figure 6.46 displays the battery SOC over the four taxi driving cycles run back to back. Four consecutive runs were chosen by selecting the four runs with the average overall fuel consumption from the normal driving style data. Time when the vehicle is in the outer zone has been coloured green and time in the inner zone coloured blue. In this representative case, using normal driving, the SOC only fluctuates between 50 and 80%, this means the charging rate could be decreased or the outer zone made smaller and the vehicle could still drive the PE zones. However, by designing the vehicle controls so that they are capable of completing the driving demand in all three driving styles a more robust set of controls have been created.

Under normal driving conditions, the new control regime pushes the battery SOC up to 80% which is 5 to 10% higher than the Prius would usually allow. The big difference compared to the current Prius controls is the amount of charging and discharging allowed, this will have a big effect on battery degradation and new battery chemistries and controls may be needed to ensure a reasonable battery lifetime. The new controls are shown to be very effective with the outer zone often increasing the battery SOC by 20%, while using charging rates that are within those regularly experienced by the Prius battery. This rise in SOC allows for large inner zones covering the whole of the major shopping areas in both Leeds and Headingley. With the taxi rank in the Leeds inner zone, it takes a long time to pass through and the drop in SOC is, therefore, high, usually around 30%, compared to Headingley, only 15%. This shows how important it is to reduce the time that the vehicle spends in the taxi rank when geofenced PE zones are being considered. The data shows that the same rated power and capacity battery could be used to drive through short sections of PE mode only zones and that it can be achieved with conventional hybrid vehicles.

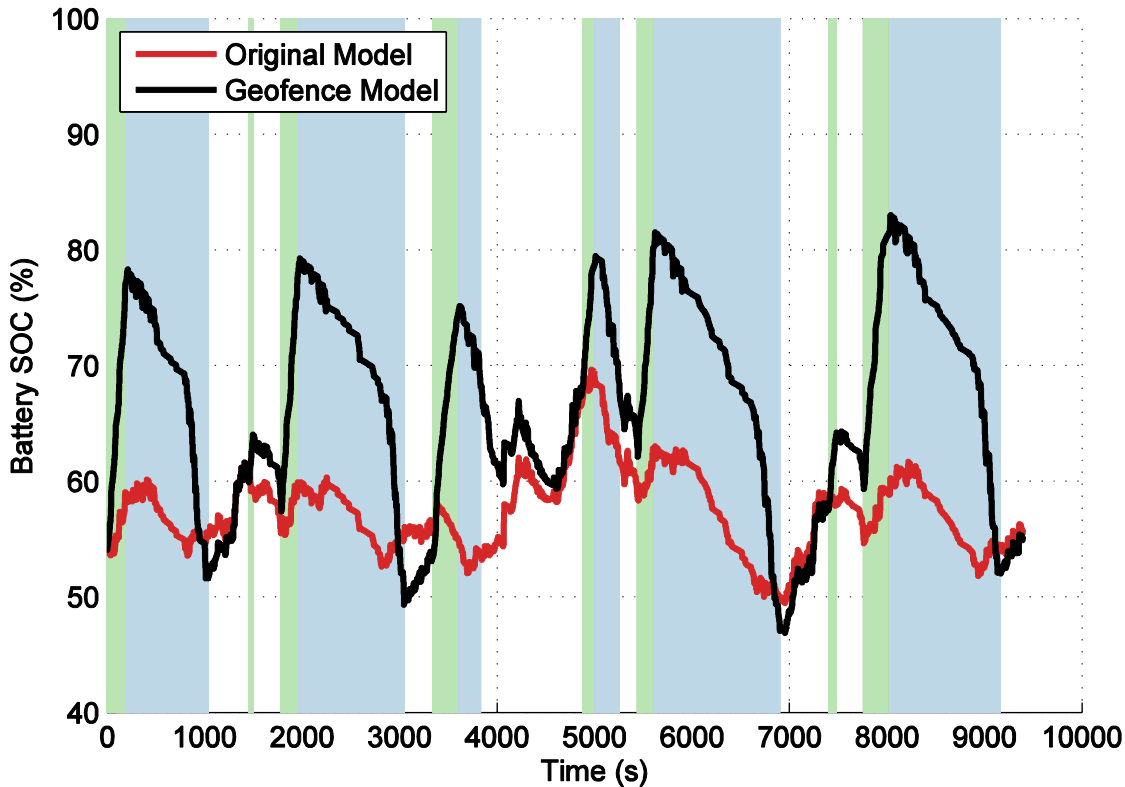


Figure 6.46: Original and geofence model battery SOC over the four taxi driving cycles. Colour coded by geofence zone. Green, outer zone. Blue, inner zone

Apart from battery degradation the other downside of geofenced PE zones is a drop in the overall system efficiency. As the boxplot in Figure 6.47 shows the geofence controls result in the engine running for much more of the cycle, although for much of that additional engine on time the engine is only idling. Over the normal driving style runs the original model has the engine on for 3.1 hours, while the geofence model has the engine on for 4.1 hours. As Figure 6.48 demonstrates this additional engine on time pushes the fuel consumption, over the four cycles, up by nearly 8% and this will be accompanied by higher emissions of all other air quality pollutants. This value should be considered a low estimate as the model does not take into account the efficiency effects of battery temperature or battery degradation with time, both of which will decrease the battery efficiency and increase the additional fuel consumption required to drive long sections in PE mode. Also as the model is further developed in the future and an engine power delay

sub-model is added this will improve the accuracy of this work by taking into account the higher battery demands which become increasingly important the longer the modelled run. The Figure also displays the PAMS test data to show that the model can represent these runs with a total error of less than 5%.

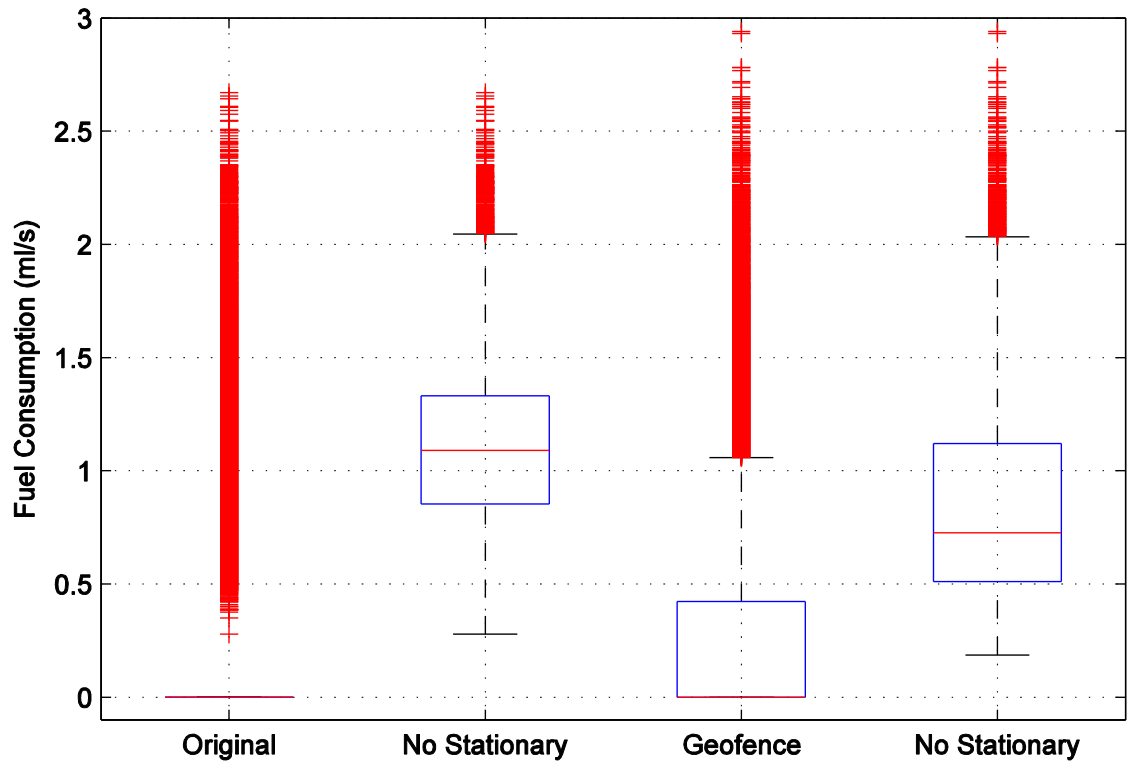


Figure 6.47: Boxplot of fuel consumption, left to right. Original model all data. Original model excluding vehicle stationary data. Geofence model all data. Geofence model excluding vehicle stationary data.

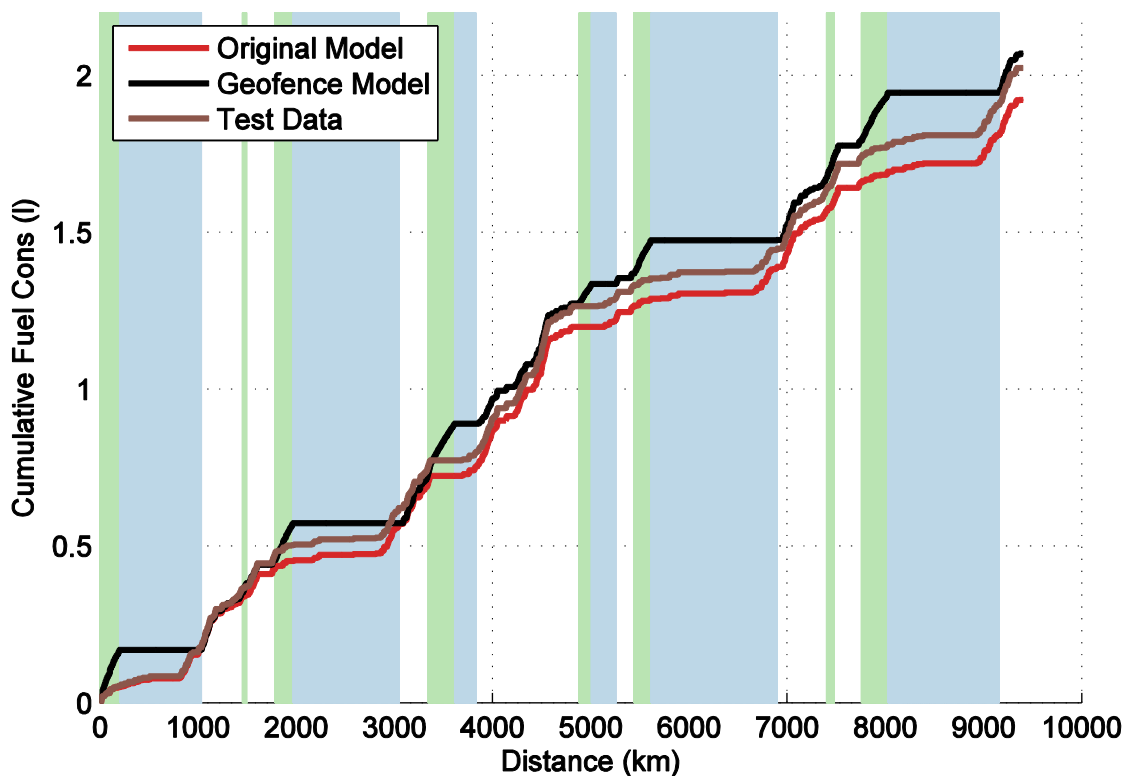


Figure 6.48: Cumulative fuel consumption, original versus geofence model, over the four taxi driving cycles. Colour coded by geofence zone. Green, outer zone. Blue, inner zone

By not considering the effects of more battery charging and discharging, over wider SOC ranges, the effects of battery temperature and battery degradation as well as the effect of engine power delay on the battery, this analysis is unable to discuss the actual emission benefits of a geofence scheme. Instead, this section is designed to provide an example of the versatility and flexibility of the model to answer questions that could not be analysed in any other way.

6.5 Conclusions

This chapter has presented the successful building and validation of a microscale CO₂ emission model based on real world PAMS data. The most common data source for model building is chassis dynamometer data. This is because there is fewer external variable that effects the data and this makes it easier to fit the model. This work has

shown that it is possible to build an accurate vehicle model using real world data. This has not been done before for a hybrid vehicle because of the difficulty and cost of collecting the internal variables required, if vehicle CAN data is not utilised. Using real world data makes fitting the model more difficult, but by including and recording all the variables that affect the vehicle on the road a more robust model can be built that better represents real world fuel consumption figures.

Other models in the literature have been validated against chassis dynamometer data (N. Kim et al., 2012; Namwook Kim et al., 2012). By validating this model against independent chassis dynamometer data it has been shown that this modelling method can meet the same standards, under a range of conditions, as models built from carefully controlled chassis dynamometer runs. The method used for collecting the validation fuel consumption data could not be more different from the method used to collect the on-road fuel consumption data. This means there are likely to be differences in the vehicles used, the test equipment accuracy and bias and the test method accuracy and bias. These differences will cause errors on top of the modelling error and yet over five very different and challenging cycles the model was able to meet the project aim of building a model with a total error of less than 5%.

Once built the model is quick and easy to run. To compile and run, at ten hertz, the five cycles, HWFET, UDDS with hot start, UDDS cold start, US06 and a steady state speed test, took 2.9, 2.4, 2.5, 2.5 and 1.6 seconds respectively. This makes it a powerful tool for studying a wide range of situations. A simple example of applying the model to a PE mode geofence has been given in this chapter. This example shows how the model allows the user to vary not just the model inputs but the component sizing and efficiency as well as the powertrain control. This allows the modeller to achieve far more with the model than simply to run the same vehicle over different drive cycles.

Models built using a similar method to the one presented here are likely to play an ever increasing role in transport research as the data required to build and run the models

becomes more readily available. These models still require a lot of time to create and this has to be weighted up against a simple data collection campaign. However, in several emerging areas such as autonomous vehicles, vehicle to vehicle communication and active traffic management, modelling will always play an important role because testing these situations in a laboratory or on the road is incredibly difficult.

Chapter 7

Conclusions

This project aimed to develop real world CO₂ emission factors for hybrid vehicles, to help overcome the wide range of repercussions that have resulted from inaccurate type approval CO₂ and fuel consumption figures. The project has successfully demonstrated real world vehicle activity data collection through the vehicle CAN. This data has been used to provide new insight into the control of the Toyota Prius, to inform Leeds City Council about the emission benefits of hybrid taxis, to provide a tailor made business case to the Leeds taxi drivers, which may encourage the uptake of hybrid taxis, and to build a microscale CO₂ emission model. Although the long term effects of this project on Leeds City Councils taxi policy and taxi drivers decision making is unknown. Overall this project has successfully fulfilled the aims set out in Section 1.2.

Two methods for delivering real world CO₂ emission factors for technology analysis, informing local policy makers and educating consumers has been presented in this work. The methods selected were microscale vehicle modelling and PAMS. Microscale emission modelling was chosen because local policy makers and consumers want emission factors that are specific to their situation. Providing location specific data through vehicle testing is not always possible due to time and economic limitations, and the fact that proposed policies can't be tested until they have been enacted, at least at a trial level. Microscopic simulation can help to overcome these issues as run times are short and theoretical scenarios can be tested. PAMS was selected because it is cheaper than PEMS testing for creating real world CO₂ emission factors and much cheaper than instrumenting the vehicle to measure internal vehicle parameters needed to analyse the vehicle and build a microscale emission model.

By combining the two methods novel research has been conducted and original results created. The two methods perform well in conjunction, each overcoming the drawbacks

of the other method. The greatest difficulty in building and validating vehicle models is input data. This can most effectively be provided by PAMS testing. The biggest obstacle to performing real world testing for every project is time and money. Once set up modelling runs are fast and cheap.

The project demonstrated PAMS testing by fitting two devices capable of recording GPS and CAN data on a 2009 third generation Toyota Prius. To prove the potential of the data collected to inform local policy makers, educate consumers, analyse complex powertrains and build microscale models the data has been validated through a number of projects.

Leeds University was asked by Leeds City Council to provide the supporting information for a DEFRA funded project on the potential of hybrid vehicles as taxis in Leeds. It was decided to use PAMS data collection to inform the CO₂ and fuel consumption sections of the project. PAMS was well suited to this project because of its very competitive price, it allows for local real world data to be collected and it is technically and economically viable to collect data over a reasonable long time. This is important because taxi runs take a long time to complete due to the very long idling periods in the taxi rank. By collecting local real world data the City Council can be confident in the results, ensuring that they will get the expected benefits from their financial investment in policies. Also, while consumers' confidence in generic emission data has fallen with the problems in type approval testing this tailored data should give the consumers, in this case, the taxi drivers, the assurances they need to invest money in low carbon vehicles knowing they will get a return on their investment.

The results of the study have shown that taxi driving patterns are unlike type approval drive cycles meaning taxi specific emission factors are needed for policy makers and drivers to select technology winners. Based on taxi specific data the petrol hybrid vehicle clearly outperforms conventional petrol and diesel vehicles on price, fuel use, CO₂ and NO_x emissions. This project has successfully proved that PAMS can be a useful tool for

providing the information needed by policy makers and consumers to make cost and emission effective choices.

Analysing vehicle powertrains under real world use is important for understanding component operation and control. This information can be used in three ways. Firstly, many studies relate emissions to vehicle activity to better understand the results (H. Christopher Frey et al., 2010; Henry Christopher Frey & Sun, 2011; Hu et al., 2016; Xu et al., 2011). This is enough when analysing conventional vehicles, but in hybrid vehicles, the same activity can result in very different emissions. In this case, to understand the emissions they need to be related to vehicle and component activity. Secondly, understanding powertrain component performance and control is an important step in checking that manufacturers are building vehicles to perform to the emission standards on the road. Thirdly, to build an emission model requires the modeller to have an in-depth understanding of the vehicle control patterns in order to design and build the model architecture. PAMS has proved a powerful tool for analysing powertrain components and control because it provides a wide range of internal variables, and control thresholds are easier to detect as the exact magnitude of parameters on which the control is based can be observed.

One of the biggest challenges in model building is creating the database needed to build and validate the model. PAMS has proved a successful method for collecting this data because it is low cost, large amounts of data can be collected in a short space of time, the wide range of real-world conditions that the model should be able to predict can be captured in the data and internal variables are collected so sub-models can be created for different drive train components. By building the model from the PAMS data and validating it, to within 5% for fuel consumption, against an independent database collected on a chassis dynamometer by Argonne National Laboratory. The model has validated the accuracy of the PAMS data used to create it, an outcome that was difficult

to achieve without fitting the vehicle with sensors to check the PAMS parameters, an exercise that would have defeated the point of conducted PAMS testing.

The microscale emission model of the Toyota Prius has been demonstrated by analysing the potential of hybrid taxis to drive through Leeds city centre in PE mode only. This scenario has been chosen for three reasons. Firstly, using geofences to force hybrid taxis to drive through central city zones in PE mode is a policy that has been considered by TfL for improving London's air quality (Transport for London, 2014). It is, therefore, feasible that it could be considered as a policy in Leeds. Secondly, the policy is location specific, with the results depending on the road layout, traffic, topography and geofence size which are all individual to a particular city. By using PAMS data from trips within Leeds the location is included in the study in a way that could not be replicated in a laboratory. Thirdly, the scenario can't be tested on the road because the infrastructure has not been created. This leaves modelling as the only tool capable of analysing the situation to provide an initial indication of the potential of the scheme. The results have shown that a geofenced zone could be instated in Leeds city centre and the PE mode demand met using a conventional hybrid vehicle with similar characteristics to the Toyota Prius. While reducing the emissions within the geofenced zone the scheme results in increased trip fuel consumption, this is likely to make it very unpopular with taxi drivers. This example exhibits the flexibility of modelling and shows how models combined with local activity data can be a powerful tool for analysing future policies for local councils. It is in these situations that are impractical to test that modelling is an essential tool and it is expected that its use at the local scale will increase as more models become available and local councils are faced with legislating new technologies like geofences and vehicle automation that they can't test.

7.1 Further Work

Each of the objectives of this thesis, laid out in Section 1.2, and their respective chapters demonstrate methods that could be used to help progress to low carbon vehicle fleets. These methods will need further work and multiple demonstrations before they are used as mainstream tools.

The PAMS data collection method presented in Chapter 3 has proved very successful for the Toyota Prius, but methods for accessing a wider range of PID on all vehicles needs to be developed. Until a wider range of parameters can be reliably collected for a large proportion of the vehicle fleet this method will not fulfil its full potential. This project has demonstrated the MAF method for collecting fuel consumption for petrol vehicles. This method can't be used for diesel vehicles and so developing and validating a fuel consumption method for diesel vehicles is the next step needed if PAMS is to be used more widely in Europe.

From 500 plus available PID only 27 were recorded using the HEM data logger. New studies are needed to examine the other PID, many of which could open up new uses for PAMS data not discussed here.

The vehicle analysis presented in Chapter 4 was supported by a lot of information already available in the literature. The next stage is to prove that this method can be applied to a new powertrain as it enters the market. This is needed to support the long term goal of analysing new vehicles to check that the controls have been optimised for real world driving and not for the test procedure.

PAMS data has been used to provide consumer information for a small group. Several papers on eco-driving have shown that it is possible to provide PAMS information to more people both in real time and after each trip (Hari et al., 2012). A much larger study collecting PAMS data through telematics, from ordinary drivers, driving their usual driving

pattern is needed to exhibit the technology. Once these studies become common they will provide the much needed data for traffic simulation and vehicle modelling.

The Toyota Prius model built here was designed to meet the accuracy criteria with the minimum computational demand. This means that there are still areas of the model such as engine power delay and battery efficiency at varying temperatures that could be further developed to improve the predictive capabilities of the model over real-world driving cycles. Modelling vehicles from PAMS data also needs to be demonstrated for other AFV vehicles to allow users to compare many new technologies in their chosen situation and select the most effective one for them.

Now the Prius model has been validated, it is a powerful research tool that can be used to study the potential of hybrid vehicles in a wide range of real-world and hypothetical situations. The model is particularly well suited to studying proposed policies that involve a change in road infrastructure. The next stage in model development is to pair the model with a traffic simulation model, this will allow researchers to analyse whole traffic systems without having to collect on-road data.

Glossary

Coast Down Test. A test that involves coasting a car from a high speed to a low speed to calculate the real world vehicle aerodynamic and rolling resistances (road load parameters) used for chassis dynamometer testing.

Chassis Dynamometer. An indoor vehicle testing laboratory. It consists of two large drums which are connected to a dynamometer which measures rotational speed and torque, and provides resistance. The vehicle wheels are placed on the drums and the vehicle is driven to match a specific speed time trace, while the dynamometer provides resistance to the drums to replicate the resistance of driving on a road.

Road Load Parameters. Vehicle resistance parameters calculated in a coast down test and used to set the driving resistance in a chassis dynamometer test to represent on-road driving demand.

PEMS. Portable Emission Measurement System is a portable laboratory fitted to a vehicle to measure emissions from the tailpipe.

PAMS. Portable Activity Measurement System is a device fitted to a vehicle to measure vehicle and component operating conditions by reading data from the vehicle communication bus (CAN bus).

Planetary Gear. A gearing device with two inputs and one output that can act as a continuously variable transmission automatic gearbox.

On-Board Diagnostics. A standardised system on the vehicle that monitors the wellbeing of the vehicle emission control systems and allows technicians to access fault codes and component operation data to assist in vehicle repair and maintenance.

Controller Area Network. A communication bus standard that defines the physical and data layers of the bus.

List of References

- AA. (2015). *Fuel Price Report*. Retrieved from <http://www.theaa.com/resources/Documents/pdf/motoring-advice/fuel-reports/december2015.pdf>
- Abuhijleh, B., & Nik, A. (2013). Economic and Environmental Benefits of Using Hybrid Taxies in Dubai-UAE. In *SB13 Dubai: Advancing the Green Agenda Technology, Practices and Policies, Dubai, United Arab Emirates*. Dubai. Retrieved from http://www.irbnet.de/daten/iconda/CIB_DC26914.pdf
- Ajtay, D. (2005). *Modal Pollutant Emissions Model of Diesel and Gasoline Engines*. Zurich. Retrieved from <http://e-collection.library.ethz.ch/eserv/eth:28554/eth-28554-02.pdf>
- Alessandrini, A., Filippi, F., Orecchini, F., & Ortenzi, F. (2006). A new method for collecting vehicle behaviour in daily use for energy and environmental analysis. *Proceedings of the Institution of Mechanical Engineers, Part D: Journal of Automobile Engineering*, 220(11), 1527–1537. <http://doi.org/10.1243/09544070JAUTO165>
- Alessandrini, A., Orecchini, F., Ortenzi, F., & Villatico Campbell, F. (2009). Drive-style emissions testing on the latest two Honda hybrid technologies. *European Transport Research Review*, 1(2), 57–66. <http://doi.org/10.1007/s12544-009-0008-3>
- Andre, M. (2005). *Vehicle Emission Measurement Collection of the ARTEMIS Database*. Lyon. Retrieved from <http://www.inrets.fr/ur/lte/publications/publications-pdf/Joumard/A3312reportJMALTE0504.pdf>
- Arata, J., Leamy, M. J., Meisel, J., Cunefare, K., & Taylor, D. (2011). Backward-Looking Simulation of the Toyota Prius and General Motors Two-Mode Power-Split HEV Powertrains. *SAE International Journal of Engines*, 4(1), 1281–1297. <http://doi.org/10.4271/2011-01-0948>

- Argonne National Laboratory. (2015). Downloadable Dynamometer Database 2010 Toyota Prius. Retrieved February 8, 2016, from <http://www.anl.gov/energy-systems/group/downloadable-dynamometer-database/hybrid-electric-vehicles/2010-toyota-prius>
- AVL. (2009). *CRUISE Vehicle System Analysis*. Graz. Retrieved from <https://www.environmental-expert.com/products/avl-cruise-202595>
- AVL. (2016). AVL CRUISE. Retrieved July 8, 2016, from https://www.avl.com/cruise/-/asset_publisher/gYjUpY19vEA8/content/avl-cruise-?inheritRedirect=false&redirect=https%253A%252F%252Fwww.avl.com%253A443%252Fcruise%253Fp_p_id%253D101_INSTANCE_gYjUpY19vEA8%2526p_p_lifecycle%253D0%2526p_p_state%253Dnormal%2526p_p_mode%253Dview%2526p_p_col
- Barlow, T. J., Boulter, P. G., & McCrae, I. S. (2007). *Scoping study on the potential for instantaneous emission modelling: summary report*. Wokingham. Retrieved from <http://www.trl.co.uk/reports-publications/trl-reports/report/?reportid=6236>
- Barrieu, E. (2011). EHRS Impact on Engine Warm up and Fuel Economy. In *Directions in Engine-Efficiency and Emissions Research Conference*. Detroit: US Department of Energy. Retrieved from http://energy.gov/sites/prod/files/2014/03/f8/deer11_barrieu.pdf
- Barth, M., An, F., Norbeck, J., & Ross, M. (1996). Modal Emissions Modeling: A Physical Approach. *Transportation Research Record*, 1520, 81–88.
- Burress, T. A., Campbell, S. L., Coomer, C. L., Ayers, C. W., Wereszczak, A. A., Cunningham, J. P., ... Lin, H. T. (2011). *Evaluation of the 2010 Toyota Prius Hybrid Synergy Drive System*. Oak Ridge. Retrieved from <http://info.ornl.gov/sites/publications/files/Pub26762.pdf>
- Cappiello, A., Chabini, I., Nam, E. K., Lue, A., & Abou Zeid, M. (2002). A statistical model

of vehicle emissions and fuel consumption. In *Proceedings. The IEEE 5th International Conference on Intelligent Transportation Systems* (pp. 801–809). IEEE. <http://doi.org/10.1109/ITSC.2002.1041322>

CH2M Hill. (2013). *Emissions Modelling: PHEM*. Bristol. Retrieved from http://www.bathnes.gov.uk/sites/default/files/bath-lez-doc04_bath_lez-emissions_modelling.pdf

Choi, D., & Koupal, J. (2011). *MOVES Validation*. Retrieved from <https://www3.epa.gov/otaq/models/moves/conference2011/validation-moves-2011.pdf>

City & County of San Francisco Office of the Mayor. (2012). San Francisco Taxis Surpass Emissions Goal. Retrieved April 20, 2016, from <http://www.sfmayor.org/?page=684>

City of Boston. (2008). Mayor Menino Announces Taxi Fleet to be Fully Hybrid by 2015. Retrieved April 29, 2016, from <http://www.cityofboston.gov/news/Default.aspx?id=3967>

City of Boston. (2009). Climate Change Bill would Allow Boston to Regulate Taxicab Standards. Retrieved April 29, 2016, from <http://www.cityofboston.gov/news/Default.aspx?id=4376>

City of Chicago. (2011). Alternative Fuels Green Taxi Program. Retrieved April 29, 2016, from http://www.cityofchicago.org/city/en/depts/cdot/supp_info/alternative_fuels.html

City of Chicago Department of Business Affairs and Consumer Protection. (2012). New Taxicab and Public Vehicle Ordinances. Retrieved April 29, 2016, from <http://www.cityofchicago.org/dam/city/depts/bacp/publicvehicleinfo/taxiindustrynotices/taxiindustrynotice12-004newtaxipublicvehicleord.pdf>

City of New York. (2006). Mayor Bloomberg And Tlc Commissioner Daus Announce Increase In Alternative Fuel Medallions For City Taxi Cabs. Retrieved April 29,

2016, from <http://www1.nyc.gov/office-of-the-mayor/news/162-06/mayor-bloomberg-tlc-commissioner-daus-increase-alternative-fuel-medallions-city>

City of New York. (2008). Mayor Bloomberg Announces New Incentive / Disincentive Program To Reach Goal Of Green Taxi Fleet. Retrieved April 29, 2016, from <http://www1.nyc.gov/office-of-the-mayor/news/455-08/mayor-bloomberg-new-incentive-disincentive-program-reach-goal-green-taxi-fleet>

City of New York. (2011). Mayor Bloomberg And Taxi Commissioner Yassky Join Senator Gillibrand And Congressman Nadler To Introduce Green Taxis Act. Retrieved April 29, 2016, from <http://www1.nyc.gov/office-of-the-mayor/news/100-11/mayor-bloomberg-taxi-commissioner-yassky-join-senator-gillibrand-congressman-nadler-to#/7>

City of New York Taxi & Limousine Commission. (2007). Commissioner's Column. Retrieved April 29, 2016, from http://www.nyc.gov/html/tlc/html/about/column_2007_06.shtml

City of New York Taxi & Limousine Commission. (2014). *TaxiCab Fact Book*. New York. Retrieved from http://www.nyc.gov/html/tlc/downloads/pdf/2014_taxicab_fact_book.pdf

Ciuffo, B., Marotta, A., Tutuianu, M., Anagnostopoulos, K., Fontaras, G., Pavlovic, J., ... Tsiakmakis, S. (2015). The development of the World-wide Harmonized Test Procedure for Light Duty Vehicles (WLTP) and the pathway for its implementation into the EU legislation. *Transport Research Board Annual Meeting*, 15–4935. Retrieved from <http://docs.trb.org/prp/15-4935.pdf>

Coelho, M. C., & Luzia, M. B. (2010). Evaluating the energy performance of a SUV hybrid electric vehicle. *Transportation Research Part D: Transport and Environment*, 15(8), 443–450. <http://doi.org/10.1016/j.trd.2010.04.003>

Committee on the Assessment of Technologies for Improving Fuel Economy of Light-

Duty Vehicles. (2015). *Cost, Effectiveness, and Deployment of Fuel Economy Technologies for Light-Duty Vehicles*. Washington DC: The National Academies Press.

Coordinating Research Council. (2010). *Review of the 2009 Draft Motor Vehicle Emissions Simulator (MOVES) Model*. Alpharetta. Retrieved from http://www.crcao.org/reports/recentstudies2011/E-68a/Final_CRC_E-68a_Report_V6.pdf

Costagliola, M. A., Prati, M. V., Mariani, A., Unich, A., & Morrone, B. (2015). Gaseous and Particulate Exhaust Emissions of Hybrid and Conventional Cars over Legislative and Real Driving Cycles. *Energy and Power Engineering*, 7(5), 181–192. <http://doi.org/10.4236/epe.2015.75018>

DeFries, T. H., Sabisch, M. A., & Kishan, S. (2013). *Light-Duty Vehicle In-Use Fuel Economy Data Collection: Pilot Study*. Austin TX. Retrieved from <http://www.theicct.org/sites/default/files/ICCT-131108 - ERG - In-Use FE Pilot-V8FInal.pdf>

DeFries, T. H., Sabisch, M., Kishan, S., Posada, F., German, J., & Bandivadekar, A. (2014). In-Use Fuel Economy and CO₂ Emissions Measurement using OBD Data on US Light-Duty Vehicles. *SAE International Journal of Engines*, 7(3), 1382–1396. <http://doi.org/10.4271/2014-01-1623>

Della Ragione, L., Meccariello, G., Prati, M. V., Costagliola, M. A., & Ragione, L. Della. (2014). Statistical evaluation of slope's effect on real emissions and fuel consumption performed with different cars in Naples urban area. *Transport Research Arena*. Retrieved from http://tra2014.traconference.eu/papers/pdfs/TRA2014_Fpaper_20308.pdf

Den Braven, K. R., Abdel-Rahim, A., Henrickson, K., & Battles, A. (2012). *Modeling Vehicle Fuel Consumption And Emissions at Signalized Intersection Approaches:*

Integrating Field-Collected Data Into Microscopic Simulation. Idaho. Retrieved from http://www.webpages.uidaho.edu/NIATT/research/Final_Reports/KLK721_N12-12.pdf

Department for Transport. (2014). *National Travel Survey: England 2014*. London. Retrieved from https://www.gov.uk/government/uploads/system/uploads/attachment_data/file/457752/nts2014-01.pdf

Department for Transport. (2016a). Plug-in car and van grants. Retrieved April 29, 2016, from <https://www.gov.uk/plug-in-car-van-grants/what-youll-get>

Department for Transport. (2016b). *Table VEH0122 Licensed vehicles by postcode district: United Kingdom*. London. Retrieved from <https://www.gov.uk/government/statistical-data-sets/all-vehicles-veh01>

Department for Transport. (2016c). *Vehicle Licensing Statistics: Quarter 4 (Oct - Dec) 2015*. London. Retrieved from https://www.gov.uk/government/uploads/system/uploads/attachment_data/file/516429/vehicle-licensing-statistics-2015.pdf

Dhameja, S. (2002). *Electric Vehicle Battery Systems*. Boston: Newnes.

DieselNet. (2013). ECE 15 + EUDC / NEDC. Retrieved June 23, 2016, from https://www.dieselnet.com/standards/cycles/ece_eudc.php

Duarte, G., Lopes, R., Goncalves, G., & Farias, T. (2013). Energy and environmental characterization of operational modes of plug-in vehicles. In *2013 World Electric Vehicle Symposium and Exhibition (EVS27)* (pp. 1–11). IEEE. <http://doi.org/10.1109/EVS.2013.6914811>

Duarte, G. O., Varella, R. A., Gonçalves, G. A., & Farias, T. L. (2014). Effect of battery state of charge on fuel use and pollutant emissions of a full hybrid electric light duty vehicle. *Journal of Power Sources*, 246, 377–386.

<http://doi.org/10.1016/j.jpowsour.2013.07.103>

Duoba, M. (2011). Engine Design, Sizing and Operation in Hybrid Electric Vehicles. In *University of Wisconsin-Madison Engine Research Center Symposium*. Madison: University of Wisconsin Madison. Retrieved from https://www.erc.wisc.edu/documents/symp11_Duoba.pdf

Duoba, M., Lohse-Busch, H., Rask, E., & Carlson, R. (2011). Control of Engine for Hybrid Vehicle Emissions. In *SAE 2011 Electronic Systems for Vehicle Propulsion Symposium*. Troy, Michigan: Society of Automotive Engineers. Retrieved from http://www.sae.org/events/training/symposia/esvp/presentations/2011/michael_duoba.pdf

Element Energy, & The International Council on Clean Transportation. (2015). *Quantifying the impact of real-world driving on total CO2 emissions from UK cars and vans*. Retrieved from <https://www.theccc.org.uk/wp-content/uploads/2015/09/Impact-of-real-world-driving-emissions-for-UK-cars-and-vans.pdf>

European Automobile Manufacturers Association. (2016). Alternative fuel vehicle (AFV) registrations: +6.4% in first quarter of 2016. Retrieved July 18, 2016, from <http://www.acea.be/press-releases/article/alternative-fuel-vehicle-afv-registrations-6.4-in-first-quarter-of-2016>

European Commission. (2011). *Roadmap to a Single European Transport Area – Towards a competitive and resource efficient transport system*. Retrieved from <http://eur-lex.europa.eu/legal-content/EN/TXT/PDF/?uri=CELEX:52011DC0144&from=EN>

European Commission. (2012). Reducing emissions from transport. Retrieved June 20, 2016, from http://ec.europa.eu/clima/policies/transport/index_en.htm

European Commission. (2016). Reducing CO2 emissions from passenger cars.

- Retrieved June 20, 2016, from
http://ec.europa.eu/clima/policies/transport/vehicles/cars/index_en.htm
- eurostat. (2015). Greenhouse gas emission statistics. Retrieved June 22, 2016, from
http://ec.europa.eu/eurostat/statistics-explained/index.php/Greenhouse_gas_emission_statistics
- Fairhurst, G. (2016). CAN Physical Layer. Retrieved June 28, 2016, from
<https://erg.abdn.ac.uk/users/gorry/eg3576/CAN-phy.html>
- Faris, W., Rakha, H., Kafafy, R., Idres, M., & Elmoselhy, S. (2011). Vehicle fuel consumption and emission modelling: An in-depth literature review. *International Journal of Vehicle Systems Modelling and Testing*, 6(3), 318–395.
<http://doi.org/DOI: 10.1504/IJVSMT.2011.044232>
- Ferris, D. (2009). *Global OBD Legislation Update (Worldwide Requirements)*. Indianapolis. Retrieved from
<http://www.sae.org/events/training/symposia/obd/presentations/2009/d1daveferris.pdf>
- Franco, V., Kousoulidou, M., Muntean, M., Ntziachristos, L., Hausberger, S., & Dilara, P. (2013). Road vehicle emission factors development: A review. *Atmospheric Environment*, 70, 84–97. <http://doi.org/10.1016/j.atmosenv.2013.01.006>
- Franco, V., Posada Sánchez, F., German, J., & Mock, P. (2014). *Real-world exhaust emissions from modern diesel cars*. Berlin. Retrieved from
http://www.theicct.org/sites/default/files/publications/ICCT_PEMS-study_diesel-cars_20141013.pdf
- Frey, H. C., Boroujeni, B. Y., Hu, J., & Liu, B. (2013). Measurement of Cold Starts and Their Contribution to Real - World Total Trip Emissions for Light Duty Gasoline Vehicles. In *Air & Waste Management Association*.
- Frey, H. C., Sandhu, G. S., Sun, Y., Lee, T., Swidan, H., Liu, B., & Babae, S. (2011).

Incorporating Vehicle Portable Emissions Measurement Systems Into the Classroom Paper. In *Air & Waste Management Association*.

Frey, H. C., & Sun, Y. (2011). Comparison of Real-world Activity, Fuel Use, and Emissions for Selected Light Duty Gasoline Vehicles Based on Driving Cycles. In *Air & Waste Management Association*.

Frey, H. C., Zhang, K., & Roupail, N. M. (2010). Vehicle-Specific Emissions Modeling Based upon on-Road Measurements. *Environmental Science & Technology*, 44(9), 3594–3600.

Gao, H. O., & Kitiratragarn, V. (2008). Taxi owners' buying preferences of hybrid-electric vehicles and their implications for emissions in New York City. *Transportation Research Part A: Policy and Practice*, 42(8), 1064–1073. Retrieved from <http://www.sciencedirect.com/science/article/pii/S0965856408000694>

Gao, Y., & Checkel, M. D. (2007). Emission Factors Analysis for Multiple Vehicles Using an On-Board, In-Use Emissions Measurement System. *SAE Technical Paper*, 2007-01–13. <http://doi.org/10.4271/2007-01-1327>

Guensler, R., Washington, S., & Sperling, D. (1993). *A Weighted Disaggregate Approach to Modeling Speed Correction Factors*. California. Retrieved from http://transaq.ce.gatech.edu/guensler/publications/reports/weighted_disaggregate.pdf

Halbach, S., Sharer, P., Pagerit, S., Rousseau, A. P., & Folkerts, C. (2010). Model Architecture, Methods, and Interfaces for Efficient Math-Based Design and Simulation of Automotive Control Systems. *SAE Technical Paper*, 2010-01–02. <http://doi.org/10.4271/2010-01-0241>

Hari, D., Brace, C. J., Vagg, C., Poxon, J., & Ash, L. (2012). Analysis of a Driver Behaviour Improvement Tool to Reduce Fuel Consumption. In *2012 International Conference on Connected Vehicles and Expo (ICCVE)* (pp. 208–213). IEEE.

<http://doi.org/10.1109/ICCVE.2012.46>

HEM Data. (2016). OBD Mini Logger. Retrieved April 13, 2016, from <http://www.hemdata.com/products/dawn/obd-mini-logger>

HM Revenue & Customs. (2016). Company Car and Car Fuel Benefit Calculator. Retrieved May 2, 2016, from <http://cccfcaculator.hmrc.gov.uk/CCF0.aspx>

House of Commons, E. A. C. (2014). *Action on Air Quality*. London. Retrieved from <http://www.parliament.uk/documents/commons-committees/environmental-audit/HC-212-for-web.pdf>

Hu, J., Frey, H. C., & Washburn, S. S. (2016). Comparison of Vehicle-Specific Fuel Use and Emissions Models Based on Externally and Internally Observable Activity Data. *Transport Research Board Annual Meeting*, 16–6315.

insuremytaxi4less. (2016). Online Quote. Retrieved May 2, 2016, from insuremytaxi4less.com

Intergovernmental Panel on Climate Change. (2014a). *Climate Change 2014 Impacts, Adaptation, and Vulnerability Summary for Policymakers*. Cambridge. Retrieved from http://www.ipcc.ch/pdf/assessment-report/ar5/wg2/ar5_wgII_spm_en.pdf

Intergovernmental Panel on Climate Change. (2014b). Organization History. Retrieved April 9, 2016, from https://www.ipcc.ch/organization/organization_history.shtml

International Energy Agency. (2009). *Transport, Energy and CO2*. Retrieved from <https://www.iea.org/publications/freepublications/publication/transport2009.pdf>

Jiménez-Palacios, J. L. (1999). *Understanding and Quantifying Motor Vehicle Emissions with Vehicle Specific Power and TILDAS Remote Sensing*. Retrieved from http://cires1.colorado.edu/jimenez/Papers/Jimenez_PhD_Thesis.pdf

Johansson, K. H., Törngren, M., & Nielsen, L. (2005). Vehicle Applications of Controller Area Network. In *Handbook of Networked and Embedded Control Systems* (pp.

741–765). Boston, MA: Birkhäuser Boston. http://doi.org/10.1007/0-8176-4404-0_32

Jones, S. (2011). System Simulation Tools for Electrified Vehicles. In *Joint EC / EPoSS / ERTRAC Expert Workshop*. Berlin. Retrieved from http://www.egvi.eu/uploads/3_1_Jones__AVLSimulationToolsForElectrifiedVehicles.pdf

Kadijk, G., & Ligterink, N. (2012). *Road load determination of passenger cars*. Delft.

Kasab, J., Shepard, D., Casadei, A., Huang, H., & Brandao, F. (2012). *Analysis of Greenhouse Gas Emission Reduction Potential of Light Duty Vehicle Technologies in the European Union for 2020–2025*.

Kawamoto, N., Naiki, K., Kawai, T., Shikida, T., & Tomatsuri, M. (2009). Development of New 1.8-Liter Engine for Hybrid Vehicles. *SAE Technical Paper*, 2009-01–10. <http://doi.org/10.4271/2009-01-1061>

Kim, N., & Rousseau, A. (2015). Thermal impact on the control and the efficiency of the 2010 Toyota Prius hybrid electric vehicle. *Proceedings of the Institution of Mechanical Engineers, Part D: Journal of Automobile Engineering*, 230(1), 1–11. <http://doi.org/10.1177/0954407015580217>

Kim, N., Rousseau, A., Lee, D., & Lohse-Busch, H. (2014). Thermal Model Development and Validation for 2010 Toyota Prius. *SAE Technical Paper*, 2014-01–17. <http://doi.org/10.4271/2014-01-1784>

Kim, N., Rousseau, A., & Rask, E. (2012). Autonomie Model Validation with Test Data for 2010 Toyota Prius. *SAE International*, 1–14. <http://doi.org/10.4271/2012-01-1040>

Kim, N., Rousseau, a., & Rask, E. (2012). Vehicle-level control analysis of 2010 Toyota Prius based on test data. *Proceedings of the Institution of Mechanical Engineers, Part D: Journal of Automobile Engineering*, 226(11), 1483–1494.

<http://doi.org/10.1177/0954407012445955>

- Koupal, J., Beardsley, M., Brzezinski, D., Warila, J., & Faler, W. (2010). *U.S. EPA's MOVES2010 vehicle emission model: overview and considerations for international application*. Ann Arbor. Retrieved from <https://www3.epa.gov/otaq/models/moves/MOVES2010a/paper137-tap2010.pdf>
- Koupal, J., Cumberworth, M., Michaels, H., Beardsley, M., & Brzezinski, D. (2003). Design and Implementation of MOVES: EPA's New Generation Mobile Source Emission Model. In *International Emission Inventory Conference*. San Diego.
- Koupal, J., Hart, C., Brzezinski, D., Giannelli, R., & Bailey, C. (2002). *Draft Emission Analysis Plan for MOVES GHG*. Ann Arbor. Retrieved from <http://www.4cleanair.org/p02008.pdf>
- Kousoulidou, M., Ntziachristos, L., Gkeivanidis, S., Samaras, Z., Franco, V., & Dilara, P. (2010). Validation of the COPERT road emission inventory model with real-use data. In *International Emission Inventory Conference*. San Antonio.
- Krimmer, M., & Venigalla, M. (2006). Measuring Impacts of High-Occupancy-Vehicle Lane Operations on Light-Duty-Vehicle Emissions: Experimental Study with Instrumented Vehicles. *Transportation Research Board, 1987*. <http://doi.org/DOI:10.3141/1987-01>
- Kuhlwein, J., Rexeis, M., Luz, R., Hausberger, S., Ligterink, N., & Kadijk, G. (2013). *Update of Emission Factors for EURO 5 and EURO 6 Passenger Cars for the HBEFA Version 3.2*. Graz. Retrieved from http://ermes-group.eu/web/system/files/filedepot/10/HBEFA3-2_PC_LCV_final_report_aktuell.pdf
- Lee, S., Lee, B., McDonald, J., Sanchez, L. J., & Nam, E. (2014). Modeling and Validation of Power-Split and P2 Parallel Hybrid Electric Vehicles. *SAE International*. <http://doi.org/10.4271/2013-01-1470>

- Leeds City Council. (2016a). Are you taxi aware? - information for passengers. Retrieved July 16, 2016, from <http://www.leeds.gov.uk/residents/Pages/are-you-taxi-aware.aspx>
- Leeds City Council. (2016b). Taxi and private hire licensing. Retrieved July 7, 2016, from <http://www.leeds.gov.uk/Business/Pages/Taxi-and-private-hire-licensing.aspx>
- Lenaers, G. (2009). Real Life CO₂ Emission and Consumption of Four Car Powertrain Technologies Related to Driving Behaviour and Road Type. *SAE Technical Paper, 2009-24-1*. <http://doi.org/10.4271/2009-24-0127>
- Liu, W. (2013). *Introduction to Hybrid Vehicle System Modeling and Control*. Hoboken: John Wiley & Sons.
- Lutsey, N. (2011). Comparison of Emissions, Energy, and Cost Impacts of Diesel and Hybrid Models in the United States in 2010. *Transportation Research Board, 2252*, 40–48. <http://doi.org/http://dx.doi.org/10.3141/2252-06>
- Luz, R., & Hausberger, S. (2010). *User Guide to the PHEM Emission Model*. Graz.
- Magana, V. C., & Munoz-Organero, M. (2015). GAFU: Using a Gamification Tool to Save Fuel. *IEEE Intelligent Transportation Systems Magazine, 7*(2), 58–70. <http://doi.org/10.1109/MITS.2015.2408152>
- Markel, T., Brooker, A., Hendricks, T., Johnson, V., Kelly, K., Kramer, B., ... Wipke, K. (2002). ADVISOR: a system analysis tool for advanced vehicle modeling. *Journal of Power Sources, 110*, 255–266.
- Marotta, A., Pavlovic, J., Ciuffo, B., Serra, S., & Fontaras, G. (2015). Gaseous Emissions from Light-Duty Vehicles: Moving from NEDC to the New WLTP Test Procedure. *Environmental Science & Technology, 49*, 8315–8322. <http://doi.org/10.1021/acs.est.5b01364>
- Marotta, A., & Tutuianu, M. (2012). *Europe-centric light duty test cycle and differences with respect to the WLTP cycle*. Ispra. Retrieved from

file:///C:/Users/pm08r/Downloads/LDNA25345ENN_002.pdf

Martin, T. (2015). *How To Use Automotive Diagnostic Scanners*. Minneapolis: Quarto Publishing Group USA Inc.

Mercedes-Benz. (2008). Vito Taxi. Retrieved July 25, 2015, from http://www.londonblacktaxi.net/kpmuktaxis_mercedes_vito_taxi.pdf

Mock, P., & German, J. (2015). *The future of vehicle emissions testing and compliance*. Berlin. Retrieved from http://www.theicct.org/sites/default/files/publications/ICCT_future-vehicle-testing_20151123.pdf

Mock, P., Kuhlwein, J., Tietge, U., Franco, V., Bandivadekar, A., & German, J. (2014). *The WLTP: How a new test procedure for cars will affect fuel consumption values in the EU*. Berlin. Retrieved from http://www.theicct.org/sites/default/files/publications/ICCT_WLTP_EffectEU_2014_1029.pdf

Mock, P., Tietge, U., Franco, V., German, J., Bandivadekar, A., Ligterink, N., ... Riemersma, I. (2014). *From Laboratory to Road*. Retrieved from http://www.theicct.org/sites/default/files/publications/ICCT_LaboratoryToRoad_2014_Report_English.pdf

Munoz-Organero, M., & Magana, V. C. (2013). Validating the Impact on Reducing Fuel Consumption by Using an EcoDriving Assistant Based on Traffic Sign Detection and Optimal Deceleration Patterns. *IEEE Transactions on Intelligent Transportation Systems*, 14(2), 1023–1028. <http://doi.org/10.1109/TITS.2013.2247400>

Nam, E. (2004). *Advanced Technology Vehicle Modeling in PERE*. Retrieved from <https://www3.epa.gov/otaq/models/ngm/420d04002.pdf>

Nam, E. (2009). *Drive Cycle Development and Real- world data in the United States* (No. WLTP-02-17). Geneva. Retrieved from

<http://www.unece.org/fileadmin/DAM/trans/doc/2009/wp29grpe/WLTP-02-17e.pdf>

National Academy of Engineering. (2011). *Assessment of Fuel Economy Technologies for Light-Duty Vehicles*. Washington DC: The National Academies Press.

National Instruments. (2014). Controller Area Network (CAN) Overview. Retrieved June 28, 2016, from <http://www.ni.com/white-paper/2732/en/>

National Renewable Energy Laboratory. (2009). Hybrid Taxis Give Fuel Economy a Lift. Retrieved April 29, 2016, from <http://www.afdc.energy.gov/pdfs/45148.pdf>

Nelson\Nygaard. (2013). *Taxi Consultant Report*. San Francisco. Retrieved from <http://www.cityofboston.gov/mayor/pdfs/bostaxiconsultant.pdf>

Netherlands Government. (2016). Bpm Tariff. Retrieved May 2, 2016, from http://www.belastingdienst.nl/wps/wcm/connect/bldcontenten/belastingdienst/individuals/cars/bpm/calculate_and_pay_bpm/bpm_tariff/bpm_tariff

OECD. (2011). *OECD Studies on Environmental Innovation Invention and Transfer of Environmental Technologies*. Paris: OECD Publishing.

Ortenzi, F., & Costagliola, M. A. (2010). A New Method to Calculate Instantaneous Vehicle Emissions using OBD Data. In *SAE World Congress & Exhibition*. <http://doi.org/10.4271/2010-01-1289>

Outils OBD Facile. (2016). OBD Modes and PIDs. Retrieved June 28, 2016, from <http://www.ouilsobdfacile.com/obd-mode-pid.php>

Pelkmans, L., Debal, P., Hood, T., Hauser, G., & Delgado, M.-R. (2004). Development of a Simulation Tool to Calculate Fuel Consumption and Emissions of Vehicles Operating in Dynamic Conditions. *SAE Technical Paper, 2004-01-18*. <http://doi.org/10.4271/2004-01-1873>

Pointel, S. (2015). Was COP21 a Failure or a Success. Retrieved June 22, 2015, from <http://steps-centre.org/2015/blog/was-cop21-a-failure-or-a-success/>

- Prati, M. V., Meccariello, G., Della Ragione, L., & Costagliola, M. A. (2015). Real Driving Emissions of a Light-Duty Vehicle in Naples. Influence of Road Grade. In *International Conference on Engines & Vehicles*. <http://doi.org/10.4271/2015-24-2509>
- Price, K. S., Wang, L., & Pauly, T. (2015). Evaluation of Field NO_x Performance of Diesel Vehicles using ECM - Provided OBD/SAEJ1979 Data. In *SAE World Congress & Exhibition*. <http://doi.org/10.4271/2015-01-1067>
- Racelogic. (2008). *VBOX II Lite 5Hz GPS Data Logger User Guide*. Buckingham. Retrieved from http://www.racelogic.co.uk/_downloads/vbox/Manuals/Data_Loggers/RLVB2L_Manual.pdf
- Racelogic. (2014). *VBOX Automotive*. Retrieved April 13, 2016, from https://racelogic.support/01VBOX_Automotive
- Rakha, H., Ahn, K., El-Shawarby, I., & Jang, S. (2004). Emission Model Development Using In-vehicle On-Road Emission Measurements. In *Transport Research Board Annual Meeting* (Vol. 2). Washington DC.
- Rakha, H., Ahn, K., & Trani, A. (2004). Development of VT-Micro model for estimating hot stabilized light duty vehicle and truck emissions. *Transportation Research Part D*, 9, 49–74.
- Rask, E., Duoba, M., Lohse-Busch, H., & Bocci, D. (2010). *Model Year 2010 (Gen 3) Toyota Prius Level-1 Testing Report*. Retrieved from <http://www.ipd.anl.gov/anlpubs/2010/06/67317.pdf>
- Ricardo Inc. (2008). *A Study of Potential Effectiveness of Carbon Dioxide Reducing Vehicle Technologies*.
- Ricardo Inc. (2016). *IGNITE*.
- Riley, R., & Tate, J. (2016). Database of third generation Toyota Prius operation over

city centre taxi test routes. Retrieved July 19, 2016, from <http://archive.researchdata.leeds.ac.uk/57/>

Ross, M. (1997). Fuel efficiency and the physics of automobiles. *Contemporary Physics*, 38(6).

Rousseau, A., Deville, B., Zini, G., Kern, J., Anderson, J., & Duoba, M. (2001). Honda Insight Validation Using PSAT. *SAE Technical Paper*, 2001-01-25. <http://doi.org/10.4271/2001-01-2538>

Rousseau, A., & Halbach, S. (2010). *Autonomie Plug&Play Software Architecture*. 2009 DOE Hydrogen Program and Vehicle Technologies Annual Merit Review. Retrieved from http://energy.gov/sites/prod/files/2014/03/f11/vss009_rousseau_2010_o.pdf

Rubino, L., Bonnel, P., Hummel, R., & Krasenbrink, A. (2007). PEMS Light Duty Vehicles Application: Experiences in downtown Milan. *SAE Technical Paper*, 2007-01-01. <http://doi.org/doi:10.4271/2007-24-0113>

San Francisco Municipal Transportation Agency. (2008). 2008 Clean Air Taxi Frequently Asked Questions. Retrieved April 29, 2016, from <https://www.sfmta.com/sites/default/files/pdfs/CAT-FAQ.pdf>

San Francisco Municipal Transportation Agency. (2015). Carbon Footprint Reports. Retrieved April 29, 2016, from [https://www.sfmta.com/sites/default/files/pdfs/Cab Companies%2527s Carbon Footprint Report July 2013_0.pdf](https://www.sfmta.com/sites/default/files/pdfs/CabCompanies%2527s%20Carbon%20Footprint%20Report%20July%202013_0.pdf)

Sandhu, G., & Frey, H. (2013). Effects of Errors on Vehicle Emission Rates from Portable Emissions Measurement Systems. *Transportation Research Board*, 2340. <http://doi.org/http://dx.doi.org/10.3141/2340-02>

Sandoval, D., & Heywood, J. B. (2003). An Improved Friction Model for Spark-Ignition Engines. <http://doi.org/10.4271/2003-01-0725>

Schäfer, F., & Basshuysen, R. van. (1995). *Reduced Emissions and Fuel Consumption in Automobile Engines*. Berlin: Springer-Verlag.

- Scora, G., & Barth, M. (2006). *Comprehensive Modal Emissions Model (CMEM), version 3.01 User's Guide*. Riverside CA. Retrieved from http://www.cert.ucr.edu/cmем/docs/CMEM_User_Guide_v3.01d.pdf
- Senger, R. D., Merkle, M. A., & Nelson, D. J. (1998). Validation of ADVISOR as a Simulation Tool for a Series Hybrid Electric Vehicle. *SAE Technical Paper, 981133*. <http://doi.org/10.4271/981133>
- Skoda. (2016). Skoda Octavia Hatch S. Retrieved May 2, 2016, from <http://cc-cloud.skoda-auto.com/gbr/gbr/en-gb>
- Smit, R., Smokers, R., & Rabe, E. (2007). A new modelling approach for road traffic emissions: VERSIT+. *Transportation Research Part D, 12*, 414–422.
- Smit, R., Smokers, R., Schoen, E., & Hensema, A. (2006). *A New Modelling Approach for Road Traffic Emissions: VERSIT+ LD - Background and Methodology*. Delft. Retrieved from [http://www.emissieregistratie.nl/ERPUBLIEK/documenten/Lucht \(Air\)/Verkeer en Vervoer \(Transport\)/Smit et al. \(2006\) A new modelling approach for road traffic emissions; VERSIT+ LD - background and methodoly.pdf](http://www.emissieregistratie.nl/ERPUBLIEK/documenten/Lucht(Air)/Verkeer%20en%20Vervoer(Transport)/Smit%20et%20al.%20(2006)%20A%20new%20modelling%20approach%20for%20road%20traffic%20emissions;%20VERSIT%20LD%20-%20background%20and%20methodoly.pdf)
- The International Council on Clean Transportation. (2014). *European Vehicle Market Statistics*. Berlin. Retrieved from http://www.theicct.org/sites/default/files/publications/EU_pocketbook_2014.pdf
- The International Council on Clean Transportation. (2015a). EPA's notice of violation of the Clean Air Act to Volkswagen. Retrieved July 15, 2016, from <http://www.theicct.org/news/epas-notice-violation-clean-air-act-volkswagen-press-statement>
- The International Council on Clean Transportation. (2015b). *The European Real-Driving Emissions Regulation*. Berlin. Retrieved from http://www.theicct.org/sites/default/files/publications/ICCTbrief_EU-RDE_201512.pdf

- The London Taxi Company. (n.d.). Performance. Retrieved July 25, 2015, from <http://london-taxis.co.uk/performance>
- The Scottish Government. (2010). Low Carbon Scotland: Public Engagement Strategy. Retrieved May 2, 2016, from <http://www.gov.scot/Publications/2010/12/23134226/1>
- The Society of Motor Manufacturers and Traders Limited. (2015). *New Car CO2 Report 2015 The 14th report*. Retrieved from http://www.smmt.co.uk/wp-content/uploads/sites/2/101924_SMMT-CO2-Report-FINAL-270415.pdf
- Thiel, C., Krause, J., & Dilara, P. (2015). *Electric vehicles in the EU from 2010 to 2014 - is full scale commercialisation near?* Retrieved from http://publications.jrc.ec.europa.eu/repository/bitstream/JRC97178/ev_registrations_report_final_online.pdf
- Toronto Atmospheric Fund. (2009). *Toronto Hybrid Taxi Pilot*. Toronto. Retrieved from <http://www.toronto.ca/taf/pdf/hybrid-taxi-oct09.pdf>
- Toyota. (2012). 2012 Toyota Prius: New Style, New Technology for the world's Best-Selling Hybrid. Retrieved April 13, 2016, from <http://media.toyota.co.uk/2012/01/2012-toyota-prius-new-style-new-technology-for-the-worlds-best-selling-hybrid/>
- Toyota. (2015a). 2015 Prius eBrochure. Retrieved May 31, 2016, from http://www.toyota.com/content/ebrochure/2015/prius_ebrochure.pdf
- Toyota. (2015b). History of the Toyota Prius. Retrieved April 13, 2016, from <http://blog.toyota.co.uk/history-toyota-prius>
- Toyota. (2015c). Prius 2015. Retrieved May 17, 2016, from http://www.toyota.com/content/ebrochure/2015/prius_ebrochure.pdf
- Toyota. (2016). New Prius. Retrieved May 2, 2016, from <https://www.toyota.co.uk/new-cars/prius/index.json?gclid=COBwxtXzrswCFQ5mGwodl1YPQQ&gclsrc=aw.ds>

Transport & Environment. (2014). Netherlands tops EU ranking of lowest CO2 emissions from new cars – Germany and Poland the laggards. Retrieved May 2, 2016, from <https://www.transportenvironment.org/press/netherlands-tops-eu-ranking-lowest-co%25E2%2582%2582-emissions-new-cars-%25E2%2580%2593-germany-and-poland-laggards>

Transport & Environment. (2015a). *Mind the Gap*. Brussels. Retrieved from https://www.transportenvironment.org/sites/te/files/publications/TE_Mind_the_Gap_2015_FINAL.pdf

Transport & Environment. (2015b). Some Mercedes, BMW and Peugeot models consuming around 50% more fuel than official results, new study reveals. Retrieved June 23, 2016, from <https://www.transportenvironment.org/press/some-mercedes-bmw-and-peugeot-models-consuming-around-50-more-fuel-official-results-new-study>

Transport & Environment. (2015c). Transport consuming most energy in developed world. Retrieved July 17, 2016, from <https://www.transportenvironment.org/news/transport-consuming-most-energy-developed-world>

Transport & Environment. (2016). Carmakers' hands tied as EU agrees CO2 targets will be based on new test. Retrieved June 23, 2016, from <https://www.transportenvironment.org/press/carmakers%25E2%2580%2599-hands-tied-eu-agrees-co2-targets-will-be-based-new-test>

Transport Canada. (2008). Hail a Hybrid Program. Retrieved May 2, 2016, from <http://data.tc.gc.ca/archive/eng/programs/environment-utsp-casestudy-cs70e-hailahybrid-811.htm>

Transport for London. (2007). Construction and Licencing of Motor Taxis for use in London. Conditions of Fitness. Retrieved July 20, 2015, from

<https://tfl.gov.uk/cdn/static/cms/documents/taxi-conditions-of-fitness.pdf>

Transport for London. (2014). *Transport Emissions Roadmap cleaner transport for a cleaner London*. London. Retrieved from <http://content.tfl.gov.uk/transport-emissions-roadmap.pdf>

Transport for London. (2015a). Have your say on the Ultra Low Emission Zone. Retrieved April 29, 2016, from <https://consultations.tfl.gov.uk/environment/ultra-low-emission-zone>

Transport for London. (2015b). New Vision for taxi and private hire services in the Capital. Retrieved July 20, 2015, from <https://tfl.gov.uk/info-for/media/press-releases/2015/new-vision-for-cleaner-greener-taxi-and-private-hire-services-in-the-capital>

Transport for London. (2015c). Taxi and private hire requirements. Retrieved April 29, 2016, from <https://tfl.gov.uk/modes/driving/ultra-low-emission-zone/taxi-and-private-hire-requirements?intcmp=35073>

Treiber, M., & Kesting, A. (2013). *Traffic Flow Dynamics: Data, Models and Simulation*. Berlin: Springer-Verlag.

Tutuianu, M., Bonnel, P., Ciuffo, B., Haniu, T., Ichikawa, N., Marotta, A., ... Heinz Steven. (2015). Development of the World-wide harmonized Light duty Test Cycle (WLTC) and a possible pathway for its introduction in the European legislation. *Transportation Research Part D*, 61(75). Retrieved from http://e3p-beta.jrc.nl/sites/default/files/documents/publications/2015_trd_wltc.pdf

UK Department for Transport. (2013). Table TAXI0101 Licenced taxis and taxi drivers: England and Wales, from 1965. Retrieved July 20, 2015, from <https://www.gov.uk/government/statistics/taxi-and-private-hire-vehicle-statistics-england-and-wales-2013>

UK Department of Energy & Climate Change. (2016). *2014 UK Greenhouse Gas*

Emissions, Final Figures. London. Retrieved from https://www.gov.uk/government/uploads/system/uploads/attachment_data/file/496942/2014_Final_Emissions_Statistics_Release.pdf

United Kingdom Government. (2016). Tax on company benefits. Retrieved May 2, 2016, from <https://www.gov.uk/tax-company-benefits/tax-on-company-cars>

United Nations Framework Convention on Climate Change. (2016). Background on the UNFCCC: The international response to climate change. Retrieved April 9, 2016, from http://unfccc.int/essential_background/items/6031.php

United States Environmental Protection Agency. (2014). Global Greenhouse Gas Emissions Data. Retrieved June 20, 2016, from <https://www3.epa.gov/climatechange/ghgemissions/global.html>

United States Environmental Protection Agency. (2016). Test Car List Data Files. Retrieved June 2, 2016, from <https://www3.epa.gov/otaq/tcldata.htm>

University of California. (2016). Comprehensive Modal Emission Model (CMEM). Retrieved July 9, 2016, from <http://www.cert.ucr.edu/cmем/>

US Environmental Protection Agency. (2002). *Methodology for Developing Modal Emission Rates for EPA's Multi-Scale Motor Vehicle and Equipment Emission System.*

US Environmental Protection Agency. (2010). Can MOVES model Hybrid-Electric vehicle? Retrieved July 9, 2016, from <https://movesepa.zendesk.com/hc/en-us/articles/212330817-Can-MOVES-model-Hybrid-Electric-vehicle->

US Environmental Protection Agency. (2012). *Motor Vehicle Emission Simulator (MOVES) User Guide for MOVES2010b.* Retrieved from <https://www3.epa.gov/otaq/models/moves/documents/420b12001b.pdf>

US Environmental Protection Agency. (2013). EPA Releases MOVES2010b Mobile Source Emissions Model Revision: Questions and Answers. Retrieved July 9, 2016,

from <https://www3.epa.gov/otaq/models/moves/documents/420f13004.pdf>

US Environmental Protection Agency. (2014). EPA Releases MOVES2014 Mobile Source Emissions Model: Questions and Answers. Retrieved July 9, 2016, from <https://www3.epa.gov/otaq/models/moves/documents/420f14049.pdf>

V.Gopal, R., & Rousseau, A. P. (2011). System Analysis Using Multiple Expert Tools. *SAE Technical Paper, 2011-01-07*. <http://doi.org/10.4271/2011-01-0754>

Valencia, M. J. (2009). US bill could pave way for hybrid taxi fleets. Retrieved April 29, 2016, from http://archive.boston.com/news/nation/washington/articles/2009/10/02/us_bill_could_pave_way_for_hybrid_taxi_fleets/

Varella, R. A., Gonçalves, G., Duarte, G., & Farias, T. (2016). Cold-Running NO_x Emissions Comparison between Conventional and Hybrid Powertrain Configurations Using Real World Driving Data. In *SAE Technical Paper*. <http://doi.org/10.4271/2016-01-1010>

Weilenmann, M., Soltic, P., & Ajtay, D. (2003). Describing and compensating gas transport dynamics for accurate instantaneous emission measurement. *Atmospheric Environment*, *37*(37), 5137–5145. <http://doi.org/10.1016/j.atmosenv.2003.05.004>

Weiss, M. A., Heywood, J. B., Drake, E. M., Schafer, A., & AuYeung, F. F. (2000). *On the Road in 2020 A Life-Cycle Analysis of New Automobile Technologies*. Cambridge MA. Retrieved from <http://citeseerx.ist.psu.edu/viewdoc/download?doi=10.1.1.22.3438&rep=rep1&type=pdf>

Weiss, M., Bonnel, P., Hummel, R., Manfredi, U., Colombo, R., Lanappe, G., ... Sculati, M. (2011). *Analyzing on-road emissions of light-duty vehicles with Portable Emission Measurement Systems (PEMS)*. Ispra. Retrieved from

http://ec.europa.eu/clima/policies/transport/vehicles/docs/2011_pems_jrc_62639_en.pdf

- Weiss, M., Bonnel, P., Kühlwein, J., Provenza, A., Lambrecht, U., Alessandrini, S., ... Sculati, M. (2012). Will Euro 6 reduce the NO_x emissions of new diesel cars? – Insights from on-road tests with Portable Emissions Measurement Systems (PEMS). *Atmospheric Environment*, 62, 657–665. <http://doi.org/10.1016/j.atmosenv.2012.08.056>
- Wu, X., Zhang, S., Wu, Y., Li, Z., Ke, W., Fu, L., & Hao, J. (2015). On-road measurement of gaseous emissions and fuel consumption for two hybrid electric vehicles in Macao. *Atmospheric Pollution Research*, 6(5), 858–866. <http://doi.org/10.5094/APR.2015.095>
- Wyatt, D. W., Li, H., & Tate, J. (2013). Examining the Influence of Road Grade on Vehicle Specific Power (VSP) and Carbon Dioxide (CO₂) Emission over a Real-World Driving Cycle. *SAE Technical Paper*, 2013-01-15. <http://doi.org/10.4271/2013-01-1518>
- Xu, Y., Yu, L., & Song, G. (2011). Improved Vehicle-Specific Power Bins for Light-Duty Vehicles in Estimation of Carbon Dioxide Emissions in Beijing. *Transportation Research Board*, 2191. <http://doi.org/http://dx.doi.org/10.3141/2191-20>
- Yang, L., Franco, V., Campestrini, A., German, J., & Mock, P. (2015). *NO_x control technologies for Euro 6 Diesel passenger cars*. Berlin. Retrieved from http://www.theicct.org/sites/default/files/publications/ICCT_NOx-control-tech_revised_09152015.pdf
- Zallinger, M., Anh, L. T., & Hausberger, S. (2005). Improving an Instantaneous Emission Model for Passenger Cars. In *Transport and Air Pollution*. Graz.
- Zhang, K. (2006). *Micro-Scale On-Road Vehicle Emissions Measurements and Modeling*. North Carolina State University.

